OPTIMISING THE FUNCTIONAL MATURITY OF KIDNEY ORGANOIDS FOR SCREENING NEPHROTOXIC DRUGS

Ying-Chen Soo

ORCID: 0000-0003-3939-6869

Thesis submitted in total fulfilment of the requirement of the

degree of Doctor of Philosophy

September 2019

Department of Paediatrics

Faculty of Medicine, Dentistry, and Health Sciences

The University of Melbourne

Australia

ABSTRACT

Kidneys are uniquely vulnerable to drug toxicity due to their role in filtering substances from the blood. Filtration and urine production takes places in specialised tubules called nephrons, which are divided into segments with functionally distinct cell types that express transporters and receptors for transporting water, solutes, or small molecules from the blood into the filtrate, or from the filtrate into the cells. Should a drug have an affinity for these transporters, it can accumulate within these cells and cause injury. As a result, there are many commonly-used pharmaceutical compounds which are nephrotoxic to some degree, which can lead to acute kidney injury in patients. The nephron segment called the proximal tubule is the most frequently affected, as proximal tubule cells express a wide array of transporters and receptors which can transport drugs, and have a high metabolic rate which is vulnerable to disruptions in cellular energy production. Developing new drugs which are less nephrotoxic has been challenging, as the *in vitro* assays and animal tests currently used to screen drugs in development for nephrotoxicity have decreased transporter and receptor expression compared to mature human proximal tubules *in vivo*. Recent advances in understanding kidney development in the embryo have led to protocols for differentiating human pluripotent stem cells to kidney organoids, which contain segmented nephrons that have proximal tubules. Hence, kidney organoids may be useful for *in vitro* nephrotoxicity screening during drug development if they show sufficient nephron maturation.

Through immunofluorescence and qRT-PCR analysis, we found that while proximal tubules in organoids expressed some proximal tubule markers to a greater degree than primary proximal tubule cells cultured in 2D, expression was still low overall compared to foetal kidney, and some transporters were absent. We then performed a bioinformatics analysis of single-cell RNA sequencing datasets generated from foetal and adult mouse and human kidneys to find signalling pathways which changed during proximal tubule maturation. Among other changes, mature proximal tubule cells showed increased fatty acid oxidation, a decreased capacity for glycolysis, and decreased TGFβ/BMP signalling, suggesting that inducing these changes *in vitro* might improve proximal tubule maturation in organoids.

To aid our characterisation of proximal tubules in organoids, we developed two reporter lines, *LRP2*:mTagBFP2 and *HNF4A*:YFP, for genes which are highly expressed in the developing proximal tubule, and confirmed that these genes and their respective reporters were co-expressed in the proximal tubules of kidney organoids. We also developed a

HAVCR1:mCherry reporter line for future use in detecting injury responses in kidney organoids. These reporter lines allowed live monitoring of proximal tubule development and function.

Using the *HNF4A*:YFP reporter, we screened for culture conditions which improved proximal tubule maturity in organoids and determined that a low-glucose, insulin-free medium designed to induce fatty acid oxidation supplemented with a small molecule inhibitor of TGFβ improved the expression of proximal tubule markers in organoids, consistent with our bioinformatics analysis. We also performed xenotransplantation of reporter organoids into immunocompromised mice to determine whether proximal tubules would mature in this environment, and found that while non-renal tissue would proliferate in the grafts, proximal tubules in transplanted organoids maintained reporter expression better than organoids maintained *in vitro* under standard conditions. Taken together, this thesis characterises proximal tubule maturation and has begun to optimise this process within kidney organoids using novel reporter tools. This represents a significant advance in facilitating improved screening of drug-induced nephrotoxicity using organoids in the future.

DECLARATION

I. This thesis contains only original work towards the Doctor of Philosophy.

II. Due acknowledgement has been made in the text of all other material used.

III. The thesis is fewer than 100,000 words in length, excluding tables, figures, bibliographies and appendices.

(Signature image omitted pursuant to University of Melbourne electronic thesis deposition requirements)

Ying-Chen Soo

PREFACE

Pursuant to the regulations governing the degree of Doctor of Philosophy at the University of Melbourne, I hereby submit that:

Declaration by author:

This thesis is composed of my original work, and contains no material previously published or written by another person except where due reference has been made in the text. I have clearly stated the contribution by others to jointly-authored works that I have included in my thesis. I have clearly stated the contribution of others to my thesis as a whole, including statistical assistance, survey design, data analysis, significant technical procedures, professional editorial advice, and any other original research work used or reported in my thesis. The content of my thesis is the result of work I have carried out since the commencement of my research higher degree candidature and does not include a substantial part of work that has been submitted to qualify for the award of any other degree or diploma in any university or other tertiary institution. I have clearly stated which parts of my thesis, if any, have been submitted to qualify for another award.

Statement of parts of the thesis submitted to qualify for the award of another degree:

None

Publications during candidature:

1. Little, M., Takasato, M., Soo, J. Y.-C. & Forbes, T. A. Recapitulating development to generate kidney organoid cultures. in *Organ Regeneration - 3D Stem Cell Culture & Manipulation* (ed. Tsuji, T.) 195–206 (2017).
2. Soo, J. Y.-C., Jansen, J., Masereeuw, R. & Little, M. H. Advances in predictive *in vitro* models of drug-induced nephrotoxicity. *Nature Reviews Nephrology* **14**, 378–393 (2018).
3. Vanslambrouck, J. M. *et al.* A toolbox to characterize human induced pluripotent stem cell–derived kidney cell types and organoids. *JASN* (2019). doi:10.1681/ASN.2019030303

Contributions by others to the thesis:

Prof. Melissa Little contributed to experiment concept and design, interpretation of experimental data, proofreading of the manuscript, and performed surgery for subcutaneous and omental xenotransplantation of organoids (Chapter 5).

Dr. Sara Howden and Dr. Jessica Vanslambrouck contributed to experiment concept and design, interpretation of experimental data, and proofreading of the manuscript.

Pei Xuan Er, Irene Ghobrial, and Dr. Santhosh Kumar provided training and technical advice for tissue culture and kidney organoid differentiation.

The MCRI Flow Cytometry & Imaging facility (Dr. Matt Burton, Dr. Eleanor Jones, Paul Lau) performed fluorescence-activated cell sorting (FACS) and provided training and technical advice for confocal microscopy.

Dr. Jitske Jansen (Radboud University) designed and performed CD13 and EPCAM-based FACS and qRT-PCR of proximal tubule cells from organoids (Chapter 2).

Dr. Belinda Phipson, Luke Zappia, and Andrew Lonsdale provided technical advice for bioinformatics analysis (Chapter 2).

The MCRI Gene Editing Facility (Dr. Sara Howden, Alison Graham, Penny McDonald) performed the initial targeting and screening of the *HNF4A*:YFP reporter line and provided advice for the targeting and screening of the *LRP2*:mTagBFP2 and *HAVCR1*:mCherry reporter lines (Chapter 3).

Dr. Kwaku Dad Abu-Bonsrah provided technical assistance with preparing cardiac maturation medium (Chapter 4).

Dr. Siebe Spijker (Leiden University Medical Centre), Michelle Scurr, and Ker Sin Tan performed surgeries for subcapsular xenotransplantation of organoids (Chapter 5). The MCRI Disease Modelling Unit provided animal welfare support.

Michelle Scurr performed paraffin embedding and sectioning of grafts as well as staining of sections (Chapter 5).

The introduction of this thesis contains text from a review (see previous section) which was co-authored with Dr. Jitske Jansen, Prof. Rosalinde Masereeuw, and Prof. Melissa Little. Dr.

Jitske Jansen and I performed the literature search, and Dr. Jitske Jansen, Prof. Rosalinde Masereeuw and I wrote the review. All authors contributed to discussion of the review's content and edited the manuscript before submission.

Unpublished scRNA-seq datasets of organoids analysed in Chapter 2 were previously characterised by Sean Wilson and others within our research group. Unpublished scRNA-seq datasets of human foetal kidneys were contributed by Jason Spence in collaboration with our research group.

ACKNOWLEDGEMENTS

I would like first of all to thank Prof. Melissa Little for her supervision and for encouraging me to persevere through this project. Thanks are also due to my co-supervisors Dr. Sara Howden and Dr. Jessica Vanslambrouck for their technical advice, feedback on experimental design, and support.

To the many members of the Kidney Regeneration group past and present whom I have had the pleasure of knowing, thank you for your advice, your patience with a student who had not touched kidneys or pluripotent stem cells prior to this project, the late-night conversations, the overabundance of cakes and treats, and the memories.

To my advisory committee members, Prof. Andrew Elefanty and Prof. Amanda Fosang, thank you for your moral support.

I am grateful to my Heavenly Father for the strength to complete this project and to my family for their listening ears.

I received funding from a Melbourne Research Scholarship and a Murdoch Children's Research Institute Top-Up Scholarship.

TABLE OF CONTENTS

LIST OF TABLES

LIST OF FIGURES

THIRD PARTY COPYRIGHT MATERIAL

Citation Information	**Location of item in thesis**	**Permission granted Y/N**
Davidson, A. J. Mouse kidney development. in *StemBook* (Harvard Stem Cell Institute, 2008). (Creative Commons Attribution license)	Pg. 3	Y
Little, M. H., Combes, A. N. & Takasato, M. Understanding kidney morphogenesis to guide renal tissue regeneration. *Nat Rev Nephrol* **12**, 624–635 (2016).	Pg. 5	Y
Little, M. & Combes, A. N. Kidney organoids: accurate models or fortunate accidents. *Genes & Development* **in press**, (2019).	Pg. 6	Y
Georgas, K. *et al.* Analysis of early nephron patterning reveals a role for distal RV proliferation in fusion to the ureteric tip via a cap mesenchyme-derived connecting segment. *Dev. Biol.* **332**, 273–286 (2009).	Pg. 6	Y
Soo, J. Y.-C., Jansen, J., Masereeuw, R. & Little, M. H. Advances in predictive in vitro models of drug-induced nephrotoxicity. *Nature Reviews Nephrology* **14**, 378–393 (2018).	Pg. 11	Y
Ran, F. A. *et al.* Genome engineering using the CRISPR-Cas9 system. *Nature Protocols* **8**, 2281–2308 (2013).	Pg. 77	Y
Paquet, D. *et al.* Efficient introduction of specific homozygous and heterozygous mutations using CRISPR/Cas9. *Nature* **533**, 125–129 (2016).	Pg. 77	Y

1 INTRODUCTION

1.1 Structure and function of the kidney

The human kidney contains approximately one million tubular structures called nephrons, which maintain homeostasis by controlling water, salt and pH levels in the blood and by filtering metabolic waste products. Each nephron is an epithelial tubule divided into specialised segments composed of distinct cell types (Figure 1.1).

At the proximal end of the nephron in the renal cortex is the renal corpuscle, which consists of a capillary tuft associated with specialised epithelial cells (podocytes) called the glomerulus, contained within an epithelial enclosure called Bowman's capsule. The podocytes and the endothelial cells of the glomerulus maintain the glomerular basement membrane, while parietal epithelial cells line the basement membrane of the Bowman's capsule. The podocytes are named for their long "foot" processes which interdigitate to form slit diaphragms. As blood enters the glomerulus through the afferent arteriole, fluid is forced across the glomerular basement membrane, while large molecules are retained in the blood because they cannot pass through the slit diaphragms. The urinary filtrate passes through the slit diaphragms and into the Bowman's capsule, where it continues into the proximal tubules and progresses along each nephron. This filtrate has the same concentration of salts and small compounds as the blood, but lacks the large proteins which were retained by the slit diaphragms and basement membrane. The efferent arteriole, carrying blood from the glomerulus, branches into capillaries that intertwine with the nephron so that substances can be exchanged between the interstitial fluid and the filtrate.

The next segment in the nephron is the proximal tubule. The proximal tubule is subdivided into three segments, S1-3, with the first two forming the proximal convoluted tubule and the third forming the proximal straight tubule or pars recta [1]. All three segments have a single layer of columnar epithelial cells attached to a basement membrane [2]. The epithelial cells are closely packed, with tight junctions composed of various proteins in between cells, and are polarised with distinct apical and basolateral surfaces that have different membrane proteins. The tight junctions are relatively leaky compared to tight junctions in other segments of the nephron [3]. The apical surface of each cell faces the lumen of the proximal tubule and has dense, relatively long microvilli forming a brush border [4]. The major role of the proximal tubule is to reabsorb substances such as ions, water, glucose, and small proteins from the

filtrate so that they are not lost in the urine. Roughly 70% of these substances present in the filtrate are reabsorbed [5]. The other major role of the proximal tubule is to secrete unwanted substances from the blood into the filtrate [6]. Proximal tubule cells have many mitochondria (occupying 22-33% of their cytoplasmic volume) to meet the energy demand of these activities, and are heavily reliant on aerobic respiration as their capacity for glycolysis is limited compared to other cell types [7,8].

The loop of Henle is divided into the descending limb extending into the inner zone of the kidney, known as the renal medulla, and the ascending limb which returns to the renal cortex. The main role of the loop of Henle is to assist the collecting duct in reabsorbing water from the urine to the degree needed to maintain homeostasis. The descending limb expresses aquaporin 1 (AQP1) and reabsorbs some water. The ascending limb actively transports NaCl via the NKCC2 transporter from the filtrate into the interstitial fluid, creating an osmotic gradient that favours the reabsorption of water from the adjacent collecting duct into surrounding blood vessels [9].

The distal tubule reabsorbs sodium, chloride, calcium, and magnesium ions from the filtrate [10]. At the beginning of the distal tubule is the macula densa, which secretes vasoconstrictors in response to salt levels in the distal tubule, controlling blood flow into the glomerulus and thereby controlling the rate of salt filtration. Salt reabsorption occurs via active transport channels, whose expression is controlled by aldosterone and parathyroid hormone so that reabsorption occurs at the rate needed to maintain homeostasis. Like the proximal tubule, the distal tubule has high numbers of mitochondria to supply energy for active transport, but compared to the proximal tubule, the distal tubule is more tolerant of mitochondrial damage [11].

The collecting duct runs close to the loop of Henle and reabsorbs water from the urine via AQP2-4 [9]. Multiple collecting ducts join each other and converge into a renal papilla in the medulla. Mice have a single papilla leading to the ureter which carries urine to the bladder, while humans have lobed kidneys with multiple papillae.

The tubules are supported by an extensive peritubular microvasculature, which is maintained by vascular endothelial growth factor (VEGF) secreted by the tubular cells [12]. Interstitial cells found throughout the kidney also contact the basement membranes of the vasculature and tubules and secrete factors supporting the maintenance and repair of these cells [13]. Immune cells such as dendritic cells and macrophages are also found in the interstitium.

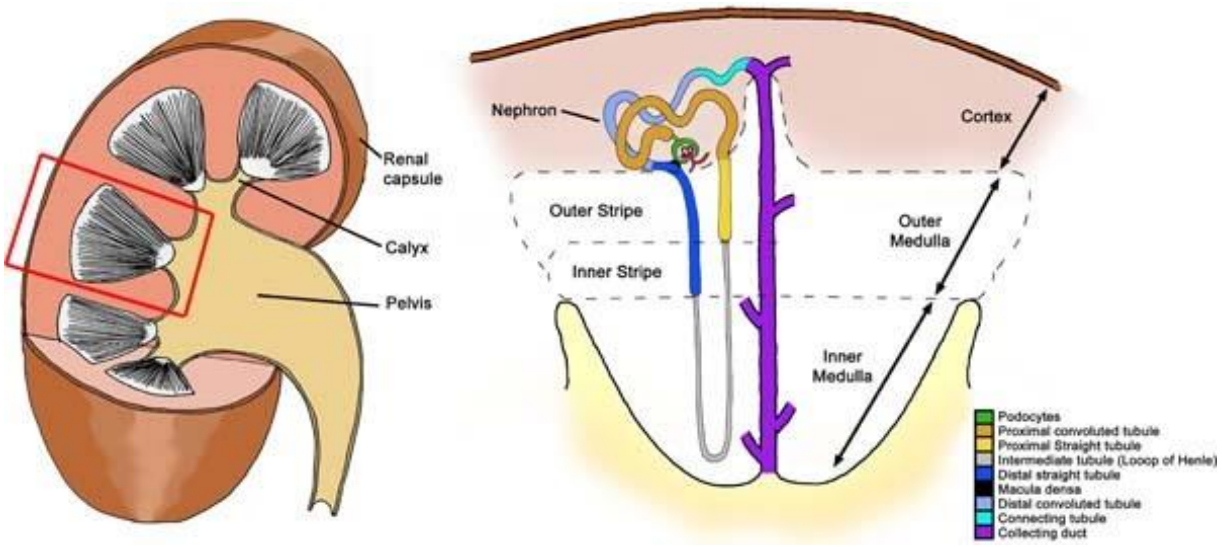

Figure 1.1 Structure of the human kidney [14]. The fibrous outer layer of the kidney is called the renal capsule. Beneath the capsule, the kidney can be divided anatomically into a peripheral zone, the renal cortex, and an inner layer, the renal medulla. Nephrons span the cortex and medulla and are composed of segments with distinct cell types and functions, marked by the colour key. Filtrate from each nephron drains into the collecting duct system, then into the calices and the renal pelvis, through to the ureter.

1.2 Kidney development and organogenesis

During embryonic development, the embryo undergoes gastrulation, specifying the populations which will give rise to the three germ layers. The posterior primitive streak is the region which gives rise to the mesoderm, which along the body trunk is divided into the paraxial, intermediate, and lateral plate mesoderm (Figure 1.2) [15]. In mammals such as mice and humans, the intermediate mesoderm gives rise to three excretory organs in sequence from anterior to posterior: the pronephros, the mesonephros, and the metanephros [16,17]. The paired pronephroi and mesonephroi degenerate in the embryo, while the metanephroi are the kidneys seen in postnatal life.

The anterior intermediate mesoderm gives rise to the paired nephric or Wolffian ducts, epithelial structures which are oriented along the anterior-posterior axis of the embryo and extend caudally as the embryo develops [16]. The pronephric and mesonephric tubules that connect with and drain into the anterior nephric ducts develop from mesenchymal progenitors undergoing mesenchymal-to-epithelial transitions, but these populations eventually degenerate. The posterior intermediate mesoderm gives rise to the metanephric mesenchyme, which forms alongside the posterior nephric duct and will give rise specifically to the metanephric kidneys. The metanephric mesenchyme induces an outgrowth from the adjacent

nephric duct called the ureteric bud [18]. In response to secreted growth factors from the metanephric mesenchyme, the ureteric bud extends towards these signals and then branches dichotomously to form the ureteric epithelium, which will mature into the collecting duct. Conversely, in response to signals from the tips of the branching ureteric tree, metanephric mesenchyme cells aggregate around the ureteric tips to form what is called a cap mesenchyme, consisting of nephron progenitors. These cells drive continued ureteric epithelial branching but can also be triggered to undergo a mesenchymal-to-epithelial transition to give rise to segmented nephrons.

The first stage of nephron formation is the formation of a pre-tubular aggregate of nephron progenitors, which receives signals from the ureteric tip and the surrounding renal stroma inducing the aggregated cells to commit to nephron formation (Figure 1.3). Sufficient signalling will induce a mesenchymal-to-epithelial transition in the pretubular aggregate to form an epithelial renal vesicle, which is polarised with a lumen and has distinct proximal and distal domains [19,20]. The renal vesicle becomes continuous with the ureteric tip at its distal end via a connecting segment and elongates to become the S-shaped body, which is patterned into proximal, medial, and distal segments that will elongate and give rise to the segments of the mature nephron [20]. As the nephron matures, the podocytes secrete VEGF to induce vascularisation of the glomeruli and start fluid filtration through the nephrons.

During kidney development, nephron progenitor commitment to forming nephrons is balanced with progenitor self-renewal as the ureteric tips continue to branch, so that new nephrons can form around the new tips. This iterative branching and nephron production continues and the kidney grows until around 36 weeks gestation in humans [21] or shortly after birth in mice [22]. At this point, the nephron progenitors all commit and are depleted. While the nephrons formed will continue to mature, no further nephrogenesis occurs.

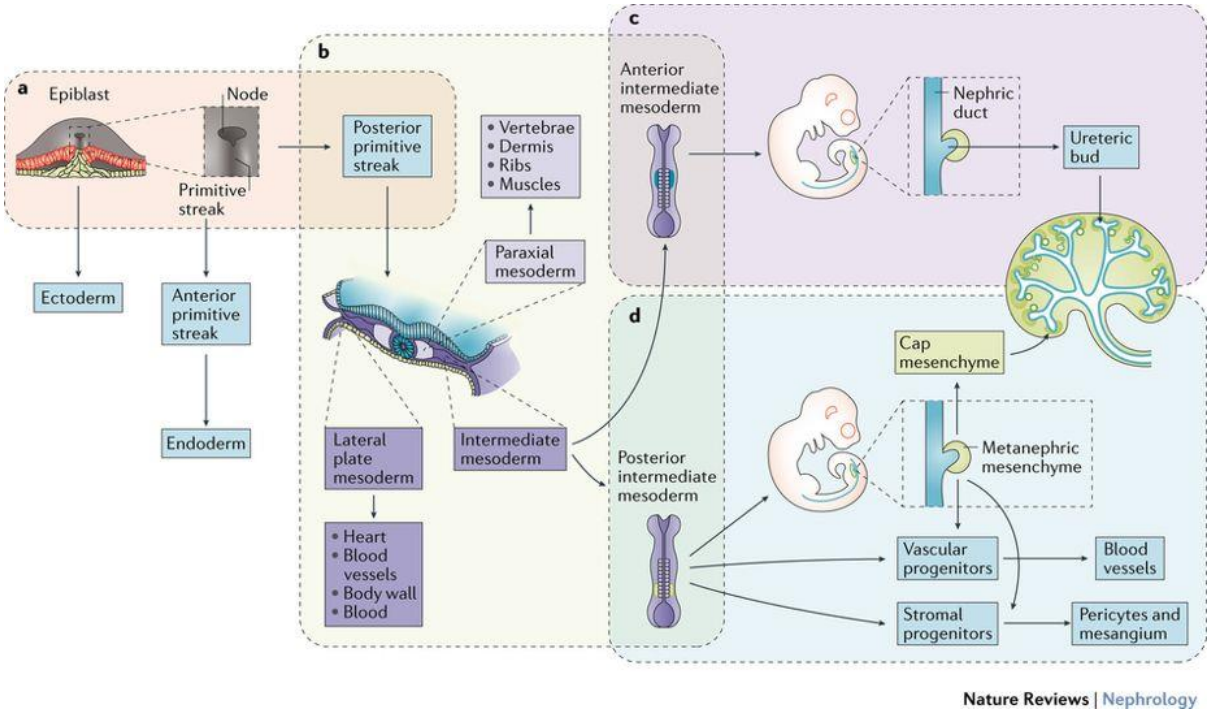

Figure 1.2 Cell populations which give rise to the kidney during embryonic development [23].

A: During gastrulation of the embryo, the epiblast gives rise to the ectoderm, mesoderm, and endoderm. The posterior primitive streak is the population which gives rise to the mesoderm. B: The mesoderm is patterned into paraxial, intermediate, and lateral plate mesoderm along the embryo's mediolateral axis, with the paraxial mesoderm closest to the neural tube. The intermediate mesoderm gives rise to the kidney and gonads. C and D: The anterior intermediate mesoderm gives rise to the nephric duct which extends caudally and forms the ureteric bud. The posterior intermediate mesoderm gives rise to the metanephric mesenchyme which attracts the ureteric bud, induces branching of the ureteric epithelium, and itself gives rise to segmented nephrons.

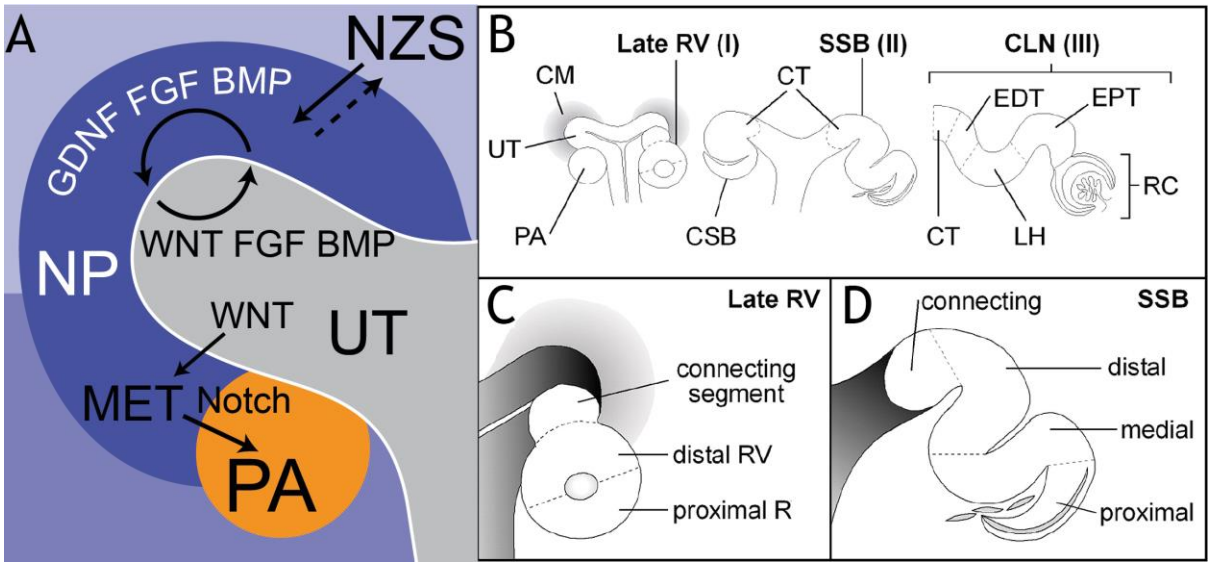

Figure 1.3 Diagram of nephron progenitor epithelialisation and nephron development (adapted from Little and Combes, in press [24] and Georgas *et al.* [25]). A: Nephron progenitors (NP) form pre-tubular aggregates (PA) at the base of a ureteric tip (UT). Signals from the ureteric tips and the nephrogenic zone stroma (NZS) to the nephron progenitors regulate the mesenchymal-to-epithelial transition (MET) of the pre-tubular aggregate to form the renal vesicle. B: The renal vesicle (RV) arises from the pre-tubular aggregate and develops transcriptionally distinct proximal and distal domains, where the distal domain is closest to the connecting segment and ureteric tip (panel C). The renal vesicle elongates into a comma-shaped body (CSB) and then an S-shaped body (SSB) connected to the ureteric tip via the connecting tubule (CT). The S-shaped body has proximal, medial, and distal domains (panel D). The S-shaped body develops further into the capillary loop nephron (CLN), which is segmented into the renal corpuscle (RC), early proximal tubule (EPT), early loop of Henle (LH), early distal tubule (EDT), and the connecting tubule.

1.3 Acute kidney injury and drug-induced nephrotoxicity

Since the mature mammalian kidney cannot produce new nephrons, it repairs itself after injury by replacing damaged tubular epithelial cells within surviving nephrons. It is debatable whether this occurs through de-differentiation and proliferation of the remaining cells or through the proliferation of a resident epithelial stem cell population [26]. Nevertheless, despite this capacity for repair, acute kidney injury is associated with increased hospitalisation costs ranging from $11,016 to $42,077 USD compared to patients without kidney injury, increased mortality, and decreased quality of life [27]. Severe or repeated acute kidney injury can also cause dysregulation of the repair process, leading to fibrosis of the renal interstitium, loss of the microvasculature, and chronic kidney disease with irreplaceable loss of nephron function [26]. Should this progress to end-stage renal disease, the only treatments currently available are

dialysis or kidney transplantation. Due to these adverse consequences, the prevention of acute kidney injury is a major healthcare concern [28].

Drug-induced kidney injury accounts for 20% of hospital- and community-acquired cases of acute kidney injury [29]. The impact of drug-induced kidney injury, mechanisms of injury to the various cell types of the kidney, and methods of characterising potential *in vitro* models of nephrotoxicity are reviewed in detail in Soo *et al*. [12], which was written and published during candidature and is included in the Appendix. Where indicated, the following sections are relevant extracts from that review.

1.3.1 Impact and challenges [12]

The specialised role of the kidney in filtering substances from the blood to maintain homeostasis, coupled with the high metabolic activity of the renal tubular epithelium, makes the kidney particularly vulnerable to drug-induced injury. A wide variety of commonly used pharmaceutical compounds cause a degree of nephrotoxicity, which has to be balanced against the utility of the compound and is often dose-limiting. Antibiotics, such as gentamicin and vancomycin, and immunosuppressive agents provided post-organ transplant, including cyclosporine A (CsA), can cause drug-induced tubular injury[30]. Lithium, frequently prescribed for bipolar disorder, can result in adverse events in the collecting duct[31]. Several epidemiological studies have shown strong associations between the use of common drugs, such as anti-retrovirals and aminoglycoside antibiotics, with increased risk of acute kidney injury[32]. Developing drug derivatives with improved renal safety profiles has proved challenging, as currently available *in vitro* screening methods are poorly predictive of toxicity in animal models or humans[33]. Preclinical trials can also fail to identify toxicity due to species-specific variation in metabolic response and gene expression.[33].

The failure of *in vitro* drug screening methods to identify nephrotoxic activity results from a combination of factors. A major contributor is the lack of valid *in vitro* cell models of the kidney[34]. A second is the lack of robust markers of injury both *in vitro* and *in vivo*[34,35]. The fact that drugs can interact with each other and/or compete for detoxification enzyme complexes complicates screening due to the difficulty of predicting what combinations of drugs may be used on a patient[36–38]. Finally, the market has failed to develop models by which to predict precise drug responses dependent upon the individual patient, such as variants in cytochrome P450 enzymes[39].

Current *in vitro* screens for compound nephrotoxicity have focused mostly on proximal tubule cells, because this segment of the nephron is a significant target of *in vivo* nephrotoxic injury. As described in section 1.1, the proximal tubules secrete xenobiotics into the filtrate and reclaim small molecules such as glucose and albumin from the filtrate via an array of transporters and receptors that can also transport drugs, potentiating toxicity. To generate energy for these processes, the proximal tubule cells are rich in mitochondria, which also makes them sensitive to disruptions of oxidative phosphorylation[40]. Further, metabolic enzymes such as beta-lyase expressed in these cells can bioactivate xenobiotics. However, nephrotoxic injury is not restricted to the proximal tubules, with all segments of the nephron, including the podocytes, distal nephrons and collecting ducts, displaying specific drug sensitivities. The kidney also contains a versatile microvasculature that is also susceptible to drug-induced injury, which causes diminished blood flow, hypoxic injury and inflammation subsequently affecting tubule function.

To develop improved *in vitro* models that can reliably predict potential human clinical nephrotoxicity, we need a solid understanding of the specific cellular targets and consequences of nephrotoxicant injury. This also requires robust and reliable mechanistic biomarkers of nephrotoxicity. The use of primary or conditionally immortalised renal epithelial cell types in 2D culture has represented the gold standard to date. However, proximal tubular epithelial cells cultured in this format display poor apical-basal polarisation and only low levels of the key transporters such as organic anion transporters (OATs) and organic cation transporters (OCTs) which mediate nephrotoxicity *in vivo*, reducing their utility as predictive tools[4,41]. Recent advances in the directed differentiation of human pluripotent stem cells to multiple renal cell types, as well as advances in microfluidic culture systems, have opened up a range of potential novel platforms for *in vitro* nephrotoxicity screening. Here, we review mechanisms of nephrotoxic injury, functional features of a tubular cell model essential for predicting toxicity, and novel *in vitro* cell models currently under development.

1.3.2 Mechanisms of nephrotoxic injury [12]

Nephrotoxicants can either selectively injure specific cell types or injure multiple cell types within the kidney, depending on their mechanism of action[30] (Figure 1.4). Direct toxicity to tubular epithelial cells has been the most extensively studied, particularly injury to the proximal tubule. Tubular epithelial cells express a wide range of transporters, many of which

are unique to each tubular segment. Hence, drugs which have an affinity for these transporters can accumulate within the cells, causing cell death in specific nephron segments. Other drugs, such as amphotericin B, cause tubular toxicity due to their affinity for cell membranes[42]. Tubular epithelial cells can also suffer injury as a result of osmotic effects, drug-induced nephrolithiasis, or secondary injury from ischaemic events. Contrast media used for angiography and similar procedures can induce nephropathy through oxidative stress and osmotic effects as well as haemodynamic changes[43].

The interstitial cells surrounding the tubules are also targets for drug toxicity. Acute interstitial nephritis is most often due to an inflammatory, non-dose-dependent response to a drug causing immunoglobulins to be deposited in tubule basement membranes, while chronic interstitial nephritis is often associated with the long-term use of drugs such as cyclosporine, which cause acute tubular injury followed by inflammatory changes and interstitial fibrosis[30].

The podocytes, which maintain the filtration barrier in the glomeruli, are also targets of drug-induced nephrotoxicity[44]. Similar to interstitial nephritis, drug-induced podocyte injury is often immune-mediated. However, certain drugs have direct toxic effects on podocytes. For example, puromycin, which is taken up via the plasma membrane monoamine transporter (PMAT, *SLC29A4*), and bisphosphonates [45–47] are thought to cause podocyte injury by disrupting their cytoskeleton [45]. Injured podocytes de-differentiate, which disrupts the glomerular filtration barrier, allowing albumin and/or other plasma proteins to leak into the urine. Depending on the extent of the proteinuria, secondary tubular damage may also occur. Severe glomerular injury and proteinuria presents as nephrotic syndrome, defined as proteinuria in excess of 3 g per day accompanied by hypoalbuminaemia, oedema, and hyperlipidemia due to the loss of plasma proteins [48].

Beyond their nephrotoxic effects on specific renal cell types, drugs can exert injurious effects on the haemodynamic regulatory mechanisms of the kidney. Renal blood flow and glomerular filtration rate (GFR) are regulated by complex mechanisms, including prostaglandin and renin-angiotensin system signalling pathways[30]. Several drug classes, such as non-steroidal anti-inflammatory drugs (NSAIDs) and angiotensin converting enzyme (ACE) inhibitors, can disrupt these pathways[49,50], reducing GFR and potentially causing renal ischaemia and cell death through excessive vasoconstriction.

The kidney also contains a highly diverse population of endothelial cells that form its microvasculature. These cells are also sensitive to drug-induced injury. Unlike the renal

tubules, these endothelial cells lack regenerative capacity[51] and hence, acute injury of the renal vasculature can predispose patients to the development of CKD[52]. Nephrotoxicants can directly affect vascular responsiveness by modulating endothelial barrier function, coagulation cascades, and/or inflammatory processes[53]. Tubulovascular cross-talk takes place through VEGF-A, which is expressed in renal tubular epithelial cells, and its receptor (VEGFR2) located almost exclusively on peritubular capillary endothelial cells[54]. This interaction is essential for the maintenance of the peritubular microvasculature. Anticancer drugs that target the VEGF pathway can induce thrombotic microangiopathy, proteinuria and hypertension[55]. Thrombotic microangiopathy involving thrombocytopenia, microangiopathic haemolytic anaemia and microvascular occlusion, can be immune-mediated and often leads to acute tubule necrosis, and drugs associated with this include quinine, cyclosporine and tacrolimus.

Assessment of the potential nephrotoxic effects of pharmaceutical compounds on different components of the kidney therefore requires the use of different model systems. Direct injurious effects of a compound on tubular cells are the easiest mechanisms to model *in vitro*, whereas injury mechanisms that require blood flow, urine or filtrate production, immune-mediated injury, or involve secondary injury are more challenging, as they require a model system in which complex cellular architecture is combined with functional components. Below we discuss current *in vitro* models that are used to assess the nephrotoxicity of pharmaceutical agents and the development of novel systems that more closely recapitulate the complexity of the kidney.

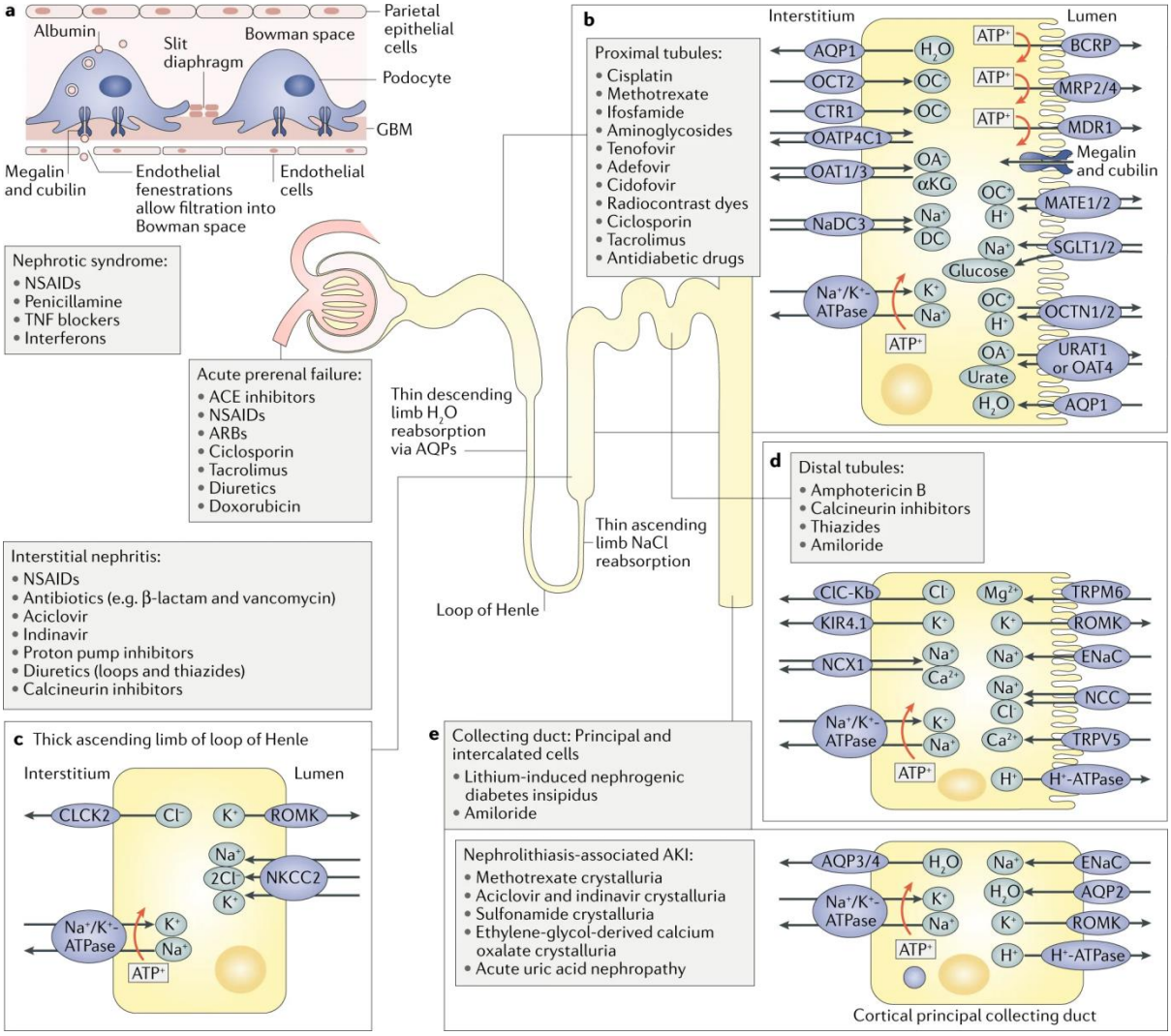

Figure 1.4 Transporters and receptors found in nephron segments and drugs which have toxic effects on each segment [12]. Drugs may also cause nephrotic syndrome through damage to the glomerular basement membrane or podocytes, acute prerenal failure due to ischaemia, interstitial nephritis, or microangiopathy.

1.3.3 Characterisation of in vitro models of nephrotoxicity [12]

1.3.3.1 Markers of functional maturity

An *in vitro* model that recapitulates the *in vivo* response of renal cells to nephrotoxicants requires appropriate expression of the transporters and receptors that interact with the drug of interest. Much work has been done to identify transporters and enzymes associated with drug-induced nephrotoxicity. The more of these markers that can be expressed at physiological levels in a model, the more likely it becomes that the model will accurately predict whether a drug will be nephrotoxic. In addition to detecting expression at the transcript and protein

level by qRT-PCR and immunostaining, transporter and endocytotic receptor function can be assayed using fluorescent substrates and inhibitors (Table 1.1). Inhibiting uptake routes will decrease intracellular fluorescence, while inhibiting efflux transporters will increase fluorescence. These transporters, receptors, and enzymes do not act in isolation. For example, drug transporters may rely on Na^+/K^+ ATPase activity to generate an electrochemical gradient. A drug may also be a substrate for multiple transporters and receptors, or become a substrate after bioactivation by an enzyme. Thus, for a model to accurately predict drug nephrotoxicity, it must express appropriate levels of all key transporters and enzymes and carry out the metabolic activities required for these transporters and enzymes to function.

The polarised, mature proximal tubule expresses a range of influx and efflux transporters which have overlapping substrate affinities, allowing for transcellular secretion of drugs and endogeneous compounds from the interstitial compartment into the filtrate. Two of the major influx transporter types are the organic anion transporters (OATs) and the organic cation transporter OCT2 expressed on the basolateral surface of the proximal tubule. OAT1-3 and OCT2 are not expressed in other nephron segments in adult humans[56,57]. OAT-mediated transport is driven by an α-ketoglutarate gradient generated by Na^+/K^+-ATPase and sodium dicarboxylate cotransporters (NaDCs) (*SLC13A3*), while OCT2 transport is electrogenic[58,59]. Multiple studies, including mouse knockout models and *in vitro* transfection models, have demonstrated that OAT1-3 and OCT2 increase sensitivity to known nephrotoxic drugs such as nucleoside analogue antivirals and cisplatin[60–64]. In addition to OCT2, copper transporter 1 (CTR1, *SLC31A1*), which is also expressed on the basolateral surface of the proximal tubule in mice, is also involved in cisplatin uptake and contributes to its toxicity[65]. Similarly, the megalin/cubilin endocytotic receptor complex expressed on the apical surface of proximal tubule cells and in podocytes also increases sensitivity to aminoglycoside, polymyxin, and glycopeptide antibiotics as these drugs bind to the receptor and are endocytosed[66,67].

Efflux transporters found in the proximal tubule include the ATP-binding cassette transporters breast cancer resistance protein (BCRP), multidrug resistance proteins (MRPs), and P-glycoprotein (P-gp), as well as the multidrug and toxin extrusion H^+ exchangers (MATEs). Most of these are expressed at the mRNA level prior to nephron formation in the developing mouse kidney (expression profiling is included in the GUDMAP database and can be searched by gene symbol using www.gudmap.org)[68,69]. If this holds true in developing human kidneys, expression of these markers does not necessarily show functional maturity of an *in vitro* model and should be interpreted with caution. Indeed, the HK-2 cell line expresses

P-gp and demonstrates efflux function under conditions where its influx transporter expression and function is close to zero[70]. Within the adult human nephron these markers are only expressed on the apical surface of the proximal tubule[71–73]. As these transporters export substances from the cell, their overexpression or upregulation attenuates toxicity of their substrates. Different affinities for these transporters could distinguish nephrotoxic drugs from less nephrotoxic derivatives[39,74,75]

Other characteristic proximal tubule transporters include sodium/glucose cotransporter 2 (SGLT2; *SLC5A2*) and aquaporin 1 (*AQP1*). SGLT2 is a target for a new class of drug for type 2 diabetes mellitus (SGLT2 inhibitors), but concerns exist that these agents might cause acute kidney injury in some patients[76,77], possibly due to increased intratubular oxidative stress, uricosuria (with or without crystal formation), or an as-yet unidentified indirect mechanism[76,77]. Further insights into the underlying mechanism of SGLT2 inhibitor nephrotoxicity could be provided using an *in vitro* model of the renal proximal tubule that expresses SGLT2[78].

In addition to transcellular active transport via transporter proteins, ATP-independent paracellular transport also occurs in the proximal tubule. The proximal tubule epithelium has a leaky barrier, characterised by a transepithelial electrical resistance (TEER) of merely 5-7 $\Omega*cm^2$, , compared to isolated renal distal tubular cells which form a less leaky monolayer and have a TEER of 630 $\Omega*cm^2$ [79,80]. Ions like sodium, chloride, potassium and, to a lesser extent, compounds such as water are reabsorbed via passive diffusion and osmosis through paracellular tight junctions to the interstitial space. . The tight junctions consist of a variety of proteins —including claudin-2, -10a, -11 and -17, occludin, and tricellulin — that form ion-selective channels, with a pore size of ~4 Å in radius[79,81]. Functional analysis has shown that claudin-2 channels facilitate cation diffusion (e.g. Na^+, K^+, Ca^{2+} and H_2O) whereas claudin-10a and possibly -17 are involved in anion diffusion. Claudin-2 expression is regulated by immune factors (e.g. IL-2, TNF-a, IL-13, IL-15, IL17) and growth factor signaling pathways (e.g. EGF, HGF, ERK1/2 and Akt pathways)[82]. Under pathophysiological conditions such as cisplatin-induced nephrotoxicity, ischemic injury or metabolic acidosis, claudin-2 expression is reduced, resulting in impaired paracellular transport of cations which may contribute to disruption of the proximal tubule epithelium [83,84]. Tight junction injury can be visualised *in vitro* by immunofluorescence or leakage of labelled inulin.

The proximal tubule also expresses a range of biotransformation enzymes such as gamma-glutamyltransferase (GGT) on the brush border, as well as cytochromes P450 (CYPs), glutathione-*S*-transferases (GSTs), flavin-containing monooxygenase, and UDP-glucuronosyltransferases (UGTs) in the cytoplasm[36,85,86]. These renal enzymes, especially CYP3A4 and -5 and UGT1A9 and -2B7, might facilitate drug detoxification and efflux[39,86,87]. This would lead to drug-drug interactions, as substrates that inhibit these enzymes could cause other drugs to accumulate in proximal tubule cells and exacerbate nephrotoxicity[88]. Various studies have demonstrated that these enzymes can also bioactivate xenobiotics, potentially exacerbating their nephrotoxic effects instead[89–91]. However, the degree to which renal biotransformation contributes to the nephrotoxic effects of pharmaceutical compounds *in vivo* is not yet clear. GGT activity in proximal tubule models has been measured using a colorimetric assay or with commercially-available kits, though a difficulty in normalising the assay readout to total protein content has been reported[92–94]. Acivicin, a GGT inhibitor, can be used to demonstrate the specificity of a chosen GGT assay[95].

The glomerulus, loop of Henle, distal tubule, and collecting duct also express transporters and receptors unique to those segments. Although some of these transporters have been linked to drug nephrotoxicity, less is known about the contributions of these transporters to nephrotoxicity than those of the proximal tubule. In principal cells of the collecting duct, lithium is absorbed via the epithelial sodium channel (ENaC), inducing downregulation of AQP2 expression, which leads to diabetes insipidus and with chronic exposure can lead to remodelling of the collecting duct characterised by loss of principal cells and an increase in the number of intercalated cells [96–98]. Distinct transporters are also responsible for the side effects of some drugs even without overt renal cell injury; for example, Mg^{2+} and Na^{+} loss following cyclosporine treatment is due to downregulation of transient receptor potential subfamily metastatin 6 (TRPM6) and Na^{+}-Cl^{-} cotransporter (NCC) in the distal tubule[99].

In summary, the sensitivity of the kidney to nephrotoxicants is mediated by a multitude of unique functional proteins that are present in distinct epithelial components of the tubule. Modelling nephrotoxicity *in vitro* therefore requires characterisation of the functional identity of the cells under study, regardless of the cell source used. Such characterisation requires substantially more than evaluation of gene expression and should also include characterisation of protein localisation and function.

Table 1.1 Substrates and inhibitors used to functionally characterise renal transporters, receptors and ion channels *in vitro.*

Nephron segment	Protein	Gene symbol	Labelled Substrate (µM)	Inhibitors (µM)	References
Glomerulus	TRPC6	*TRPC6*	Fura-2-AM (10)	2-aminoethoxydiphenyl borate (100)	Sonneveld et al. Am J Pathol, 2014[100] Ambrus et al., J Cell Mol Med, 2015[101]
	Megalin	*LRP2*	FITC-human serum albumin (*Km* 4.5 mg/ml)	Equimolars of Transferrin or IgG	Eyre, Am J Physiol Ren Physiol, 2007[102]
Proximal tubule	OAT1	*SLC22A6*	Fluorescein (*Km* 0.8 ± 0.1)	Para-aminohippuric acid (IC_{50} 18 ± 4) Probenecid (IC_{50} 12.7 ± 5) Kynurenic acid (IC_{50} 6 ± 1)	Nieskens et al. AAPS J, 2016[62] Jansen et al. Sci Rep, 2016[103]
	OAT3	*SLC22A8*	Fluorescein (*Km* 3.7 ± 0.5)	Estrone Sulfate (IC_{50} 2.1 ± 0.3) Probenecid (IC_{50} 1.9 ± 0.6) Kynurenic acid (IC_{50} 6 ± 1)	Nieskens et al. AAPS J, 2016[62] Jansen et al. Sci Rep, 2016[103]
	OCT2	*SLC22A2*	ASP^+ (*Km* 36.4±6.8)	TPA (IC_{50} 16 ± 2) Metformin (IC_{50} 3.9 ± 1.2) Cimetidine (IC_{50} 8 ± 2) Verapamil (IC_{50} 10 ± 2)	Kido et al. J Med Chem, 2011[104] Schophuizen et al. Pflug Arch, 2013[105]
	BCRP	*ABCG2*	Hoechst 33342 (1.25) Fluorescein (1)	KO143 (IC_{50} 4.4 ± 0.9) MK571 (IC_{50} 5.1 ± 0.9) PSC833 (IC_{50} 1.3 ± 0.3)	Caetano-Pinto et al., Mol Pharmaceutics, 2016[106] Jansen et al. Sci Rep, 2016[103]

Nephron segment	Protein	Gene symbol	Labelled Substrate (µM)	Inhibitors (µM)	References
	MRPs	*ABCC2* *ABCC4*	CMFDA (1.25) Fluorescein (1)	KO143 (IC_{50} 2.7 ± 0.2) MK571 (IC_{50} 6.4 ± 1.3) PSC833 (IC_{50} 1.0 ± 0.2)	Caetano-Pinto et al., Mol Pharmaceutics, 2016[106] Jansen et al. Sci Rep, 2016[103]
	P-gp	*ABCB1*	Calcein-AM (1)	KO143 (IC_{50} 2.5 ± 0.5) MK571 (IC_{50} 10.2 ± 3.1) PSC833 (IC_{50} 0.7 ± 0.5) Zosuquidar (0.07)[a]	Caetano-Pinto et al., Mol Pharmaceutics, 2016[106] Shaik et al., Drug Metab Disp, 2007[107]
	MATE-2K	*SLC47A2*	n.d.	Pyrimethamine[b]	Kusuhara et al., Clin Pharmacol Ther, 2011[108] Ito et al, Clin Pharmacol Ther, 2012[109]
	Megalin	*LRP2*	FITC- bovine serum albumin (*Km* 126 µg/ml) RAP-GST (2.5 µg/ml) rhodamine-dextran (5 µM) Alexa488-dextran (10 µg/ml)	RAP (IC_{50} 0.02)[c]	Wilmer et al., Cell Tissue Res, 2010[110] Zhai et al., Kidney Int, 2000[111] Caetano-Pinto et al., Mol Pharmaceutics, 2016[106] Freedman, Nat Commun, 2015[112] Takasato, Nature, 2015[113]
Distal tubule	NCC	*SLC12A3*	$^{22}Na^{+}$ (2 µCi/ml)	Hydrochlorothiazide (100) Spironolactone (100) Metolazone (0.3 ± 0.001)	Markadieu et al., Am J Physiol Ren Physiol, 2012[80] Moreno et al., J Biol Chem, 2006[114]
	TRPV5	*TRPV5*	Fluo-4 (2 µM)	Ruthenium red (10 µM)	Andrukhova *et al.* EMBO J, 2014[115]

Nephron segment	Protein	Gene symbol	Labelled Substrate (µM)	Inhibitors (µM)	References
Collecting duct	ENaC	*SCNN1A*	Lithium (10mM, unlabeled)	Amiloride (10 µM)	Kortenoeven, Kidney Int, 2009[96]

[a] IC_{50} abacavir inhibition. Zosuquidar 1 µM is a potent inhibitor of P-gp mediated calcein efflux (Unpublished data). [b]Inhibits efflux of N-methylnicotinamide and metformin in low micromolar range. [c]concentration used in assay 1 µM[110]

1.3.3.2 Readouts of injury

Most *in vitro* models of nephrotoxicity rely on general cytotoxicity measures such as cell death, cytoskeletal defects, mitochondrial function, lactate production, or ATP content as a measure of injury. The assumption is that in a relatively homogenous population of renal cells, any compound that is cytotoxic to these cells is nephrotoxic. This assumption fails, however, when using a model that has more than one cell type by design. In addition, these cytotoxicity responses might only reflect advanced stages of injury elicited by high doses of the drug, and therefore might fail to detect subtle injury that could still lead to acute or chronic kidney injury *in vivo*.

The past decade has witnessed a push to identify biomarkers of renal injury with improved specificity and sensitivity over the current standards of serum creatinine (SCr) and blood urea nitrogen (BUN)[116]. The fact that many of these biomarkers are proteins that are upregulated in response to injury led to the assumption that their *in vitro* expression could be used as a readout of the nephrotoxic potential of a given drug. However, not all biomarkers with potential utility *in vivo* are reliable indicators of nephrotoxicitiy *in vitro*.

Kidney injury molecule 1 (KIM-1), also known as hepatitis A virus cellular receptor 1 (encoded by *HAVCR1*), is a type I membrane glycoprotein that is expressed in the liver, in activated immune cells, and in proximal tubules following injury[117,118]. Following acute kidney injury, KIM-1 is expressed on the apical surface of proximal tubule cells where it acts as a phagocytic receptor, enabling the removal of apoptotic cell debris by surviving cells[119]. The KIM-1 ectodomain is shed into the urine following metalloprotease cleavage, enabling it to be used as a biomarker of kidney injury [117]. The demonstration that urinary KIM-1 concentration is a more sensitive and specific readout of *in vivo* kidney injury in rats and humans than SCr and BUN led to FDA (Food and Drug Administration) and EMA (European Medicines Agency) approval of KIM-1 as one of seven biomarkers to be used in addition to SCr and BUN for monitoring drug-induced nephrotoxicity in pre-clinical trials [120–123]. However, KIM-1 has not performed as well in *in vitro* models, with a number of studies of primary proximal tubule cells or cell lines being unable to consistently detect significant differences in KIM-1 expression between controls and cultures exposed to nephrotoxicants[124–127]. These inconsistent findings might suggest that additional cell types are required within the organ for KIM-1 expression to be induced or that deficits exist in the *in vitro* cell models with respect to their cellular identity and/or response to injury.

Heme oxygenase 1 (HO-1, encoded by *HMOX1*) is a 32 kDa enzyme that is induced in response to oxidative stress[128]. Within the kidney, HO-1 is expressed following injury to the proximal tubules, glomeruli, or interstitial cells, and is upregulated in renal mononuclear phagocytes in response toinjury [129]. One study showed that levels of plasma and urinary HO-1 are significantly higher in rats and humans with acute kidney injury compared to levels in healthy controls, although sample sizes used in that study were smaller than those of studies that have validated the specificity of other novel biomarkers, such as the 2008 and 2010 studies validating the performance of KIM-1[121,122,130]. A study that performed transcriptional profiling of an *in vitro* primary proximal tubule cell model exposed to nephrotoxins showed that *HMOX1* was the marker that correlated positively with dose for the largest number of nephrotoxic compounds tested[131]. HO-1 expression also showed greater specificity and sensitivity for distinguishing between nephrotoxic and non-nephrotoxic compounds than the cell viability measures of cell death and ATP levels. Moreover, upregulation of HO-1 expression was detectable by immunofluorescence in a kidney-on-a-chip model following exposure to cadmium chloride, whereas KIM-1 expression was not detectable before exposure and only marginally increased after exposure, suggesting that the HO-1 response to this nephrotoxic metal is more robust than that of KIM-1 *in vitro*[131].

Interleukin-6 (IL-6) is a multifunctional cytokine that is expressed by macrophages, endothelial cells, and fibroblasts, whereas interleukin-8 (IL-8) attracts neutrophils and is expressed by a number of immune cells as well as by endothelial and epithelial cells[132]. In the kidney, tubular epithelial cells and podocytes produce these interleukins as part of an inflammatory response following most types of injury, including ischaemia–reperfusion injury and pyelonephritis[133–136]. The potential utility of IL-6 and IL-8 as *in vivo* biomarkers of acute kidney injury is unclear, but a pilot study that assessed the effects of gentamicin and cadmium chloride on primary proximal tubule cells from two different donors showed greater upregulation of IL-6 and IL-8 than KIM-1 levels in response to the compounds[126]. Upregulation of IL-6 and IL-8 expression also occurs in conditionally immortalised proximal tubule cell lines in response to uremic toxins[137]. Together these findings suggest that IL-6 and IL-8 could be used as readouts of injury *in vitro*.

Neutrophil gelatinase-associated lipocalin (NGAL), also known as lipocalin 2 (encoded by *LCN2*), is expressed in maturing granulocytes and in various epithelial tissues including the stomach, lung, and kidney[138]. The healthy kidney filters serum NGAL through the glomerulus whereupon it is endocytosed by the proximal tubule[139]. Kidney injury leads to

upregulation of NGAL levels in the distal tubules and collecting ducts, and shedding of NGAL into the urine[140]. The utility of urinary NGAL as a clinical biomarker of acute kidney injury is, however, limited by the finding that inflammation affects NGAL levels [122,141–143]. NGAL is expressed at relatively high levels in proximal tubule cells *in vitro*, which may indicate the poor phenotype retention of proximal tubule cells when cultured using standard techniques, as NGAL is not upregulated in mouse or rat proximal tubules following injury *in vivo*[35,126,127]. NGAL might be useful as a marker of distal tubule and collecting duct injury *in vitro*, though this possibility has not been extensively investigated.

1.3.4 Preclinical screens for nephrotoxicity [12]

Preclinical testing of drug candidates using animal models is required to study safety and efficacy on a systems biology level before moving to clinical studies. However, animal pharmacokinetic profiles often differ considerably from those of humans; hence, animal models are often poor predictors of adverse drug effects of drug disposition in humans [144,145]. This mismatch between animal and human outcomes is largely due to the many differences in drug transporter and metabolising enzyme expressions between species[146]. For example, expression levels of Oct1 and -2 are comparable in the rodent kidney, whereas OCT2 predominates in the human kidney[147,148]. Similarly, renal expression of BCRP is much higher in male FVB mice and Wistar Hanover rats than in humans[72]. Other transporters, such as MATE2-K, have only been detected in humans[147]. Transporter expression and function can also differ between different non-human animal species. For example, renal expression of BCRP is lower in female Sprague-Dawley rats than in female C57BL/6J mice[149]. In the process of developing polymyxin analogues, a compound that was selected for further investigation on the basis of promising safety results in rats was subsequently found to be nephrotoxic in dogs[33]. Sex can also influence transporter expression and hence drug kinetics, which creates the potential for toxicity screen results to differ between sexes[150,151]. In rats, for example, sex differences have been observed in the expression of tubule transporters and tight junction proteins, including claudin-2, AQP1, NCC, and ENaC[152].

The differences in transporter expression between animals and humans, and between different non-human species, limit the utility of animal models for studying adverse drug effects. The development of more suitable and predictive *in vitro* models is therefore key to providing more reliable measures of the efficacy and safety of novel drug candidates in early stages of their development. In addition, the development of such *in vitro* models will greatly reduce

preclinical toxicity testing in animals. Of note, in the area of cardiotoxicity, the FDA is the process of validating induced pluripotent stem cell (iPSC)-derived human cardiomyocytes as a model in which to screen compounds for cardiac toxicity[153].

1.3.5 Available and developing in vitro nephrotoxicity models [12]

1.3.5.1 Primary and immortalised cell lines

In vitro models for nephrotoxicity screening commonly use primary human renal proximal tubule cells, usually acquired from cadaveric specimens and cultured in 2D. However, primary cells display large inter-donor variability, have limited expansion capacity, and are prone to dedifferentiation and loss of transporter expression[4,34,126,154]. To overcome difficulties in expanding primary proximal tubule cells, lines of immortalized or conditionally immortalized proximal tubule cells have been developed using oncogenes (e.g. E6/E7 or SV40T) or telomerase (e.g. TERT1)[94,110,155]. Although TERT1-immortalised renal proximal tubule cells can undergo at least 90 population doublings and possess several characteristics of proximal tubule cells, including microvilli, tight junctions, GGT activity, endocytic activity of aprotinin, and functional drug transporters, the functional characteristics of early and late passage cells have not been compared[94,156]. Conditionally immortalized proximal tubule cells exhibit tight junctions, endocytic activity, OCT2 and P-gp function, and UGT activity, but like all renal proximal tubule cells in 2D culture, these ciPTECs lose OAT1 and OAT3 expression unless the proteins are transduced[62,105,110,157].

The difficulty in maintaining transporter and metabolic function in primary cells and cell lines, and in reaching levels of transporter function comparable to those observed *in vivo* are likely to result from the use of static 2D culture formats. *In vitro* renal transport or toxicity assays often use primary proximal tubule cells or cell lines cultured in a monolayer on a permeable support system, such as a Transwell® insert, that is coated with an extracellular matrix[95,103,110,131]. The insert is placed in a well with media on top of the insert, immersing the cells, and at the bottom, where media can diffuse through the permeable support. Hence, cells with appropriate transporters can transport substances from one side to the other. The major advantages of this system are that it is simple and that transporter and barrier function can be assayed by analysing substrate content on the top and bottom of the Transwell® insert. However, the simplicity of this model also results in the loss of the environmental cues to which kidney tubules are normally exposed *in vivo*, such as fluid flow across the apical surface or signals from other adjacent cell types[41,154,158]. This deficiency has led to the

development of more complex 3D culture systems and systems in which more than one renal cell type can be investigated, although of note, Transwell® inserts are still commonly used as a base for kidney organoids and renal tissue arrays which are discussed later.

1.3.5.2 Kidneys-on-a-chip

We define kidneys-on-a-chip as renal cells that are seeded in a microfluidic device that allows flow of media across the cell surface(s) (Figure 1.5B)[154]. One of the first studies of this technology seeded primary human proximal tubule cells on 2D chips with apical and basolateral media compartments, and demonstrated that fluid flow across the apical surface stimulated P-gp expression and function, and induced the formation of tight junctions and columnar morphology [2]. Cells in fluidic culture were also better protected by cimetidine from cisplatin-induced apoptosis than were cells in static culture, although OCT2 function and expression were not directly assessed and injury marker expression was not determined by the researchers.

Although cells grown on 2D microfluidic chips demonstrate better proximal tubule cell function than cells grown in static cultures, 3D chip designs might more closely replicate the architecture of the proximal tubule and may offer further improvements (Figure 1.5C). Indeed, a bioprinting approach has been used to fabricate a 3D chip containing a convoluted tubule filled with a fugitive ink within a gelatin-fibrinogen matrix. After flushing the fugitive ink to create a hollow tubule within the matrix, this tubule was seeded with immortalised proximal tubule cells[159], which similar to the 2D chips, could then be perfused with media to provide fluid flow and administer test compounds to the apical surface of the cells. Epithelial cells cultured within these 3D models had higher expression of megalin and greater albumin uptake than cells cultured under static conditions and on 2D microfluidic chips, indicative of greater functional maturity. These bioprinted cells also showed evidence of tight junction damage following exposure to cyclosporine; however, the expression of injury markers was not assessed.

Although these 3D bioprinted chips are an improvement on static and 2D designs, further improvements are needed to develop ‘vascular’ networks that surround the tubule in order to gain access to the basolateral surface of the printed proximal tubule [159]. A 2014 study described the development of chips for modelling human vasculature, which contained a collagen matrix and two parallel 3D channels that could be perfused independently[160]. This system has since been used to culture primary human proximal tubule cells, seeding one

channel with the cells and using the second channel as a cell-free pseudo-vascular channel[95]. Proximal tubule cells cultured in this three-dimensional flow-directed microphysiological system demonstrated GGT activity and SGLT2-mediated transport of a fluorescent glucose analogue, indicating the presence of mature, functional proximal tubule cells. Perfusion of the OAT substrates para-aminohippurate or indoxyl sulfate through the pseudo-vascular channel was followed by their detection in the 'proximal tubule' effluent, suggesting transepithelial transport. Moreover, the amount of each substrate in the effluent relative to the inflow was decreased in the presence of probenecid, an OAT and MRP inhibitor, suggesting active transport of each substrate via OATs and/or MRPs, although the use of high concentrations of probenecid might have compromised cell metabolism[161]. Nevertheless, this study demonstrates that primary proximal tubule cells cultured in this chip design show characteristic functions of this cell type, and that the pseudo-vascular channel can be used to administer compounds to the basolateral surface of these cells, although nephrotoxic injury responses were not determined in this study.

Several chips with vascular channels have been designed and could also be used to model injury to the renal and extra-renal microvasculature. One microfluidic device, for example, seeded with human microvascular endothelial cells has been used for modelling haematologic diseases[162]. Activation of these endothelial cells with tumour necrosis factor (TNF) resulted in decreased flow and microchannel occlusion, whereas exposure of the cells to Shiga-like toxin 2 resulted in the formation of thrombi that occluded the microchannels, indicating that this design would be suitable for studying drug-induced thrombotic microangiopathy. More recently, a protocol has been developed for isolating human kidney peritubular microvascular endothelial cells (HKMECs) and culturing them in a microfluidic device[163]. These HKMECs had a markedly different transcriptional profile from that of human umbilical vein endothelial cells (HUVECs) cultured under the same conditions and showed lower angiogenic potential and increased responsiveness to flow, demonstrating that the kidney microvasculature has specific properties that might not be replicated in models that use other endothelial cell types or lack physiological features such as flow.

Modelling the interactions between renal tubular cells and the microvasculature during injury requires the use of chips with dedicated renal epithelial tubules, vasculature seeded with appropriate endothelial cells, and possibly pericytes incorporated into the extracellular matrix of the chip[164]. Advances in the past couple of years have led to the development of high-throughput platforms with vascularised micro-organs in a 96-well format, with the intent of

recreating tissues with multiple cell types for rapid screening of large drug libraries. So far, however, the micro-organs studied with these platforms have been restricted to simple architectures, such as tumour models, and renal models have not yet been produced with this design[165,166].

Most kidneys-on-a-chip systems to date have used primary proximal tubule cells; however, it should also be possible to seed chips with hPSC-derived proximal tubule cells or other tubular cells. Although no system has yet assessed multiple nephron cell types on a single chip, a 2017 study reported the development of a "glomerulus-on-a-chip", in which hPSC-derived podocytes were seeded on one side of a porous membrane and primary endothelial cells were seeded on the other[167]. The chip design also permitted cyclic stretching of the membrane to model the mechanical strain of blood pulsation in glomeruli *in vivo*. As no specific molecular biomarker of podocyte injury has been identified, the researchers used albumin leakage across the membrane as a readout of injury following adriamycin exposure. Although extensive characterisation of the hPSC-derived podocytes was not carried out, evidence for the differential retention of albumin and inulin across the chip membrane suggests the existence of barrier function.

Kidneys-on-a-chip have also been used in *in vitro* systems to model multi-organ toxicity and pharmacodynamics, whereby the kidney chip is functionally coupled (via the manual transfer of media) or physically coupled to *in vitro* models of other organ systems[168,169]. One 2017 study demonstrated that human proximal tubules on a chip showed increased KIM-1 production and cell death in response to aristolochic acid I when a hepatocyte-containing chip was coupled upstream, compared to when the proximal tubule chip was isolated, consistent with bioactivation of aristolochic acid I by hepatocytes[169]. This study provides proof-of-concept that a multi-organ *in vitro* model can assess the nephrotoxicity of a test compound and its metabolites. The benefits of multi-organ models and the challenges of designing them have been discussed elsewhere[168].

Kidneys-on-a-chip are advantageous as they afford precise control over the spatial arrangement of different cell types and the perfusion of test compounds, making them a potentially valuable tool for nephrotoxicity screening. Further improvements in the engineering and design of these chips to enable the study of multiple "tubules" in parallel will facilitate high-throughput screening[154]. However, additional characterisation of injury marker expression of renal cells cultured on chips is required to enable rapid assessment of injury.

1.3.5.3 Biofunctionalised hollow fibres

A 2015 study showed that conditionally immortalized proximal tubule epithelial cells could be seeded onto the exterior surface of hollow fibres coated with an extracellular matrix, creating biofunctionalised hollow fibres with a monolayer of cells (Figure 1.5E)[170]. The proximal tubule cells grown on these fibres demonstrated improved tight junction formation and OAT1 expression compared to that of the same cells cultured in 2D even in the absence of flow through the fibres, suggesting that the 3D culture itself improved the expression of these markers. The integrity of the tight junction and OAT1 function were confirmed using FITC-labelled inulin leakage and fluorescein uptake assays, respectively, demonstrating that both the basolateral and apical surfaces of the cells are accessible for testing compounds. Flow through the basolateral compartment is also possible. Exposure of these hollow fibres to uremic toxins increased IL-6 expression and induced leakage of FITC-labelled inulin, indicating disruption of the epithelial tight junctions[171]. It should be noted that the convex arrangement of tubular epithelial cells on the exterior of the hollow fibre is not reflective of their arrangement *in vivo*, which is a caveat that should be addressed in future designs.

1.3.5.4 Engineered renal tissue arrays

Tissue arrays are a form of multicellular 3D culture that have been used for *in vitro* hepatotoxicity screening and have now been adapted for the assessment of nephrotoxicity in renal tissue (Figure 1.5F)[93,172]. To generate these renal tissue arrays, a suspension of renal fibroblasts and HUVECs in a proprietary gel were bioprinted into Transwells® to create a 3D interstitial layer[93], after which a second suspension of primary human proximal tubule cells was bioprinted over the interstitial layer. This method produced a 3D tissue array consisting of a monolayer of proximal tubule cells with a thicker interstitial layer on their basolateral side. The proximal tubule cells in these arrays expressed polarised, functional P-gp, OAT1, OAT3, OCT2, and SGLT2 transporters and showed angiotensin-converting enzyme (ACE) and GGT activity. The arrays also had TEER values of 18.1 $\Omega*cm^2$, higher than those seen in proximal tubule cells *in vivo* but better than values typical of cells cultured in static 2D systems. The proximal tubule cells desquamated and proliferated in response to cisplatin, whereas cimetidine exhibited protective effects. Furthermore, the interstitial layer showed a fibrotic response to TGF-β. To our knowledge, this is one of the first proof-of-concept models of renal fibrosis *in vitro*.

Renal tissue arrays allow the co-culture of multiple renal cell types and enable investigation of injury to different cell types, with control over the spatial arrangement of cell types and media access to the basolateral and apical surfaces of proximal tubule cells. Current designs involve bioprinting of cells into 24-well Transwell® plates, which enable moderate-throughput toxicity screens. However, rapid readouts of proximal tubule injury will be required to increase throughput, and so further characterisation of injury markers is needed. Improved tissue array designs that permit laminar flow (possibly requiring microfabrication similar to that used for kidneys-on-a-chip) might further improve the functional maturity of the proximal tubule cells cultured in these tissue arrays[93].

1.3.5.5 Pluripotent stem cell (PSC)-derived renal cells and organoids

Most of the improved culture models described in the previous sections have been shown to improve the functional maturity of primary renal epithelial cells, suggesting that they may be able to model nephrotoxicity more accurately than what was previously achievable. However, these improved models do not resolve the issue of primary cell supply or inter-donor variation, and aside from the development of a PSC-derived "glomerulus-on-a-chip" and engineered tissue arrays containing fibroblasts and endothelial cells, these models have typically been restricted to proximal tubular cells. While the proximal tubule is indeed the major target of drug-induced nephrotoxicity, interactions with other cell types may improve the functional maturity of proximal tubule cells *in vitro* and hence the fidelity of the model [173,174].

Pluripotent stem cells (PSCs) are cells which can be differentiated into any somatic cell type. For many species including mouse and human, PSCs can be derived from the inner cell mass of a developing embryo (embryonic stem cells, ESCs) or by "reprogramming" adult somatic cells into a pluripotent state through induced overexpression of the transcription factors OCT4, SOX2, c-MYC, and KLF4, creating induced pluripotent stem cells (iPSCs) [175]. In humans the use of iPSCs sidesteps the ethical issues associated with deriving human ESCs. Depending on the specific reprogramming protocol, other transcription factors such as LIN28 may also be overexpressed, though the basic principle is the same [176]. Transient overexpression of reprogramming factors is sufficient to produce iPSC lines which can be propagated *in vitro*, so overexpression can be stopped by excising the reprogramming transgenes [177–179] or by using non-integrating vectors [176] to minimise potential side effects. In recent years, protocols have been developed to generate kidney tissue from PSCs which

contain patterning and segmenting nephrons and transcriptionally match Trimester 1 human kidney. As these represent complex 3D models of kidney tissue, these may represent improved models of the proximal tubules and hence provide a more predictive screening tool that is applicable to all nephron cell types.

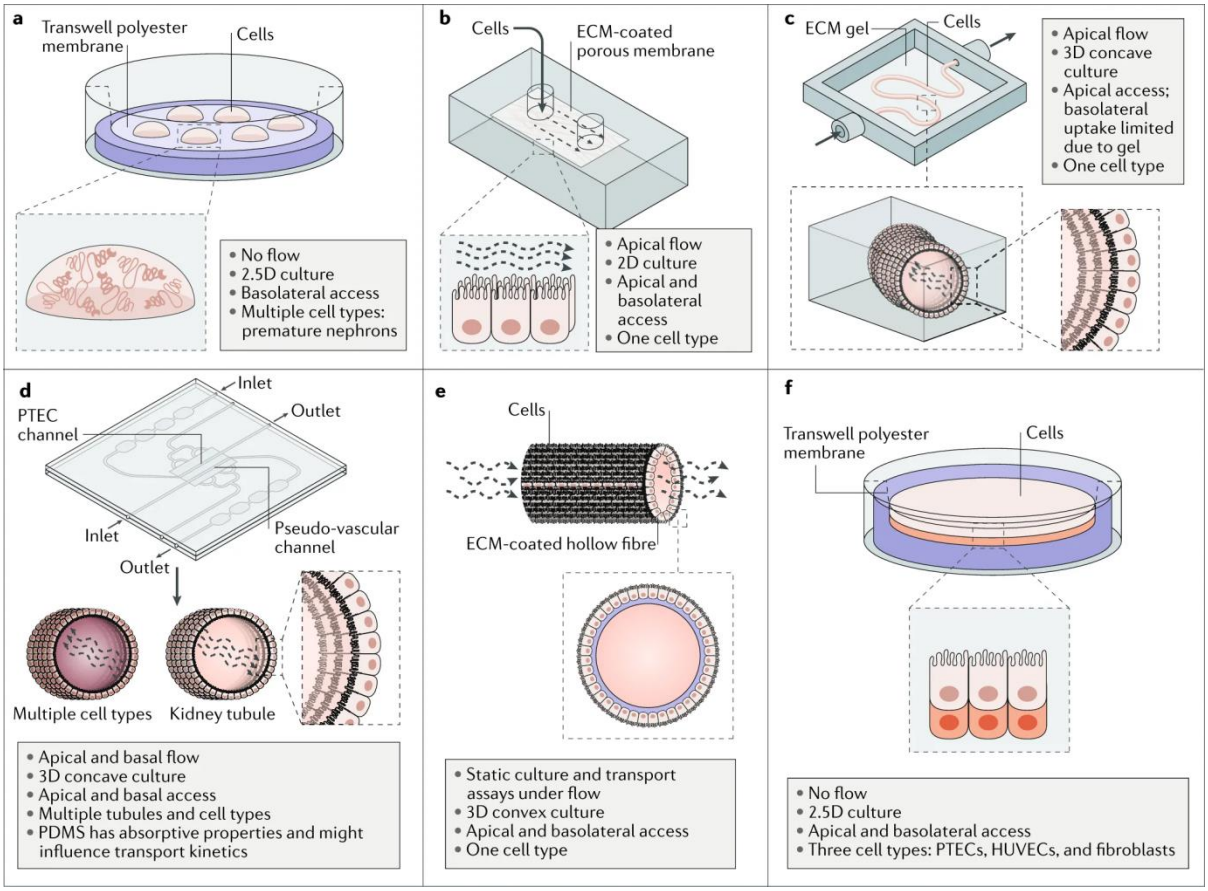

Figure 1.5 Novel culture platforms for modelling nephrotoxicity *in vitro*. [12]. A: Kidney-on-a-chip allowing flow across a cell monolayer. B: Engineered renal tissue array consisting of proximal tubule cells, HUVECs, and fibroblasts, arranged on a transwell. C: Organoids consisting of multiple immature nephrons and interstitial cells. D: Kidney-on-a-chip with parallel 3D channels to model vasculature and tubules. E: Kidney-on-a-chip consisting of a perfusable convoluted 3D tubule within an extracellular matrix. F: Biofunctionalised hollow fibre seeded with proximal tubule cells on the external surface.

1.4 Derivation of kidney tissues from pluripotent stem cells

While some protocols for differentiating human PSCs to renal cells claim to produce pure populations of specific cell types such as podocytes or proximal tubule cells in a 2D culture format for ease of use, markers of other nephron segments are often detected, suggesting that these protocols generate mixed populations of cells or that the individual cells have not been differentiated to a mature proximal tubule phenotype [180–184]. With an increased understanding

of kidney development and how cells are differentiated to generate the kidney *in vivo*, five seminal protocols have been developed for generating three-dimensional, self-organising kidney tissues from PSCs, which possess distinct nephron segments as well as endothelial and stromal cells (Figure 1.6) [112,113,185–187]. Adaptations of these protocols have also been made for generating kidney organoids in suspension culture, facilitating large scale expansion of organoids in bioreactors [188,189]. These protocols vary in the culture format, the growth factors and small molecules used, and the timing of growth factor addition, but generally start by differentiating PSCs to posterior primitive streak. This typically involves some combination of bone morphogenetic protein (BMP) signalling with recombinant BMP4, low concentrations of activin A, and/or canonical Wnt signalling using recombinant Wnt or small molecule activators such as CHIR99021 (CHIR) [18,186,190,191].

The next step is to induce intermediate mesoderm (Figure 1.6). As previously discussed, the ureteric epithelium arises from the anterior intermediate mesoderm, while the nephron progenitors arise from the posterior intermediate mesoderm. The Takasato protocol published by our group claims to simultaneously induce both anterior and posterior intermediate mesoderm with a phase of Wnt activation followed by a switch to fibroblast growth factor (FGF) signalling, based on the postulation that posterior intermediate mesoderm cells *in vivo* are mesoderm cells which are exposed to Wnt signalling longer, while anterior intermediate mesoderm cells migrate away from the Wnt source as the embryo elongates [113]. In contrast, the Morizane protocol [187] aims to produce primarily posterior intermediate mesoderm and nephron progenitors using a period of activin A exposure after specifying primitive streak.

Following intermediate mesoderm induction, nephrons will spontaneously form in continued culture [112,186], but Wnt signalling can be used to trigger synchronised nephrogenesis [113,185,187]. After continued culture to allow nephrons to proliferate and mature, the kidney organoids contain segmented, contiguous nephrons with glomeruli, proximal tubules, and distal tubules, as well as endothelial and stromal cells [192]. Bulk RNA sequencing of Takasato organoids [113] and single-cell RNA sequencing of Takasato and Morizane organoids [193] show that the cell types in these organoids are transcriptionally similar to those in trimester 1 and 2 human foetal kidneys, opening up the possibility of using organoids as an *in vitro* model of the developing human kidney.

While organoid differentiation protocols were based on kidney development *in vivo* and produce recognisable renal cell types, they are not a perfect model of kidney development.

Off-target cell types such as melanoma-like cells, neuron-like cells, and muscle-like cells often develop alongside the renal cells [193–195]. Organoid nephrons do not merge into collecting ducts with a single exit point for urine, unlike nephrons in embryonic kidneys. Even in protocols like the Takasato protocol which produce a ureteric epithelium-like population, there are no ureteric tips to attract nephron progenitors, and the process of iterative branching and nephron formation is absent, limiting the number of nephrons which an organoid can have. The organoid endothelial network is not directly perfusable *in vitro*, and organoid glomeruli maintained *in vitro* generally remain avascular, so there is no fluid filtration in organoid nephrons.

Despite these limitations, since the first protocols for deriving kidney organoids from pluripotent stem cells were developed, these protocols have been used and modified for various applications ranging from modelling human kidney development *in vitro* to drug and toxicity screening, disease modelling, and tissue engineering for renal replacement therapy (Table 1.2). Of these applications, modelling development and tissue engineering are more challenging, as they rely on aspects of kidney development such as iterative nephrogenesis which are not replicated in organoids, though modified protocols have been designed to begin addressing these challenges [196]. Disease modelling of congenital kidney diseases has been a more immediately-accessible application, as the main requirement is that the affected renal cell types are present in organoids and functionally mature enough to express the gene with the disease-causing mutation and demonstrate the phenotype. So far, organoids differentiated from patient-derived iPSCs have been used to model ciliopathies [197], cystic kidney disease [198], and congenital nephrotic syndrome [199,200]. Based on this, it is likely that organoids can model some forms of drug-induced nephrotoxicity. While modelling toxicity from immune-mediated renal injury or haemodynamic or osmotic dysregulation is currently out of reach, it should be possible to model direct injury to specific renal cell types, especially injury to the proximal tubule, provided these cells express the transporters, receptors, and/or metabolic pathways which underpin their vulnerability to nephrotoxic drugs as previously discussed.

Table 1.2 Modifications to kidney organoid differentiation protocols (adapted from Little and Combes, in press [24]).

Culture format	Reference	Endpoint	Potential application or technical advance	Differentiation protocol adapted
Suspension culture	Cruz *et al*. 2017 [198]	Organoid derived tubular cyst	Disease modelling	Freedman *et al*. 2015
	Przepiorski *et al*. 2018 [189]	Organoids from embryoid bodies cultured in suspension	Scale-up of cells Toxicity screening Disease modelling	Takasato *et al*. 2015
	Kumar *et al*. 2019 [188]	Micro-organoids formed in suspension	Scale-up of cells Drug screening	Takasato *et al*. 2015
Bioprinting	Czerniecki *et al*. 2018 [201]	Differentiation in multiwell format after plating with liquid handling robot	Optimisation of differentiation High content screening	Freedman *et al*. 2015
	Higgins *et al*. 2018 [202]	Extrusion bioprinting of intermediate mesoderm to automate organoid production	Disease modelling Increased throughput Drug/toxicity screening Improved quality control	Takasato *et al*. 2015
New iPSC-derived structures	Taguchi *et al*. 2017 [196]	Combined culture of nephron progenitors and collecting duct to form more complex kidney *in vitro*	Improved developmental model Tissue replacement	New protocol
	Leuning *et al*. 2019 [203]	Revascularisation of human kidney scaffold with iPSC-derived endothelium	Tissue replacement	Orlova *et al*. 2014 [204]
Isolated features or cell types	Musah *et al*. 2017 [167]	Directed differentiation to podocytes	Toxicity screening Disease modelling	New protocol
	Yoshimura *et al*. 2019 [200]	Directed differentiation to podocytes	Drug/toxicity screening Disease modelling	Taguchi *et al*. 2014
	Taguchi *et al*. 2017 [196]	Optimisation of collecting duct differentiation	Improved developmental model Tissue replacement	New protocol
	Hale *et al*. 2018 [199]	Isolation of intact glomeruli from organoids	Drug/toxicity screening Disease modelling	Takasato *et al*. 2015
Changes in scaffolds for culture	Gupta *et al*. 2019 [205]	Scaffolding organoids on silk	Scale-up of structure	Morizane *et al*. 2015
	Garreta *et al*. 2019 [206]	Differentiation on hydrogels	Improved maturation	Takasato *et al*. 2015
Application of flow *in vitro*	Musah *et al*. 2017 [167]	Glomerulus on chip co-culture with endothelium	Drug/toxicity screening Disease modelling	New protocol
	Homan *et al*. 2019 [207]	Organoid culture within PDMS chamber with fluid flow	Improved developmental model Functional maturation	Morizane *et al*. 2015

Culture format	Reference	Endpoint	Potential application or technical advance	Differentiation protocol adapted
Transplantation for vascularisation	Garreta *et al*. 2019 [206]	Culture on chicken chorioallantoic membrane	Functional maturation Vascularisation	Takasato *et al*. 2015
	Sharmin *et al*. 2016 [208]	Renal subcapsular transplantation	Vascularisation	Taguchi *et al*. 2014
	Bantounas *et al*. 2018 [209]	Subcutaneous transplantation	Vascularisation	Takasato *et al*. 2015
	van den Berg *et al*. 2018 [210]	Renal subcapsular transplantation	Vascularisation Functional maturation	Takasato *et al*. 2015
	Tanigawa *et al*. 2018 [211]	Renal subcapsular transplantation	Disease modelling	Taguchi *et al*. 2014
	Gupta *et al*. 2019 [205]	Renal subcapsular transplantation	Vascularisation	Morizane *et al*. 2015

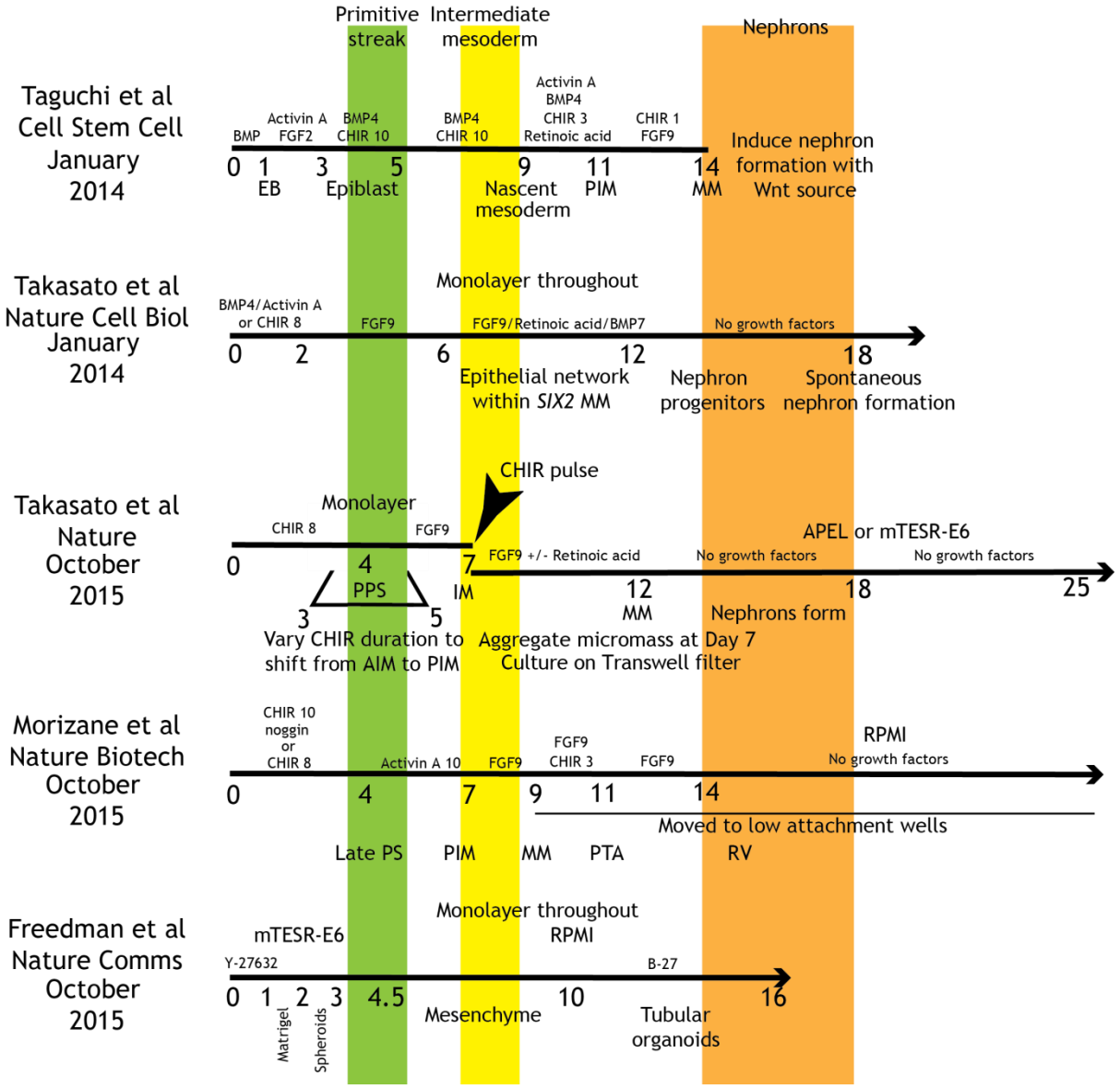

Figure 1.6 Comparison of protocols for directed differentiation of human pluripotent stem cells to kidney tissue, highlighting differentiation to primitive streak, intermediate mesoderm, and formation of nephrons in each protocol (adapted from Little and Combes, in press [24]).

Days are marked on each timeline, with the start of differentiation at day 0. APEL = APEL medium; CHIR = CHIR99021, small molecule Wnt agonist; mTeSR-E6 = E6 minimal differentiation medium. RPMI = Roswell Park Memorial Institute 1640 medium. Numbers after reagent abbreviations indicate concentration in μM. AIM = anterior intermediate mesoderm; EB = embryoid body; IM = intermediate mesoderm; MM = metanephric mesenchyme; PIM = posterior intermediate mesoderm; PS = primitive streak; PPS = posterior primitive streak; PTA = pretubular aggregate; RV = renal vesicle.

1.5 Characterisation and optimisation of kidney organoids as a nephrotoxicity screening platform

Preliminary evidence suggested that the proximal tubule cells in kidney organoids generated from the protocols listed above were capable of specific injury responses to known nephrotoxic drugs. The proximal tubule cells in Morizane organoids expressed *HAVCR1* (KIM-1) in response to cisplatin and gentamicin, although in the latter case apoptosis was also observed in cells which did not express proximal tubule markers [112,187]. Similarly, Takasato organoids had proximal tubules which were capable of endocytosing dextran and undergoing apoptosis after cisplatin exposure [113]. However, further characterisation of the functional maturity of organoid proximal tubules is required to determine if these injury responses occur via the same pathways as they do *in vivo*, and to determine if these responses are consistent across other culture formats, such as micro-organoids in suspension [188]. Hence, the first aim of this project was to characterise the maturity of nephrotoxicant-responsive proximal tubules within human iPSC-derived kidney organoids. Since most cell types in organoids are analogous to foetal human kidney, it was also possible that organoid proximal tubules were not sufficiently mature to accurately model drug-induced nephrotoxicity. Given that organoid protocols were originally designed based on kidney organogenesis *in vivo*, we also aimed to examine the maturation of the proximal tubule *in vivo* using bioinformatics to shed light on how proximal tubule maturation could be improved in organoids *in vitro*, and to develop tools and approaches for validating our findings *in vitro*.

While organoids maintained *in vitro* do not have vascularised glomeruli or fluid filtration, as previously discussed, transplanting organoids into immunocompromised mice induces vascularisation of the organoids and improves the functional maturity of their glomeruli (Table 1.2). This could also induce the maturation of the proximal tubules to a degree not seen *in vitro*, and create a "humanised" *in vivo* system which can filter substances through glomeruli and secrete or reabsorb drugs using the transporters and receptors expressed in humans, which differ from those expressed in mice. Such a system would have much lower throughput than *in vitro* screening, but might provide a useful adjunct to *in vitro* screening for characterising mechanisms of drug-induced injury.

1.6 Summary and research aims

There is an unmet need for predictive *in vitro* models of nephrotoxicity which can be used to study drug renal safety profiles during drug development. Advances have been made in

developing and characterising new *in vitro* models to meet this need, one of which is the development of PSC-derived kidney organoids. There is preliminary evidence showing that the proximal tubules within organoids are capable of specific injury responses when exposed to known nephrotoxic compounds. Further characterisation of organoid proximal tubules is required to demonstrate their suitability as a platform for nephrotoxicity screening, and to optimise them if their functional maturity is lacking.

The aims of this project were to:

i) Characterise the maturity of nephrotoxicant-responsive proximal tubules within human iPSC-derived kidney organoids

ii) Determine possible approaches for optimising proximal tubule maturity *in vitro* based on analysis of proximal tubule maturation *in vivo*

iii) Generate reporter iPSC lines to assist in characterising proximal tubule maturity and injury responses in kidney organoids

iv) Develop culture conditions to optimise proximal tubule maturity *in vitro*

v) Characterise the effect of xenotransplantation on proximal tubule maturity in organoids

2 BIOINFORMATICS ANALYSIS OF PROXIMAL TUBULE MATURATION *IN VIVO* TO UNDERSTAND REQUIREMENTS FOR MATURATION IN ORGANOIDS

2.1 Background

2.1.1 Renal cell types found in kidney organoids and their maturity

As previously described in Chapter 1, many protocols have been developed for differentiating human pluripotent stem cells to kidney organoids containing segmented nephrons. The two organoid protocols used in this project were the Takasato *et al*. protocol, in which organoids are cultured on an air-liquid interface on a permeable filter or Transwell®, and the Kumar *et al*. micro-organoid protocol, where micro-organoids are cultured in suspension under gentle swirling [188,212]. Takasato organoids typically contain at least a hundred nephrons, while Kumar micro-organoids contain six to ten nephrons each. The nephrons in both are segmented into glomeruli, proximal tubules, distal tubules, and connecting segments or ureteric epithelium, which can be identified by expression of cell type-specific markers [113,188]. (Note that while these markers are specific to certain cell types within the kidney, these proteins can be found in other tissue types.) Both organoids and micro-organoids contain stromal and vascular populations, although micro-organoids have a smaller proportion of stroma [113,188]. RNA sequencing of whole kidney organoids showed that they were transcriptionally similar to trimester 1 human kidney, and micro-organoids were similar to Transwell® organoids [113,188].

While kidney organoids are not anatomically or developmentally equivalent to human adult kidneys, they can still be useful *in vitro* models of certain cellular processes, provided the cell type of interest is sufficiently mature to carry out the process being studied. Proof-of-concept studies have demonstrated that organoids can model congenital nephrotic syndrome, which are caused by structural defects in the glomeruli [199,200] as well as cystic kidney disease [198] and ciliopathies [197], as demonstrated using organoids differentiated from patient-derived iPSCs. Glomeruli isolated from organoids also showed dose-dependent injury responses to doxorubicin, which is specifically toxic to podocytes [199]. However, it is not yet clear if organoid proximal tubules are sufficiently mature to model proximal tubule-specific drug-induced injury. Organoid proximal tubules were capable of endocytosing dextran and albumin, showing that their endocytotic pathways typically develop to a functional level, and

some groups (including our own) have claimed that treating organoids with cisplatin and gentamicin induced proximal tubule-specific cell death at low doses [113,187,188].

In Chapter 1 we discussed in detail mechanisms of drug-induced injury to different segments of the nephron, and the *in vitro* models of nephrotoxicity which have been studied to date [12]. The proximal tubule is vulnerable to drug injury primarily because of its expression of unique transporter proteins and the reliance of proximal tubule cells on mitochondrial oxidative phosphorylation to meet the cells' high energy demand. The transporters provide a route of entry for drugs which have an affinity for those transporters, allowing the drugs to reach toxic intracellular concentrations, while the high energy demand makes proximal tubule cells sensitive to mitochondrial damage. Hence, to accurately model drug-induced nephrotoxicity *in vitro*, the proximal tubule cells in the model must express functional transporters and should have the appropriate metabolic phenotype. However, as discussed in Chapter 1, 2D culture models using primary proximal tubule cells or cell lines either do not have sufficient transporter function or show dedifferentiation and injury responses under normal conditions, impairing their ability to predict the nephrotoxic potential of a drug.

Therefore, the aims of this chapter are:

i) to understand what level of maturity exists within the proximal nephrons of kidney organoids, based on their expression of key markers, and

ii) to compare this to the transcriptional changes occur during proximal tubule development and maturation in both mouse and human kidney development *in vivo.*

This information may assist in identifying approaches that might be used to improve proximal tubule maturation *in vitro*.

For the purposes of this analysis, the markers used to define developing and mature proximal tubule cells included the transcription factor *HNF4A*, which regulates the expression of multiple genes expressed in the proximal tubule [213], the SLC family transporters *SLC22A6* and *SLC22A2*, and the megalin-cubilin endocytotic complex (gene symbols *LRP2* and *CUBN* respectively).

2.1.2 scRNA-seq and snRNA-seq analyses of proximal tubules in vitro and in vivo

Single cell RNA sequencing (scRNA-seq) and single nucleus RNA sequencing (snRNA-seq) have become popular techniques for analysing cellular phenotypes within complex,

heterogeneous tissues such as the kidney [214]. The major advantage of these techniques is the ability to analyse single cell transcriptomes, which can reveal cell type-specific signatures that would be masked in bulk RNA sequencing of the tissue [215]. While there are many different commercial platforms and methodologies, the basic workflow is similar. First, single cells or single nuclei are isolated from a sample, captured, and lysed for reverse transcription of their RNA. Depending on the platform, the reverse transcription primers also include PCR adaptors for next-generation sequencing, cell barcodes to identify transcripts from a single cell, and/or unique molecular identifiers (UMIs) to identify single mRNA molecules. cDNA is then amplified by PCR, sequenced, and mapped to genes. The output, in brief, is a matrix of cells, genes, and the abundance or counts of each transcript within each cell, which can then be analysed with a wide variety of bioinformatics software packages.

Over the course of this project, multiple scRNA-seq and snRNA-seq datasets of human iPSC-derived organoids as well as mouse and human foetal and adult kidneys became available to us, either from within our group or from publications and collaborations [194,195,216,217] (Jason Spence, unpublished data). In most of these bioinformatics analyses, unsupervised algorithms (i.e. without user input to define "important" genes) had been used to group cells into clusters based on their transcription profile. The researchers had then identified the renal cell types each cluster represented based on their expression of known marker genes. Each cell type could then be studied to determine their similarities or differences with other cell types identified in the same dataset, or with cells of the same nominal type from other datasets.

For this project, these datasets were used to provide further evidence of functional maturity (or lack thereof) of proximal tubules in organoids. Proximal tubules from *in vivo* samples were also studied to determine which genes and pathways distinguished proximal tubules from other renal cell types, and to determine how active pathways changed across age in proximal tubules. We then discuss how these findings might inform optimisations to our organoid culture protocol to improve proximal tubule maturity.

2.2 Methods

For the initial analysis of proximal tubule maturity in organoids by qRT-PCR and immunofluorescence microscopy, organoids were differentiated from the C32 or 1502.3 iPS cell lines in APEL and micro-organoids were differentiated from the *HAVCR1*:mCherry iPS cell line in E6 (see Chapter 7 for details on standard cell culture and differentiation methods and cell lines used in this project). At D7+18 for the organoids and D7+19 for the micro-

organoids, samples were prepared for qRT-PCR and immunofluorescence as detailed in Chapter 7.

This chapter also describes the analysis of a number of datasets generated in this laboratory or in others. We describe here how this data was generated and analysed.

2.2.1 scRNA-seq and snRNA-seq sample preparation, library preparation, and sequencing

Samples were dissociated into single cells as described in their respective publications (Table 2.1A). For the adult human kidney dataset, nuclei were harvested instead of single cells [195]. Samples for single datasets were run in parallel on a Chromium 10x Single Cell Chip (10x Genomics) and cDNA libraries for each cell were prepared using a Chromium Single Cell Library Kit (10x Genomics). Libraries were then sequenced on a next-generation sequencing platform of the researchers' choice.

2.2.2 scRNA-seq and snRNA-seq quality control and analysis

Quality control and targeted re-analysis of each dataset was performed using the Seurat R package (v2.3.4 for organoid and mouse datasets, v3.0.0 for human foetal and adult kidney datasets) [218]. The number of UMIs (unique molecular identifiers) and the number of unique genes detected per cell can be used as a rough indicator of cell quality; stressed cells or empty cell captures will have very few UMIs or genes, while cell doublets or multiplets will have abnormally high numbers of UMIs and genes [219]. Hence, prior to analysis, cells with fewer than 500 unique genes or more than 125,000 UMIs were filtered. The number of cells, average number of UMIs and unique genes per cell in each filtered dataset is listed in Table 2.1 as an approximate measure of sequencing depth.

The general workflow for analysis of proximal tubule cells in these datasets began with unsupervised clustering of cells based on their transcriptional profiles using Seurat, and then identifying clusters containing proximal tubule cells. Identification was either based on expression of *HNF4A* and other markers we selected, or simply based on the cluster identities given by the authors of the original analyses. We then used Seurat to look for genes which were differentially expressed between clusters of interest. For comparing cells between two datasets, integrated analyses must be performed for cells to cluster by their biological types instead of by dataset-specific differences. Where possible, we integrated entire datasets using Seurat prior to clustering and identification of proximal tubule cells in the combined dataset. This was less successful when comparing datasets with very different populations of cells, as

when comparing foetal and adult kidney datasets. In these cases, we identified proximal tubule cells in each dataset and then integrated only the proximal tubule cells.

Table 2.1: scRNA-seq and snRNA-seq datasets analysed in this project.

Sample type	**Number of samples**	**Number of cells**	**nUMI / cell (average)**	**nGene / cell (average)**	**Additional notes**	**Citation (if published)**
D7+18 organoids (CRL1502-C32)	3	7004	10494	2930	-	Phipson *et al.*[194]
D7+18 organoids (CRL2429-derived *MAFB*:mTagBFP2 / *GATA3*:mCherry dual reporter) in E6 medium	3	3513	16559	3790	Integrated analysis with organoids in E6 + RA medium where noted	Unpublished
D7+18 organoids (CRL2429-derived *MAFB*:mTagBFP2 / *GATA3*:mCherry dual reporter) in E6 + RA medium	3	1668	15100	3697	Integrated analysis with organoids in E6 medium where noted	Unpublished
E18.5 embryonic mouse kidneys (C57Bl/6)	6 (3 pairs)	5639	9171	3128	-	Combes *et al.*[216]
4-8 week adult mouse kidneys (C57Bl/6 wild-type and lineage-tagged)	7 (single kidneys, 4 wild-type, 3 lineage-tagged)	21773	2875	1143	-	Park *et al.*[217]
96d foetal human kidney	1	5674	11639	3291	Integrated analysis with 108d foetal human kidney where noted	Jason Spence, unpublished data

Sample type	Number of samples	Number of cells	nUMI / cell (average)	nGene / cell (average)	Additional notes	Citation (if published)
108d foetal human kidney	1	6181	13394	3653	Integrated analysis with 96d foetal human kidney where noted	Jason Spence, unpublished data
62y adult human kidney	1 (2 technical replicates)	4524	3934	1802	snRNA-seq instead of scRNA-seq	Wu *et al.*[195]

2.3 Proximal tubules in organoids cultured *in vitro* express some proximal tubule markers but not others

For the initial analysis of proximal tubule maturity, D7+18 whole organoids cultured in APEL on Transwell® inserts according to the method of Takasato *et al.* [212] and D7+19 whole swirler micro-organoids cultured in E6 according to the method of Kumar *et al.* [188] were analysed by qRT-PCR to compare their expression of *SLC22A6*, *SLC22A2*, and *CUBN* to RPTECs and human foetal kidney (HFK) (n = 2).

SLC22A6 and *CUBN* expression in RPTECs was lower than in HFK, suggesting that RPTECs in 2D culture had lost expression of these functional markers, consistent with previous observations [41]. Organoids had higher expression of *CUBN* and *SLC22A6* than RPTECs, with a more marked difference for *CUBN*, but lower expression of *SLC22A2*, while swirlers had slightly higher *CUBN* expression than RPTECs and lower *SLC22A6* and *SLC22A2* expression (Figure 2.1A). This may suggest that the proximal tubules within swirler organoids are less mature. Both organoids and swirlers had lower expression of these genes than HFK. This suggests that while organoids have a transcriptomic profile similar to trimester 1 human kidney, they lack expression of key genes and therefore it is likely that their proximal tubules are not functionally equivalent.

As whole organoids and whole swirlers were used for this analysis, it was possible that lower expression of proximal tubule markers in organoids and swirlers compared to HFK was

because of differences in the proportion of proximal tubule cells, rather than differences in proximal tubule maturity. To determine if this was the case, D7+19 organoids differentiated from the 1502.3 cell line were dissociated and stained with antibodies against EPCAM and CD13 (alanyl aminopeptidase, gene symbol *ANPEP*) to sort proximal tubule cells by FACS. EPCAM marks all tubular epithelial cells in the kidney organoid, while CD13 within the developing kidney is a cell surface marker which is restricted to the proximal tubule [195,220]. qRT-PCR analysis was then performed on the double negative, EPCAM$^+$, and EPCAM$^+$ CD13$^+$ fractions. The EPCAM$^+$ CD13$^+$ fraction was enriched for expression of *SLC22A6*, *SLC22A2*, and *CUBN* over the EPCAM$^+$ and double negative fractions, as expected, and now had higher expression of *SLC22A6* and *CUBN* than RPTECs, suggesting that proximal tubule cells in organoids indeed had higher expression of these markers than RPTECs cultured in 2D (Figure 2.1B). However, *SLC22A6* and *SLC22A2* expression in the EPCAM$^+$ CD13$^+$ fraction was still lower than in HFK, showing that potential differences in the proportion of proximal tubule cells in organoids and in HFK cannot completely account for the lower expression of these markers in whole organoids.

Our group previously performed scRNA-seq of 3,513 cells from D7+18 *MAFB*:mTagBFP2/*GATA3*:mCherry whole organoids cultured in E6 and 1,668 cells from the same cell line cultured in E6 with retinoic acid (Sean Wilson *et al*., unpublished data). After these datasets were integrated, unsupervised clustering separated cells into 11 clusters (Figure 2.1C) [218]. The cell populations these clusters represented were identified in the previous analysis based on their expression of known cell type markers. The proximal tubule cluster showed significant, specific expression of *HNF4A*, *CUBN*, and *LRP2*, as expected, but there were few to no cells which expressed *SLC22A6*, *SLC22A8*, or *SLC22A2*. This was consistent with the qRT-PCR analysis performed for this project showing low expression of *SLC22A6* and *SLC22A2* in organoids compared to HFK.

It was also possible that *SLC22A6*, *SLC22A8*, and *SLC22A2* mRNA levels were not an accurate representation of protein expression. Other groups have observed poor correlation between mRNA levels of the SLC family genes in liver and kidney samples and protein expression as measured by liquid chromatography/tandem mass spectrometry [93,221]. We confirmed that cubilin (CUBN) and HNF4α were expressed at the protein level in LTL$^+$ proximal tubules in organoids (Figure 2.1D). Cubilin localised to the apical surface of proximal tubules and HNF4α to the nucleus of each cell, as expected. However, our attempts to detect SLC22A6 by immunofluorescence were inconclusive. SLC22A6 in mature kidneys

is specific to the proximal tubule and localises to the basolateral membrane. The apparent staining for SLC22A6 in D7+21 C32 organoids did not correspond to LTL^+ tubules or $ECAD^+$ LTL^- tubules. To determine if this was because SLC22A6 was absent in organoids or if this was because our immunofluorescence staining protocol was not optimised for this antibody, we fixed fresh-frozen adult human kidney sections (Zyagen) as a positive control and stained them with peanut agglutinin (PNA) and antibodies against cubilin, SLC22A6, and SLC22A2. As PNA stains the distal tubule [222], PNA staining and cubilin staining were mutually exclusive, and cubilin showed clear brush border staining, as expected (Figure 2.1D). However, anti-SLC22A6 and anti-SLC22A2 showed non-specific staining in both PNA^+ and $CUBN^+$ tubules and was not restricted to the basolateral surface of cells. Hence, this immunofluorescence staining protocol would not have been able to specifically detect SLC22A6 or SLC22A2 protein in organoids even if it had been present.

In summary, organoids cultured using our standard protocols expressed some functional markers, namely *CUBN* and *LRP2*, at the transcript and protein level, but transcript-level expression was not equivalent to human foetal kidney, and other key markers such as the SLC family transporters were only expressed at low levels based on mRNA, if at all. We concluded that further optimisation of organoid culture methods was required to improve proximal tubule maturity.

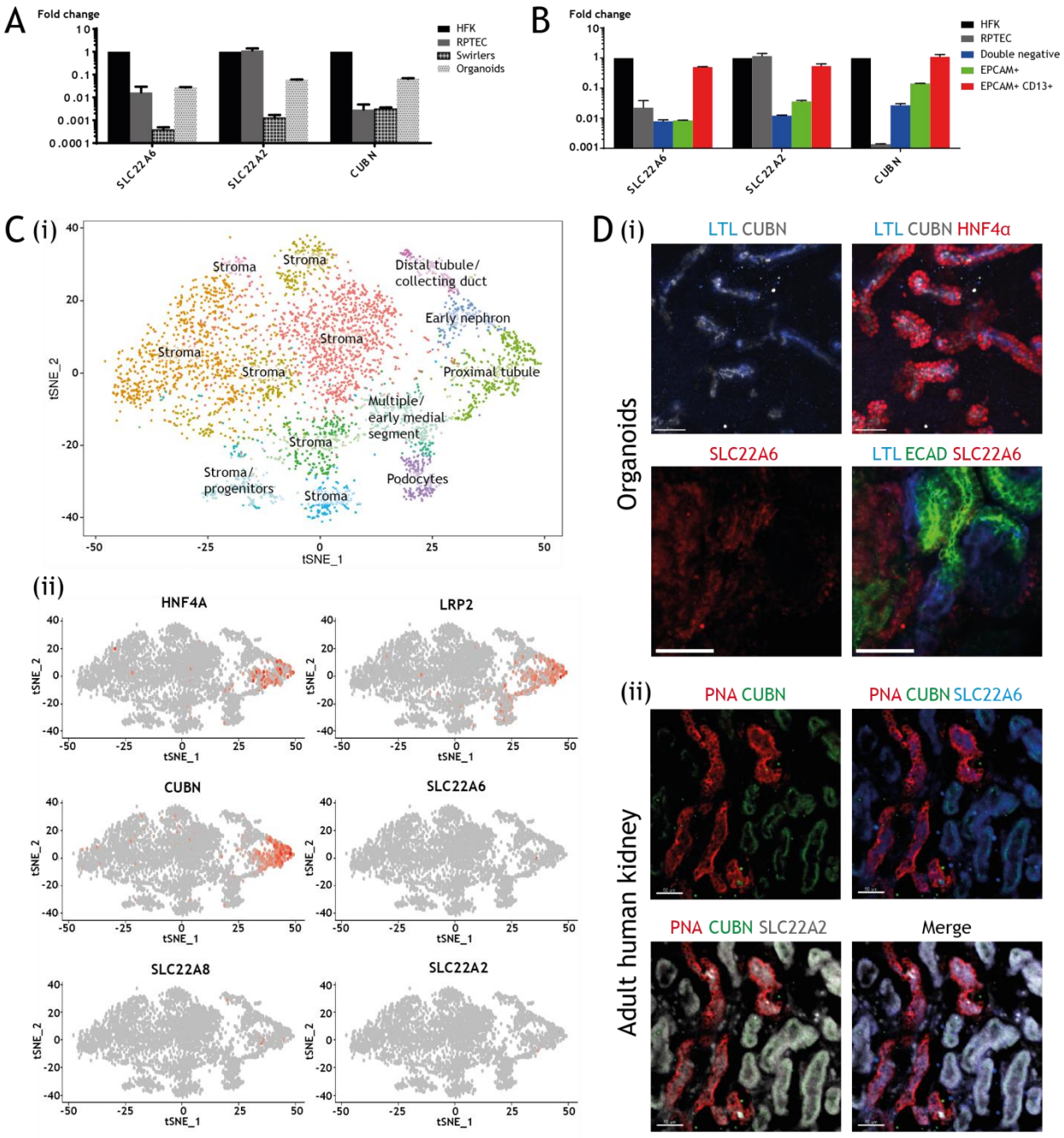

Figure 2.1 Characterisation of proximal tubule marker expression in organoids cultured *in vitro* at RNA and protein level. A: qRT-PCR comparison of proximal tubule marker expression in human foetal kidney (HFK), primary proximal tubule cells (RPTEC), D7+19 swirler micro-organoids (swirlers) and D7+18 Transwell® organoids. n = 2 biological replicates, error bars ± SEM. B: qRT-PCR comparison of proximal tubule marker expression in FACS fractions of Transwell® organoids compared to HFK and RPTEC. C: (i) tSNE plot showing unsupervised clustering of cells from scRNA-seq of organoids and (ii) feature plots showing which clusters express proximal tubule markers. D: Immunofluorescence staining for proximal tubule markers in (i) organoids and (ii) control adult human kidney sections. Anti-SLC22A6 and SLC22A2 antibodies did not detect these markers in organoids or in adult human kidney sections. LTL: *Lotus tetragonolobus* lectin. CUBN: cubilin. SLC22A6: organic anion transporter 1. SLC22A2: organic cation transporter 2.

2.4 Proximal tubule maturation in organoids cultured in different media types

2.4.1 Proximal tubules in organoids differentiated and cultured in E6 have higher expression of early proximal tubule markers than those differentiated and cultured in APEL

Over the course of this project, our group developed multiple variations of the Takasato organoid culture protocol. One of these was a switch to E6 as the basal medium for differentiation of iPSCs and organoid maintenance, as the basal medium (APEL) used in the Takasato protocol as published[212] was discontinued. To determine if this switch had any effect on proximal tubule maturation, Seurat integrated analysis was used to combine two datasets produced and analysed by others in our group: scRNA-seq of D7+18 whole organoids cultured in E6 (also briefly discussed in section 2.1.2) and scRNA-seq of D7+18 whole organoids cultured in APEL[194], so that proximal tubule cells from both datasets could be identified after unsupervised clustering and compared (Figure 2.2A).

One major limitation of this analysis is that these datasets were not originally produced with the aim of characterising differences between organoids cultured in E6 and APEL, and were produced from different cell lines at different times. Nonetheless, after unsupervised clustering of the combined dataset, most of the clusters had contributions from both datasets, indicating that clusters primarily reflected distinctions between renal cell types as opposed to experiment-specific differences, though cells within clusters were often visibly separated by dataset (Figure 2.2B). While some clusters were dominated by cells from the E6 or APEL dataset, extensive characterisation of the cell types present in these clusters was beyond the scope of this project. As the proximal tubule cluster (based on *HNF4A* expression) had cells from both datasets, we looked for genes which were differentially expressed between E6 proximal tubule cells and APEL proximal tubule cells (Figure 2.2C).

The top 20 genes which were upregulated in E6 proximal tubule cells included metallothioneins (Figure 2.2C). This was specific to E6 proximal tubule cells, and not a general effect of culturing organoids in E6 (Figure 2.2C). Metallothioneins are cysteine-rich proteins which have roles in zinc and copper transport and also scavenge free radicals and reactive oxygen species [223]. In proximal tubules *in vivo*, they are normally expressed at low levels, but can be upregulated in response to zinc supplementation, or high glucose concentrations and oxidative stress [223,224]. Both E6 and APEL basal media have high concentrations of glucose (~17.5 mM and ~15.1 mM respectively) compared to normal non-

fasting serum glucose levels (< 8 mM), and hence may well trigger the high glucose response in proximal tubules. However, given how similar the glucose concentrations are, it is not clear why E6 proximal tubule cells upregulate metallothionein expression so strongly compared to APEL proximal tubule cells. There are a number of possible explanations. One is that while E6 and APEL have similar concentrations of glucose and inorganic salts, APEL contains recombinant human albumin, which may mitigate oxidative stress induced by the media, possibly in concert with other antioxidants. Conversely, E6 may contain a compound which exacerbates the response. Another possible reason is that metallothioneins are being upregulated in response to one or more factors other than glucose which are present in higher concentrations in E6. In any case, while mature proximal tubules should be able to upregulate metallothioneins in response to certain stressors, exhibiting the stress response in baseline culture is not desirable.

Other genes which were significantly upregulated in E6 proximal tubule cells included *JAG1*, *HNF1B*, and *CUBN* (Figure 2.2D). *JAG1* and *HNF1B* are expressed in renal vesicles and S-shaped bodies and are required to form the medial segment of the early nephron (detailed in Chapter 1), which gives rise to the proximal tubule and loop of Henle [225]. *JAG1* expression drops as the medial segment matures into the proximal tubule, so *JAG1* expression in E6 proximal tubules may reflect a less mature state compared to APEL proximal tubules. However, the upregulation of *CUBN* in E6 proximal tubule cells argues against this, as *CUBN* is also expressed in adult proximal tubules *in vivo.* It may be that E6 proximal tubule cells have a more established identity compared to APEL proximal tubule cells, even though proximal tubule cells in both E6 and APEL are immature compared to proximal tubules *in vivo*.

Another point suggesting that APEL proximal tubule cells have a less established identity is their higher average expression of *WT1* and *MAFB* compared to E6 proximal tubule cells (Figure 2.2D). *WT1* and *MAFB* are transcription factors which are expressed in the most proximal end of the S-shaped body, which gives rise to podocytes [20]. Indeed, the cells with the strongest expression of *WT1* and *MAFB* are on the lower right of the combined proximal tubule cluster, closest to the cluster expressing definitive podocyte markers, while the opposite pattern is seen with *HNF4A* (Figure 2.2A). However, because cell clustering was unsupervised, it is possible that the cells expressing *MAFB* and *WT1* which were included in this cluster represent cell types other than genuine early proximal tubule cells.

SPP1 was upregulated in E6 compared to APEL (Figure 2.2D). *SPP1* is expressed in healthy adult distal tubules and distal loop of Henle, but is upregulated in adult proximal tubules during the repair stage following acute injury [226,227]. The upregulation of *SPP1* in E6 proximal tubules may reflect ongoing development of an early proximal tubule (which often involves pathways similar to those seen in tissue repair), or a stress response similar to the observed upregulation of metallothioneins [26].

Other proximal tubule markers which are expressed in both early and adult proximal tubules such as *LRP2* and *HNF4A* were expressed in both E6 and APEL proximal tubules, but were not differentially expressed between the media types, while more definitive markers such as *SLC22A6* and *SLC22A2* were absent in both media types (Figure 2.2D). Hence, both media types can produce early proximal tubules which express some functional markers, but not mature proximal tubules.

Considering all the above points, the change in our organoid differentiation and culture protocol to using E6 as the basal medium instead of APEL may have improved expression of medial segment markers and some early functional proximal tubule markers such as *CUBN*, but also strongly increased expression of metallothioneins, suggesting an undesirable stress response, and had no effect on the expression of definitive proximal tubule markers. We continued to use organoids cultured in E6 (or E6 supplemented with all-*trans*-retinoic acid, discussed in the following section) as a baseline while investigating potential improvements to culture conditions, instead of attempting to re-create APEL.

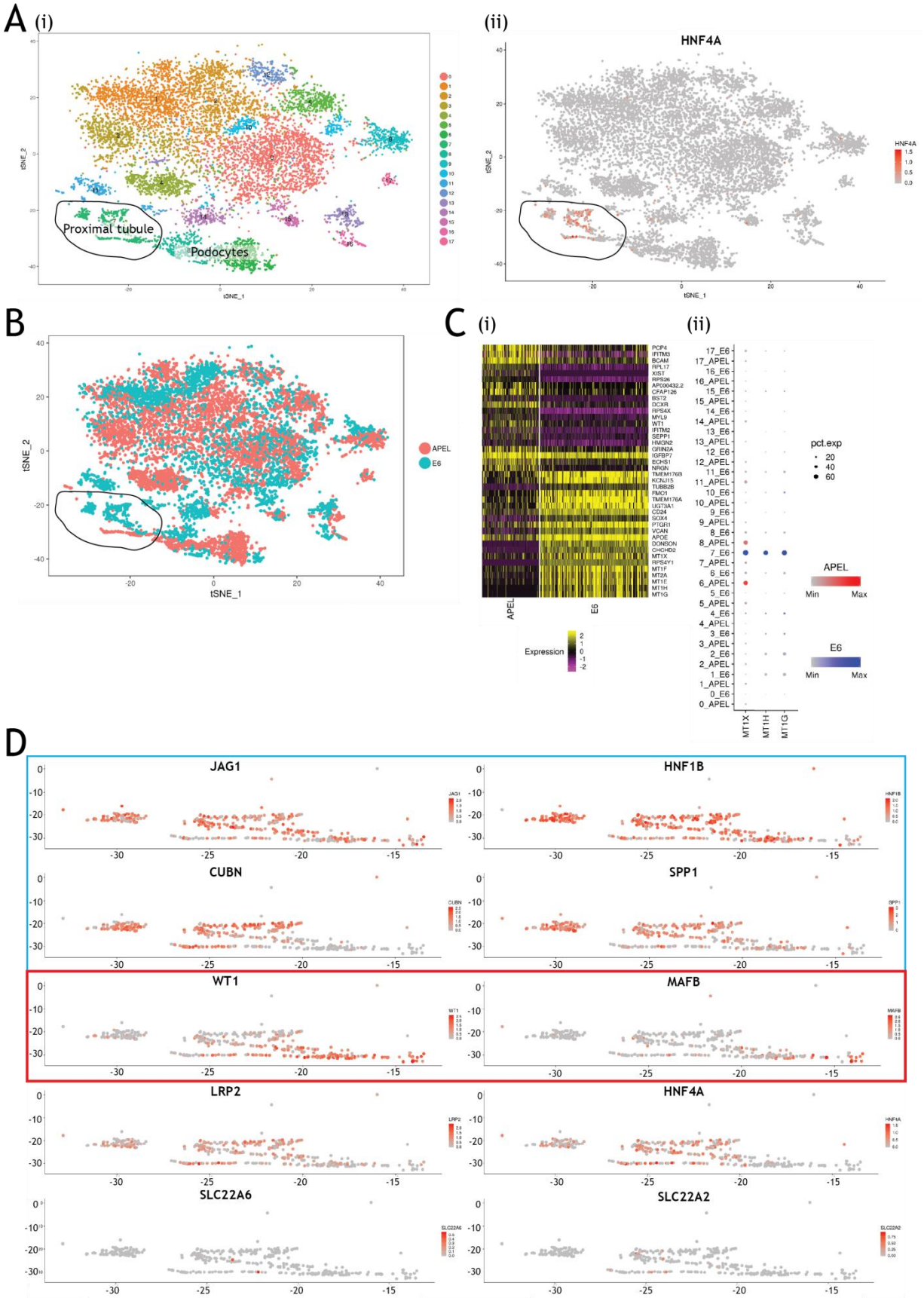
A
(i)
Proximal tubule
Podocytes
tSNE_1
tSNE_2
(ii)
HNF4A
B
APEL
E6
C
(i)
(ii)
Expression
pct.exp
Min
Max
D
JAG1
HNF1B
CUBN
SPP1
WT1
MAFB
LRP2
HNF4A
SLC22A6
SLC22A2

Figure 2.2 scRNA-seq comparison of proximal tubule cells between D7+18 organoids cultured in E6 and D7+18 organoids cultured in APEL. A: (i) Unsupervised clustering of the combined dataset identified 17 clusters. Clusters with significantly increased *HNF4A* expression shown in (ii) compared to other clusters were considered proximal tubule cells for further analysis. B: tSNE plot of the combined dataset labelled by media type. C: (i) Heatmap showing the top 20 differentially upregulated and downregulated genes between APEL and E6 proximal tubule cells. (ii) Split dot plot showing expression of metallothioneins across all clusters, coloured by media type. Dot size corresponds to the percentage of cells in a given cluster which express the corresponding gene, and dot shading shows the scaled average expression of the gene across those cells. D: Feature plots comparing cell type marker expression in APEL and E6 proximal tubule cells. Plots outlined in blue and red are markers which were significantly upregulated in E6 and APEL respectively ($p < .05$). Plots without outlines are markers of interest which were not significantly differentially expressed at $p < .05$.

2.4.2 All-trans-retinoic acid added to E6 medium does not improve or hinder proximal tubule maturation

Another variation of the Takasato organoid protocol made after the switch to using E6 as the basal medium was the addition of all-*trans*-retinoic acid (RA) at D7+5 of organoid culture, after the withdrawal of FGF9 (see Chapters 1 and 7 for more details), as supplementation with either 9-*cis*-retinoic acid or all-*trans*-retinoic acid increases the nephron number and size of embryonic rat kidney explants grown *in vitro* [228]. Retinoic acid binds and activates retinoic acid nuclear receptor (RAR) transcription factors, which form heterodimers with retinoid X receptor (RXR) and activate the transcription of target genes [229]. Retinoic acid signalling from the cortical stroma to ureteric buds is required for ureteric bud branching during renal development [230]. It may also play a role in nephron segmentation, as inhibition of retinoic acid signalling in zebrafish embryos causes a loss of pronephric podocytes and the segments which are analogous (based on gene expression) to the mammalian proximal tubule [231,232]. Hence, to determine if retinoic acid supplementation affected the maturation of organoid proximal tubules, we analysed a scRNA-seq dataset (the combined dataset briefly discussed in section 2.1.2) of organoids cultured in E6 alone (E6) and E6 with all-*trans*-retinoic acid (E6RA) which was previously generated and analysed by others in our group (Sean Wilson *et al*., unpublished data).

Prior unsupervised clustering after combining E6 and E6RA datasets with integrated analysis produced 11 clusters which were identified based on their expression of known marker genes (Figure 2.3A). Most clusters, including the proximal tubule cluster, had contributions from both E6 and E6RA datasets, showing that clustering most likely reflects differences between

cell types as opposed to technical differences between datasets (Figure 2.3B). A heatmap of genes which passed the threshold for statistical significance for being differentially expressed between E6 and E6RA proximal tubule cells showed very little difference in average expression of these genes, suggesting that retinoic acid supplementation had little effect on organoid proximal tubules (Figure 2.3C). No dramatic differences in the expression of early proximal tubule markers (*HNF4A*, *CUBN*, and *LRP2*) were observed, while the solute channel transporters (*SLC22A6*, *SLC22A8*, and *SLC22A2*) were absent from both E6 and E6RA. Hence, we concluded that retinoic acid supplementation did not improve or hinder proximal tubule maturation. However, at this stage our group routinely used E6 supplemented with retinoic acid to improve differentiation of renal progenitors and podocyte maturation (Sean Wilson *et al*., unpublished data), so later experiments in this project continued to use E6 supplemented with retinoic acid as a baseline condition which we sought to improve upon.

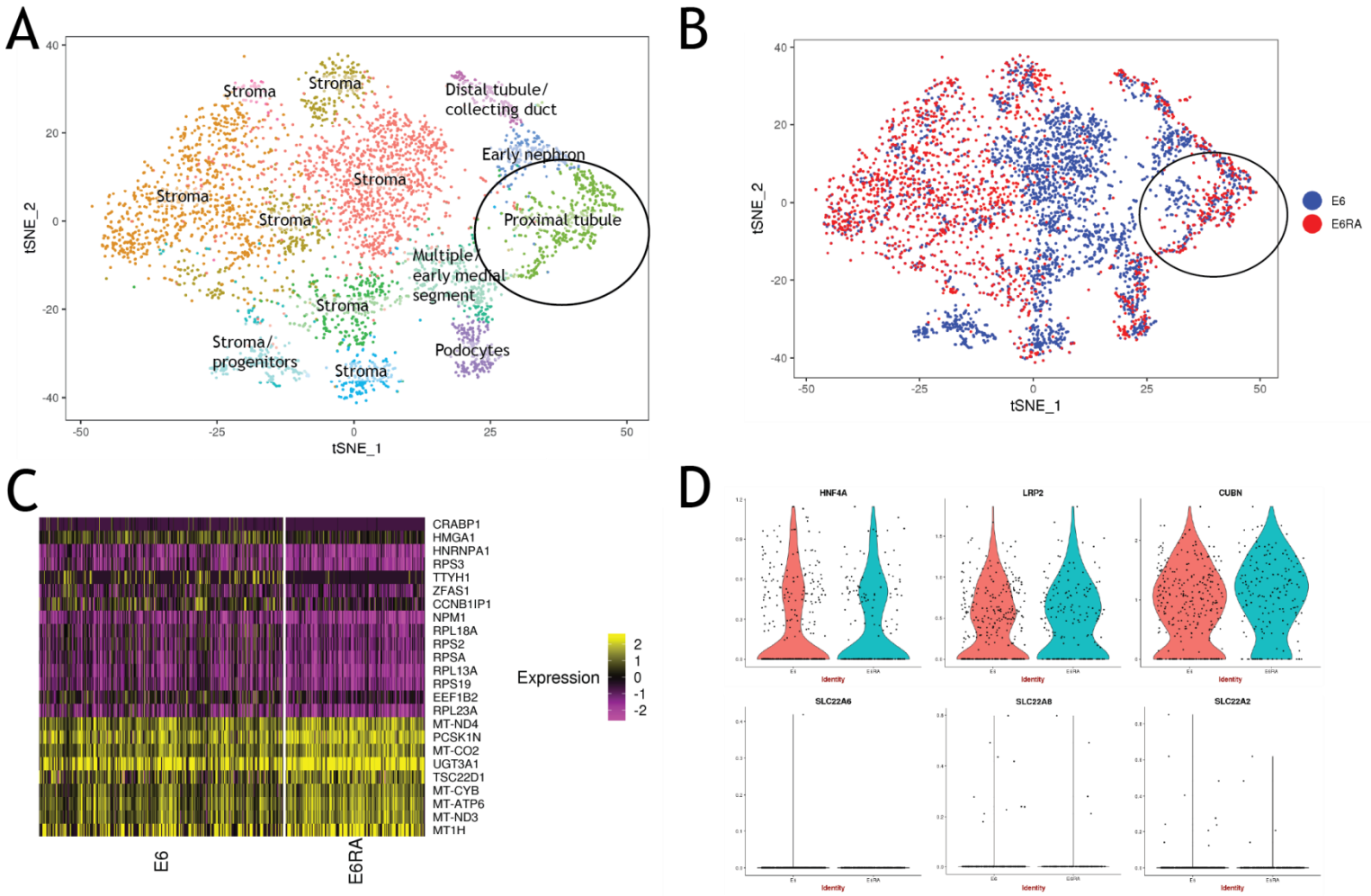
A
Stroma
Stroma
Distal tubule/
collecting duct
Early nephron
Stroma
Stroma
Stroma
Proximal tubule
Multiple/
early medial
segment
Stroma
Stroma/
progenitors
Podocytes
Stroma
tSNE_2
tSNE_1
B
tSNE_2
tSNE_1
E6
E6RA
C
CRABP1
HMGA1
HNRNPA1
RPS3
TTYH1
ZFAS1
CCNB1IP1
NPM1
RPL18A
RPS2
RPSA
RPL13A
RPS19
EEF1B2
RPL23A
MT-ND4
PCSK1N
MT-CO2
UGT3A1
TSC22D1
MT-CYB
MT-ATP6
MT-ND3
MT1H
Expression
E6
E6RA
D
HNF4A
LRP2
CUBN
SLC22A6
SLC22A8
SLC22A2
Identity

Figure 2.3 scRNA-seq comparison of proximal tubule cells between D7+18 organoids cultured in E6 alone (E6) and D7+18 organoids cultured in E6 with retinoic acid (E6RA). A: tSNE plot of unsupervised clustering of cells from D7+18 organoids (same data as in Figure 2.1, included here for ease of comparison.) B: tSNE plot of cells from D7+18 organoids cultured in E6 or E6RA, labelled by media type. C: Heatmap of genes which are differentially expressed between E6 proximal tubule and E6RA proximal tubule at $p < .05$. None of the genes had an average log-fold change > 0.5. D: Violin plots comparing proximal tubule marker expression in E6 and E6RA proximal tubule cells. Y-axis represents log-normalised expression while the shaded area represents the proportion of cells at a given expression level.

2.5 scRNA-seq comparison of early and mature proximal tubule cells in mouse and human kidneys

2.5.1 Rationale and method

As expression of functional markers was limited in organoid proximal tubules in all the culture conditions we have discussed so far, we concluded that they needed to mature further before they could be used as a reliable nephrotoxicity model. The initial patterning of organoid nephrons into distinct segments would also benefit from optimisation, as the proportion of cell types (both renal cells and non-renal off-targets) has been found to vary between organoids differentiated using the same protocol in different experiments [194].

While the regulation of nephron progenitor self-renewal and initial nephron formation has been extensively studied, there are fewer studies investigating the signals regulating nephron segmentation and maturation. To determine the signals and pathways which drive proximal tubule patterning and maturation *in vivo* so that we could replicate those signals *in vitro*, we analysed existing scRNA-seq and snRNA-seq datasets of mouse [216,217] and human kidney samples (Jason Spence, unpublished data) [195] at different ages, and searched for the KEGG (Kyoto Encyclopaedia of Genes and Genomes) pathway annotations of upregulated and downregulated genes.

In the scope of this analysis, the differentially-expressed genes we found can be categorised into two broad classes. The first class includes the functional proximal tubule markers such as *LRP2* and *SLC22A2* which were pointed out in section 2.1. These genes are required to perform some function which a mature proximal tubule *in vivo* has, such as endocytosis or organic cation transport, but are not necessarily involved in the development or maturation of the proximal tubule. Pathway analysis may still indicate that these genes are targets of one or more specific signals, which could potentially be replicated *in vitro*. The second class

includes genes which regulate the expression of functional markers, or are parts of signalling pathways. The pathways associated with these genes are more likely to play a role in overall renal development or in differentiation and maturation of the proximal tubule specifically, depending on which cell types express these genes.

2.5.2 Comparison of early and mature proximal tubule cells in E18.5 mouse kidney

First, a targeted analysis of a previously-generated and analysed scRNA-seq dataset of 6752 cells from E18.5 mouse kidneys was performed [216]. The previous analysis identified 15 clusters of cells, which were then labelled based on their expression of known markers. Two of these clusters were labelled early proximal tubule (EPT) and proximal tubule (PT) (Figure 2.4A).

Both EPT and PT expressed the proximal tubule markers we observed in organoids (*Hnf4a*, *Lrp2*, *Cubn*), but expression of the markers which were lacking in organoids (*Slc22a6*, *Slc22a8*, *Slc22a2*) was higher in PT (Figure 2.4B). Based on this, we hypothesised that differences in gene expression and the associated signalling pathways between both EPT and PT compared to the other cell types, or the differences between EPT and PT, would highlight pathways which drive proximal tubule maturation. Monocle [233–235] pseudotime analysis is a method of ordering cells in scRNA-seq datasets into a branched trajectory based on their gene expression levels relative to each other. Previous Monocle analysis of nephron cell clusters within this dataset placed EPT cells between PT cells and earlier developmental stages, supporting the interpretation of the EPT cluster as immature proximal tubule cells (Figure 2.4C).

Genes which were significantly upregulated in EPT and PT as a whole compared to the rest of the E18.5 mouse kidney included the proximal tubule markers known to mediate nephrotoxicity, as well as genes associated with oxidative phosphorylation, carbon metabolism, amino acid biosynthesis, gluconeogenesis, fatty acid metabolism, AMPK signalling, and parathyroid hormone and prolactin responses (Figure 2.4D). The mature proximal tubule is much more reliant on mitochondrial fatty acid oxidation to supply energy for active transport compared to other renal cell types and is capable of gluconeogenesis [40,236]. Parathyroid hormone and prolactin signalling also modulate calcium, phosphate, and sodium reabsorption by the proximal tubule [237–239]. Hence, the pathways upregulated in our EPT and PT clusters were broadly consistent with literature describing the function, metabolic activity, and signalling pathways of the mature proximal tubule. While the

proximal tubules in a late pre-natal mouse kidney may still not be functionally equivalent to adult proximal tubules, the fact that these phenotypes are already apparent at a transcriptional level during development suggests that it might be possible to induce some of these functions in an organoid *in vitro*.

Several genes, such as *Hnf4a*, *Prkaa2*, *Met*, *Tgfb1*, *Fzd2*, *Fzd7*, and *Hk1*, were upregulated or downregulated in EPT and PT compared to the rest of the E18.5 kidney but had similar average expression, or lack thereof, between EPT and PT (Figure 2.4D and E). This suggests that the pathways associated with these genes are activated or deactivated relatively early as the nephron is patterned into segments and then persist as the proximal tubule matures.

Hnf4a and *Prkaa2* were highlighted in this analysis as components of AMPK signalling which were upregulated in EPT and PT (Figure 2.4D). *Hnf4a* is a transcription factor which regulates the expression of multiple proximal tubule markers, including the SLC transporters [213]. However, our analysis in this project indicates that while *Hnf4a* expression may be necessary to develop and maintain the proximal tubule phenotype, it is not sufficient for expression of SLC transporters. The endogenous ligands of Hnf4α are fatty acids, but to activate Hnf4α, binding of coactivators such as PGC-1 (*Ppargc1a*) is required, and no small molecule agonists of Hnf4α have been made available to date [240]. *Prkaa2* encodes the catalytic alpha-2 subunit of the AMP-activated protein kinase, which is an energy sensor that acts to increase ATP production and decrease energy demand [241]. Because many proximal tubule transporters require ATP, AMPK activity in the proximal tubule may regulate their activity and expression. AMPK activation increases glucose reabsorption in the proximal tubule and decreases creatine transporter (*SLC6A8*) and Na^+-coupled phosphate transporter (*SLC34A1*) activity, but the effects of AMPK on other ATP-dependent transporters in the proximal tubule have not been extensively studied [241]. AMPK activation downregulates Hnf4α expression in pancreatic β-cells [242]. If AMPK activation has the same effect in the kidney, it would reduce expression of Hnf4α-regulated transporters. Hence, AMPK inhibition may be a method of maintaining Hnf4α expression to allow maturation of proximal tubules *in vitro*, in concert with manipulation of other signalling pathways seen during maturation.

Met, *Ghr*, *Fgfr3* and *Fgfr4* were receptors which were upregulated when comparing EPT and PT cells to other cell types, but not between EPT and PT (Figure 2.4D). *Met* encodes the receptor tyrosine kinase c-Met, which binds hepatocyte growth factor (HGF). Inhibiting HGF activity in mouse embryonic kidney explants impairs ureteric bud branching, podocyte

formation, and proximal tubule proliferation, showing that it is required for these processes [243]. In the presence of HGF, proximal tubule cells cultured *in vitro* proliferate, have more microvilli, and will form tubules with lumens if cultured in 3D [244,245]. Hence, HGF might aid proximal tubule proliferation or differentiation in organoids.

As for *Ghr* (growth hormone receptor), few studies have examined the role of growth hormone signalling in normal renal development. Overexpression of growth hormone in mice leads to increased numbers of proximal tubule cells without increased cell volume, but only if insulin-like growth factor 1 (*Igf1*) is also present, while overexpression of growth hormone causes glomerular hypertrophy in both $Igf1^{+/+}$ and $Igf1^{-/-}$ backgrounds [246]. This effect of growth hormone on proximal tubule cells suggests that growth hormone regulates their proliferation and is consistent with the analysis in this project. However, this analysis did not show a direct mechanism for the glomerular changes, as *Ghr* expression in podocytes in this dataset was very low. In postnatal life, growth hormone increases phosphate reabsorption in the proximal tubule of juvenile rats [247]. However, in our analysis, *Ghr* expression decreased between the EPT and PT clusters, indicating that growth hormone signalling might not be crucial for proximal tubule maturation.

Fgfr3 and Fgfr4 are two of four fibroblast growth factor receptors (FGFRs) which bind the various FGFs with different specificities and downstream effects [248]. FGF signalling is crucial throughout vertebrate and invertebrate embryonic development and for tissue maintenance in adults. In the mouse embryo, Fgf9 is weakly expressed in the primitive streak and highly expressed in the paraxial and intermediate mesoderm; the latter population gives rise to the ureteric epithelium and nephron progenitors [249]. FGF signalling also plays a role in proliferation and self-renewal of the nephron progenitors [250]. However, it is not clear if Fgfr3 or Fgfr4 specifically have any role in nephron segmentation, as global $Fgfr3^{-/-}$, $Fgfr4^{-/-}$, or $Fgfr3^{-/-}$ $Fgfr4^{-/-}$ mice have various defects including growth retardation, but do not show the gross renal structural defects of *Fgfr1* or *Fgfr2* conditional knockouts [251,252]. In adult mice, Fgfr3 and Fgfr4 are receptors for Fgf23, which increases phosphate excretion in the proximal tubule [253]. Few studies have aimed to determine if loss of Fgfr3 and/or Fgfr4 causes any subtle defects in proximal tubule patterning or function beyond altered phosphate regulation. Nevertheless, the ability to respond to regulatory signals for maintaining serum phosphate is required in a mature proximal tubule and arises relatively early, based on analysis of this dataset.

As described previously in section 2.1.1, the mature proximal tubule is sensitive to drug-induced injury partly because of its reliance on mitochondrial oxidation to meet the energy demand of its transport activity. Hence, directing proximal tubule metabolism towards fatty acid oxidation *in vitro* might improve their functional maturity and their ability to mirror the *in vivo* response to nephrotoxic drugs. Many of the upregulated genes which were annotated for gluconeogenesis and fatty acid metabolism pathways were also annotated as peroxisome proliferator-activated receptor (PPAR) targets. The PPAR family consists of three nuclear receptors (PPARα, PPARγ, and PPARδ – previously called PPARβ) which bind fatty acids or their metabolites and form heterodimers with retinoid X receptors (RXRs) to control the transcription of multiple target genes to regulate metabolism [254]. Based on this, it is likely that they have a role in maintaining the metabolic signature of the proximal tubule. While this analysis did not detect statistically significant upregulation of PPAR genes in EPT or PT, RT-PCR of RNA from kidney sections in previous studies demonstrate that *Ppara, Pparg,* and *Ppard* are expressed in mouse kidneys from E17.5, and *in situ* hybridisation and immunofluorescence staining of kidney sections shows that *Ppara* and *Pparg* are expressed in the adult rat proximal tubule [255–257]. However, these studies conflict on the site of expression of the different PPAR genes. Yang *et al.*[255] found *Ppara* mRNA in the cortical proximal tubules and *Pparg* in the inner medulla of embryonic mouse kidneys, while Lyu *et al.*[257] found both PPARα and PPARγ staining in LTL^+ proximal tubules in adult mouse kidneys, and not $CD28K^+$ cortical distal tubules.

CUBN and *LRP2* expression in proximal tubules is enhanced by PPARα and PPARγ agonists [258,259]. The effect of PPAR agonists on proximal tubule markers aside from the genes involved in gluconeogenesis and fatty acid oxidation suggests that PPARs also regulate the expression of other genes which define the proximal tubule. This is consistent with investigations which found that the promoter regions of proximal tubule-specific genes were enriched for PPARα or PPARγ binding sites [213,257,260]. Considering our current analysis and the studies available, we hypothesised that PPAR agonists may be useful for driving proximal tubule maturation *in vitro*.

Genes which were downregulated in EPT and PT compared to other cell types in the E18.5 mouse kidney included cell cycle-associated genes, genes associated with Wnt signalling, transforming growth factor beta/bone morphogenic protein (TGFβ/BMP) signalling, the Notch target transcription factor *Hes1*, and the enzymes *Pkm* (pyruvate kinase M) and *Hk1*

(hexokinase 1) (Figure 2.4E). The downregulation of the latter enzymes suggests a metabolic switch away from glycolysis.

Wnt and Notch signalling regulate the formation and development of multiple embryonic tissues and organs, including the kidney. Wnt signalling from ureteric tips to nephron progenitors induces the formation of the pretubular aggregate [250]. Following this, *Wnt4* expression in the pretubular aggregate triggers a mesenchymal-to-epithelial transition of the aggregated cells, giving rise to the renal vesicle which develops into the nephron [19,261,262]. There is also some evidence that a β-catenin gradient (indicating canonical Wnt signalling) from high to low activity along the axis of the early nephron regulates its patterning into distal, medial, and proximal segments which give rise to the functionally distinct segments of the mature nephron [263,264]. We also observed that *Lgr4* was upregulated in EPT, but decreased in PT (Figure 2.4D). *Lgr4* is a receptor for R-spondins, which enhance Wnt signalling by maintaining Wnt receptors on the surface of the cell, so this was consistent with a role for Wnt signalling in nephron patterning or proliferation [265]. However, the downregulation of the Wnt receptors *Fzd2* and *Fzd7* in EPT and PT, especially when compared to the podocytes (which develop at the most proximal end of the early nephron, where Wnt signalling is lowest) and distal tubule, suggests that past a certain stage in their differentiation, cells committed to the proximal tubule fate are not reliant on Wnt signalling (Figure 2.4E). Similarly, the downregulation of the Notch target *Hes1* in EPT and PT suggests that while Notch signalling is important for differentiation of the pretubular aggregate and specifying tubular epithelium [266], it is not a major driver of proximal tubule maturation.

The TGFβ signalling pathway is involved in multiple processes throughout embryonic development including stem cell maintenance, cell fate determination, and organogenesis, as well as in maintenance and repair of adult tissues [267,268]. In general, TGFβ, BMP, and the ligands activin and nodal bind to their respective cell surface receptors (type II receptors), which then phosphorylate and activate type I receptors. These then phosphorylate Smad proteins which activate transcription of target genes. TGFβ and/or BMP signalling are required both for nephron progenitor maintenance and differentiation of progenitors into tubules [269–271]. However, in mature proximal tubules, TGFβ signalling inhibits re-differentiation of tubular cells to the proximal tubule phenotype following acute kidney injury, and this is associated with a persistent glycolytic state instead of recovery of oxidative phosphorylation [272,273]. Hence, inhibiting TGFβ signalling after early proximal tubules are formed may aid the *in vitro* differentiation of proximal tubules.

To examine genes which changed specifically during maturation, a comparison of genes which were differentially expressed between EPT and PT was also performed (Figure 2.5A). The pathways upregulated and downregulated in PT compared to EPT were broadly similar to the pathways upregulated and downregulated in both clusters compared to the rest of the E18.5 mouse kidney (Figure 2.5B and C). However, in these pathways, some new target genes, ligands, and/or receptors emerged. For example, *Smad7* and *Bmp4* were both expressed in EPT but downregulated in PT (Figure 2.5C). *Smad7* expression is induced by TGFβ and inhibits Smad-dependent canonical TGFβ and BMP signalling as a negative feedback mechanism [274]. *Bmp4* regulates ureteric budding and elongation, but its role in nephron patterning or proximal tubule maturation, if any, has not been extensively studied [275,276]. Nevertheless, downregulation of *Smad7* along with other TGFβ target genes and with *Tgfb1* indicates downregulation of TGFβ signalling in PT compared to EPT.

Taken together, the changes which occur during proximal tubule maturation in an embryonic mouse kidney include metabolic shifts away from glycolysis to oxidative phosphorylation of fatty acids, which involves PPAR target genes, and a downregulation of signals which are required earlier for nephron formation and patterning such as TGFβ signalling.

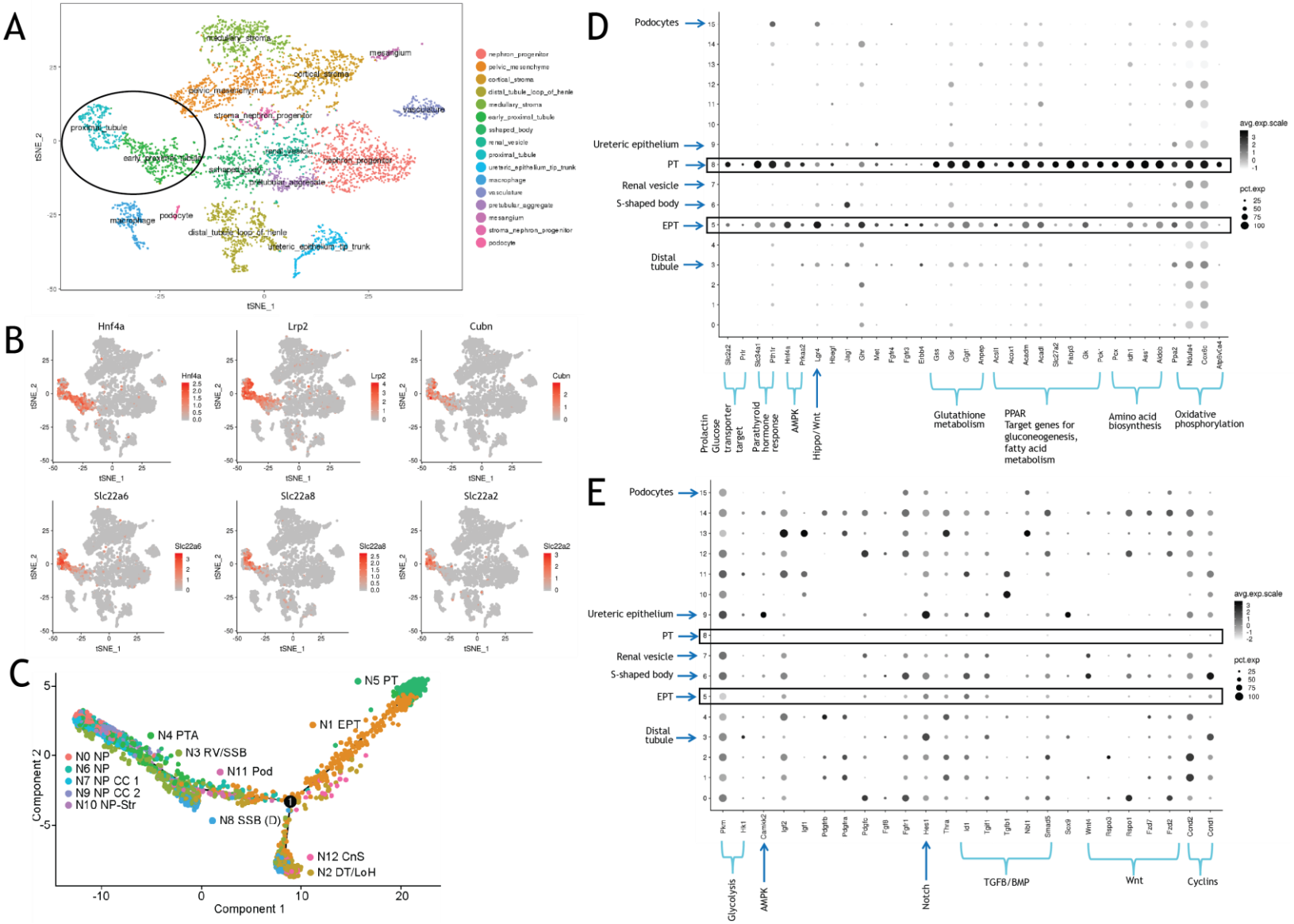
A
B
C
D
E
tSNE_1
tSNE_2
Component 1
Component 2
Hnf4a
Lrp2
Cubn
Slc22a6
Slc22a8
Slc22a2
N0 NP
N4 PTA
N3 RV/SSB
N11 Pod
N6 NP
N7 NP CC 1
N9 NP CC 2
N10 NP-Str
N8 SSB (D)
N5 PT
N1 EPT
N12 CnS
N2 DT/LoH
Podocytes
Ureteric epithelium
PT
Renal vesicle
S-shaped body
EPT
Distal tubule
avg.exp.scale
pct.exp
Prolactin
Glucose transporter target
Parathyroid hormone response
AMPK
Hippo/Wnt
Glutathione metabolism
PPAR Target genes for gluconeogenesis, fatty acid metabolism
Amino acid biosynthesis
Oxidative phosphorylation
Glycolysis
AMPK
Notch
TGFB/BMP
Wnt
Cyclins

Figure 2.4 scRNA-seq analysis comparing early and mature proximal tubule cells (EPT and PT respectively) in E18.5 mouse kidney to other cell types [216]. A: tSNE plot of clusters identified in the original analysis and the cell types they represent. The proximal tubule and early proximal tubule clusters are circled. B: Feature plots showing expression of proximal tubule markers across the clusters. C: Pseudotime trajectory arranging cells from the nephron lineage into a progression from nephron progenitors (NP) and progenitor-like stroma, to renal vesicles and S-shaped bodies (RV/SSB), podocytes, and proximal and distal tubular fates (adapted from Combes *et al.*[216]). The EPT cluster is closer to other clusters on the trajectory than the PT cluster, which is expected if they represent less and more mature proximal tubule cells respectively. D: Dot plot showing the expression of selected genes which are upregulated in EPT and PT compared to the rest of the E18.5 mouse kidney across every cluster. Clusters of interest are labelled on the vertical axis, and genes on the horizontal axis. The pathways these genes represent are also briefly described. Dot size corresponds to the percentage of cells in a given cluster which express the corresponding gene, and dot shading shows the scaled average expression of the gene across those cells. E: Dot plot showing the expression of selected genes which are downregulated in EPT and PT compared to the rest of the E18.5 mouse kidney across every cluster.

A

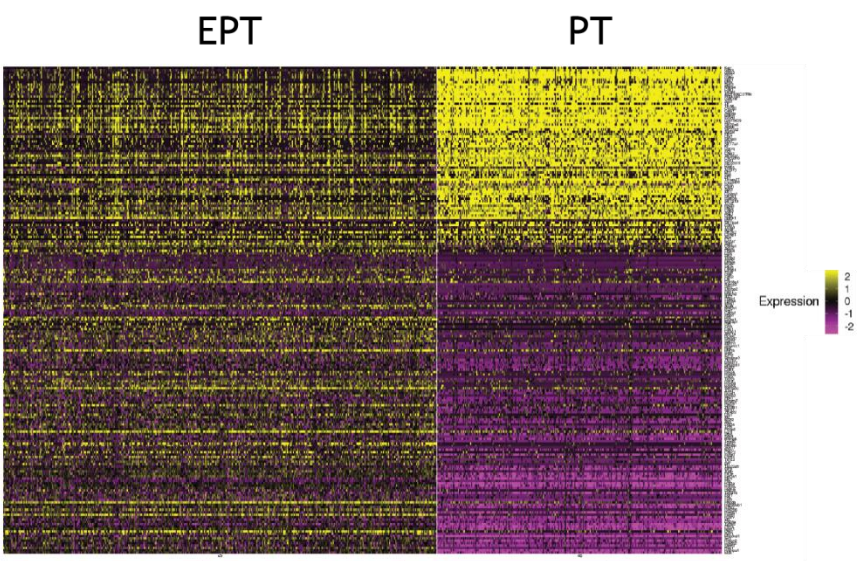
EPT
PT
Expression
2
1
0
-1
-2

B

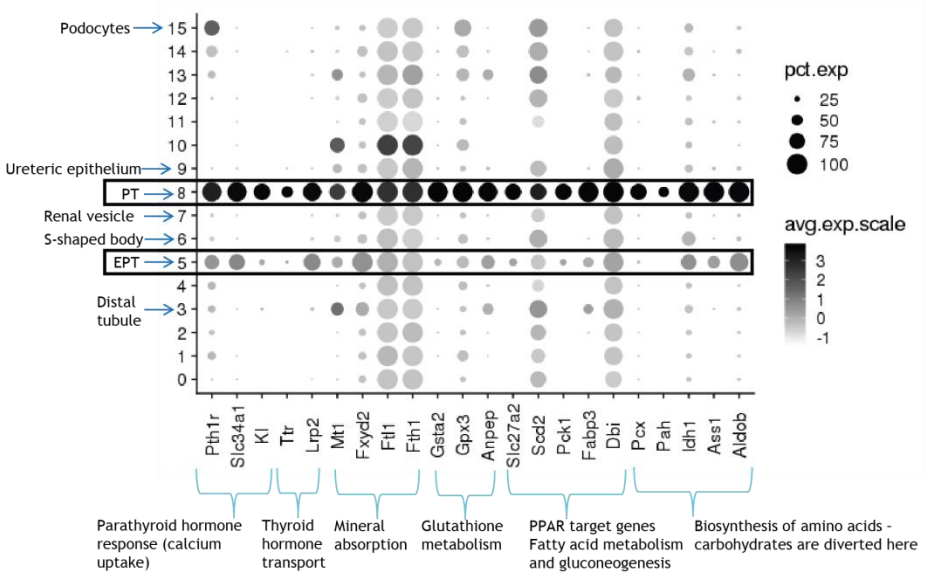
Podocytes
Ureteric epithelium
PT
Renal vesicle
S-shaped body
EPT
Distal tubule
15
14
13
12
11
10
9
8
7
6
5
4
3
2
1
0
pct.exp
25
50
75
100
avg.exp.scale
3
2
1
0
-1
Pth1r
Slc34a1
Kl
Ttr
Lrp2
Mt1
Fxyd2
Ftl1
Fth1
Gsta2
Gpx3
Anpep
Slc27a2
Scd2
Pck1
Fabp3
Dbi
Pcx
Pah
Idh1
Ass1
Aldob
Parathyroid hormone response (calcium uptake)
Thyroid hormone transport
Mineral absorption
Glutathione metabolism
PPAR target genes Fatty acid metabolism and gluconeogenesis
Biosynthesis of amino acids - carbohydrates are diverted here

C

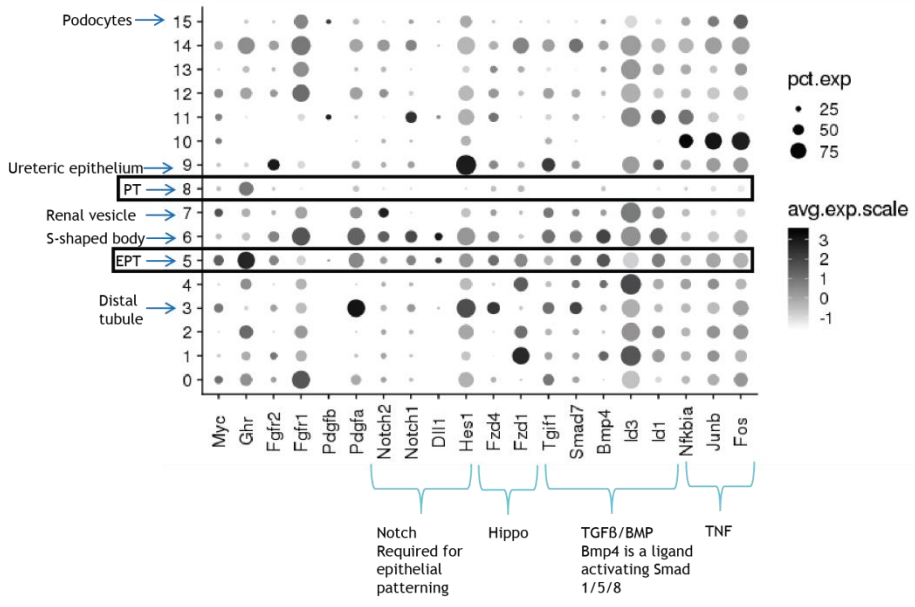
Podocytes
Ureteric epithelium
PT
Renal vesicle
S-shaped body
EPT
Distal tubule
15
14
13
12
11
10
9
8
7
6
5
4
3
2
1
0
pct.exp
25
50
75
avg.exp.scale
3
2
1
0
-1
Myc
Ghr
Fgfr2
Fgfr1
Pdgfb
Pdgfa
Notch2
Notch1
Dll1
Hes1
Fzd4
Fzd1
Tgif1
Smad7
Bmp4
Id3
Id1
Nfkbia
Junb
Fos
Notch Required for epithelial patterning
Hippo
TGFB/BMP Bmp4 is a ligand activating Smad 1/5/8
TNF

Figure 2.5 Differentially-expressed genes between early and mature proximal tubule cells (EPT and PT) in E18.5 mouse kidney [216]. A: Heatmap of genes that have an average log-fold change in expression > 1 between EPT and PT, as well as differentially-expressed ligands, receptors, and transcription factors. B and C: Dot plot showing the expression of selected genes which are upregulated and downregulated respectively in PT compared to EPT across every cluster. Clusters of interest are labelled on the vertical axis, and genes on the horizontal axis. The pathways these genes represent are also briefly described. Dot size corresponds to the percentage of cells in a given cluster which express the corresponding gene, and dot shading shows the scaled average expression of the gene across those cells.

2.5.3 Comparison of proximal tubule cells between E18.5 and adult mouse kidney follows the trends shown in the E18.5 mouse kidney

In the previous section, prior analysis of E18.5 mouse kidney scRNA-seq had identified EPT and PT clusters which represented early and more mature proximal tubule cells respectively, based on their expression of functional markers such as the SLC transporters. Hence, we inferred that other transcriptional differences between these two clusters would shed light on how proximal tubule cells mature. However, since these were cells from an embryonic mouse kidney, the PT cluster may not represent fully mature proximal tubule cells. Because of this, we sought to compare the EPT and PT cells from the E18.5 mouse kidney with proximal tubule cells from a published adult mouse kidney dataset[217].

One major caveat in this analysis is that there may be uncontrolled differences between the E18.5 mouse dataset and the adult mouse dataset, such as differences in sequencing depth, sex of the samples, and/or mouse lines. Nevertheless, after re-clustering cells from the adult mouse kidney dataset, proximal tubule cells were identified based on clusters which significantly upregulated *Hnf4a* (Figure 2.6A). There was one cluster which upregulated *Hnf4a* but also showed strong specific expression of *Xist* (X-inactive specific transcript), showing sex-specific transcriptomic differences between these cells and the other proximal tubule clusters (Figure 2.6A). As characterising these differences was beyond the scope of this project, the *Xist* cluster was excluded from the downstream analysis. A tSNE plot after integration of E18.5 and adult proximal tubule cells showed little separation between E18.5 and adult cells, showing that cells were not separating primarily by dataset, though there was separation between E18.5 EPT and PT cells (Figure 2.6C).

Genes which were differentially expressed between E18.5 and adult proximal tubule cells generally showed a trend in expression between EPT, PT, and adult cells, as expected if these clusters represented less to more mature cells, though some exceptions were apparent (Figure

2.7A). Many of the genes which were upregulated or downregulated in the adult cells were broadly similar to those upregulated or downregulated between EPT and PT. In particular, genes associated with gluconeogenesis were upregulated, and genes associated with Wnt, FGF, and Notch signalling were downregulated (Figure 2.7B).

Some genes which were expected to be upregulated in a more mature proximal tubule state, such as *Slc22a6* and *Slc22a2*, were not upregulated between E18.5 PT and adult cells (Figure 2.7B). One possible explanation is that only a fraction of adult proximal tubule cells expressed what we considered to be mature markers such as *Slc22a6* and *Slc22a2* (Figure 2.6Aii), possibly reflecting the segmentation of the adult proximal tubule into convoluted and straight segments, which would skew the average expression of these markers. We also note that some genes such as *Col4a3* and *Col4a4*, which have not previously been associated with proximal tubule cells *in vivo*, were upregulated in a small fraction of adult cells (Figure 2.7B). Further studies on how the proximal tubule sub-segments develop during maturation are required to validate these findings as well as to fully characterise the changes which occur in proximal tubule cells from the foetal to the adult state.

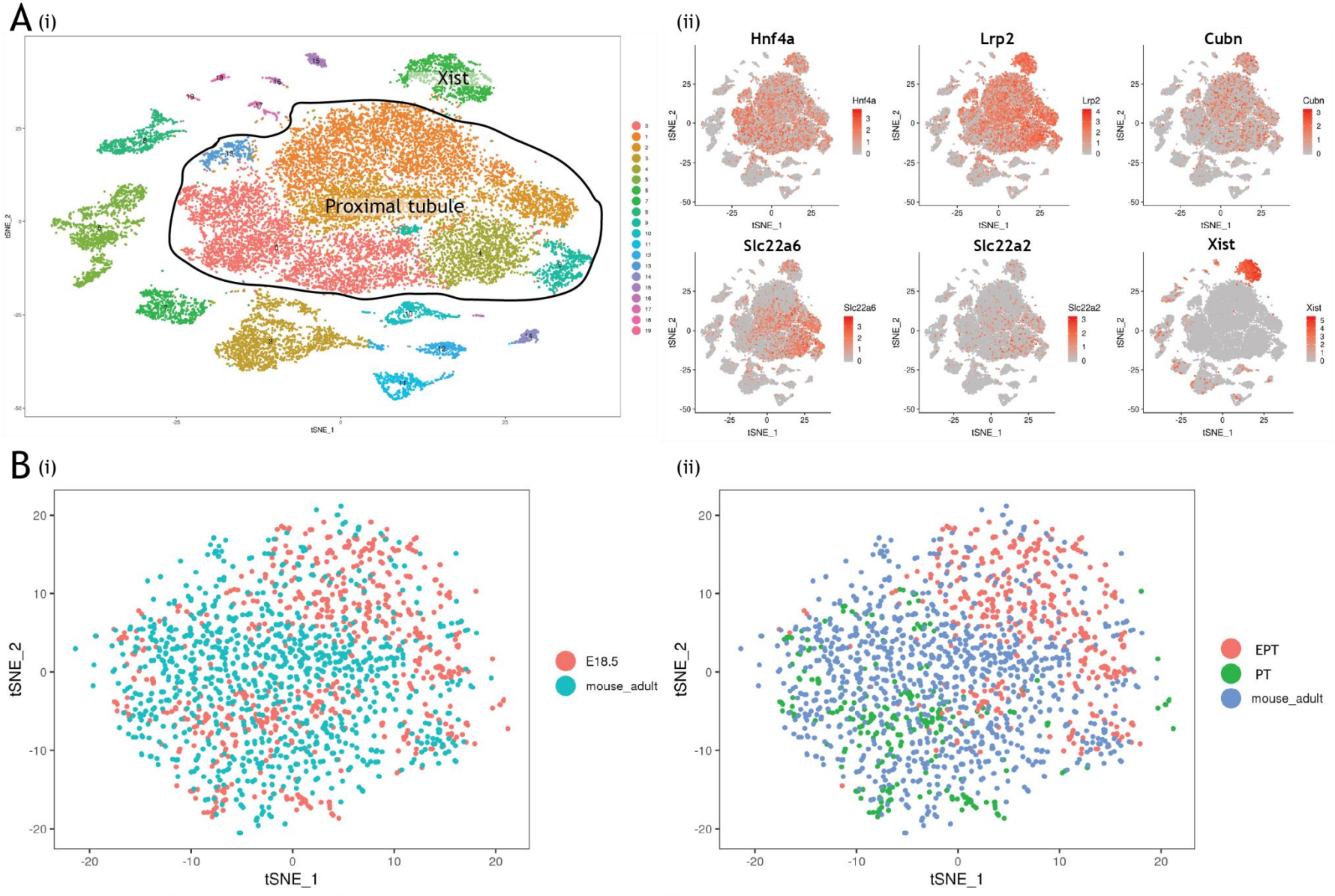
A (i)
Xist
Proximal tubule
tSNE_1
tSNE_2
(ii)
Hnf4a
Lrp2
Cubn
Slc22a6
Slc22a2
Xist
B (i)
E18.5
mouse_adult
(ii)
EPT
PT
mouse_adult

Figure 2.6 Unsupervised clustering of proximal tubule cells from E18.5[216] and adult mouse kidney[217]. A: (i) tSNE plot of clusters obtained by re-clustering cells from the adult mouse kidney dataset and (ii) feature plots showing expression of proximal tubule markers and *Xist* across those clusters. Clusters with significantly increased *Hnf4a* expression compared to other clusters were considered proximal tubule cells and used for further analysis, with the exception of the *Xist* cluster. B: tSNE plot of E18.5 and adult proximal tubule cells aligned by integrated analysis, labelled (i) by origin and (ii) with visual distinction between E18.5 EPT and PT.

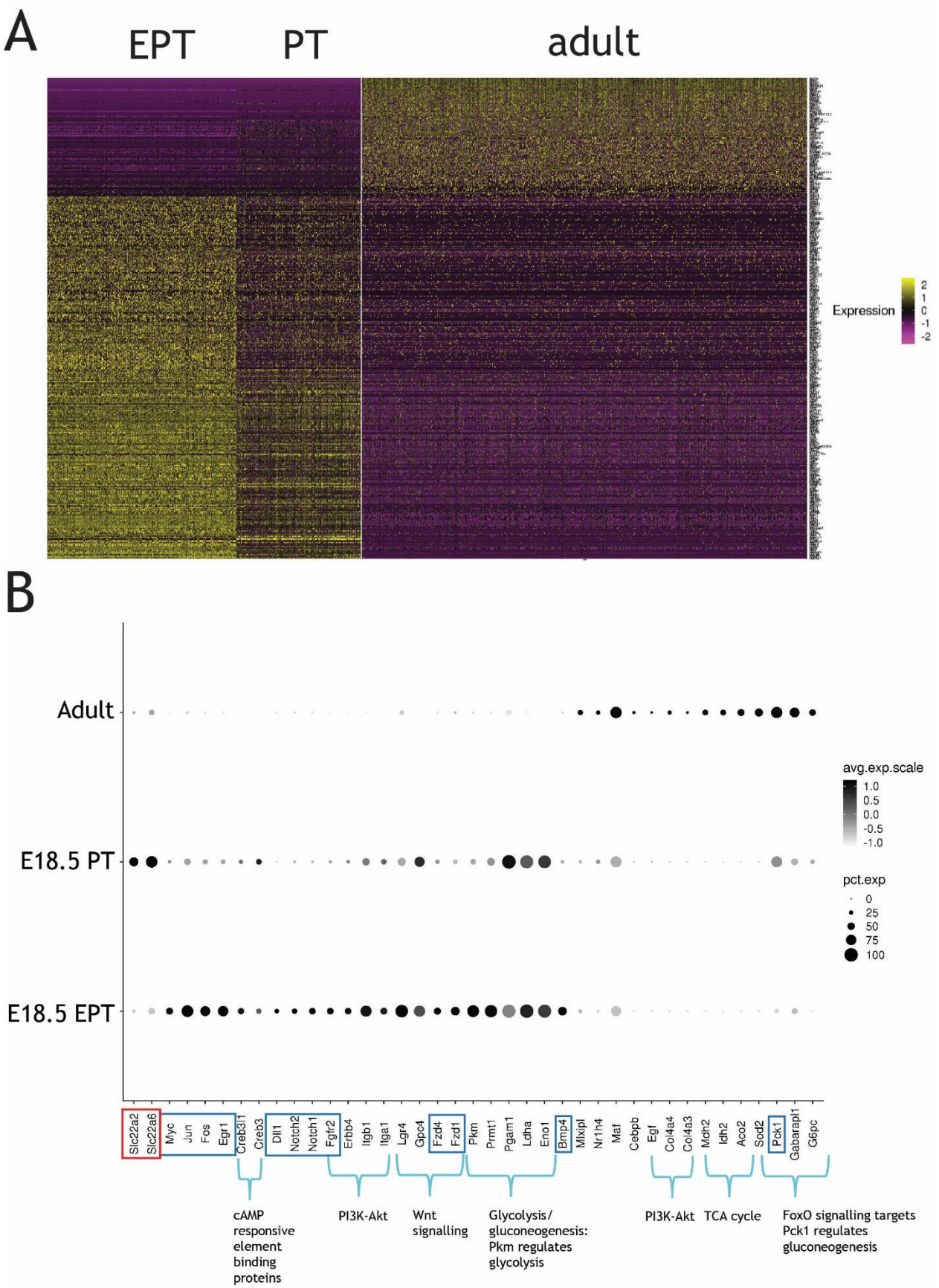
A
EPT
PT
adult
Expression
2
1
0
-1
-2
B
Adult
E18.5 PT
E18.5 EPT
avg.exp.scale
1.0
0.5
0.0
-0.5
-1.0
pct.exp
0
25
50
75
100
Slc22a2
Slc22a6
Myc
Jun
Fos
Egr1
Creb3l1
Creb3
Dll1
Notch2
Notch1
Fgfr2
Erbb4
Itgb1
Itga1
Lgr4
Gpc4
Fzd4
Fzd1
Pkm
Prmt1
Pgam1
Ldha
Eno1
Bmp4
Mlxipl
Nr1h4
Maf
Cebpb
Egf
Col4a4
Col4a3
Mdh2
Idh2
Aco2
Sod2
Pck1
Gabarapl1
G6pc
cAMP responsive element binding proteins
PI3K-Akt
Wnt signalling
Glycolysis/ gluconeogenesis: Pkm regulates glycolysis
PI3K-Akt
TCA cycle
FoxO signalling targets Pck1 regulates gluconeogenesis

Figure 2.7 Differentially-expressed genes between E18.5[216] and adult mouse kidney[217] proximal tubule cells. A: Heatmap of genes that have an average log-fold change in expression > 1 between E18.5 and adult proximal tubule cells, as well as differentially-expressed ligands, receptors, and transcription factors. B: Dot plot showing the expression of selected genes which are differentially expressed in adult proximal tubule cells compared to E18.5 proximal tubule cells. Clusters of interest are labelled on the vertical axis, and genes on the horizontal axis. The pathways these genes represent are also briefly described. Dot size corresponds to the percentage of cells in a given cluster which express the corresponding gene, and dot shading shows the scaled average expression of the gene across those cells. Blue boxes indicate genes which showed the same trend in expression between EPT and PT as between E18.5 cells and adult cells, while red boxes indicate genes which showed an opposite trend.

2.5.4 Comparison of proximal tubule cells in human foetal kidney and human adult kidney

While the mouse has often been used to model renal development, there are differences in gene expression during renal development between mice and humans [20,277]. Hence, we sought to compare human foetal and adult proximal tubule cells to determine if the pathways which changed during human proximal tubule maturation were similar to those we identified in the mouse, using human foetal kidney scRNA-seq datasets made available by our collaborators (Jason Spence, unpublished data) and a published human adult kidney snRNA-seq dataset [195] (Table 2.1). snRNA-seq was used for the adult kidney dataset instead of scRNA-seq as the researchers noted the difficulty of dissociating their adult kidney samples to single cells. While comparisons between scRNA-seq and snRNA-seq datasets of similar tissues have been published [278,279], including the study from which we accessed the human adult kidney dataset [195], this still introduces a major technical difference between the datasets being compared in this analysis.

Cells from each dataset were re-clustered and proximal tubule clusters with significant upregulation of *HNF4A* were identified as before (Figure 2.8). Similar to the embryonic and adult mouse datasets, *SLC22A6, SLC22A8,* and *SLC22A2* expression were observed in subsets of proximal tubule cells (Figure 2.8A and B). The foetal proximal tubule cluster also contained a subset of cells which did not express *HNF4A*, *LRP2*, or *CUBN*, though this was not labelled as a separate cluster at the clustering resolution used (Figure 2.8A). After integration of cells from the foetal and adult proximal tubule clusters, a tSNE plot showed overlaps between both cell types, showing that cells were not separating primarily by dataset (Figure 2.9A). Pathways associated with differentially-expressed genes were then identified (Figure 2.9B and C).

Functional markers such as *LRP2*, *CUBN*, *SLC22A6*, and *SLC22A2* were upregulated in the adult proximal tubule cells compared to foetal proximal tubule cells, as expected (Figure 2.9B). However, we noted that *FGFR3* and *FGFR4*, which were upregulated in mature mouse proximal tubule, were downregulated in this comparison, in contrast to previous reports showing that *FGFR3* and *FGFR4* are expressed more strongly in human adult kidneys compared to foetal kidneys (Figure 2.9C) [280]. This may reflect technical issues with gene capture or mapping in the adult human kidney dataset, as we also noted that *AQP1* was completely absent, even though *AQP1* expression in the proximal tubule is well-established (Figure 2.9C) [281]. Hence, if a pathway is upregulated or downregulated in both our mouse and human analyses, this suggests that the pathway is conserved in mouse and human proximal tubule maturation and that manipulating the pathway *in vitro* may improve organoid proximal tubules, but if a pathway change is only present in one set of comparisons, we cannot necessarily conclude that a species difference exists.

While signalling receptors such as *PPARA* and *PPARG* were upregulated in the human adult proximal tubule, as expected from the upregulation of their target genes seen in mice, the target genes were not (Figure 2.9B and C). Similarly, some genes associated with amino acid synthesis and glucose metabolism which were significantly upregulated in the adult mouse were either downregulated or expressed in a smaller proportion of cells in adult human proximal tubules compared to foetal human proximal tubules (Figure 2.9B). Activin receptors, *BMP1RB*, and *SMAD2* were upregulated, which was unexpected given the downregulation of TGF/BMP signalling targets (Figure 2.9B and C). Other receptors which were upregulated included thyroid hormone receptors (*THRB*), prolactin receptor (*PRLR*), *IGF1R*, *INSR*, *MET*, and *GHR*. *Met*, *Ghr*, and *Prlr* (prolactin receptor) in the mouse E18.5 dataset were upregulated when comparing EPT and PT cells to other cell types, but not between EPT and PT. Adding ligands for these receptors *in vitro* may aid proximal tubule proliferation and may or may not aid maturation.

Similar to the mouse kidney, glycolytic enzymes, TGFβ/BMP target genes, the Notch target *HES1*, and the Wnt receptors *FZD1* and *FZD7* were downregulated between foetal and adult human proximal tubule cells (Figure 2.9B and C). This suggests that shifting metabolism away from glycolysis and/or inhibiting TGFβ/BMP, Notch, or Wnt signalling after tubules have been formed may aid proximal tubule maturation in human iPSC-derived organoids.

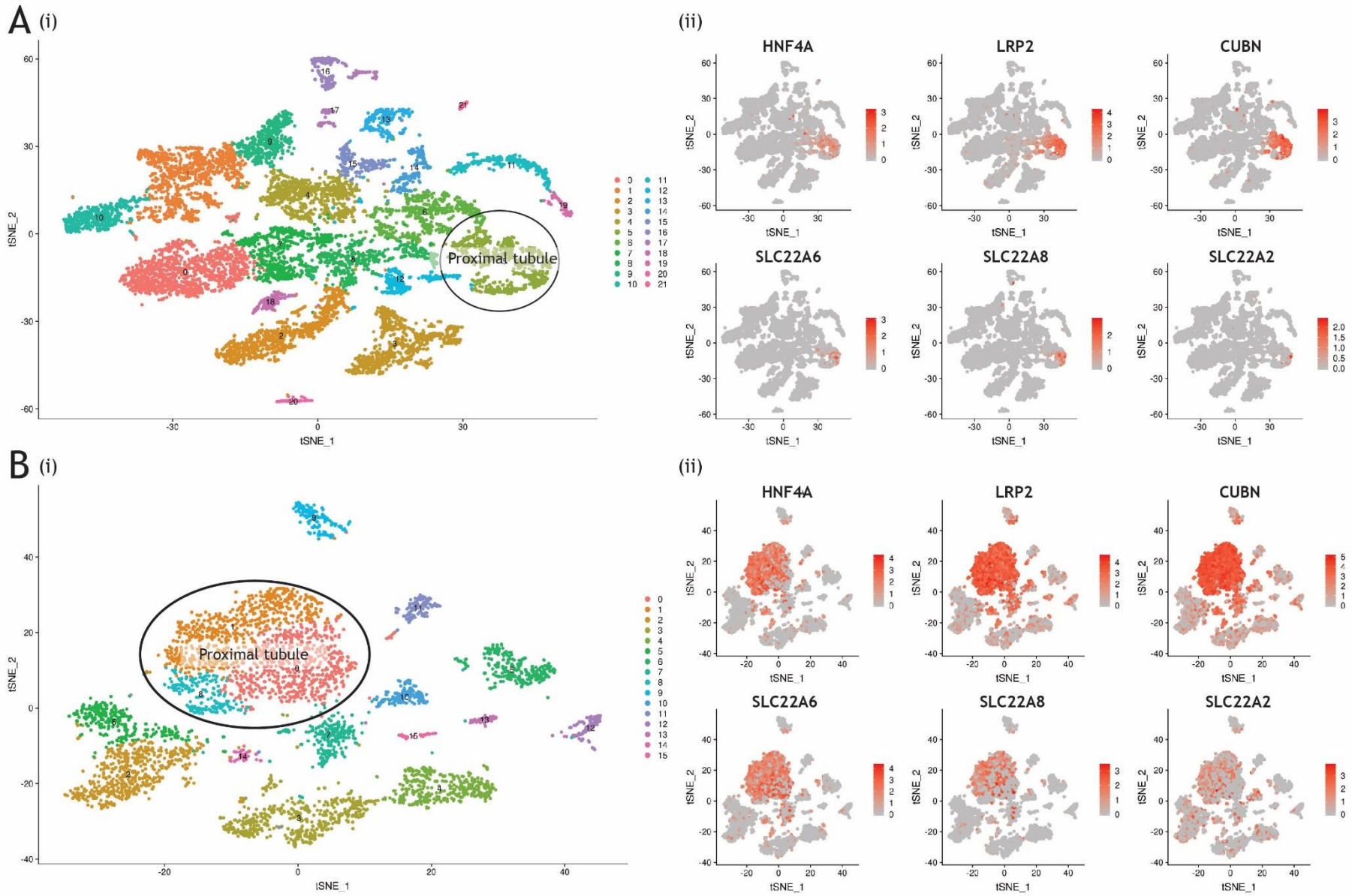
A (i)
Proximal tubule
tSNE_1
tSNE_2
(ii)
HNF4A
LRP2
CUBN
SLC22A6
SLC22A8
SLC22A2
B (i)
Proximal tubule
(ii)
HNF4A
LRP2
CUBN
SLC22A6
SLC22A8
SLC22A2

Figure 2.8 Unsupervised clustering of proximal tubule cells from foetal (Jason Spence, unpublished data) and adult human kidney[195]. A: (i) tSNE plot of clusters obtained by re-clustering cells from the foetal human kidney dataset and (ii) feature plot showing expression of *HNF4A* across those clusters. Clusters with significantly increased *HNF4A* expression compared to other clusters were considered proximal tubule cells and used for further analysis. B: (i) tSNE plot of clusters obtained by re-clustering cells from the adult human kidney dataset and (ii) feature plot showing expression of *HNF4A* across those clusters.

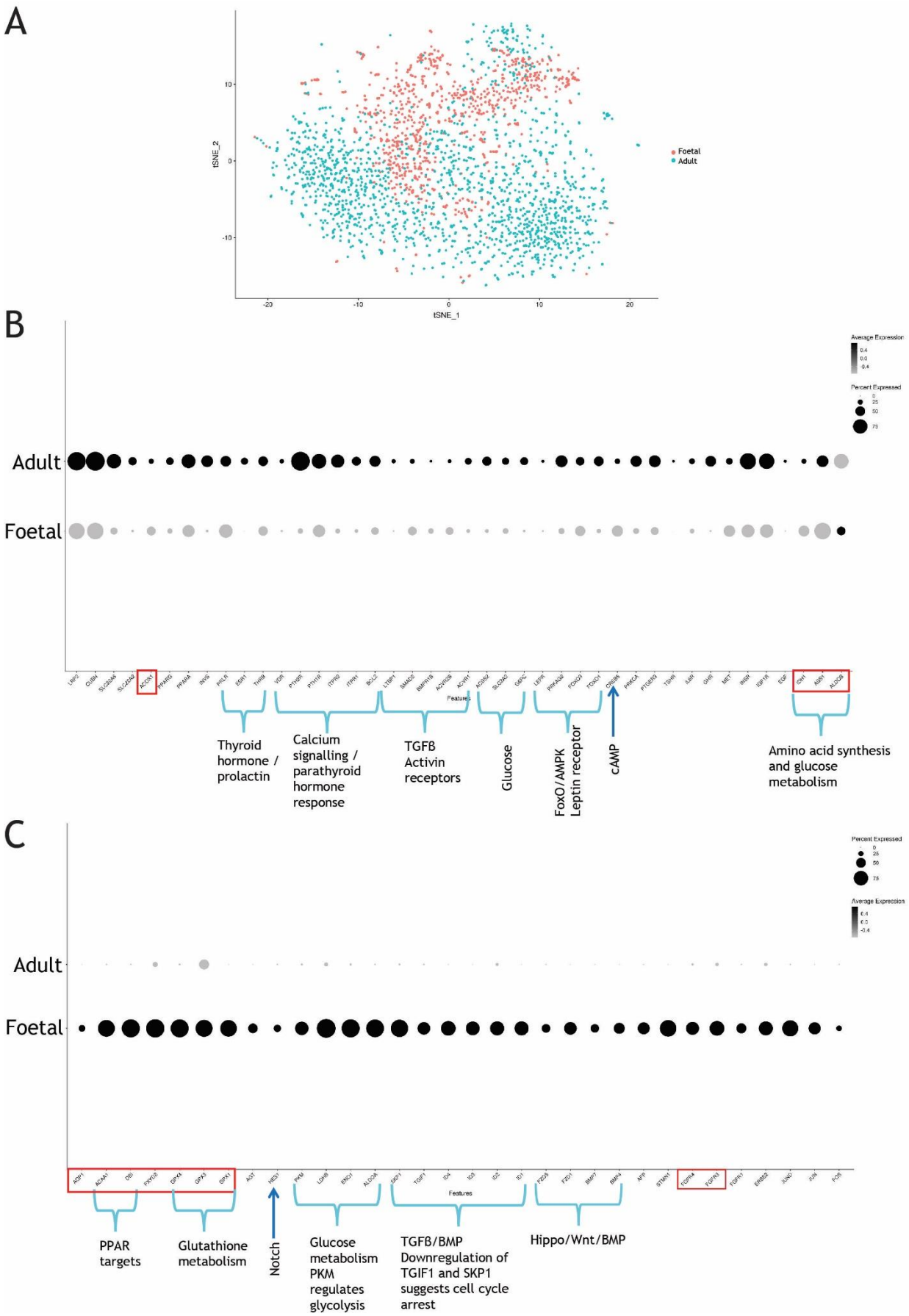
A
tSNE_2
tSNE_1
Foetal
Adult
B
Adult
Foetal
Average Expression
Percent Expressed
Features
Thyroid hormone / prolactin
Calcium signalling / parathyroid hormone response
TGFß Activin receptors
Glucose
FoxO/AMPK Leptin receptor
cAMP
Amino acid synthesis and glucose metabolism
C
Adult
Foetal
Percent Expressed
Average Expression
Features
PPAR targets
Glutathione metabolism
Notch
Glucose metabolism PKM regulates glycolysis
TGFß/BMP Downregulation of TGIF1 and SKP1 suggests cell cycle arrest
Hippo/Wnt/BMP

Figure 2.9 Integrated analysis of proximal tubule cells from foetal (Jason Spence, unpublished data) and adult human kidney[195] showing selected differentially-expressed genes. A: tSNE plot of integrated foetal and adult proximal tubule cells, labelled by origin. Integration was performed using the Seurat R package. B and C: Dot plot showing the expression of selected genes which are upregulated and downregulated respectively in adult proximal tubule cells compared to foetal proximal tubule cells. Clusters of interest are labelled on the vertical axis, and genes on the horizontal axis. The pathways these genes represent are also briefly described. Dot size corresponds to the percentage of cells in a given cluster which express the corresponding gene, and dot shading shows the scaled average expression of the gene across those cells. Red boxes indicate selected genes which were upregulated between foetal and adult mouse proximal tubule cells, but not between foetal and adult human proximal tubule cells.

2.6 Discussion

2.6.1 Summary of pathways implicated in proximal tubule proliferation and maturation which can be manipulated in vitro to improve organoid proximal tubules

In this chapter, we sought to understand the baseline maturity of the proximal tubule generated in our existing differentiation protocols, examine how this changed with alternations to media conditions, and then compare this to foetal and adult proximal tubules *in vivo* in both the mouse and human. Based on the low expression of functional markers such as the SLC transporters in our organoid proximal tubules, we concluded that the proximal nephron segment in kidney organoids generated using any of our available methods is immature and may not accurately model drug-induced nephrotoxicity. By studying the process of proximal tubule maturation inferred from single cell transcriptional profiling of foetal and adult mouse and human kidneys, we may be able to improve our organoid culture methods.

In vivo, an early proximal tubule has the capacity to respond to HGF, R-spondin, FGF signalling via FGFR3 and FGFR4, and growth hormone. It also develops a differential sensitivity to AMPK signalling. As the proximal tubule matures, it continues shifting away from glycolysis to fatty acid oxidation involving PPAR target genes, and downregulates pathways which are required for development of the early nephron such as Wnt, TGFβ/BMP, and Notch signalling. Hence, to encourage proliferation of proximal tubule cells *in vitro*, we could add R-spondin, FGFs, and/or HGF. The use of R-spondin and FGFs together with TGFβ/BMP inhibition would be similar to published protocols for generating epithelial organoids from adult stem cells found in tissues such as the intestines and liver [282]. While the presence of adult stem cells in the nephron is debatable, this method has also been applied to

create “tubuloids” from primary renal epithelial cells, showing that these factors support proliferation of renal cells [283].

To encourage maturation of those tubules, we could supply fatty acids in the media and stimulate fatty acid oxidation by inhibiting glycolysis and/or activating PPARs, and also inhibit AMPK, Wnt, TGFβ/BMP, and/or Notch signalling. Inducing shifts to fatty acid oxidation has been shown to improve the maturity of iPSC-derived cardiac organoids, which, like proximal tubules, favour fatty acid oxidation *in vivo* [284,285]. TGFβ inhibition during patterning of iPSC-derived renal vesicles prior to tubule formation suppresses tubular fates in favour of podocytes [200], showing that these early patterning pathways must be inhibited only after tubule formation, if the aim is to support proximal tubule proliferation and maturation.

2.6.2 Limitations of the current work and alternative analyses

One major limitation of our analysis which we have highlighted throughout this chapter is that we have compared proximal tubule cells between different datasets that were not all created with the same aim, which introduces uncontrolled differences between the proximal tubule cell states we have compared. Some of the published datasets used here also showed anomalies, such as *Xist* expression in a dataset prepared exclusively from male samples [217], or complete absence of *AQP1* transcripts in the adult human kidney dataset [195]. One method of reducing the effect of these uncontrolled differences would be to identify proximal tubule cells in each dataset and find differentially-expressed genes between these cells and other cell types in their respective datasets, as we did in section 2.5.2. The upregulated and downregulated genes and pathways could then be compared between datasets in a qualitative fashion to see if different genes or pathways are upregulated or downregulated in comparison to other renal cell types when proximal tubules mature from the embryonic to the adult state.

We have also shown that in both adult mouse and human kidneys, the SLC transporters were only expressed in a subset of proximal tubule cells. This may reflect segmentation of the adult proximal tubule into convoluted and straight segments. As we wished to increase SLC transporter expression in our organoid proximal tubules to model drug-induced toxicity which is mediated by these transporters, we might have compared foetal proximal tubule cells directly to SLC-expressing adult cells to determine specifically which pathways change as proximal tubule cells adopt this phenotype. Another related analysis would have been to determine if proximal tubule segmentation was detectable in foetal proximal tubule cells by using the adult datasets as a reference, a method available in the newest version of Seurat [218],

and to study changes which occur with maturation from a foetal to an adult state in each specific segment. Overall, the segmentation of the proximal tubule as it develops is an area that requires further research.

While we have identified several pathways which change during proximal tubule maturation which we may be able to influence *in vitro*, this analysis has not provided an exhaustive list of such pathways or determined the relative importance of the pathways we identified. There are packages available for processing scRNA-seq data to infer gene regulatory networks and hence master regulators of different cell states in a dataset in an unsupervised fashion [286,287]. This has also been shown to be a robust method of comparing cell types between different datasets, as conserved regulatory networks can be used to identify cell types.

2.6.3 Characterising changes to proximal tubules in vitro in response to culture conditions

To model drug-induced nephrotoxicity *in vitro*, we need proximal tubule cells which express the transporters and metabolic phenotype that make them uniquely vulnerable to drug toxicity. However, testing for expression of these transporters by immunofluorescence and qRT-PCR quickly becomes impractical to perform across all possible variations we could make to our culture protocol based on our analysis. To screen for effects of these variations on organoid proximal tubules, we could develop a proximal tubule reporter line so that changes can be quickly screened through fluorescent imaging, before promising conditions are identified for further characterisation.

We have not yet discussed pathways which may influence proximal tubule maturation but are difficult to manipulate *in vitro* using our culture system, such as fluid shear stress. Microfluidic devices have been used to culture primary proximal tubule cells under flow, and this has been shown to increase their expression of tight junction proteins and transporter function [2,95,154,159]. Seeding iPSC-derived proximal tubule cells into these devices may be another method of creating functionally mature iPSC-derived proximal tubule cells for modelling drug-induced toxicity.

In summary, we have shown that while organoids we are currently capable of producing have identifiable proximal tubules, these do not express all the features of a mature proximal tubule, and this persisted across the different basal media we have used. Through analysis of proximal tubules in the foetal and adult mouse and human to determine which pathways are upregulated or downregulated as proximal tubules mature *in vivo*, we have identified HGF,

FGFs, R-spondin, and growth hormone as factors which may encourage proliferation of proximal tubules *in vitro*. We have also identified upregulation of PPAR target genes for fatty acid oxidation and inhibition of glycolysis and of AMPK, Wnt, TGFβ/BMP, and/or Notch signalling after early proximal tubule formation as potential methods of increasing proximal tubule maturity *in vitro*.

3 GENERATION AND VALIDATION OF REPORTER LINES FOR CHARACTERISING PROXIMAL TUBULES IN KIDNEY ORGANOIDS

3.1 Background

3.1.1 Generation of reporter PSC lines for in vitro models of the kidney using the Cas9 system

One advantage of PSC-derived models of the kidney is that reporter PSC lines can be created to identify, track, and characterise cell types and states of interest. Several groups, including our own, have described the generation or use of fluorescent reporter lines for identifying nephron progenitors, lineage tracing of cells within kidney organoids to compare their development to what was known about kidney development *in vivo*, and to study the maturation of glomeruli in different culture platforms or after xenotransplantation [208,210,288–290].

To generate cell type-specific reporter lines, a reporter gene (typically encoding a fluorescent protein) is inserted into a locus known to be expressed in the cell type of interest. The first step is to induce a targeted DNA double-strand break at that locus. A double-strand break in eukaryotic genomic DNA can be repaired through non-homologous end joining (joining the broken strands end-to-end, an error-prone process) or homology-directed repair, which requires a homologous repair template [291,292]. Hence, if a DNA repair template which includes the reporter construct is provided, the reporter construct can be integrated into the gene of interest when the double-strand break is repaired (Figure 3.1).

Multiple methods are available for producing targeted DNA double-strand breaks to make these specific genetic modifications, including meganucleases, zinc finger nucleases, transcription activator-like effector nucleases (TALENs), and more recently the RNA-guided endonucleases, which are derived from an adaptive anti-phage defence found in bacteria known as the clustered regularly interspaced short palindromic repeats (CRISPR)/Cas9 system [291–297]. The Cas9 system has gained popularity because unlike the other methods listed, its target site is specified by a guide RNA, which is much easier to customise for a desired target compared to the DNA-binding protein domains used in the other methods. The CRISPR/Cas9 complex recognises DNA which is complementary to a 20-nucleotide region within the guide RNA [297]. Provided that the complementary sequence is immediately followed by a protospacer adjacent motif (5'-NGG for the most commonly used

Streptococcus pyogenes system), the Cas9 nuclease then induces a double-strand break in the DNA 3-4 base pairs upstream of the protospacer adjacent motif. Hence, a reporter construct can be inserted into a gene of interest through DNA repair as previously described, by introducing Cas9, a short guide RNA targeting a sequence specific to the gene of interest, and a DNA repair template including the reporter construct into host cells (Figure 3.1). The reporter construct should have synonymous base changes in the target site or protospacer adjacent motif, to prevent Cas9 cleavage of the successfully-integrated reporter construct [298].

The CRISPR/Cas9 system is a simple and efficient method for gene editing, but some undesirable outcomes can occur during the gene editing process. Off-target cleavage is possible since Cas9 can tolerate multiple mismatches within the guide sequence, depending on their position and distribution [299–301]. Tools are publicly available for designing guide RNAs and predicting off-target activity *in silico* (e.g. Cas-OFFinder), to aid selection of guide RNAs which induce efficient on-target cleavage and have low off-target activity [302,303]. Variants of Cas9 with reduced mismatch tolerance and hence reduced off-target activity have also been designed [304,305]. To verify that a given cell line does not have off-target modifications, Sanger sequencing of predicted off-target sites can be performed, and more comprehensive methods including whole genome sequencing, DNA double-strand breaks mapping, GUIDE-Seq and Digenome-seq have been described [306–309].

Undesirable "on-target" indel mutations can also be introduced at the target site, even in cells where the reporter construct has been successfully integrated, if a double-strand break was induced in both alleles of the target gene and one allele was repaired by non-homologous end joining instead of homology-directed repair [298]. One strategy to reduce the frequency of such mutations is to use a Cas9-Geminin fusion protein, which is proteolytically degraded in the late M and G1 phase of the cell cycle where non-homologous end joining is the dominant repair pathway [310].

We used the workflow developed by Howden *et al*. for generating reporter iPSC lines using CRISPR/Cas9 (see section 3.2 for details) [311]. Briefly, fibroblasts were electroporated to simultaneously introduce episomal reprogramming plasmids, Cas9-Geminin mRNA, a plasmid for transcribing the guide RNA, and a plasmid with the reporter construct. This simultaneous reprogramming and gene editing strategy allows clonal iPS colonies to be selected and screened by PCR for successful reporter insertion without antibiotic selection or single-cell dissociation and replating.

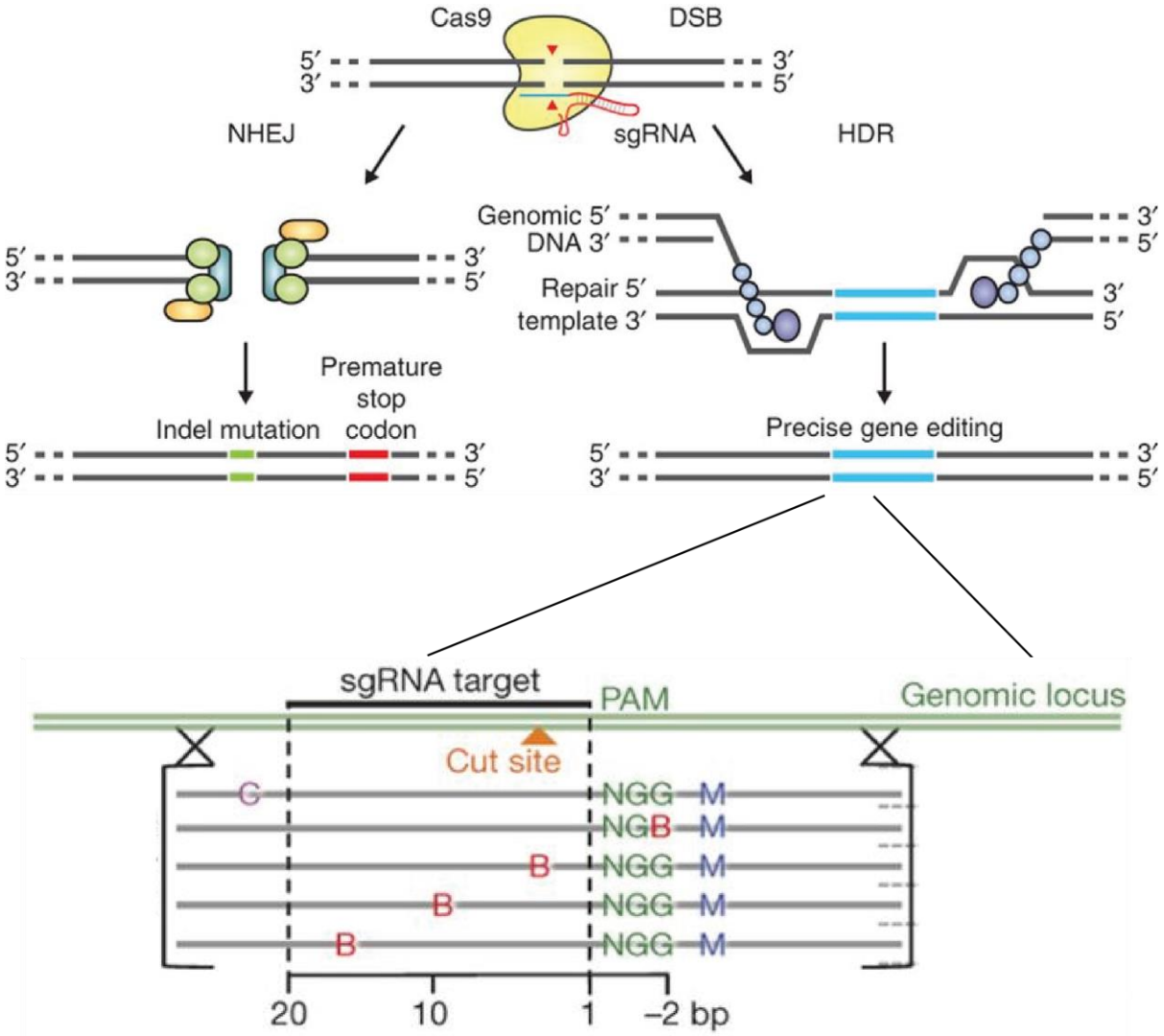

Figure 3.1 Schematic of CRISPR/Cas9 gene editing (adapted from Ran *et al.*[312] and Paquet *et al.*[313]) . The CRISPR/Cas9 complex recognises a target site in DNA which is complementary to the guide sequence within the sgRNA and induces a double-strand break (DSB). This can be repaired by non-homologous end joining (NHEJ), which is error-prone and may introduce indel mutations, or by homology-directed repair (HDR). In gene editing to create a reporter line, a repair template for HDR which contains the reporter construct is provided, so that the reporter construct is integrated into the gene when the DSB is repaired. The repair template can also include synonymous base changes (red Bs) within the target site or protospacer adjacent motif (PAM) so that once the reporter construct is integrated, it cannot be re-targeted and cleaved by the CRISPR/Cas9 complex.

3.1.2 Genes for proximal tubule reporter lines

To generate a reporter line for characterising proximal tubule cells, we first had to identify genes which were specifically expressed in the proximal tubule. Previous analysis of a scRNA-seq dataset from E18.5 mouse kidney (described in Chapter 2) identified genes which

were specific to the early proximal tubule and proximal tubule clusters and showed high average log-fold changes, suggesting strong expression. From these, we selected target genes which had a well-described role in the mature proximal tubule according to previous literature. Hence, to characterise proximal tubules in organoids, we created two proximal tubule reporter iPSC lines, *LRP2*:mTagBFP2 and *HNF4A*:YFP (Table 3.1). The role of these genes in the proximal tubule is detailed later in this chapter.

A fluorescent or bioluminescent reporter of proximal tubule injury would be a useful tool for high-throughput *in vitro* screening for nephrotoxicity. As discussed in Chapter 1, much work has been done to identify potential biomarkers of renal injury *in vivo* which have better sensitivity and specificity than the current standard measures of kidney function (serum creatinine and blood urea nitrogen) [12,116]. In a clinical setting, these biomarkers can be functional biomarkers associated with loss of glomerular barrier function or tubular reabsorption (i.e. proteins or molecules found in serum which would not normally appear in the urine), tubular cell proteins which are released into the urine following epithelial cell injury, or proteins which are upregulated by the renal cells themselves in response to injury [139]. Of these, upregulated proteins may represent suitable loci for creating a proximal tubule injury reporter line. Based on a review of the literature (elaborated on in Chapter 1 and later in this chapter), we chose *HAVCR1* (KIM-1) as the target gene for an injury reporter line [12].

In summary, our aims for this chapter were:

i) to develop *LRP2*:mTagBFP2 and *HNF4A*:YFP fluorescent reporter lines for characterising proximal tubule differentiation

ii) to develop a *HAVCR1*:mCherry fluorescent reporter line for detecting proximal tubule injury *in vitro*

iii) to validate these reporter lines by differentiating them into kidney organoids and confirming appropriate reporter expression.

3.1.2.1 *LRP2* (Megalin)

LRP2 (low density lipoprotein-related receptor 2, also known as megalin) is located on chromosome 2 (2q31.1) and is a multiligand endocytotic receptor expressed in multiple tissues. *LRP2* expression was previously detected in kidney organoids generated by our group using bulk RNA-seq [113]. During renal development in humans, *LRP2* is expressed in the

medial segment of the S-shaped body [20]. In the adult human, *LRP2* is highly expressed in the proximal tubule and to a lesser extent in podocytes [314,315]. LRP2 mediates the nephrotoxicity of certain drugs, including aminoglycoside antibiotics, as evidenced by studies demonstrating that the toxicity of these drugs is attenuated in conditional *Lrp2* knockout models or when Lrp2 ligand binding is inhibited [66,67]. As LRP2 is expressed during renal development and in organoids, has sustained or increased expression in mature proximal tubules, and has a functional role in mediating nephrotoxicity, we decided that *LRP2* was a suitable locus for targeting to generate a proximal tubule reporter line. We selected a blue fluorescent protein as the reporter for this cell line for two reasons. The first was that we intended to assay proximal tubule function by visualising the uptake of fluorescent substrates, most of which intrinsically emit green fluorescence. The second was to facilitate future use of this reporter construct with the *HAVCR1*:mCherry reporter construct (described later in this chapter) to create a dual reporter line after the completion of the current project. We chose mTagBFP2 as it is photostable, fast-maturing, and one of the brightest blue proteins available to date [316,317].

3.1.2.2 HNF4α

Hepatocyte nuclear factor 4 alpha (HNF4α) is located on chromosome 20 (20q13.12) and is a transcription factor which is expressed in multiple tissues, including the liver, pancreas, gut, and kidney [318]. There are multiple isoforms which are transcribed from two promoters with differing tissue specificities [318]. In the kidney, the shorter transcripts from the P1 promoter are predominant [318]. Within the mouse and rat kidney, *Hnf4a* expression is specific to early and mature proximal tubules [216,319]. Several genes expressed in mature proximal tubules, including functional markers such as the solute channel transporters, have HNF4α binding sites in their promoters, suggesting that HNF4α regulates their expression [213,260]. In support of this, a specific *HNF4A* missense mutation in humans is associated with autosomal dominant Fanconi renotubular syndrome, a disorder where reabsorption of water and organic solutes by the proximal tubule is impaired [319]. Kidney-specific deletion of *Hnf4a* in rats leads to Fanconi-like symptoms, consistent with a role for Hnf4α in regulating the expression of proximal tubule transporter proteins [319]. Given that *HNF4A* within the kidney is expressed specifically in developing and mature proximal tubules and is likely to be a key regulator of the mature proximal tubule phenotype, we chose *HNF4A* as another suitable locus for a proximal tubule reporter line. Despite our previously stated preference for a blue reporter, blue fluorescent proteins are still generally considered challenging to detect [317], and this was indeed the case with the equipment available to us. Hence, yellow fluorescent protein (YFP)

was chosen as the reporter for this cell line, even though we could not spectrally separate it from green fluorescence for proximal tubule function assays.

3.1.2.3 *HAVCR1* (KIM-1)

Kidney injury molecule 1 (KIM-1; gene symbol *HAVCR1*) is located on chromosome 5 (5q33.3) and is a type I membrane glycoprotein that is expressed in the liver, in activated immune cells, and in proximal tubules following injury [117,118]. In injured proximal tubule cells, KIM-1 acts as a phagocytic receptor, enabling surviving tubular cells to remove apoptotic debris [119]. In rats and humans *in vivo*, urinary KIM-1 concentration is a more specific and sensitive readout of acute kidney injury than serum creatinine and blood urea nitrogen, and is approved by the FDA and EMEA as a biomarker for monitoring drug-induced nephrotoxicity in pre-clinical trials in addition to standard serum creatinine and blood urea nitrogen measurements [120–123]. However, in an *in vitro* setting, a number of studies of primary proximal tubule cells or cell lines were unable to consistently detect significant differences in KIM-1 expression between controls and cultures exposed to nephrotoxicants [124–127]. We hypothesised that this was because the models used were not adequately replicating the *in vivo* proximal tubule identity, or lacked additional renal cell types which were required for inducing KIM-1 expression [12]. To determine if our organoids could more accurately replicate the *in vivo* injury response, we proceeded to target *HAVCR1* to create a specific reporter of proximal tubule injury.

Table 3.1 Reporter lines generated for characterising proximal tubules in organoids.

Gene targeted	NCBI reference sequence	Common name	Reporter	Targeting approach	Parental line	Reporter expression
LRP2	NM_004525.3	Megalin	mTagBFP2	3', T2A polyA	CRL-2429 (ATCC)	Proximal tubule
HNF4A	NM_001287182.2	HNF4α	YFP	3', T2A polyA	PCS-201-010 (ATCC)	Proximal tubule
HAVCR1	NM_001308156.1	KIM-1	mCherry	5', T2A	CRL-2429 (ATCC)	Proximal tubule after acute injury

3.2 Methods

3.2.1 Simultaneous gene editing and reprogramming of fibroblasts

All reporter lines used in this project were generated according to the method of Howden *et al.* [311]. Guide RNAs (sgRNAs) for the genes of interest were designed by entering regions of each gene into http://www.rgenome.net/cas-designer/, then selecting sgRNAs which had binding sites close to the intended knock-in site and had low predicted off-target activity (Table 3.2). Reporter templates were ordered as double-stranded linear DNA fragments (gBlocks, Integrated DNA Technologies). Oligonucleotides for sgRNAs were ligated into pSMART-sgRNA (Sp) plasmids (Addgene ID 80427), while gBlocks were ligated into pDNR-Dual plasmids (Clontech), hereafter sgRNA and template plasmids respectively. Plasmids were transformed into DH5α chemically competent cells (Bioline, catalogue number BIO-85047) according to manufacturer's instructions for expansion and then purified using a Plasmid Midi Kit (QIAGEN).

For reprogramming and gene targeting, fibroblasts were transfected using the Neon® Transfection System (Thermofisher). Commercially available fibroblasts were maintained in T175 flasks. Transfections were performed two days after cells were passaged. On the day of transfection, fibroblasts were detached with TrypLE Select, re-suspended in fibroblast medium and centrifuged at 300 ×g for 3 minutes. Then, cells were re-suspended in PBS and cell density was determined with a haemocytometer, before centrifuging and gently re-suspending cells in Resuspension Buffer R to a final density of 1×10^7 cells/mL. A Neon® pipette station was set up with a Neon® tube and 3 mL Electrolytic Buffer E2 and set to 1400 V, 20 ms, two pulses. The cell transfection mixture in Table 3.4 was aspirated into a 100 µL Neon® tip and cells were electroporated according to manufacturer's instructions. Cells were immediately transferred to a 6-well plate with 2 mL pre-warmed fibroblast medium and incubated at 37° C. Where needed, fibroblast medium was changed after 24 hours to remove cell debris. On day 3 or 4 after transfection, fibroblast medium was removed and replaced with TeSR-E7 (Stemcell Technologies) supplemented with 100 µM sodium butyrate. Media was changed every two days until iPSC colonies appeared two weeks post-transfection. At this point, the media was changed to E8 medium (Thermofisher) and changed daily. When iPSC colonies reached ~1 mm in diameter, individual colonies were picked and placed into separate wells of 24-well plates coated with Matrigel.

Table 3.2 sgRNA sequences for gene editing of reporter lines.

Line	Sequence (5'→3')
HAVCR1:mCherry	GACCACTTGAGGATGCATTA
LRP2:mTagBFP2	GGAGTTGGGTCTCTTCTCGA
HNF4A:YFP	TTCCCCACTGTGCCGCTTT

Table 3.3 Oligonucleotides for encoding protospacers. N denotes the sequence of the gene-specific sgRNAs in Table 3.2. The underlined G residue indicates the transcription start site and replaces the first residue of the sgRNA sequence if the sequence does not already begin with G.

Oligonucleotide	Sequence (5'→3')
sgRNA-top	CACC**G**NNNNNNNNNNNNNNNNNNN
sgRNA-bottom	AAACNNNNNNNNNNNNNNNNNNNC

Table 3.4 Mixture for transfecting fibroblasts with reprogramming and gene editing factors.

Component	Amount
Fibroblast suspension (1×10^7 cells/mL in Resuspension Buffer R)	100 µL
pEP4 E02S ET2K (reprogramming)	2.5 µg
pEP4 E02S EN2L (reprogramming)	2.5 µg
pEP4 E02S EM2K (reprogramming)	2.5 µg
pSimple-miR302/367 (reprogramming)	2.5 µg
Template plasmid (gene editing)	5 µg
sgRNA plasmid (gene editing)	2 µg
EBNA1 mRNA (gene editing)	5 µg
Cas9-Geminin mRNA (gene editing)	5 µg

3.2.2 iPSC clone screening and genotyping

Once iPSC colonies in 24-well plates had grown to a suitable size, they were split to replica plates and maintained with standard feeder-free iPSC culture methods. Cells in the original plate were allowed to grow to confluence. These cells were then dissociated with TrypLE Select, re-suspended in 50 µL TE buffer, and placed in a boiling water bath for 5-10 minutes for rapid extraction of DNA. PCR screening was performed on 5 µL of each sample using the reagents, conditions, and primers in Table 3.5, Table 3.6 and Table 3.7 respectively. Products were run at 100 V for 1 hour on 1% agarose gel (Bioline) with GelRed or RedSafe and then imaged on a G:BOX system (Syngene).

To confirm successful knock-in of the reporter in positive clones and to determine whether clones were heterozygous or homozygous for the reporter, cells were dissociated with TrypLE Select and harvested in PBS for genomic DNA extraction using a DNeasy Blood and Tissue Kit (Qiagen). This was to facilitate PCR of longer amplicons compared to the initial colony screen when needed. PCR was performed on 5 µL of each sample using the reagents, conditions, and primers in Table 3.5, Table 3.6 and Table 3.7 respectively.

For heterozygous clones, the untargeted allele was sequenced to determine if mutations had been introduced at the target site. The region of the untargeted allele surrounding the target site was amplified by PCR using primers 1 and 3 for each line. PCR products were treated with 1 µL exonuclease I (NEB) and 1 µL rAPid alkaline phosphatase (Sigma) at 37° C for 30 minutes, followed by enzyme inactivation at 80° C for 10 minutes. Treated products were then sequenced using the BigDye Terminator v3.1 Cycle Sequencing Kit (Thermofisher) and the primers in Table 3.8 according to manufacturer's instructions. Cycling conditions are listed in Table 3.9. Capillary separation and base-calling of the sequencing products was performed by the Australian Genome Research Facility.

All lines generated were checked for karyotypic abnormalities by SNP analysis (Illumina Infinium GSA-24 v1.0) performed by Victorian Clinical Genetics Services and confirmed to be mycoplasma-free through the MCRI Tissue Culture Team.

Gene editing and screening for the *HNF4A*:YFP cell line was performed by the MCRI Gene Editing Facility.

Table 3.5 General PCR reagents.

Component	Volume (µL)	Final concentration
GoTaq® Green Master Mix (2×) (Promega)	12.5	1×
Forward primer (10 µM)	1	400 nM
Reverse primer (10 µM)	1	400 nM
Nuclease-free H_2O	5.5	-

Table 3.6 General PCR cycling conditions, performed on a C1000 Touch™ Thermal Cycler (Bio-Rad) or a Veriti™ 96-Well Thermal Cycler (Thermofisher).

Temperature (°C)	Time	Cycles
95	3 min	1
95	22 s	35
55	22 s	
72	1 min	
72	7 min	1

Table 3.7 PCR primers for reporter iPSC clone screening and genotyping.

Line	Name	Sequence (5'→3')
HAVCR1:mCherry	Primer 1: KIM-1 F	GCTCCACGTCCACCAGAGG
	Primer 2: mCherry R	GAGCCGTACATGAACTGAGG
	Primer 3: KIM-1 seqR	TCTGGTCCTGCTCACTAG
LRP2:mTagBFP2	Colony screen: BFP2 screen2F	CACCGTGGACAACCATCACT
	Colony screen: BFP2 screen2R	TGAAGGTCTTGCTGCCGTAG
	Primer 1: LRP2 screenF	TGTGACACAGGAGGGAATGA
	Primer 2: BFP2 screenR	GCTTCATGTGCATGTTCTCC
	Primer 3: LRP2 seqR-Out	GTGGCCCCTATCAACATAGC
HNF4A:YFP	Primer 1: HNF4A seqF	CGATCCAGGGAAGATCAAGC
	Primer 2: T2A screenR	GGATTCTCCTCCACGTCACC
	Primer 3: HNF4A 3' R	CAGCCGTTAGGGTCTTAGCA

Table 3.8 PCR primers for sequencing reporter iPSC lines.

Line	Targeted/untargeted allele	Primer sequences (5'→3')
HAVCR1:mCherry	Untargeted	TCTGGTCCTGCTCACTAG
LRP2:mTagBFP2	Untargeted	GTGGCCCCTATCAACATAGC

Table 3.9 Cycling conditions for sequencing of PCR products with BigDye Terminator v3.1, performed on a C1000 Touch™ Thermal Cycler (Bio-Rad) or a Veriti™ 96-Well Thermal Cycler (Thermofisher).

Temperature (°C)	Time	Cycles
96	1 min	1
96	10 s	25
50	5 s	
60	4 min	

3.2.3 Drug toxicity screening of HAVCR1:mCherry reporter line

Swirler micro-organoids were differentiated from the *HAVCR1*:mCherry reporter line using the methods described in Chapter 7. At D7+18, micro-organoids were treated with saline (control), 20 μM DBL™ cisplatin, saline with an efflux inhibitor cocktail MKKOP (5 μM MK571, 5 μM KO143, and 5 μM PSC833 [Sigma]) or cisplatin with MKKOP. After incubation for 24 hours, micro-organoids were taken for flow cytometry, immunofluorescence, and qRT-PCR analysis as described in Chapter 7.

3.3 Targeting of fluorescent reporters and screening for successful targeting

3.3.1 CRL-2429 LRP2:mTagBFP2

Using the simultaneous reprogramming and gene targeting method described in section 3.2, mTagBFP2 was targeted to the 3' end of *LRP2* in CRL-2429 fibroblasts (Figure 3.2A). We verified successful ligation of sgRNA into plasmids by Sanger sequencing. To verify ligation of the homologous repair template with the reporter construct into the template plasmid, we performed a restriction digest using *Eco*RI and *Sty*I, which would produce two bands (2638 bp and 1992 bp) in plasmids with the repair template, but only one in plasmids without (Figure 3.2B and C).

After gene editing and reprogramming of fibroblasts using the sgRNA plasmid and template plasmid, four heterozygous targeted clones were identified (Figure 3.2D). Two clones (6 and 12) had indels in the untargeted allele identified by Sanger sequencing, and two clones had mixed chromatogram peaks after the target site, suggesting that they were mixtures of clones with and without indels, or with different indels, at the target site (Figure 3.3A).

Though attempts to subclone the putative mixed clones were unsuccessful, we concluded that differentiation of the pure mutated clones into organoids with developing proximal tubules would not be impaired, for the following reasons. As late premature stop codons are less likely to trigger nonsense-mediated decay than early premature stop codons, mRNA transcribed from the slightly truncated mutant alleles may still be functional [320]. Assuming that this mRNA is translated, the resulting protein would have a truncated cytoplasmic domain lacking a synectin (*GIPC1*) binding motif [321] (Figure 3.3B). *Gipc1*-null mice develop proteinuria and show perturbed Lrp2 localisation in their proximal tubules (in addition to extra-renal changes), showing that synectin binding is required for Lrp2-dependent endocytosis [322,323]. However, the *Gipc1*-null phenotype is milder than the *Lrp2*-null

phenotype, as *Lrp2*-null mice die shortly after birth [324]. This suggests that loss of synectin binding does not lead to complete loss of LRP2 function, although the compensatory mechanism may still rely on the synectin binding motif. It is also possible that the function of Lrp2 which is linked to *Lrp2*-null lethality is not endocytosis *per se*. Nevertheless, even if the mutant allele is completely non-functional, the reporter construct for this cell line should not lead to knockout of the targeted allele, and no *LRP2* haploinsufficiency or dominant-negative phenotype has been reported to date. Hence, we considered it likely that clones 6 and 12 could still be differentiated into organoids with proximal tubules. Clone 6 was chosen for subsequent experiments. No chromosomal abnormalities were detected by molecular karyotyping.

3.3.2 PCS-201-010 HNF4A:YFP

Construct design, targeting, and screening of this reporter line were performed by the MCRI Gene Editing Core Facility. As nonsense mutations in *HNF4A* are known to cause autosomal dominant disorders such as young-onset diabetes [325], the targeting strategy and reporter construct were designed to avoid disrupting *HNF4A* expression. YFP was targeted to the 3' end of *HNF4A* variant 8 (which has eight exons instead of ten, and is one of the variants transcribed from the kidney-predominant P1 promoter[318]) in PCS-201-010 fibroblasts (Figure 3.2A). Clone 16 was identified as a homozygous targeted clone (Figure 3.2D). No chromosomal abnormalities were detected by molecular karyotyping.

3.3.3 CRL-2429 HAVCR1:mCherry

mCherry was targeted to the 5' end of *HAVCR1* in CRL-2429 fibroblasts (Figure 3.2A). As before, successful ligation of sgRNA plasmids was verified by Sanger sequencing. Ligation of template plasmids was verified by a restriction digest with *Kpn*I, which would produce three bands (2781 bp, 980 bp, and 340 bp) in plasmids with the repair template, and only one band in plasmids without (Figure 3.2B and C). Of the three targeted clones, clone 1 was heterozygous and harboured a large deletion in the untargeted allele which was detectable by PCR (Figure 3.2D). Clones 18 and 47 were heterozygous targeted clones with no mutations in the untargeted allele (Figure 3.3A). Clone 18 was chosen for subsequent work, as no chromosomal abnormalities were detected by molecular karyotyping prior to the experiments conducted for this project. However, later G-banding performed by collaborators (Washington University) detected a balanced translocation between the long arms of chromosomes 9 and 22 [t(9;22)(q22;q13)].

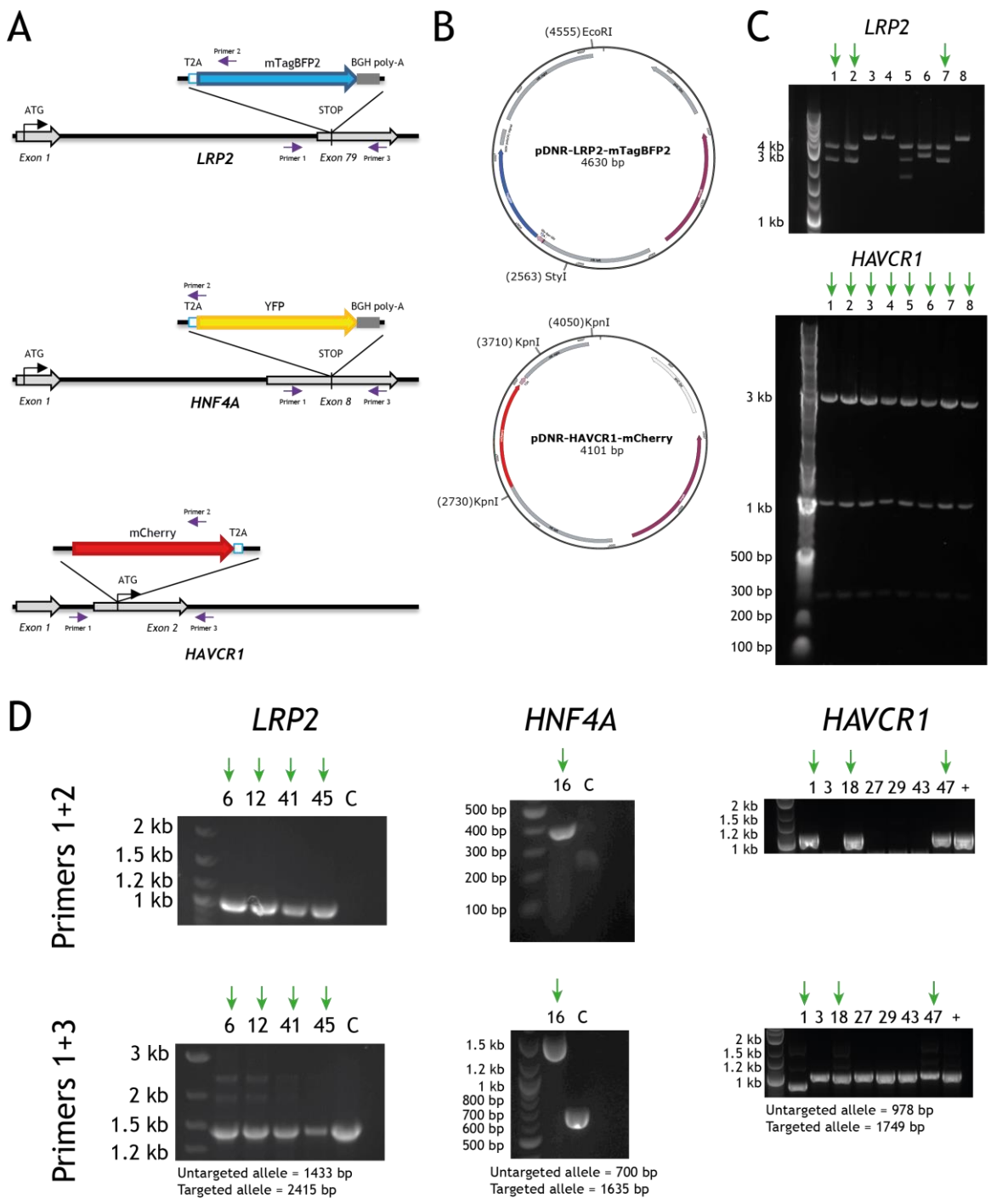
A
Primer 2
T2A
mTagBFP2
BGH poly-A
ATG
STOP
Exon 1
LRP2
Primer 1
Exon 79
Primer 3
Primer 2
T2A
YFP
BGH poly-A
ATG
STOP
Exon 1
HNF4A
Primer 1
Exon 8
Primer 3
Primer 2
mCherry
T2A
ATG
Exon 1
Primer 1
Exon 2
Primer 3
HAVCR1
B
(4555) EcoRI
pDNR-LRP2-mTagBFP2
4630 bp
(2563) StyI
(4050)KpnI
(3710) KpnI
pDNR-HAVCR1-mCherry
4101 bp
(2730)KpnI
C
LRP2
1 2 3 4 5 6 7 8
4 kb
3 kb
1 kb
HAVCR1
1 2 3 4 5 6 7 8
3 kb
1 kb
500 bp
300 bp
200 bp
100 bp
D
LRP2
HNF4A
HAVCR1
Primers 1+2
6 12 41 45 C
2 kb
1.5 kb
1.2 kb
1 kb
16 C
500 bp
400 bp
300 bp
200 bp
100 bp
1 3 18 27 29 43 47 +
2 kb
1.5 kb
1.2 kb
1 kb
Primers 1+3
6 12 41 45 C
3 kb
2 kb
1.5 kb
1.2 kb
Untargeted allele = 1433 bp
Targeted allele = 2415 bp
16 C
1.5 kb
1.2 kb
1 kb
800 bp
700 bp
600 bp
500 bp
Untargeted allele = 700 bp
Targeted allele = 1635 bp
1 3 18 27 29 43 47 +
2 kb
1.5 kb
1.2 kb
1 kb
Untargeted allele = 978 bp
Targeted allele = 1749 bp

Figure 3.2 Targeting strategies and screening for proximal tubule and injury reporter lines. A: Reporter constructs, knock-in sites, and binding sites of the screening primers used for the *LRP2*, *HNF4A*, and *HAVCR1* (KIM-1) reporter lines. T2A sequences encode a self-cleaving T2A peptide, allowing expression of the endogenous protein and the reporter from the same promoter without disrupting the function of either protein [326]. B: Maps of the template plasmids for the *LRP2* and *HAVCR1* reporter lines, showing plasmid features (white and purple arrows), the repair template including the reporter gene (grey blocks flanking blue and red arrows respectively), and the restriction sites which distinguish successfully ligated plasmids. C: Gel electrophoresis of restriction digest screening to detect ligation of *LRP2* and *HAVCR1* reporter constructs into plasmids to use in gene editing. Green arrows indicate clones with the expected number of bands for successfully ligated plasmids. (Apparent band sizes may have been altered by the addition of GelRed prior to electrophoresis). D: PCR screening for successfully targeted iPSC clones of *LRP2*, *HNF4A*, and *HAVCR1* reporter lines. Primer 1 binds outside the insertion site, while primer 2 binds to the reporter construct (see panel A). Hence amplification with primers 1+2 indicates successful targeting in at least one allele in a given clone. Green arrows indicate targeted clones. Primers 1+3 flank the insertion site and produce a shorter band when an untargeted allele is present and can be preferentially amplified (i.e. in heterozygous targeted clones which have one targeted allele detected by primer 1+2 PCR and one untargeted allele, or in untargeted clones), but produce a longer band in homozygous clones where only the targeted allele is present. The amplification bias is such that the longer band is often weak or absent in heterozygous clones[311]. C = untargeted iPSC control, + = pooled DNA from electroporated cells, expected to contain both targeted and untargeted cells.

A

LRP2:mTagBFP2

HAVCR1:mCherry

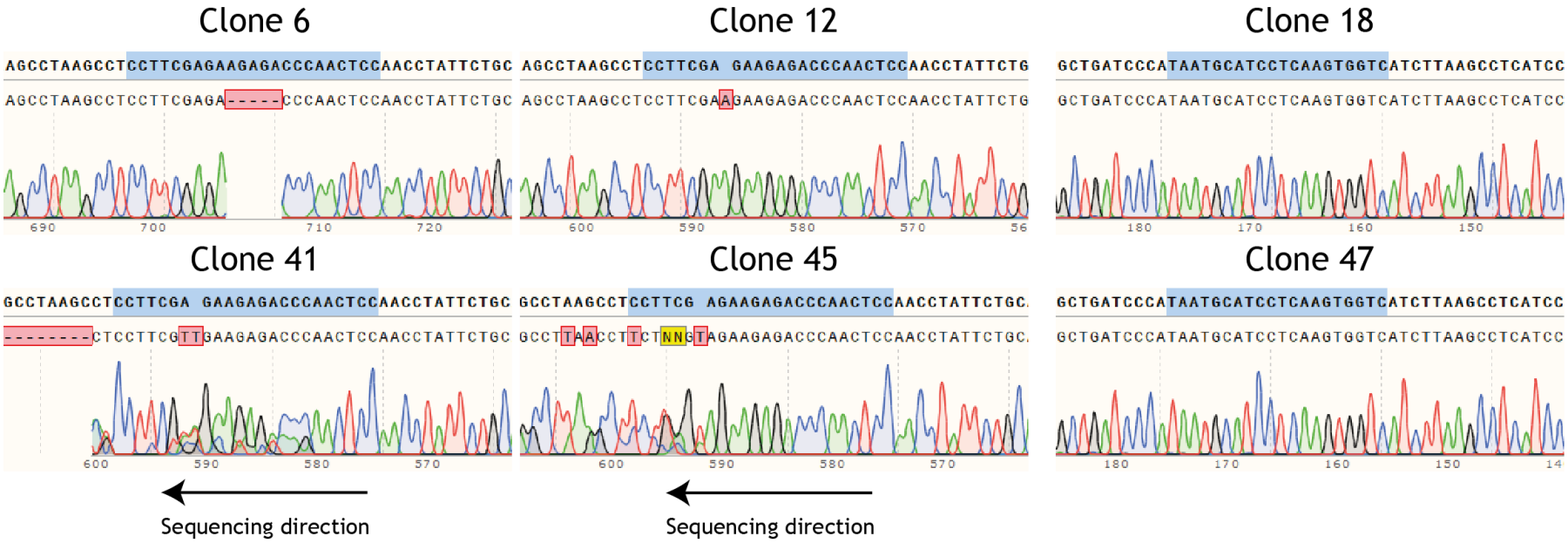

B

Wild type	CCT	TCG	AGA	AGA	GAC	CCA	ACT	CCA	ACC	TAT	TCT	GCA	ACA	GAA	GAC	ACT	TTT	AAA	GAC	ACC	GCA	AAT	CTT	GTT	AAA	GAA	GAC	TCT	GAA	GTA	TAG	
	Pro	Ser	Arg	Arg	Asp	Pro	Thr	Pro	Thr	Tyr	Ser	Ala	Thr	Glu	Asp	Thr	Phe	Lys	Asp	Thr	Ala	Asn	Leu	Val	Lys	Glu	Asp	Ser	Glu	Val	*	
Clone 6	CCT	TCG	AGA	---	--C	CC	AAC	TCC	AAC	CTA	TTC	TGC	AAC	AGA	AGA	CAC	TTT	TAA	AGA	CAC	CGC	AAA	TCT	TGT	TAA	AGA	AGA	CTC	TGA	AGT	ATA	G
	Pro	Ser	Arg			Pro	Asn	Ser	Asn	Leu	Phe	Cys	Asn	Arg	Arg	His	Phe	*														
Clone 12	CCT	TCG	AAG	AAG	AGA	CCC	AAC	TCC	AAC	CTA	TTC	TGC	AAC	AGA	AGA	CAC	TTT	TAA	AGA	CAC	CGC	AAA	TCT	TGT	TAA	AGA	AGA	CTC	TGA	AGT	ATA	G
	Pro	Ser	Lys	Lys	Arg	Pro	Asn	Ser	Asn	Leu	Phe	Cys	Asn	Arg	Arg	His	Phe	*														

Figure 3.3 Sequence validation of proximal tubule and injury reporter lines. A: Sanger sequencing of the untargeted alleles in heterozygous clones obtained from gene editing showing mutations in all *LRP2*:mTagBFP2 clones and no mutations in *HAVCR1*:mCherry clones. Bold sequence indicates wild-type. Bases highlighted in blue indicate the Cas9 target site, where Cas9-induced indels will occur if present. Bases or dashes in red indicate indels in the clones found by alignment to the wild-type sequence. Yellow Ns indicate base-calling failure. The sudden appearance of mixed signals when sequencing past the target site suggested that clones 41 and 45 were mixed clones. B: Comparison of DNA sequence and predicted amino acid sequence in wild-type *LRP2* and the untargeted alleles of clones 6 and 12. The indels cause a short frameshift (red) and introduce a premature stop codon. If the transcript is stable and is translated, the resulting protein would have a truncated cytoplasmic domain which lacks the GIPC binding motif (blue in wild-type).

3.4 Validation of differentiation and reporter expression in *LRP2:*mTagBFP2 and *HNF4A:*YFP reporter lines

LRP2:mTagBFP2 and *HNF4A*:YFP iPSCs were differentiated into kidney organoids using standard protocols (refer to Chapter 7 for more details). For both cell lines, fluorescent protein expression was detectable in tubules upon live microscopy and in dissociated organoids by flow cytometry, although YFP was consistently easier to detect using these methods (Figure 3.4A).

Immunofluorescence staining showed that the organoids differentiated from these reporter cell lines had developing glomeruli ($NPHS1^+$), proximal tubules (LTL^+), distal tubules ($ECAD^+$), and ureteric epithelium ($GATA3^+$), consistent with our differentiations of other cell lines (Figure 3.4A). In both cell lines, fluorescent protein was co-expressed with the targeted gene and with other markers of the developing proximal tubule (Figure 3.4B). Tubules expressing fluorescent protein were also capable of albumin uptake, a hallmark of proximal tubules (Figure 3.4C) [12]. This also suggests that the heterozygous mutation observed in the untargeted allele of the *LRP2*:mTagBFP2 reporter line does not lead to total loss of endocytotic function, even if there was an as-yet-undetermined reduction in uptake rate or capacity.

After FACS to isolate cells which expressed reporter proteins, *LRP2* and *HNF4A* expression was enriched in reporter$^+$ cells, while *GATA3* (a marker of ureteric epithelium and renal stroma which is not expressed in the proximal tubule) was depleted (Figure 3.4D). *LRP2* expression was also enriched in the YFP^- population relative to the undissociated, whole organoid, suggesting that there were cells that express *LRP2* without expressing *HNF4A*. This is consistent with reports that *LRP2* is also expressed in podocytes in humans [315]. However,

in immunofluorescence staining of our organoids, mTagBFP2 expression was strongest in tubules which were LRP2^{+}, and we were not able to detect LRP2 in podocytes (Figure 3.4Bi). Taken together, these findings show that the *LRP2*:mTagBFP2 and *HNF4A*:YFP reporter lines identify developing proximal tubules in organoids.

Live images and flow cytometry over the course of organoid culture showed that the percentage of mTagBFP2^{+} cells increased from D7+8 (where fluorescence was nearly undetectable) to D7+14 and then decreased at D7+19, while YFP^{+} cells were first observable at D7+8 and increased until D7+18 (Figure 3.5). Consistent with observations throughout this project, YFP^{+} cells showed more distinct separation from non-specific fluorescent events than mTagBFP2^{+} cells and YFP^{+} tubules were more easily detected by live microscopy. The earlier appearance of *HNF4A*-driven YFP compared to *LRP2*-driven mTagBFP2 was consistent with predictions from the bioinformatics analysis and literature review described in previous chapters. HNF4α is a transcription factor regulating the proximal tubule phenotype that is expressed at roughly the same level in the early and mature proximal tubule, while LRP2 is a functional protein that is expressed in both early and mature proximal tubule but is also significantly upregulated in the mature proximal tubule compared to the early proximal tubule. This provides a brief demonstration of how the *LRP2*:mTagBFP2 and *HNF4A*:YFP reporter lines can be used to monitor proximal tubule development *in vitro*.

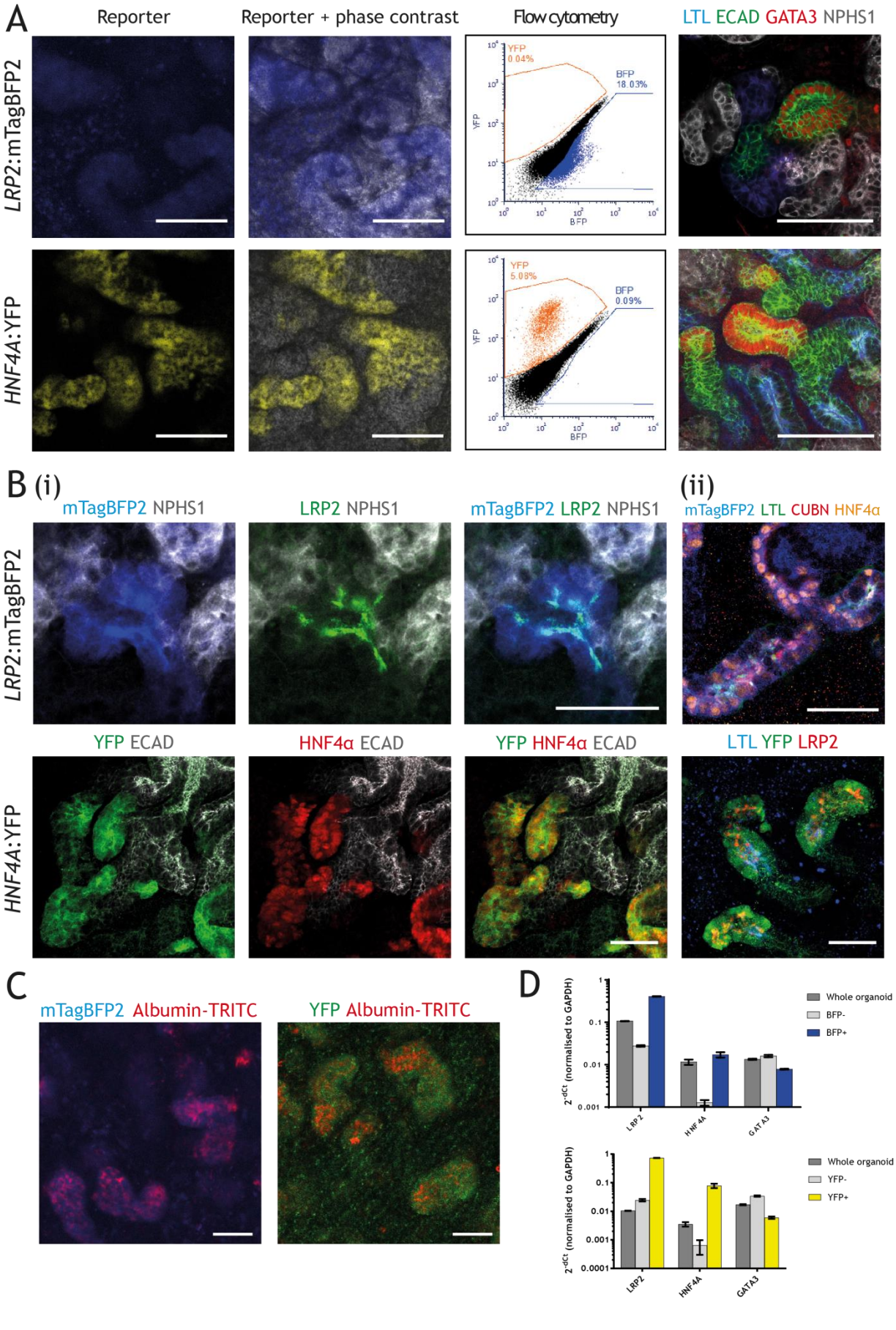
A
Reporter
Reporter + phase contrast
Flow cytometry
LTL ECAD GATA3 NPHS1
LRP2:mTagBFP2
HNF4A:YFP
YFP 0.04%
BFP 18.03%
YFP 5.08%
BFP 0.09%
B (i)
mTagBFP2 NPHS1
LRP2 NPHS1
mTagBFP2 LRP2 NPHS1
(ii)
mTagBFP2 LTL CUBN HNF4α
YFP ECAD
HNF4α ECAD
YFP HNF4α ECAD
LTL YFP LRP2
C
mTagBFP2 Albumin-TRITC
YFP Albumin-TRITC
D
2-dCt (normalised to GAPDH)
Whole organoid
BFP-
BFP+
LRP2
HNF4A
GATA3
Whole organoid
YFP-
YFP+

Figure 3.4 Validation of *LRP2*:mTagBFP2 and *HNF4A*:YFP reporter lines for monitoring proximal tubule development. A: Live microscopy and flow cytometry of D7+13-16 organoids (scale bars 100 μm). Separation between fluorescent protein $(FP)^+$ and FP^- populations was more distinct for YFP than mTagBFP2. Immunofluorescence staining of D7+18 organoids differentiated from these cell lines showed that glomeruli ($NPHS1^+$), proximal tubules (LTL^+), distal tubules ($ECAD^+$) and collecting ducts ($ECAD^+$ $GATA3^+$) were all present. Scale bars 100 μm. B: Immunofluorescence staining of D7+16-18 organoids for (i) fluorescent reporters and the targeted loci (LRP2 and HNF4α), as well as markers of the glomerulus and distal tubule (NPHS1 and ECAD), and (ii) fluorescent reporters and markers of the proximal tubule (LTL, CUBN, LRP2, and HNF4α). Scale bars 50 μm. C: Live microscopy of albumin labelled with TRITC in tubules expressing fluorescent reporters. Scale bars 50 μm. D: qRT-PCR of whole organoid lysates and FACS fractions ($reporter^+$ and $reporter^-$) from *LRP2*:mTagBFP2 organoids (D7+15) and *HNF4A*:YFP organoids (D7+18). Results from 3 technical replicates. Error bars ± SEM.

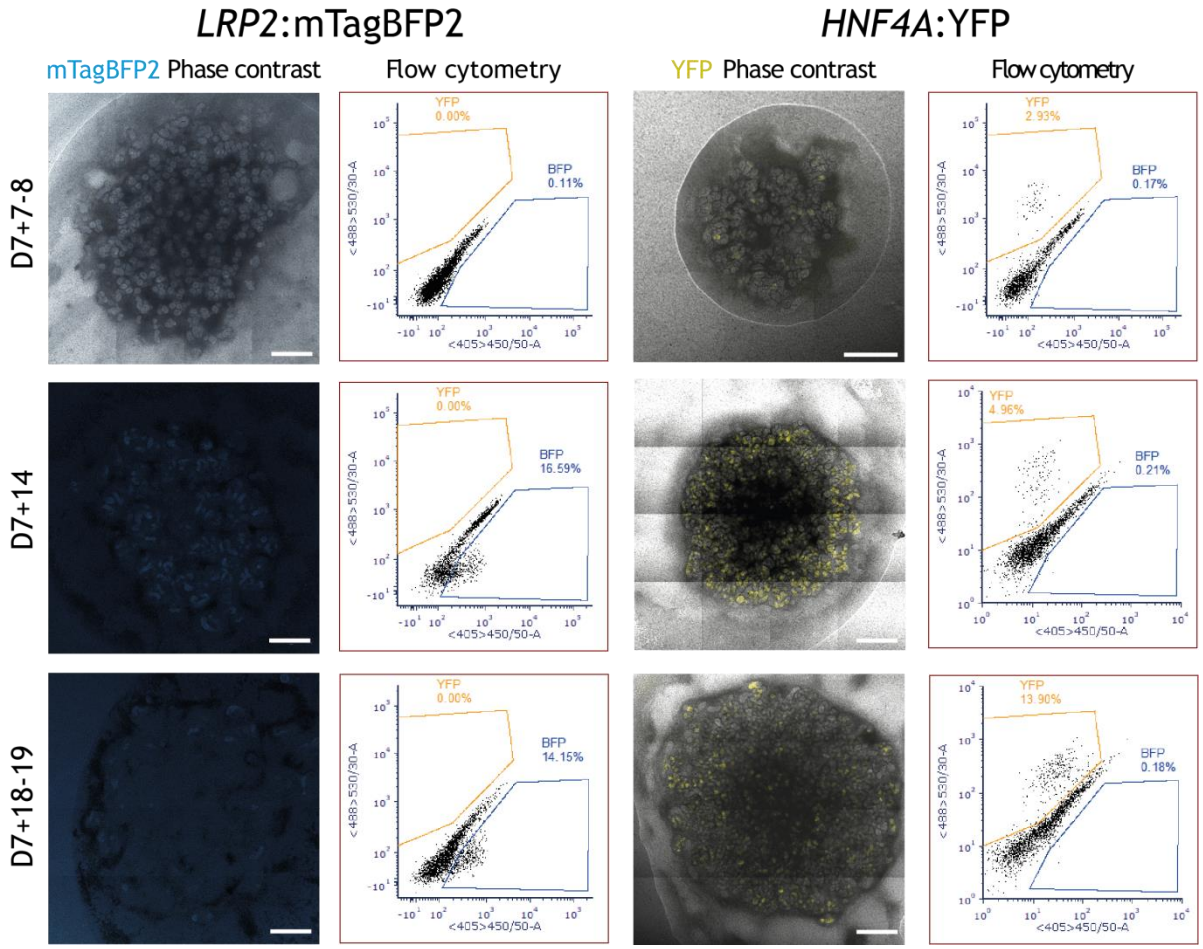

Figure 3.5 Live microscopy and flow cytometry show changes over time in the percentage of cells expressing mTagBFP2 (left, in blue) and YFP (right, in yellow) in organoids from the respective reporter lines. Flow cytometry gating for mTagBFP2 was performed using *HNF4A*:YFP organoids as a negative control, and vice versa. Phase contrast was omitted from D7+14 and D7+19 *LRP2*:mTagBFP2 images for visibility. For the *LRP2*:mTagBFP2 line, background subtraction was performed using ZEN image processing software (Zeiss) based on autofluorescence in 493-574 nm. Scale bars 500 µm.

3.5 Differentiation of *HAVCR1*:mCherry reporter into organoids and micro-organoids and their response to nephrotoxicants

To determine whether the *HAVCR1*:mCherry reporter line would be a useful tool for investigating nephrotoxic injury to the proximal tubule, we differentiated *HAVCR1*:mCherry reporter iPSCs to organoids using our standard protocol (details in Chapter 7), alongside a reporter line which expressed mCherry from an unrelated locus (*GATA3*:mCherry) as a control. A pilot assay was performed where *HAVCR1*:mCherry organoids were exposed to 20 µM cisplatin for 24 hours from D7+18. However, while we were able to detect specific red

fluorescence in tubules in the *GATA3*:mCherry organoids, which served as a positive control, we were unable to do so for *HAVCR1*:mCherry organoids (Figure 3.6A).

Kumar *et al*. [188] developed a method for culturing kidney micro-organoids in suspension, in contrast to the transwell-based culture used for most experiments during this project. We hypothesised that the smaller size of the micro-organoids and the suspension culture would allow any drugs in the culture medium to access cells more easily. Hence, for further investigation of the *HAVCR1*:mCherry reporter line, we differentiated *HAVCR1* reporter iPSCs to micro-organoids. However, like standard transwell organoids, *HAVCR1*:mCherry micro-organoids did not show red fluorescence in tubules after exposure to cisplatin (Figure 3.6A).

To confirm that this was not due to technical issues in detecting mCherry by live microscopy, micro-organoids were stained for proximal tubule markers and further analysed by qRT-PCR, flow cytometry, and immunofluorescence. *HAVCR1*:mCherry micro-organoids developed proximal tubules which were LTL^+ and $CUBN^+$, consistent with previous characterisation of proximal tubules in organoids differentiated using our standard methods [113] (Figure 3.6B). However, qRT-PCR of micro-organoids showed low expression of key SLC transporters compared to human foetal kidney or primary proximal tubule cells (Figure 3.6C). When micro-organoids were exposed to cisplatin, no significant change in *HAVCR1* (KIM-1) expression was observed between control and cisplatin conditions by qRT-PCR, and no increase in mCherry expression was detected by flow cytometry (Figure 3.6C and D). Immunofluorescence staining did not specifically detect mCherry expression in LTL^+ tubules either, although weak KIM-1 staining was observed (Figure 3.6D). Due to the lack of positive or negative controls for KIM-1 staining, non-specific binding of the KIM-1 antibody could not be ruled out. Increased cleaved caspase-3 staining was observed in organoids exposed to cisplatin, compared to controls, showing that the dose used was high enough to induce cell death (Figure 3.6D). However, this increased cell death was generally not within $HNF4\alpha^+$ segments. Therefore, cisplatin-induced injury in the micro-organoids was not specific to the proximal tubules, in which case KIM-1 expression would not have been expected to increase.

In addition to the influx transporters which serve as a route of entry for nephrotoxic drugs, proximal tubule cells also express efflux transporters such as MDR1 (gene symbol *ABCB1*), MRP4 (gene symbol *ABCC4*), BCRP (gene symbol *ABCG2*) and MATE-1 (gene symbol *SLC47A1*). MDR1, MRP4, and BCRP in particular are expressed more widely and earlier in

renal development compared to most of the influx transporters implicated in nephrotoxic injury of the proximal tubule [71,327,328]. *SLC47A1* expression in micro-organoids was also closer to (but still lower than) expression in human foetal kidney and primary proximal tubule cells, compared to the expression of *SLC22A2*, *SLC22A6*, or *CUBN*. Hence, it was possible that an imbalanced expression of these efflux transporters compared to influx transporters was making the micro-organoids resistant to cisplatin-induced injury. We hypothesised that inhibiting efflux transporters during drug exposure might exacerbate an injury response to detectable levels. However, while increased *HAVCR1* expression was observed by qRT-PCR in micro-organoids exposed to cisplatin and an efflux inhibitor cocktail (MKKOP) compared to micro-organoids exposed to MKKOP alone, this increase was not statistically significant ($p > .05$) (Figure 3.6C). Consistent with this finding, MKKOP did not increase mCherry expression or increase apoptosis of proximal tubule cells (Figure 3.6D).

We concluded that the proximal tubules in micro-organoids were insufficiently mature to demonstrate specific nephrotoxic injury, considering the low expression of influx transporters and endocytotic receptors in micro-organoids, and the non-specific apoptotic response of micro-organoids to cisplatin with or without efflux inhibitors. Hence, lack of mCherry expression following injury was more likely due to a failure to replicate the *in vivo* KIM-1 injury response, rather than an inherent defect in the reporter line.

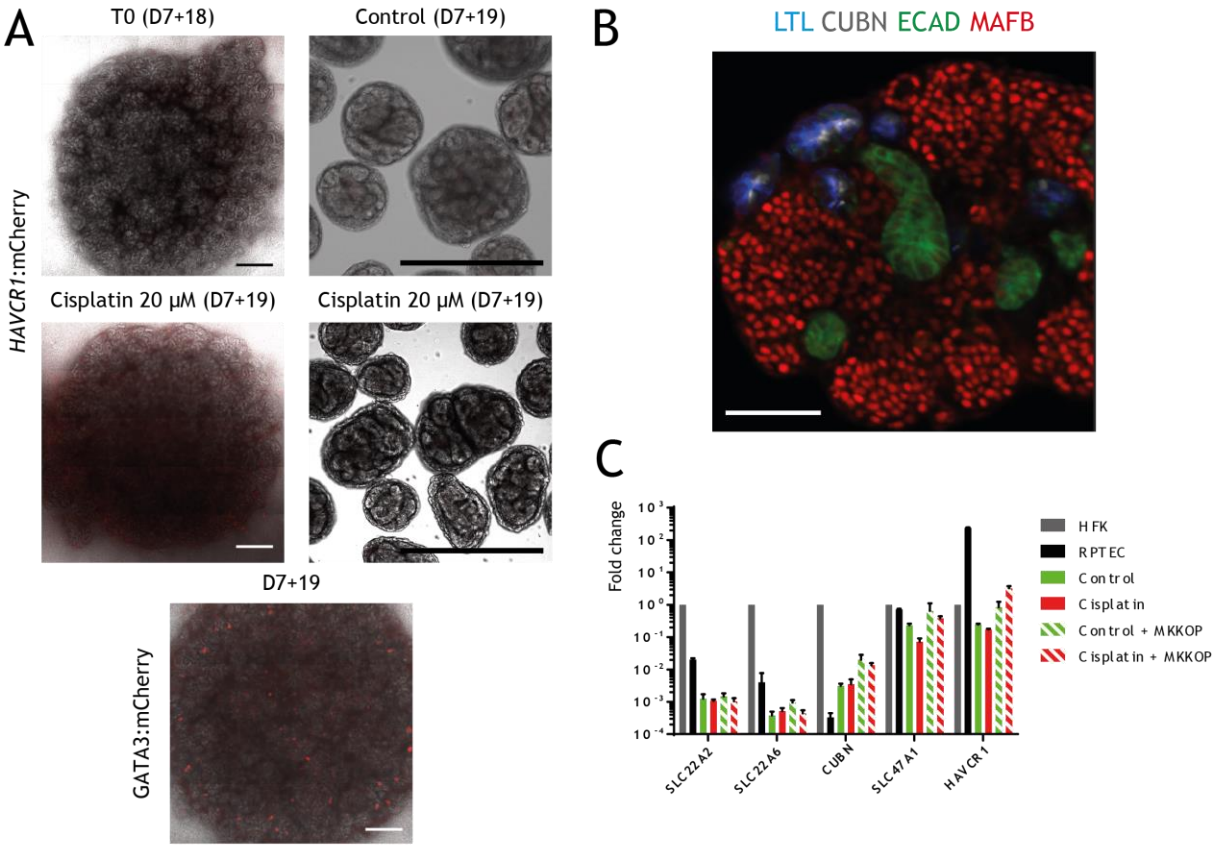
A
T0 (D7+18)
Control (D7+19)
HAVCR1:mCherry
Cisplatin 20 µM (D7+19)
Cisplatin 20 µM (D7+19)
D7+19
GATA3:mCherry
B
LTL CUBN ECAD MAFB
C
Fold change
HFK
RPTEC
Control
Cisplatin
Control + MKKOP
Cisplatin + MKKOP
SLC22A2
SLC22A6
CUBN
SLC47A1
HAVCR1

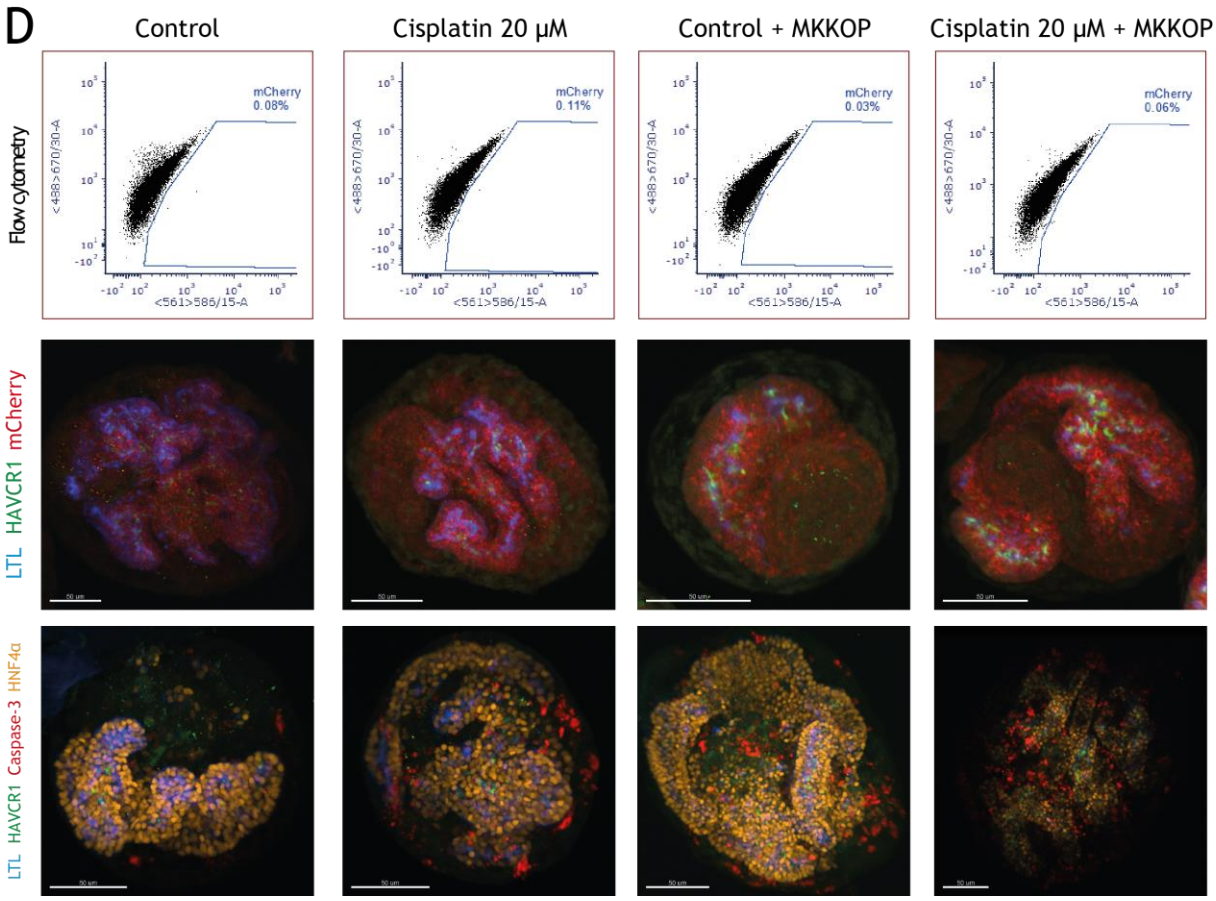
D
Control
Cisplatin 20 µM
Control + MKKOP
Cisplatin 20 µM + MKKOP
Flowcytometry
mCherry 0.08%
mCherry 0.11%
mCherry 0.03%
mCherry 0.06%
<488>670/30-A
<561>586/15-A
LTL HAVCR1 mCherry
LTL HAVCR1 Caspase-3 HNF4α

Figure 3.6 Investigation of the *HAVCR1*:mCherry reporter line for monitoring drug-induced injury to the proximal tubule. A: Live microscopy of *HAVCR1*:mCherry transwell organoids (left) and micro-organoids (right) with and without cisplatin exposure. Live microscopy of *GATA3*:mCherry transwell organoids served as a positive control for mCherry signal. Scale bars 500 μm. B: Immunofluorescence staining of micro-organoids differentiated from the*HAVCR1*:mCherry reporter line showed that glomeruli ($MAFB^+$), proximal tubules (LTL^+ $CUBN^+$), and distal tubules and/or collecting ducts (LTL^- $ECAD^+$) were all present. C: qRT-PCR comparing proximal tubule marker expression in micro-organoids to HFK and RPTEC. D: Flow cytometry and immunofluorescence staining of micro-organoids exposed to cisplatin with or without MKKOP. Scale bars 50 μm.

3.6 Discussion

3.6.1 Summary of objectives accomplished

The objective for this phase of the project was to generate reporter lines for identifying the proximal tubule in kidney organoids, and for characterising proximal tubule injury. We have demonstrated that the *LRP2*:mTagBFP2 and *HNF4A*:YFP reporter lines can be differentiated into kidney organoids and shown that reporter expression corresponds to the developing proximal tubule by immunofluorescence staining of whole organoids and qRT-PCR of FACS-purified fractions. We have also shown the development of a *HAVCR1*:mCherry reporter line for proximal tubule injury. While we could not detect mCherry expression following exposure of micro-organoids differentiated from this reporter line to a known nephrotoxicant, we concluded from immunofluorescence staining and qRT-PCR analysis that this could be due to immaturity of the proximal tubules resulting in failure to induce a specific injury response, consistent with our analysis in Chapter 2, rather than a defect in the reporter line (though this has not been ruled out).

3.6.2 Limitations of the current work

As previously discussed, the *LRP2*:mTagBFP2 clone used in this project is heterozygous and has a mutation on the untargeted allele. We predicted, based on existing literature and our targeting strategy, that the mutation would not be detrimental to an extent which would affect our aim of characterising reporter expression from this locus, or justify re-generating the reporter line within the limited time frame of this project. Preliminary assays showed that proximal tubules in organoids generated from this reporter line were capable of albumin uptake, suggesting that if any defect in LRP2-mediated endocytosis existed, activity was not completely lost, which supported our predictions. However, in the long term, we would re-

target this locus to generate a new reporter line with no mutations to address this and the limitations discussed in the following paragraphs.

A recurring difficulty in the analysis of the *LRP2*:mTagBFP2 line was the low fluorescence intensity of mTagBFP2 driven from this locus, seen in both live microscopy and flow cytometry. While this may have been consistent with the challenges inherent in detecting blue fluorescent proteins (e.g. the need to use low laser powers to avoid phototoxicity), we had expected from previous bulk RNA sequencing of organoids and the bioinformatics analysis in Chapter 2 that *LRP2* would be sufficiently strongly expressed [113]. Our group and our collaborators have also previously generated and used a *MAFB*:mTagBFP2 podocyte reporter line with no particular difficulty [210,298]. However, based on our group's scRNA-seq analysis of organoids, *MAFB* is much more strongly expressed in organoid podocytes than *LRP2* is expressed in organoid proximal tubules, so it is possible that *LRP2* expression still fails to drive enough mTagBFP2 expression to be reliably detected.

Another possible contributing factor is that *MAFB* is a nuclear transcription factor that is folded in the cytoplasm (the *MAFB*:mTagBFP2 reporter is a heterozygous knockout that does not fuse any endogenous localisation signals to mTagBFP2, in any case), while *LRP2* is a cell surface protein that is folded in the endoplasmic reticulum[298]. As mTagBFP2 in the *LRP2*:mTagBFP2 reporter is translated from the 3' end of the *LRP2* transcript, mTagBFP2 would be folded in the endoplasmic reticulum like LRP2, even though T2A cleavage separates it from the LRP2 protein during translation. There are reports that mTagBFP2 undergoes detrimental post-translational modification when folded in the endoplasmic reticulum, such as inappropriate disulphide bond formation and N-glycosylation, and that this produces non-fluorescent mTagBFP2 molecules [329]. Hence, it is possible that low mTagBFP2 intensity in our reporter line is due to low production of correctly-folded, fluorescent mTagBFP2, even if *LRP2* is strongly expressed. This is roughly consistent with our observation that mTagBFP2 in proximal tubules can be easily detected by immunofluorescence staining, where the anti-mTagBFP2 antibody might be less sensitive to the conformation of the protein. To determine if misfolded mTagBFP2 is indeed present, we could perform non-reducing Western blots of the *LRP2*:mTagBFP2 organoids. Ultimately, retargeting this locus to generate a reporter line with no mutations would also give us an opportunity to use a different reporter protein (such as a secretion-optimised TagBFP) or a different targeting strategy (e.g. producing a heterozygous knockout).

Though we have shown that our nephrotoxic injury model using our *HAVCR1*:mCherry line did not upregulate *HAVCR1* and therefore would not have upregulated mCherry even in a correctly-targeted reporter line, we have not yet demonstrated that mCherry expression corresponds to *HAVCR1* expression. While we attempted to induce specific nephrotoxic injury with cisplatin, the major route of entry of cisplatin into proximal tubule cells is via basolateral organic cation transporters (OCTs, discussed in detail in Chapter 1) [12]. As OCTs are not highly expressed in our organoids based on our bioinformatics analysis, we did not perform further investigation of dose or exposure time responses to cisplatin in our model. Other drugs such as gentamicin, which enters proximal tubule cells via receptor-mediated endocytosis, may have produced a more marked injury response. Another method of verifying reporter co-expression with *HAVCR1* would be to differentiate this cell line to a hepatocyte lineage, provided that the protocol used for doing so produces hepatocytes which are sufficiently mature to express normal levels of *HAVCR1*.

The *HAVCR1*:mCherry clone (clone 18) used in this project had no detectable chromosomal abnormalities by molecular karyotyping, but later G-banding close to the end of this project detected a balanced translocation, which is known to be undetectable by molecular karyotyping. Hence, we are screening the other clone generated in this project (clone 47) for chromosomal abnormalities, to determine whether it can be used in future work.

3.6.3 Alternative approaches for designing proximal tubule and injury reporter lines

Our choice of *LRP2* and *HNF4A* as the target loci for these reporter lines was partly based on prior scRNA-seq analysis of E18.5 mouse kidneys showing that these genes were specific to early and mature proximal tubule clusters and that *Lrp2* increased with maturation while *Hnf4a* remained level [216]. Other choices were possible. For example, *Slc22a6* (Oat1) is also expressed in both of these cell clusters, and is a functional marker that increases with maturation and is known to mediate nephrotoxicity[216,330]. Since the anti-SLC22A6 antibodies available to us were not suitable for immunofluorescence, this reporter would have enabled a visual readout of SLC22A6 expression that we would not have otherwise. However, our analysis of organoids cultured using our standard methods in Chapter 2 showed low *SLC22A6* expression, and so this reporter would not have been validated until culture conditions which induced *SLC22A6* expression had been identified.

In the time since our *LRP2* and *HNF4A* reporter lines were designed, human foetal kidney and human adult kidney scRNA-seq or snRNA-seq datasets have been published[20,195]. FACS

and qRT-PCR of reporter^{+} cells in our reporter lines suggested that some cells which did not express *HNF4A* were expressing *LRP2*, which was not predicted by our analysis of the E18.5 mouse dataset or by immunofluorescence characterisation of our organoids, but was consistent with literature describing *LRP2* expression in human podocytes[315]. For future work, the human datasets might give more consistent predictions regarding cell type-specific loci which can be used to create reporter lines for cell types of interest.

HAVCR1 was chosen for our injury reporter line based on our literature review on markers of acute kidney injury. Since then, an extensive RNA-seq characterisation of a mouse ischaemia-reperfusion model of kidney injury at multiple time points post-injury has found that *Havcr1* expression peaked dramatically 2 days post-injury and returned to basal expression levels after 1 week [227]. While this is a rapid rise in a pre-clinical or clinical setting, analysis of this and similar profiling data might reveal markers which are even more strongly and rapidly upregulated and might be more suitable for an *in vitro* readout of injury. These include markers such as *SOX9*, *IL6*, and *HMOX1* (haem oxygenase 1, HO-1), the latter two of which show some evidence of discriminating between known nephrotoxic and non-nephrotoxic compounds *in vitro* [126,127,131,227,331]. There is also evidence that HO-1 can be used as a biomarker of acute kidney injury *in vivo*, though it is not yet clear whether markers like these are specific to proximal tubule injury or are broadly expressed by injured renal cells [130,332].

3.6.4 Potential uses of our reporter lines and future work

The proximal tubule reporter lines generated in this project have been used for rapid, qualitative determination of maintenance of proximal tubule identity and/or viability under different culture conditions and following xenotransplantation (discussed in detail in Chapter 5), allowing us to identify and further investigate conditions which may improve proximal tubule maturity. Nephron segmentation and determination of the proximal tubule identity over time in different culture conditions can also be investigated with high-resolution live imaging of these reporter lines.

Proximal tubule function can be assayed *in vitro* with fluorescent substrates of the solute channel transporters, such as fluorescein and ASP^{+}, and a combination of influx and efflux inhibitors; transporter-mediated uptake should be specific to proximal tubule cells, and efflux inhibitors should increase fluorescence while influx inhibitors decrease fluorescence[12,170,333]. Endocytosis in proximal tubules can also be observed with labelled albumin or

dextran[12,112,113]. Our reporter lines allow identification of proximal tubules during live imaging and will therefore enable assays of proximal tubule function in complex, multicellular *in vitro* models such as kidney organoids.

High-content imaging allows the rapid quantitation of multiple cellular features *in vitro* for comparison of cell phenotypes between different experimental conditions, provided that those cellular features can be visualised. Hence, high-content imaging of our reporter lines will enable rapid, quantitative comparisons of proximal tubules in organoids between different culture conditions. If the reporter is for a marker that increases in expression as the proximal tubule matures (e.g. *LRP2* or *SLC22A6*), fluorescence intensity of the reporter can also be correlated with maturity. The functional assays described earlier can also be used in conjunction with the reporter lines to quantitate proximal tubule function. Finally, if a sufficiently mature *in vitro* model of the proximal tubule can be obtained, an injury reporter line, such as the *HAVCR1* reporter, could be used to rapidly screen compounds for nephrotoxicity.

In conclusion, we have generated two reporter lines (CRL-2429 *LRP2*:mTagBFP2 and PCS-201-010 *HNF4A*:YFP) and shown that they mark the developing proximal tubule in organoids, and generated a proximal tubule injury reporter line (CRL-2429 *HAVCR1*:mCherry). Validation of the proximal tubule reporters has also been published in Vanslambrouck *et al*. [290] as part of a range of reporter lines for identifying and characterising multiple different renal cell types. Reporters for these loci will be useful tools for further characterisation of proximal tubule development and injury in organoids.

4 SCREENING CONDITIONS FOR IMPROVING PROXIMAL TUBULE MATURATION IN KIDNEY ORGANOIDS

4.1 Background

In Chapter 2 we found that organoid proximal tubules cultured using our published methods express some functional markers, such as the endocytotic receptors *CUBN* and *LRP2*, but other functional markers such as the SLC transporters *SLC22A6* and *SLC22A2* were only expressed at low levels. Because of this, we concluded that organoid proximal tubules were not sufficiently mature to model drug-induced toxicity *in vitro*, as specific toxicity to the proximal tubule is often mediated by drug interactions with these transporters [12]. Making iPSC-derived tissues which are sufficiently mature for a specific purpose, whether this is disease modelling, drug screening, or cellular therapy, is an ongoing challenge in multiple fields [334,335]. A common approach to this challenge is to identify media conditions which increase the expression and function of markers of maturity, and then culture the iPSC-derived tissue in this media after the initial differentiation. One advantage of this approach is that it does not require any specialised culture platform or expertise other than that required for the initial differentiation.

To determine what media conditions might increase proximal tubule marker expression *in vitro*, a bioinformatics analysis of foetal and adult mouse and human proximal tubules was performed to identify pathways which were upregulated or downregulated during maturation (discussed in Chapter 2). One of the pathways which was identified as differentially upregulated between proximal tubules and other renal cell types, as well as between early and mature proximal tubules, was fatty acid oxidation, which was consistent with prior literature showing that this is the major energy source in the proximal tubule *in vivo* [40]. *In vitro*, cells are often predominantly glycolytic due to the high glucose content of most culture media relative to normal serum concentrations [336]. Taking this into consideration, we hypothesised that switching the carbon source in culture medium from glucose to fatty acids would improve proximal tubule maturation.

Another change which could shift proximal tubules from glycolysis to fatty acid oxidation is to remove insulin from the culture media. Insulin receptors and insulin-like growth factor (IGF) receptors, which can both bind either insulin or IGFs with differing affinities, are expressed in the ureteric epithelium, nephron progenitors, as well as in developing and

mature nephrons [337,338]. In mature proximal tubules *in vivo*, insulin increases glucose uptake via increased SGLT2 activity and inhibits gluconeogenesis [339]. *In vitro*, insulin together with the high glucose concentrations typical in culture media were shown to increase cellular proliferation and glycolysis in primary proximal tubule cells [340]. Hence, we hypothesised that omitting insulin from the culture medium in concert with altering glucose and fatty acid concentrations would reduce glycolysis in our proximal tubules.

Our targeted bioinformatics analysis of proximal tubules in foetal and adult mouse and human kidneys also identified several other pathways which change as the proximal tubule segment is first defined, and pathways which change during proximal tubule maturation. We hypothesised that we could manipulate these pathways *in vitro* to stimulate proximal tubule proliferation or maturation. Owing to time constraints, we could not investigate all of the pathways we identified. Nevertheless, among our findings was that *Lgr4*, *Fgfr3*, and *Fgfr4* were differentially upregulated in the early and mature proximal tubule, while TGFβ/BMP signalling was downregulated in these cell populations. Hence, we also hypothesised that a "proliferation medium" containing R-spondin 1, which is a ligand for LGR4, as well as FGFs and a small molecule inhibitor of TGFβ signalling (SB 431542), could induce the proliferation of proximal tubule cells prior to switching organoids to a maturation medium.

We also identified TGFβ/BMP signalling downregulation between the early and mature proximal tubule, showing that this change continues as the proximal tubule matures, and found that several genes which were associated with fatty acid oxidation in the mature proximal tubule were PPAR targets. Based on this, we hypothesised that adding a TGFβ inhibitor or PPARγ agonist to maturation medium would improve proximal tubule maturity compared to control conditions or the maturation medium alone.

While our bioinformatics analysis clearly demonstrated that not all renal cells which express *HNF4A* express SLC transporters even in adult kidneys, previous studies have claimed that overexpression of *Hnf4a* and *Hnf1a* in mouse fibroblasts is sufficient to induce SLC expression and function [213]. The fibroblast media in that study contained epidermal growth factor (EGF), T3, dexamethasone (a corticosteroid), and cholera toxin (an adenylate cyclase activator), which individually or in combination may have influenced SLC expression upon *Hnf4a* and *Hnf1a* overexpression. To determine if adenylate cyclase activation would aid proximal tubule maturation, we also investigated the addition of forskolin to maturation medium.

Our aims in this chapter were:

i) to determine if the maturity of organoid proximal tubules could be improved by manipulating glucose and fatty acid concentrations in a defined, insulin-free culture medium to reduce glycolysis

ii) to determine if proliferation and/or maturation of proximal tubules could be improved by manipulating key signalling pathways which were identified through prior bioinformatics analysis of proximal tubules *in vivo*

iii) to demonstrate the utility of our proximal tubule reporter lines (discussed in Chapter 3) in these investigations.

4.2 Methods

A defined medium for testing the effect of glucose and palmitic acid concentrations on organoid maturation was prepared according to Table 4.1. The basal medium components were mixed first. Palmitic acid stock was prepared by dissolving palmitic acid in 100% ethanol at 50° C. Recombinant human albumin and fatty acid aliquots were prepared by pipetting the required volumes of fatty acid stocks into aliquots of albumin, mixing well, and incubating at 37° C for 2 hours until the solution was clear. Glucose (G7528, Sigma) stock was prepared in dH_2O and added as needed.

Proliferation medium consisted of E6 basal medium with 10 μM SB 431542 (Sigma) to inhibit TGFβ signalling, 50 ng/mL R-spondin 1 (R&D Systems), and 600 ng/mL FGF2 (Merck).

Cardiac maturation medium was prepared according to Mills *et al*. [284]. Ingredients are listed in Table 4.2. Palmitic acid stock was prepared by dissolving palmitic acid in DMSO (Sigma) and conjugated to albumin in B-27 by pipetting the required volume into B-27 aliquots, mixing well, and incubating at 37° C for 2 hours and shaking at 1200 rpm until the solution was clear.

Small molecules and growth factors added to the cardiac maturation medium were added to the following final concentrations: 10 μM SB 431542 (SB), 1 μM rosiglitazone (Rz), 19.4 mg/L insulin (INS), 1 μM forskolin (F).

Table 4.1 Base for defined medium for titration of glucose and palmitic acid concentrations in organoid culture.

Basal medium			
Component	**Supplier**	**Catalogue number**	**Volume (mL)**
DMEM, no glucose, no glutamine, no phenol red	Thermofisher	A1443001	50
Sodium bicarbonate (27 mg/mL stock)	Sigma	S3817	1
Sodium selenite (100 µg/mL stock)	Sigma	S5261	0.007
L-ascorbic acid 2-phosphate sesquimagnesium salt hydrate (32 mg/mL stock)	Sigma	A8960	0.1
Holo-transferrin (10 mg/mL stock)	Sigma	T0665	0.05
GlutaMAX	Thermofisher	35050-061	0.5
Recombinant human albumin and fatty acids			
Albumin (100 mg/mL stock)	Albumedix	-	2.5
Linoleic acid	Sigma	L1376	0.005
Linolenic acid	Sigma	L2376	0.005
Palmitic acid (100 mM stock)	Sigma	P5585	As needed

Table 4.2 Base for cardiac maturation medium repurposed for optimising maturation in kidney organoids.

Basal medium			
Component	**Supplier**	**Catalogue number**	**Volume (mL)**
DMEM, no glucose, no glutamine, no phenol red	Thermofisher	A1443001	50
L-ascorbic acid 2-phosphate sesquimagnesium salt hydrate (32 mg/mL stock)	Sigma	A8960	0.1
GlutaMAX	Thermofisher	35050-061	0.5
Glucose (1 M stock)	Sigma	G7528	0.05
Antibiotic-Antimycotic	Thermofisher	15240062	0.25
B-27 and palmitic acid			
B-27™ supplement, minus insulin	Thermofisher	A1895601	1
Palmitic acid (100 mM stock)	Sigma	P5585	0.05

4.3 Defined medium with recombinant human albumin and without insulin increases *CUBN*, *SLC22A2*, and *HNF4A* expression in organoids

To determine if switching the carbon source in culture media from glucose to fatty acids would increase proximal tubule maturity, organoids were differentiated and cultured according to standard methods up to D7+7 to allow renal vesicles to differentiate and segment, before switching to a medium with varying concentrations of glucose or palmitic acid, or maintained in E6 with all-*trans*-retinoic acid as a control (Figure 4.1A). The concentrations of glucose and palmitic acid used were based on Mills *et al*. [284] or chosen to match the glucose concentration of E6. Three whole organoids from each condition were lysed for qRT-PCR of proximal tubule markers. The role of *CUBN*, *LRP2*, *SLC22A2*, and *HNF4A* in the proximal tubule has been discussed in Chapter 2 and Chapter 3. *SLC5A2* (common name SGLT2, sodium/glucose cotransporter 2) is expressed on the apical membrane of mature proximal tubules for active reabsorption of glucose from the renal

filtrate [341]. *EPCAM* expression was also determined as a rough measure of the tubular epithelial content of each organoid in case the change in media caused general proliferation or suppression of epithelial cells which would skew proximal tubule marker expression in the whole organoid.

Organoids cultured in metabolic media with no glucose suffered extensive cell death visible by brightfield microscopy regardless of the palmitic acid concentration (not shown), and RNA yields from these organoids were not suitable for qRT-PCR. All other organoids cultured in metabolic media showed a non-significant decrease in *EPCAM* expression compared to the control, regardless of glucose or palmitic acid concentration, suggesting that any increases in proximal tubule marker expression were not due to general epithelial proliferation (Figure 4.1C). *CUBN* expression significantly increased compared to the control in organoids which received no palmitic acid and 1 mM glucose, and *SLC22A2* expression significantly increased in all conditions receiving 17.5 mM glucose regardless of palmitic acid content. All metabolic media conditions showed significant increases in *CUBN* and *SLC22A2* expression as a proportion of *EPCAM* expression. *HNF4A* expression as a proportion of *EPCAM* was always increased in metabolic media compared to the control, but was only statistically significant in four conditions: 0 μM palmitic acid + 1 mM glucose, 10 μM palmitic acid + 1 mM glucose, 10 μM palmitic acid + 17.5 mM glucose, and 100 μM palmitic acid + 17.5 mM glucose. Increased *CUBN* and *SLC22A2* expression would suggest that organoids in metabolic media have a greater capacity to respond to nephrotoxic drugs which are transported via these pathways compared to organoids in standard media. It is also possible that increased *CUBN*, *SLC22A2*, and *HNF4A* expression as a proportion of *EPCAM* was due to an increased proportion of proximal tubule cells relative to other tubular epithelial cell types rather than maturation of the proximal tubule cells present. Further characterisation with immunofluorescence, qRT-PCR of markers for other tubular segments, or quantification with proximal tubule reporter lines could be performed to determine if this was the case.

Since the largest changes in proximal tubule marker expression were always between the control and the metabolic media conditions (Figure 4.1C), the basal metabolic media itself was responsible for most of the improved marker expression. One major difference between the basal metabolic media and E6 was the inclusion of recombinant human albumin with essential lipids (see section 4.2 for details). Albumin binds bioactive molecules such as lipids and growth factors and thus can have a wide variety of effects on cells in culture, from modulating the effects of growth factors to mitigating toxicity from media components or

substances secreted by cells [342,343]. This may be especially pertinent given that proximal tubules and podocytes endocytose albumin *in vivo*, and we and others have shown that organoid proximal tubules can accumulate labelled albumin [188,290], potentially allowing albumin in the culture medium to also exert cell type-specific intracellular effects. We have also shown in Chapter 2 using bioinformatics analysis that in E6, organoid proximal tubules upregulate metallothioneins, which is a typical oxidative stress response, while this upregulation was not observed in APEL which contains recombinant human albumin [223,224,344]. While that analysis also had a number of uncontrolled differences detailed in Chapter 2, E6 and APEL have similar concentrations of most other components, so the result, together with our observations in this chapter, suggests that albumin mitigates oxidative stress in organoids, especially in proximal tubules. However, any effect of albumin supplementation to organoid proximal tubules or other organoid cell types is likely to have multiple mechanisms of action.

The other major difference between the basal metabolic media and E6 was the omission of insulin from the metabolic media. We previously hypothesised that omitting insulin from the media would reduce glycolysis and improve proximal tubule maturation. However, changing the concentration of glucose or palmitic acid did not produce statistically significant changes between metabolic media conditions. This suggests that if omitting insulin had any benefit in addition to the effect of albumin supplementation, the benefit was not necessarily due to a metabolic shift away from glycolysis. *SLC5A2* expression did not differ significantly between control and metabolic media conditions, indicating that insulin in the control did not upregulate SGLT2 expression or activity as it does *in vivo*, which also suggests that further optimisation of proximal tubule maturity is required [345,346].

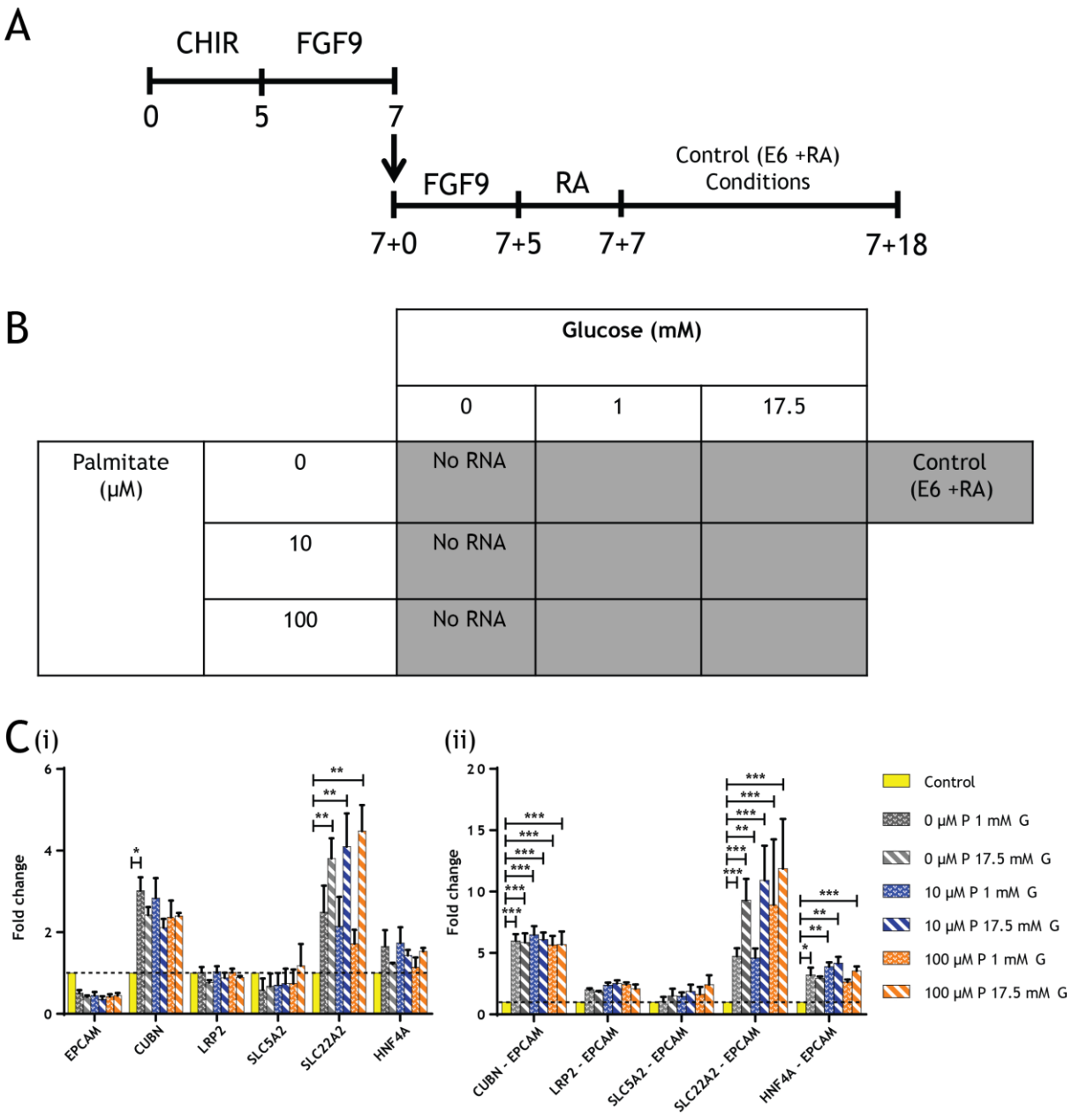

Figure 4.1 Timeline of organoid culture and qRT-PCR of proximal tubule markers in organoids cultured in E6 +RA (control) and metabolic media with varying concentrations of glucose and palmitic acid. A: Timeline of organoid culture showing the standard differentiation and organoid aggregation in E6 basal medium with the stated growth factors, followed by switching to control or metabolic media conditions at D7+7. B: Diagram of glucose and palmitic acid concentrations in metabolic media. Conditions with 0 mM glucose did not produce suitable RNA for qRT-PCR due to extensive cell death. C: qRT-PCR of proximal tubule markers in organoids at D7+18. Data are presented as fold changes relative to the control, (i) normalised by GAPDH expression and (ii) as a proportion of normalised EPCAM expression. G = glucose, P = palmitic acid. n = 3 organoids from the same experiment, error bars ± SEM. Statistical significance for each gene across treatment groups was determined using two-way ANOVA and Tukey's post-test analysis of normalised (ΔCt) values (* $p < .05$, ** $p < .01$, *** $p < .001$).

4.4 Screening effects of epithelial proliferation medium, maturation medium, and small molecules on proximal tubule patterning and maturation

In section 4.3, we demonstrated that proximal tubule marker expression in organoids increased when the culture medium was switched to a defined medium with albumin and essential lipids and without insulin. The objective was to change the carbon source in the medium by adding varying concentrations of glucose and palmitic acid, to investigate the effect of changes in carbon source on proximal tubule maturation. However, we found that the change in the basal medium itself created the greatest improvement, while shifts in glucose and palmitic acid concentration only produced modest changes in proximal tubule marker expression.

These results contrast a similar approach for cardiac tissue which showed that switching media carbon source altered the contraction force of iPSC-derived cardiac organoids depending on the glucose and palmitic acid concentration, strongly suggesting that a metabolic switch had occurred [284]. A possible explanation for this was that the cardiac organoid maturation medium included B-27, a commercially-available supplement which includes a number of proteins, lipids, and hormones [347]. One of those hormones is triiodothyronine (T3), which stimulates mitochondrial biogenesis and fatty acid oxidation in most tissues, including the heart and kidney [348,349]. Therefore, it is possible that additional factors were required to induce a shift from glycolysis to fatty acid oxidation in proximal tubules. Including these factors might also influence other aspects of proximal tubule maturation, such as increased Na^+/K^+ ATPase activity or increased sodium chloride transport [350]. Other hormones present in B-27 include corticosterone and progesterone [347]. Glucocorticoids, like corticosterone, enhance bicarbonate reabsorption in the proximal tubule [351,352], while progesterone mediates a wide range of sex-specific differences seen in transporter expression in the proximal tubule [353–356]. Hence, we hypothesised that a published "maturation medium" would have a greater effect on proximal tubule maturation than our previous approach.

In Chapter 3 we described the generation and validation of two reporter iPSC lines, a *LRP2*:mTagBFP2 line and a *HNF4A*:YFP line, which mark the proximal tubule when differentiated into organoids. YFP expression was consistently easier to detect on live imaging and showed clearer separation from background fluorescence in flow cytometry. Here, we describe the use of the *HNF4A*:YFP reporter to screen the effects of a proliferation

medium and a maturation medium on organoid proximal tubules compared to organoids maintained in standard conditions (Figure 4.2).

On D7+11 of organoid culture, prior to switching to proliferation medium (T_0), YFP^+ tubules were clearly visible by live microscopy, consistent with our previous observations (Figure 4.3). At D7+17, after organoids had been maintained in E6 with retinoic acid as a control or proliferation medium for 6 days, YFP^+ tubules were visible in both conditions, but YFP^+ tubules in proliferation medium did not appear longer or more abundant, which was unexpected. At D7+24, after organoids had been maintained in control medium, proliferation medium, or switched to maturation medium with the stated small molecules for 6 days, YFP^+ tubules were much less prominent in organoids in E6 +RA or continued proliferation compared to organoids which had been switched from proliferation medium to maturation medium. Differences in tubular morphology were evident between E6 +RA, continued proliferation, and maturation medium organoids.

Organoids were dissociated at D7+25 for flow cytometry analysis of YFP^+ cells. However, we found that continued proliferation and maturation medium (MM) organoids had very low yields (<1% live cells) of YFP^+ cells (Figure 4.4A). Given that YFP^+ tubules were readily visible by live microscopy prior to dissociation, this was unexpected and may have been due to depletion of proximal tubules during dissociation. Because of this, we could not accurately quantify the proportion of proximal tubule cells present in each condition. Nevertheless, YFP^+ cells differed in brightness between conditions (Figure 4.4B). Out of the organoids dissociated at D7+25, organoids in any form of MM without insulin had brighter YFP^+ cells than organoids maintained in E6 +RA, while adding insulin to MM reduced YFP brightness, especially when combined with the other small molecules. The concentrations of small molecules and growth factors used were consistent with screens for morphological changes performed by others in our lab group (unpublished data) and with previously published doses [357]. YFP^+ cells were brightest in MM +SB and MM –INS +SB +Rz +F, followed by MM +Rz and MM alone, suggesting that TGFβ inhibition via SB and PPARγ activation via rosiglitazone enhanced the effect of MM. MM +F showed no dramatic improvement in YFP brightness over MM alone.

None of the conditions had brighter YFP^+ cells than organoids dissociated at D7+12, showing that MM did not increase YFP expression *per se* (Figure 4.4B). Instead, we infer that organoids cultured using our standard methods initially strongly express *HNF4A* in

developing proximal tubules, but this expression declines over time as organoids are maintained in E6 with retinoic acid, and this decline can be slowed by switching to a proliferation medium followed by a maturation medium with a TGFβ inhibitor, a PPAR agonist, or both. We should note that there was no strong evidence that our proliferation medium induced proliferation of proximal tubule cells, as YFP^+ cells did not appear more abundant in live microscopy of organoids cultured in proliferation medium at D7+17 or D7+25. Based on these screening results, we focused on characterising the effect of maturation medium on proximal tubules in organoids.

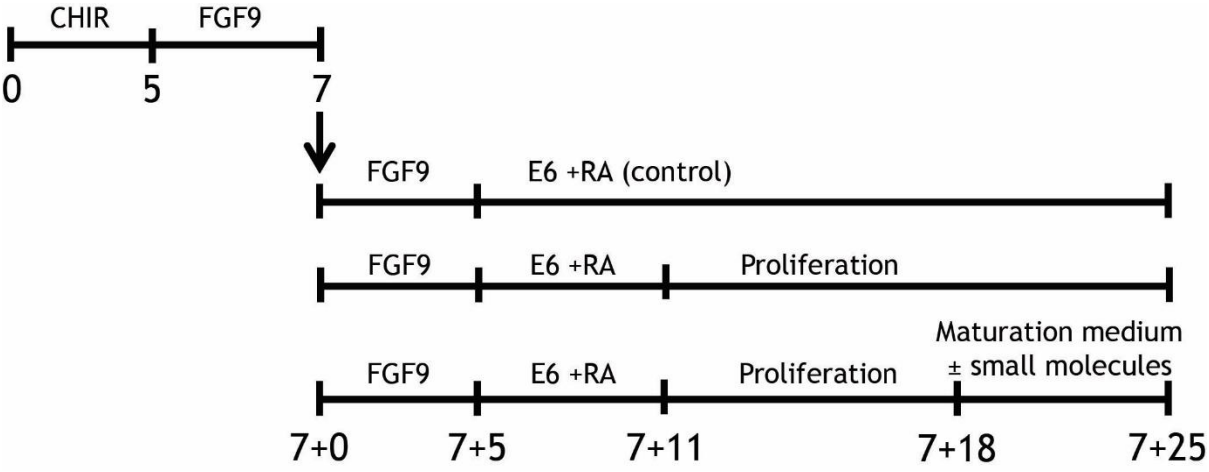

Figure 4.2 Timeline of organoid culture showing the standard differentiation and organoid aggregation in E6 basal medium with the stated growth factors, followed by switching to control or proliferation media at D7+11 and maturation media at D7+18. Numbers under the timeline denote days, with the start of differentiation at day 0 and organoid aggregation at day 7+0.

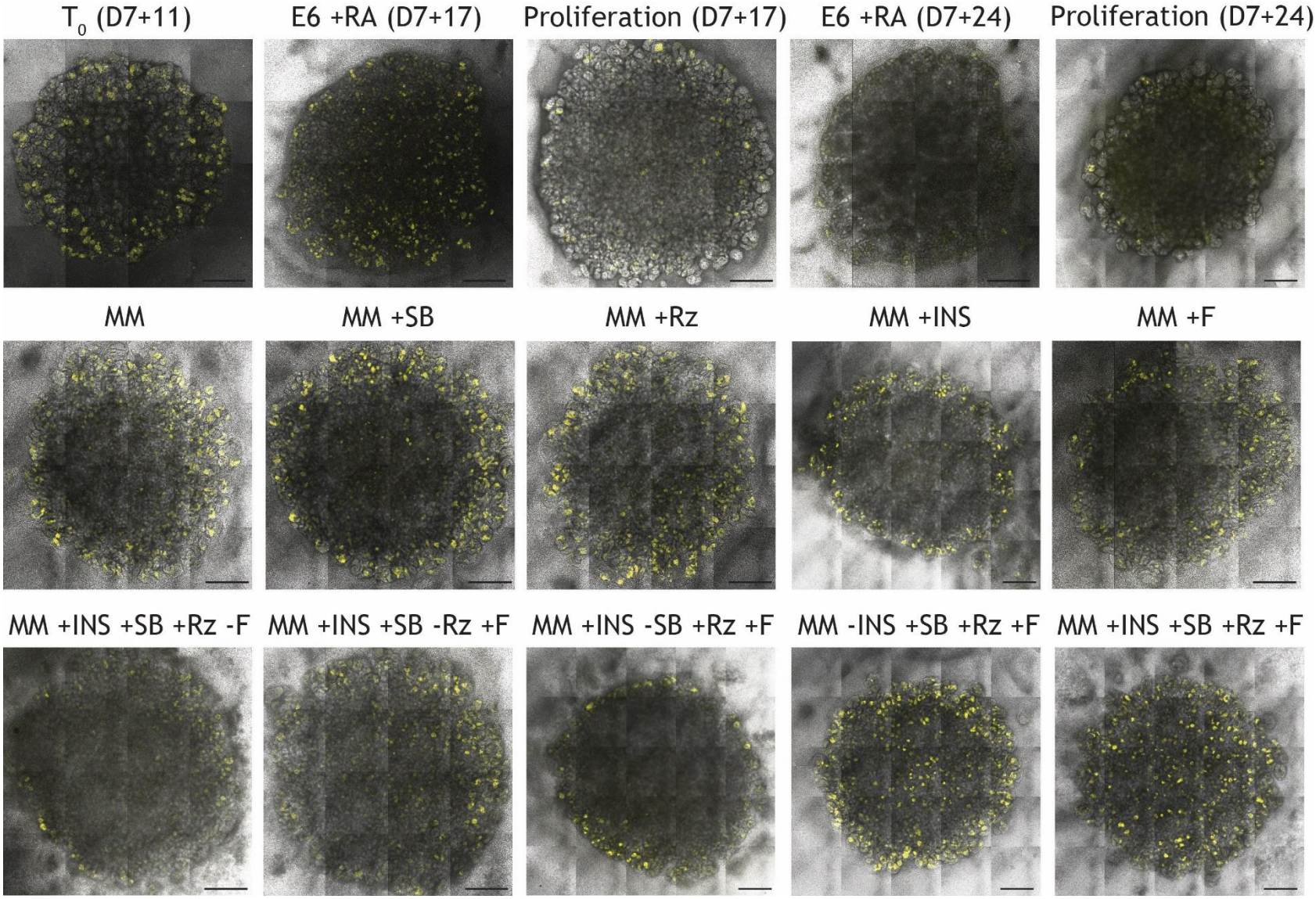
T0 (D7+11)
E6 +RA (D7+17)
Proliferation (D7+17)
E6 +RA (D7+24)
Proliferation (D7+24)
MM
MM +SB
MM +Rz
MM +INS
MM +F
MM +INS +SB +Rz -F
MM +INS +SB -Rz +F
MM +INS -SB +Rz +F
MM -INS +SB +Rz +F
MM +INS +SB +Rz +F

Figure 4.3 Live microscopy of *HNF4A*:YFP reporter organoids cultured in E6 +RA or proliferation medium followed by cardiac maturation medium (MM) with or without additives showing YFP expression in tubules. Brightness was adjusted using the automatic "best fit" threshold in the ZEN image analysis program (Zeiss) for all images. Images are representative of four organoids from the same experiment. Scale bars 500 µm.

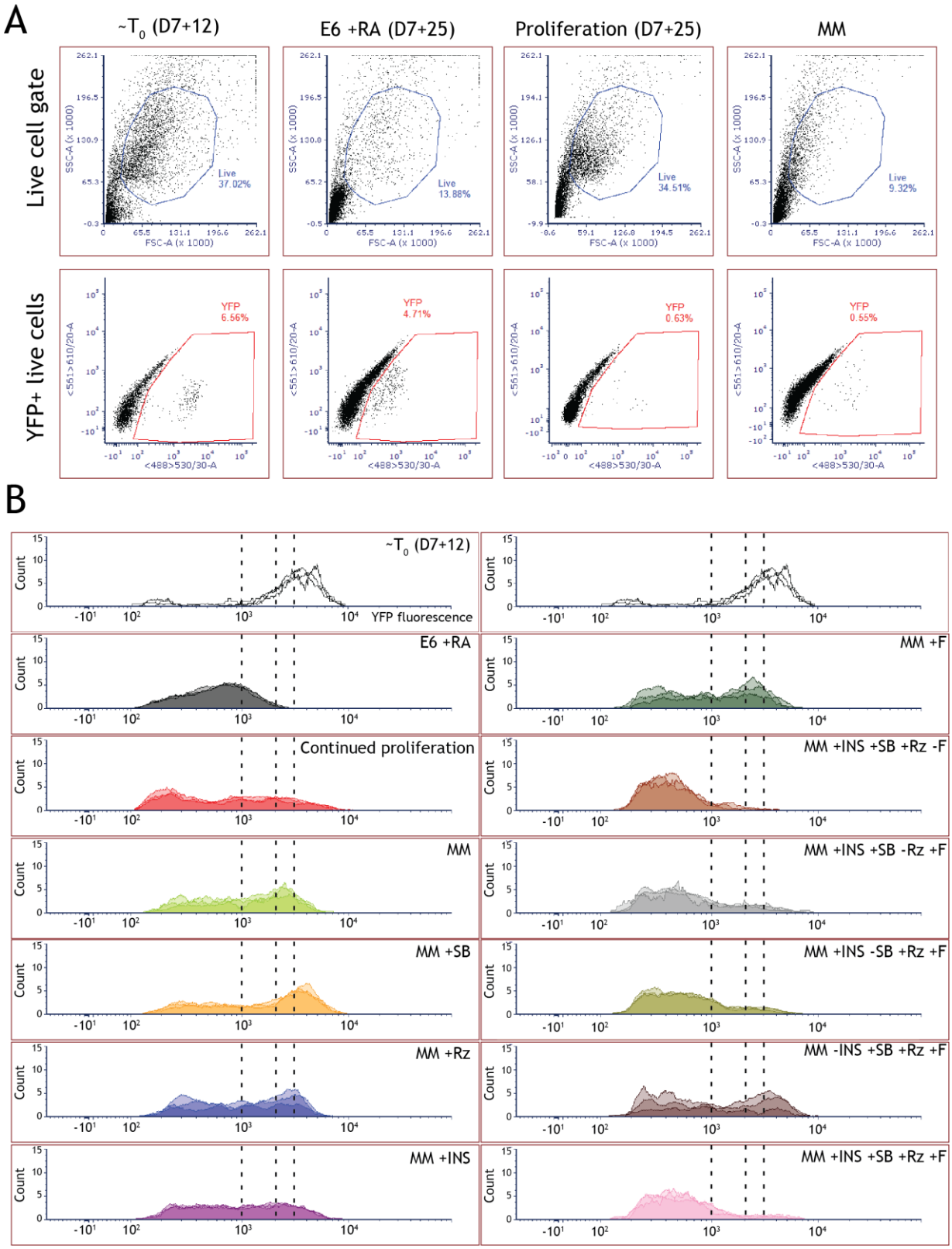
A
~T0 (D7+12)
E6 +RA (D7+25)
Proliferation (D7+25)
MM
Live cell gate
YFP+ live cells
Live 37.02%
Live 13.88%
Live 34.51%
Live 9.32%
YFP 6.56%
YFP 4.71%
YFP 0.63%
YFP 0.55%
SSC-A (x 1000)
FSC-A (x 1000)
<561>610/20-A
<488>530/30-A
B
~T0 (D7+12)
E6 +RA
Continued proliferation
MM
MM +SB
MM +Rz
MM +INS
MM +F
MM +INS +SB +Rz -F
MM +INS +SB -Rz +F
MM +INS -SB +Rz +F
MM -INS +SB +Rz +F
MM +INS +SB +Rz +F
Count
YFP fluorescence

Figure 4.4 Flow cytometry analysis of *HNF4A*:YFP reporter organoids cultured in E6 +RA or proliferation medium followed by cardiac maturation medium (MM) with or without additives. A: Flow cytometry plots showing gates for live single cells (side scatter area SSC-A vs. forward scatter area FSC-A), YFP+ live cells for specific conditions, and representative yields of these populations. B: Histograms showing YFP fluorescence intensity in YFP+ events (gated as in panel A) at T_0 prior to applying media conditions, and in each media condition, normalised to 1000 events. Both the T_0 plots at the top of each column of plots represent the same samples. Each plot shows events from three organoids. Black dashed lines are visual aids for comparing histograms. SB = SB 431542. Rz = rosiglitazone. INS = insulin. F = forskolin.

4.5 Characterising the effects of maturation medium and small molecules on proximal tubule maturation

To determine if switching organoids to maturation medium without proliferation medium was sufficient to support *HNF4A* expression in proximal tubules, we cultured organoids according to standard protocols. At D7+11, organoids were either maintained in E6 with retinoic acid as a control or switched to maturation medium with small molecules. At D7+18, organoids were imaged and dissociated for flow cytometry.

Similar to our previous observations, while YFP^+ tubules were visible in all conditions at D7+18, they were less prominent in organoids in E6 +RA (Figure 4.5A). Organoids in MM again showed an unexpectedly low apparent yield of YFP^+ cells after dissociation despite a better yield of live cells, showing that the low YFP^+ yield was not an unintended effect of the proliferation medium, but was inherent to MM (Figure 4.5B). MM, MM +Rz, and MM +INS had brighter YFP^+ cells than E6 +RA but were also dimmer than organoids at T_0 from the previous experiment, while organoids switched to MM +SB or MM +SB +Rz had the brightest YFP^+ cells (Figure 4.5C). While differences between MM, MM +Rz, and MM +INS were not as prominent as before, on the whole these results mirrored our screening experiment and showed that proliferation medium was not necessary to support *HNF4A* expression in organoids over what was possible in E6 +RA, as well as suggesting that maturation medium with TGFβ inhibition would improve proximal tubule maturity.

Another set of organoids was cultured for qRT-PCR and immunofluorescence characterisation of the effects of MM +SB and MM +SB +Rz on proximal tubules, compared to organoids at T_0 and organoids maintained in E6 +RA. All conditions had a non-significant drop in *EPCAM* expression compared to T_0 (Figure 4.5A). Expression of proximal tubule markers was always significantly lower in organoids maintained in E6 +RA compared to T_0,

with the exception of *SLC5A2* which had low expression in all conditions. In contrast, MM +SB and MM +SB +Rz showed significant increases in *CUBN*, *LRP2*, and *SLC22A2* expression as a proportion of *EPCAM* expression compared to both T_0 and E6 +RA, showing increased proximal tubule maturity with respect to these transport pathways. Both MM conditions showed a non-significant decrease in *SLC47A1* compared to T_0, though expression was higher than in E6 +RA. MM +SB +Rz also showed a significant drop in *HNF4A* expression compared to MM +SB, which was not expected from their similar YFP brightness but suggested that PPARγ activation by rosiglitazone did not synergise with TGFβ inhibition.

Immunofluorescence analysis of organoids from each condition showed that $NPHS1^+$ glomeruli, LTL^+ proximal tubules, $ECAD^+$ distal tubules and $ECAD^+$ $GATA3^+$ ureteric epithelium were all present as expected (Figure 4.5B). However, in MM +SB and MM +SB +Rz, the LTL^+ tubules were also strongly $ECAD^+$. While ECAD expression in proximal tubules was previously claimed by our group to be a marker of increased maturation [113], and other groups have observed ECAD antibody staining in adult human proximal tubules [358], there is little evidence of ECAD expression in mature proximal tubules at the mRNA level, based on our bioinformatics analysis of published datasets in Chapter 2 [195,216,217]. It is possible that the antibodies we and other groups have used to detect ECAD are cross-reacting with other cadherins which are expressed in the mature proximal tubule, such as cadherin-6 [359]. Further characterisation with qRT-PCR or an antibody panel will be required to determine if this was the case, or whether the proximal tubules in MM +SB were aberrantly expressing true ECAD. Regardless of the explanation, this change in cadherin expression might explain the difficulty we faced in reliably quantifying YFP^+ cells by flow cytometry after organoids are cultured in maturation medium.

As discussed in Chapter 2, we did not have antibodies which could reliably detect SLC transporters in whole mount immunofluorescence. Staining for YFP, LRP2, and CUBN in T_0 and E6 +RA organoids showed strong apical staining of LRP2 and CUBN in YFP^+ tubules, as expected (Figure 4.5C). However, while MM +SB and MM +SB +Rz had increased *LRP2* and *CUBN* mRNA by qRT-PCR, staining for protein decreased compared to T_0 and E6 +RA, and CUBN staining in particular occurred in aggregates rather than along the apical membrane. Other markers of the mature proximal tubule include CD13 and AQP1. In T_0, CD13 and AQP1 staining was sporadic, and typically occurred where LTL staining was weaker (Figure 4.7). Faint CD13 and AQP1 staining were observed in YFP^+ LTL^+ tubules in E6 +RA, while most YFP^+ LTL^+ tubules in MM +SB and MM +SB +Rz expressed CD13 on

the apical membrane. This suggests that CD13, AQP1, and LTL are expressed in subpopulations of organoid proximal tubules and gain wider expression over time, and that MM +SB and MM +SB +Rz improves CD13 expression compared to continued culture in E6 +RA. Further work will be required to validate changes to AQP1 and CD13 expression at the mRNA level, and to determine if the observed changes in CUBN localisation and widened CD13 expression impact the function of these proximal tubules.

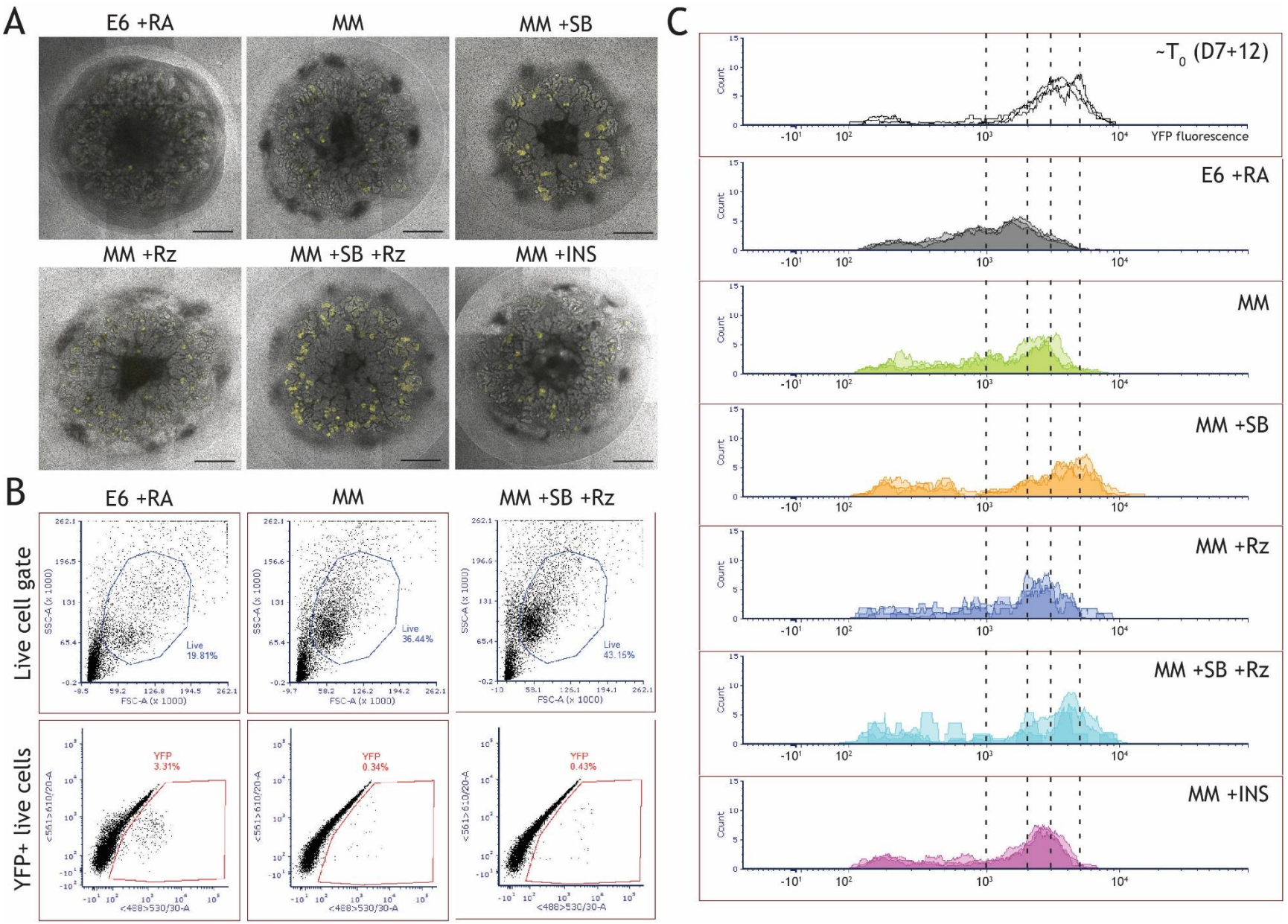
A
E6 +RA
MM
MM +SB
MM +Rz
MM +SB +Rz
MM +INS
B
E6 +RA
MM
MM +SB +Rz
Live cell gate
YFP+ live cells
Live
19.81%
Live
36.44%
Live
43.15%
YFP
3.31%
YFP
0.34%
YFP
0.43%
SSC-A (x 1000)
FSC-A (x 1000)
<561>610/20-A
<488>530/30-A
C
~T0 (D7+12)
YFP fluorescence
E6 +RA
MM
MM +SB
MM +Rz
MM +SB +Rz
MM +INS
Count

Figure 4.5 Live microscopy and flow cytometry analysis of *HNF4A*:YFP reporter organoids cultured in E6 +RA and cardiac maturation medium (MM) with or without additives. A: Live microscopy of organoids at D7+18 showing YFP in tubules. Brightness was adjusted using the automatic "best fit" threshold in the ZEN image analysis program (Zeiss) for all images. Images are representative of six organoids from the same experiment. Scale bars 100 μm. SB = SB 431542. Rz = rosiglitazone. INS = insulin. B: Flow cytometry plots showing gates for live single cells (side scatter area SSC-A vs. forward scatter area FSC-A), YFP+ live cells for specific conditions, and representative yields of these populations. C: Histograms showing YFP fluorescence intensity in YFP+ events (gated as in panel B) at T_0 prior to applying media conditions, and in each media condition, normalised to 1000 events. The T_0 plot represents the T_0 samples presented in Figure 4.4. Each plot shows events from three organoids. Black dashed lines are visual aids for comparing histograms.

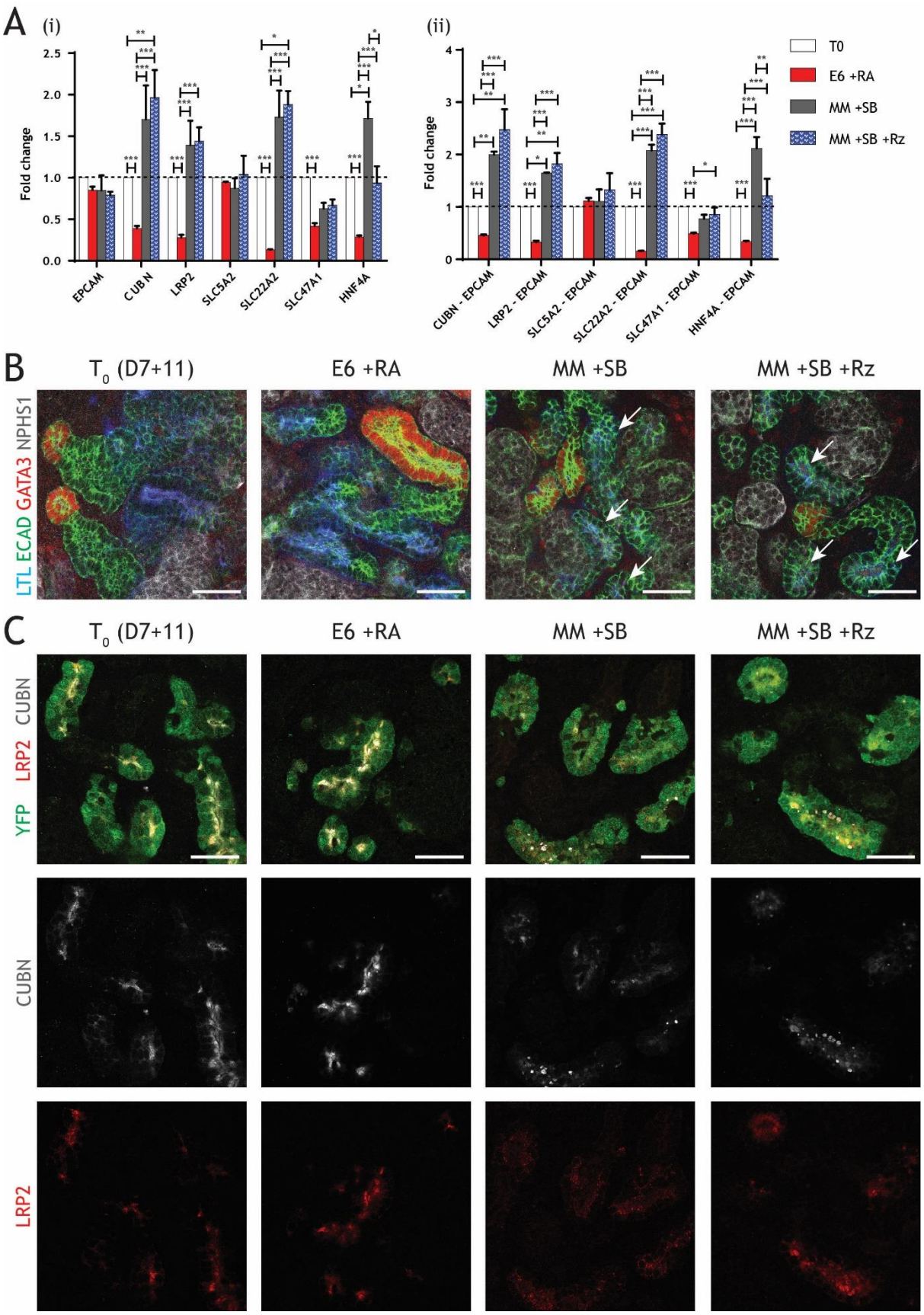
A
(i)
Fold change
EPCAM
CUBN
LRP2
SLC5A2
SLC22A2
SLC47A1
HNF4A
(ii)
Fold change
CUBN - EPCAM
LRP2 - EPCAM
SLC5A2 - EPCAM
SLC22A2 - EPCAM
SLC47A1 - EPCAM
HNF4A - EPCAM
T0
E6 +RA
MM +SB
MM +SB +Rz
B
T0 (D7+11)
E6 +RA
MM +SB
MM +SB +Rz
LTL ECAD GATA3 NPHS1
C
T0 (D7+11)
E6 +RA
MM +SB
MM +SB +Rz
YFP LRP2 CUBN
CUBN
LRP2

Figure 4.6 qRT-PCR and immunofluorescence analysis of *HNF4A*:YFP reporter organoids prior to media switching (T_0) and cultured in E6 +RA or cardiac maturation medium with small molecules. A: qRT-PCR for proximal tubule markers. Data are presented as fold changes relative to T_0, (i) normalised by *GAPDH* expression and (ii) as a proportion of normalised *EPCAM* expression. n = 3 organoids from the same experiment, error bars ± SEM. Statistical significance for each gene across treatment groups was determined using two-way ANOVA and Tukey's post-test analysis of normalised (ΔCt) values (* $p < .05$, ** $p < .01$, *** $p < .001$). B: Immunofluorescence staining of organoids from each condition showed that glomeruli ($NPHS1^+$), proximal tubules (LTL^+), distal tubules ($ECAD^+$) and collecting ducts ($ECAD^+$ $GATA3^+$) were all present. Arrows mark LTL^+ segments which are also strongly $ECAD^+$. Scale bars 50 µm. C: Immunofluorescence staining of organoids from each condition for YFP and the apical endocytotic receptors LRP2 and CUBN, illustrating changes in CUBN localisation. Scale bars 50 µm.

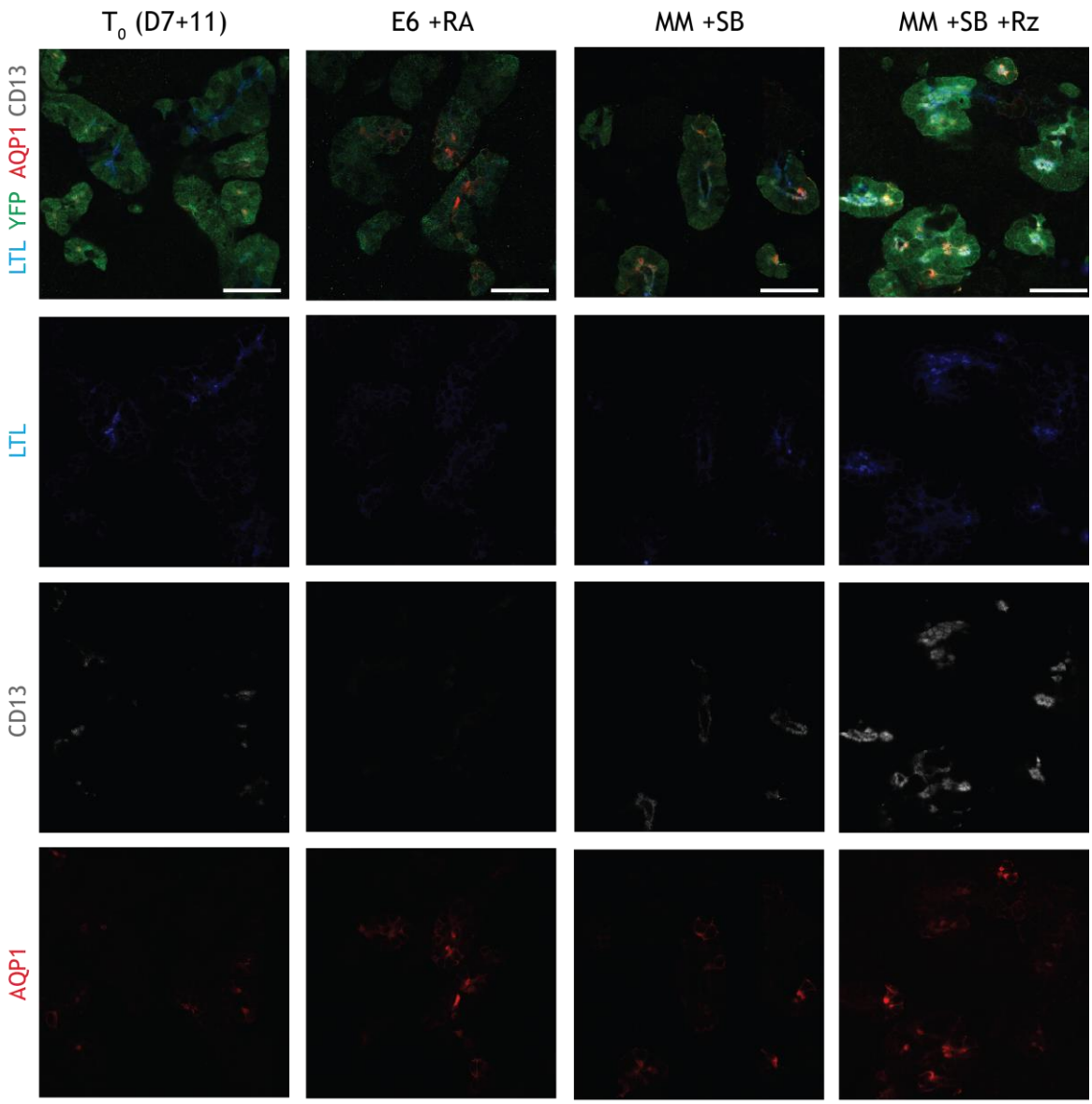

Figure 4.7 Further immunofluorescence analysis of *HNF4A*:YFP reporter organoids prior to media switching (T_0) and cultured in E6 +RA or cardiac maturation medium with small molecules. Organoids from each condition were stained for YFP and the apical proximal tubule markers LTL, AQP1 and CD13, illustrating changes in the distribution of these markers along YFP^+ tubules. Scale bars 50 µm.

4.6 Discussion

4.6.1 Summary of findings, inferences, and alternative approaches for optimising proximal tubule maturity

Based on the analysis of proximal tubule cells in scRNA-seq datasets of foetal and adult mouse and human kidneys described in Chapter 2 and based on prior literature, several pathways were identified which were differentially expressed between early and mature proximal tubules. We hypothesised that manipulating these pathways *in vitro* with changes in media composition, growth factors, or small molecules could potentially induce proximal tubule proliferation or maturation in organoids, maturation being defined as increased expression of markers which have been shown to mediate drug-induced nephrotoxicity *in vivo*. These included pathways indicating a shift away from glycolysis towards fatty acid oxidation. To optimise the maturation of proximal tubules in iPSC-derived organoids, we first hypothesised that a defined medium with varying concentrations of glucose and palmitic acid would improve the expression of proximal tubule markers in organoids by inducing a carbon source shift. The change in basal medium improved *CUBN* and *SLC22A2* expression compared to standard culture conditions. This was promising given that *SLC22A2* was one of the proximal tubule markers which had low expression in organoids, based on our analysis in Chapter 2. However, varying the glucose and palmitic acid concentration in the defined medium had little effect on its own, suggesting that either the carbon source shift had not occurred or it was not a major driver of proximal tubule maturation under these culture conditions.

The *HNF4A*:YFP reporter line described in Chapter 3 which marks developing proximal tubules in organoids was then used to screen the effects of manipulating other pathways which were previously identified by bioinformatics analysis, through live imaging and flow cytometry of YFP^+ cells in organoids. Quantifying the proportion of YFP^+ cells in dissociated organoids was unexpectedly challenging, possibly due to changes in cadherin expression in proximal tubules which were later detected by immunofluorescence staining.

Contrary to our expectations, we found little evidence by live imaging that E6 media supplemented with R-spondin 1, TGFβ inhibitor, and FGF2 induced proximal tubule proliferation. R-spondin 1 was added to this medium based on our finding that *Lgr4*, an R-spondin receptor, was differentially upregulated in early proximal tubules in the mouse embryonic kidney (detailed in Chapter 2). However, compared to other cell types which

expressed *Lgr4*, such as the distal tubule, podocytes, and ureteric epithelium, the proximal tubule had lower expression of the Wnt receptors *Fzd2* and *Fzd7*. As the canonical role of LGR stimulation by R-spondin is to maintain Wnt receptors on the cell surface, this suggests that early proximal tubule cells might not demonstrate a canonical response to R-spondin. Likewise, FGF2 was added based on observed upregulation of *Fgfr3* and *Fgfr4* in mouse embryonic proximal tubule. However, as *Fgfr3* and *Fgfr4* knockouts in mice do not produce the structural defects seen in *Fgfr1* or *Fgfr2* conditional knockouts [251,252], it is possible that the role of FGFR3 and FGFR4 in the proximal tubule is not to drive proliferation or specify the proximal tubule phenotype. Identifying cell type-specific pathways in the kidney to identify changes which can be made to the culture system to develop or suppress specific cell types is an approach that has been suggested by a few groups, including our own, but these results highlight the need to validate the pathways thus identified [195,200,216].

In Chapter 2 we also showed that proximal tubules shift from glycolysis to fatty acid oxidation as they mature, and that they downregulate TGFβ/BMP signalling. Consistent with these observations, a published insulin-free "maturation medium" used to induce carbon source shifts in cardiac organoids [284], used in combination with a TGFβ inhibitor, sustained YFP expression in organoids better than continued culture in E6 with all-*trans*-retinoic acid, which caused YFP expression to decline over time. As *HNF4A in vivo* is expressed in early proximal tubules and continues to be expressed in mature proximal tubules, sustained YFP expression suggested improved maintenance of proximal tubule cells and possibly improved maturation.

Due to time constraints, we did not characterise metabolic activity in organoids in these experiments or perform a factorial screen with components or groups of components in the maturation medium. Hence, it remains possible that the benefit of maturation medium was due to albumin and hormone supplementation and/or removal of insulin, similar to what we observed in section 4.3, rather than the hypothesised shift towards fatty acid oxidation in organoid proximal tubules. As dependence on mitochondrial fatty acid oxidation is a known feature of the mature proximal tubule [40], metabolic activity and mitochondrial function of organoids in maturation medium should be studied further. Other approaches for promoting fatty acid oxidation in organoids, along with maturation medium, might include inhibitors of glycolytic enzymes or of HIF1α (hypoxia-inducible factor 1α), which is an approach that has been used for iPSC-derived cardiac organoids [360].

A PPARγ agonist was added to the maturation medium as many of the genes which are involved in fatty acid oxidation in the proximal tubule were PPAR targets (detailed in Chapter 2). However, adding a PPARγ agonist to maturation medium with TGFβ inhibition caused a significant drop in *HNF4A* expression in whole organoids compared to maturation medium and TGFβ inhibition alone, without causing a large change in YFP brightness. One possible explanation for these findings was that PPARγ activation in this context caused another cell population to expand. However, *HNF4A* expression as a proportion of *EPCAM* was also affected, and no expansion of non-proximal tubule epithelium which would express *EPCAM* but not *HNF4A* was observed on immunofluorescence staining for nephron segments. Hence, PPARγ activation was not necessarily beneficial to maintenance of the proximal tubule phenotype or to maturation. PPARα agonists may be a better candidate for inducing fatty acid oxidation in proximal tubules, as PPARα activation maintained fatty acid oxidation in proximal tubules in mouse models of cisplatin-induced acute kidney injury [361].

Further characterisation of *HNF4A*:YFP organoids switched to maturation medium with TGFβ inhibition, compared to organoids before media switching (T_0) and organoids maintained in E6 with all-*trans*-retinoic acid, showed that organoids switched to maturation medium had higher *CUBN*, *LRP2*, and *SLC22A2* expression and increased CD13 staining compared to organoids maintained in E6 and organoids at T_0. More studies, such as functional assays with labelled albumin or fluorescent SLC22A2 substrates, are required to determine if increased expression of *CUBN*, *LRP2*, and *SLC22A2* corresponds with increased function of these pathways.

The fact that continued culture in E6 with retinoic acid caused YFP brightness and proximal tubule marker expression to decline over time while maturation medium with TGFβ inhibition improved marker expression over the same time period suggests that it is possible to maintain organoids in maturation medium for longer than we have previously thought feasible. As some markers such as *SLC5A2* were still not strongly expressed, a longer period in culture may be required for further maturation. For comparison, in this experiment organoids were maintained in maturation medium for up to 6 days, while for differentiation of iPSC-derived neurons the maturation phase after the initial differentiation can take one to seven months depending on the protocol and desired neuron type [362,363].

Maturation medium with TGFβ inhibition also induced aggregation of CUBN protein and ECAD expression in the proximal tubule, which there is little evidence of at the mRNA level

in vivo. Comprehensive profiling of the effect of maturation medium on organoid proximal tubules could be performed by FACS of proximal tubule cells followed by bulk RNA sequencing, or through scRNA-seq. This will also help to determine the biological significance of the observed changes in CUBN and ECAD expression, how they might impact the ability of these proximal tubules to accurately model the behaviours of tubules *in vivo*, and how culture conditions might be optimised further if these changes are detrimental. Ultimately, culture conditions which improve proximal tubule metabolism and transporter function will allow organoids to model drug-induced toxicity more accurately.

4.6.2 Limitations of the current work

As previously discussed, flow cytometry measurements of the proportion of proximal tubule cells in *HNF4A*:YFP organoids in maturation medium appeared to be unreliable, as <1% of live cells were YFP^+, which was not consistent with the appearance of the organoids on live fluorescent microscopy or immunofluorescence staining for YFP. Without quantitating the proportion of YFP^+ cells in organoids, it becomes more difficult to determine if increased expression of proximal tubule markers seen in whole organoid qRT-PCR was due to increased maturity of proximal tubule cells or an increased proportion of proximal tubule cells within the whole organoid. The latter might occur as a result of proximal tubule cell proliferation, or a bias in nephron segmentation towards the proximal tubule. Organoid qRT-PCR showed that organoids in control and maturation medium had similar levels of *EPCAM* expression, and there were no obvious segment biases seen in immunofluorescence staining for each nephron segment, so proximal tubule maturation was still the most likely explanation for the increase in marker expression. Nevertheless, for trials of other media conditions, a rapid method of quantitating proximal tubule cells, such as high-content imaging of a reporter line, will still be required to quickly identify conditions which cause proliferation or nephron patterning biases, and distinguish these from conditions which induce maturation.

While YFP brightness in a *HNF4A*:YFP reporter line was used to identify conditions which improved proximal tubule maturation in this experiment, *HNF4A* is not strongly differentially expressed between early and mature proximal tubules *in vivo*. The fact that we were able to show a significant increase in *HNF4A* expression in this experiment under certain conditions highlights the relative immaturity of proximal tubules in organoids cultured under standard conditions compared to early proximal tubules *in vivo*. However, we might also expect that the capacity of a *HNF4A*-driven reporter to give a rapid readout of proximal tubule maturity

will become limited as organoid culture conditions are optimised further. To address this, we could use a reporter line for a gene which is differentially expressed between early and mature proximal tubules such as a *LRP2*:mTagBFP2 reporter line re-made as described in Chapter 3, or possibly a *SLC22A6* or *SLC22A2*-driven reporter.

The aim of this experiment was to identify culture conditions which would induce proximal tubule maturation, defined as an increased expression of proximal tubule markers, to optimise organoids for modelling nephrotoxicity *in vitro*. However, these culture conditions might also attenuate the injury response to nephrotoxic drugs and lead to underestimation of their effects. For example, TGFβ inhibition ameliorates the nephrotoxic effects of cyclosporine in mouse models [364]. Further optimisation will be required to determine if certain factors and/or small molecules can be removed from the culture medium after proximal tubules have matured to a certain stage, to avoid any unintended interactions with the drugs being tested.

4.6.3 Future work to optimise a platform for modelling nephrotoxicity in vitro

Because organoids are composed of heterogenous cell populations, it is possible that conditions which optimise proximal tubule maturation may be detrimental for other cell types. For example, cells in most nephron segments other than the proximal and distal tubule favour glucose as an energy source instead of fatty acids [365]. Hence, to use organoids to model nephrotoxicity to multiple cell types, such as proximal tubules and podocytes, the effect of any optimised maturation medium on each cell type of interest must be characterised. Alternatively, conditions can be developed to deliberately skew differentiation towards a specific renal cell type, as a recent paper demonstrated for podocytes [200]. Isolated iPSC-derived proximal tubule cells could then be used to seed microfluidic devices, which allow precise control of fluid administration to the basolateral and apical surfaces of the proximal tubule cells for nephrotoxicity testing [2,95,154,159].

This chapter has demonstrated the use of a proximal tubule reporter line to screen and characterise modifications to culture media which were predicted to induce proximal tubule proliferation or maturation based on prior bioinformatics analysis. Screening by flow cytometry and live imaging was still relatively low-throughput. High-content imaging of organoids differentiated from proximal tubule reporter lines will allow rapid screening for media conditions which induce proximal tubule proliferation and/or maturation, and characterisation of functional markers in each condition. Should conditions with sufficient proximal tubule function be identified, a proximal tubule injury reporter such as the

HAVCR1:mCherry line described in Chapter 3 can also be used to characterise the injury response of organoids to known nephrotoxicants under those media conditions, to determine if they will accurately model the *in vivo* response.

In summary, using a reporter line to screen for media conditions which improve proximal tubule maturity, we found that a low-glucose, insulin-free medium supplemented with B-27, palmitic acid and a TGFβ inhibitor improved the expression of proximal tubule markers in organoids compared to standard culture conditions. Further iterative optimisation on these media conditions to drive other pathways which drive proximal tubule maturation *in vivo* can be performed using reporter lines as described here or through high-content screening. Comprehensive characterisation of transcriptomic and functional changes in the proximal tubule under these media conditions can also be carried out. Organoids cultured in optimised media conditions with sufficient proximal tubule transporter function may become a useful tool for modelling drug-induced toxicity *in vitro*.

5 IMPROVING PROXIMAL TUBULE MATURITY IN ORGANOIDS THROUGH XENOTRANSPLANTATION

5.1 Background

In Chapter 4 we discussed the challenge of making organoids with proximal tubule cells which are sufficiently mature to model drug-induced nephrotoxicity, and identified optimisations which could be made to the culture media to induce maturation. Aside from altering media conditions, another approach for maturing iPSC-derived tissues and organoids is to transplant them into an immunocompromised animal in a highly vascularised tissue, such as on the abdominal mesentery (the omentum), in the lymph nodes, or under the renal capsule [366–370]. The organoid might then attract an ingrowth of host vasculature, providing a supply of nutrients, hormones, and other metabolites. For kidney organoids, vascularisation of the glomeruli and subsequent fluid filtration into the tubules would also replicate nephron function to some extent and provide fluid shear stress to induce glomerular and tubular maturation [371]. Such an environment would be more similar to normal kidney development than continued culture *in vitro*.

Embryonic rat kidneys transplanted onto the omental fat pad or under the renal capsule of adult rats will develop nephrons with host vasculature [372], showing that transplantation into these sites is permissive for nephron differentiation and development. Suspensions of ESC-derived nephron progenitors and developing tubules injected subcutaneously into mice differentiated and matured into glomeruli and tubules which expressed markers of the glomeruli, proximal tubule, loop of Henle, distal tubule, and ureteric epithelium [209]. However, transplant maturation in the mouse took 12 weeks, and the graft also developed non-renal tissues such as cartilage. This approach also required nephron progenitors to be injected instead of differentiated nephrons, as suspensions of differentiated cells were less capable of re-associating after injection.

In contrast to the approach of implanting nephron progenitors, Sharmin *et al*. [208] induced nephrogenesis in human iPSC-derived nephron progenitors *in vitro* and implanted them under the renal capsule of immunocompromised mice for up to 20 days. The iPSC-derived renal tissue gave rise to glomeruli with host vasculature which developed slit diaphragms and double-layered basement membranes between the podocytes and fenestrated endothelial cells, similar to glomeruli *in vivo*. This showed that xenotransplantation could be used to mature

iPSC-derived renal tissue. The transplant procedure used agarose "spacers" under the renal capsule which were soaked in vascular endothelial growth factor (VEGF) to attract host vasculature. While the implanted tissue would not differentiate without the spacers due to physical pressure from the host renal capsule, soaking the spacers in exogenous VEGF was not strictly necessary for the developing glomeruli to vascularise, consistent with VEGF production from the glomeruli themselves [208]. van den Berg *et al.*[210] demonstrated that organoids which are cultured *in vitro* increase their production of VEGF over time, and organoids which have been cultured for up to 18 days after the induction of nephrogenesis are capable of drawing host vasculature into their glomeruli and of connecting host and organoid-derived vasculature when transplanted under the renal capsule [210]. Organoids cultured *in vitro* for longer prior to transplant were also less fragile and did not require spacers for transplantation. Nevertheless, similar to Sharmin *et al.* [208], van den Berg *et al.* [210] observed double-layered basement membranes and fenestrated endothelium within transplanted glomeruli after 28 days. Based on these results showing that transplantation induces maturation and slit diaphragm formation in iPSC-derived glomeruli, the Sharmin protocol has subsequently been used to model defects in slit diaphragm formation in glomeruli derived from a congenital nephrotic syndrome patient [211].

As xenotransplantation of organoids has been shown to be a useful method of maturing iPSC-derived glomeruli to make them more accurate models, it is possible that transplantation would also improve the maturity of proximal tubules. Tubules in organoids transplanted under the renal capsule develop peritubular capillaries and microvilli [210], and tubules in human foetal kidneys and organoids transplanted into lymph nodes for 6-8 weeks show expression of the early proximal tubule markers LTL and LRP2 as well as specific accumulation of dextran [368]. However, characterisation of tubular maturation after xenotransplantation has been less extensive compared to characterisation of glomerular maturation.

While the main aim of this project was to develop an *in vitro* model of nephrotoxicity, transplantation could be used to determine if organoid proximal tubules are capable of maturing to the degree required to model drug-induced injury. Hence, the aims in this chapter were to develop a xenotransplantation method suitable for our purposes, and to compare proximal tubule marker expression in organoids transplanted into immunocompromised mice with organoids prior to transplant or maintained *in vitro*, to determine if transplantation improved proximal tubule maturity.

5.2 Methods

Organoids were differentiated from the *LRP2*:mTagBFP2 and *HNF4A*:YFP reporter lines described in Chapter 3 using standard methods, and then taken for transplant between D7+9 and D7+12 of culture. Pre-transplant controls were also fixed for immunofluorescence and histology staining.

Transplants were performed in one of three sites per mouse: subcutaneously (along the skin of the back), on the omental fat pad, or under the renal capsule (subcapsular transplant). All animal experimental protocols were approved by the Murdoch Children's Research Institute Animal Ethics Committee (reference numbers A873 and A888). For subcutaneous and omental transplants, 8 week-old NSG (genotype NOD.Cg-Prkdc scid II2rg tm1WjI/SzJ/arc) female mice (Jackson Laboratories) were injected subcutaneously with buprenorphine (0.1 mg/kg) 30 minutes prior to surgery for pain relief and anaesthetised with isoflurane for surgery. Surgery was performed on a heat mat to maintain temperature at 37° C. For subcutaneous transplants, an incision was made on the dorsum of the animal's neck to create a pocket into which 1-2 whole organoids were placed. For omental transplants, the abdominal fat was exposed with a midline incision and 3-4 whole organoids were placed on the abdominal fat and secured with TISSEEL fibrin glue (Baxter Healthcare). Incisions were closed with silk sutures.

Mice were euthanised by cervical dislocation prior to sample harvest. For subcutaneous and omental transplants, samples were harvested after 19 days. Subcapsular transplants followed the method in van den Berg *et al.* [210] with the following changes: recipient mice were 10 weeks old, and whole organoids were transplanted at D7+11 or D7+12 and harvested after 21 days.

Surgeries were performed by Melissa Little, Michelle Scurr, Siebe Spijker and Ker Sin Tan from within our lab group. Paraffin embedding, sectioning and staining was performed by Michelle Scurr.

5.3 Grafts are overgrown with non-renal tissue but surviving tubules maintain proximal tubule phenotype

Subcutaneous transplantation was trialled as the surgery was relatively easier to perform and less stressful for the experimental animals. As noted in section 5.1, Bantounas *et al.* [209] reported success with this approach. However, at the point of harvest, these grafts proved

difficult to locate and not all the grafts were successfully retrieved. Histological staining of grafts harvested from subcutaneous transplants from both the *HNF4A*:YFP and *LRP2*:mTagBFP2 cell lines showed overgrowth of non-tubular, non-renal tissue surrounding scattered patches of tubules (Figure 5.1A). The non-tubular tissue surrounding the tubules resembled fat. While no vascular tissue was detected near the tubules in these sections, immunofluorescence staining for MECA-32, which specifically stains mouse endothelial cells, showed ingrowth of MECA-32$^+$ host vasculature in some of the grafts (Figure 5.1B). Staining with an antibody specific to the human homologue of the nuclear protein Ku80 (hKu80) showed that most of the non-renal tissue surrounding the tubules was hKu80$^-$, suggesting that this was subcutaneous fat from the host that was extracted when attempting to retrieve the grafts. However, isolated nuclei were hKu80$^+$, showing that some of the fat cells were derived from the organoid and not the host.

Grafts from omental transplants were likewise difficult to retrieve. However, in contrast to the subcutaneous transplants, vascularisation of glomeruli was visible in at least one section (Figure 5.2A). The non-tubular tissue in the omental grafts resembled fibroblasts instead of fat. Whole mount staining of a successfully-retrieved *LRP2*:mTagBFP2 omental graft showed mTagBFP2$^+$ proximal tubules (Figure 5.2B). Staining for PECAM1 in both human and mouse endothelial cells showed a vascular network which was loosely associated with the proximal tubules. Not all of the PECAM1$^+$ vasculature was MECA-32$^+$, suggesting that this network was composed of both organoid-derived (human) and host-derived (mouse) vasculature. Association of MECA-32$^+$ host vasculature with the tubules was also seen in sections (Figure 5.2C). Strong staining for hKu80 was seen throughout the graft, showing that the non-renal tissue seen in histological sections was largely derived from the organoid, in contrast to the subcutaneous transplants.

Grafts from subcapsular transplants were easier to retrieve as they were confined by the renal capsule and would not move from the transplant site. The required expertise for both transplantation and retrieval from this site was developed within the lab during the course of this PhD project. However, similar to the subcutaneous and omental transplants, the graft showed overgrowth of non-renal tissue surrounding patches of tubules (Figure 5.3Ai). A graft retrieved at day 2 post-transplant did not demonstrate non-tubular overgrowth, showing that this occurred over time as the transplants were maintained *in vivo* (Figure 5.3Aii). Overgrowth only occurred in transplanted organoids, as organoids fixed at the time of transplant (D7+11) or maintained *in vitro* for an equivalent span of time as the transplants

(D7+33) had a much larger proportion of glomerular and tubular tissue (Figure 5.3Aiii and iv). As with the omental transplants, MECA-32$^+$ host vasculature was seen in association with the surviving tubules, and the non-renal tissue in the grafts was positive for hKu80 (Figure 5.3B). The areas of tubules within the grafts maintained reporter expression which was detectable by live microscopy, while tubules in organoids maintained *in vitro* to an equivalent age declined in fluorescence intensity, becoming comparable to background fluorescence in *HNF4A*:YFP organoids or nearly undetectable in *LRP2*:mTagBFP2 organoids (Figure 5.4).

HNF4A:YFP grafts retrieved from subcapsular transplants showed specific uptake of TRITC-labelled albumin in YFP$^+$ tubules similar to organoids prior to transplant (T_0), showing that they retained their capacity for endocytosis, while organoids maintained *in vitro* had noticeably dimmer YFP fluorescence, such that it was difficult to gauge the specificity of albumin uptake (Figure 5.5A). This suggests that organoid proximal tubules lose their phenotype during continued culture *in vitro*, similar to our observations in Chapter 4. Immunofluorescence staining of whole mounts showed that grafts and organoids maintained *in vitro* had AQP1$^+$ vasculature associated with the tubules, which was absent in T_0 organoids (Figure 5.5B). However, T_0 organoids and graft tubules had LTL and CUBN localised to the apical membrane of YFP$^+$ tubules and occasional expression of AQP1 in tubular cells, while organoids maintained *in vitro* did not show proper LTL and CUBN localisation or AQP1 expression in YFP$^+$ tubules (Figure 5.5B).

Taken together, transplanted organoids showed evidence for retention of proximal tubular identity, although the transplanted tissue as a whole became dominated by non-renal tissue over time *in vivo* regardless of the transplant site or cell line used. By the time of harvest, only a few proximal tubules remained within each graft. In contrast, maintaining organoids *in vitro* in standard conditions caused proximal tubules to degenerate even though vascular cells developed over that span of time, while the remaining proximal tubules in transplanted organoids maintained their reporter expression and their capacity for endocytosis. From this we can conclude that, as previously reported [210,368], the transplantation of kidney organoids can induce ingrowth of a host-derived vascular supply that maintains tubular identity and potentially improves maturation.

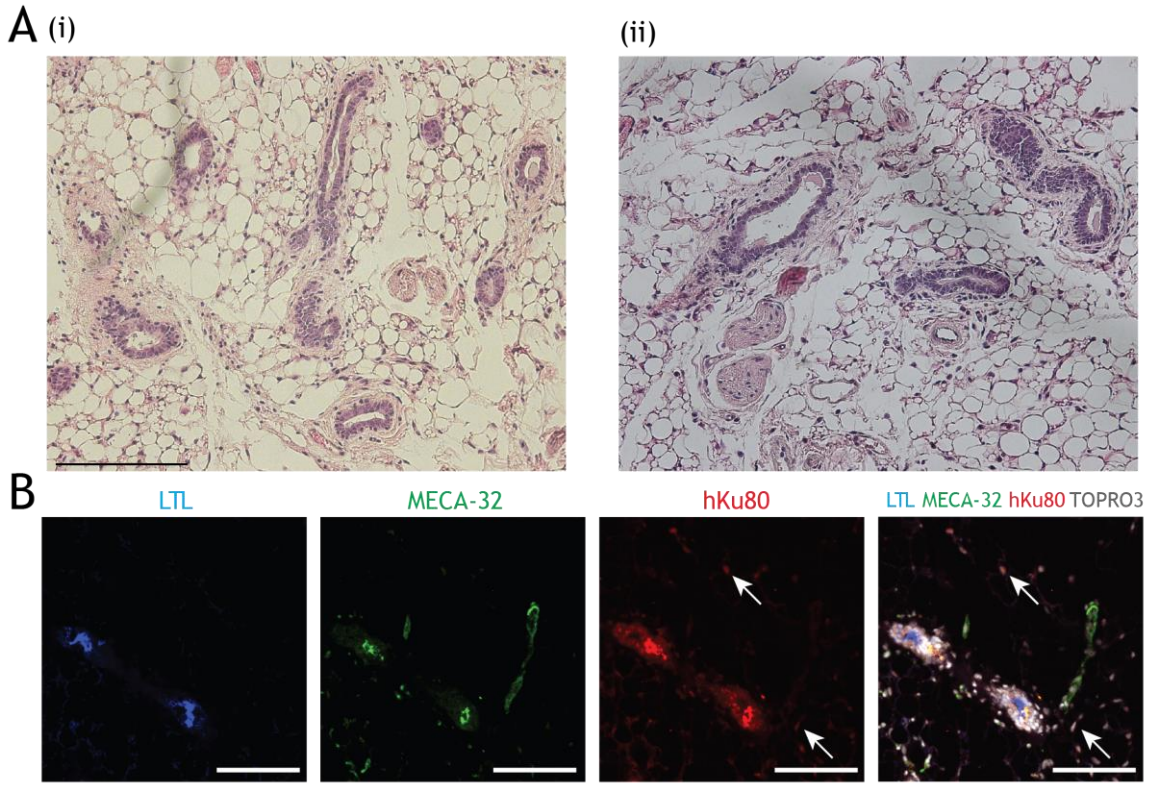

Figure 5.1 Paraffin-embedded sections and whole mounts of organoids transplanted subcutaneously. A: Haematoxylin and eosin (H&E) stains of a (i) *HNF4A*:YFP organoid and (ii) *LRP2*:mTagBFP2 organoid transplanted subcutaneously at D7+9 and retrieved after 21 days *in vivo*. B: Immunofluorescence staining of an organoid transplanted subcutaneously at D7+9, retrieved after 21 days *in vivo*, and sectioned. LTL marks proximal tubules. MECA-32 marks mouse vasculature and hKu80 marks human nuclei. TOPRO3 stains all nuclei. White arrows mark examples of $hKu80^{+}$ human nuclei. All scale bars 100 µm.

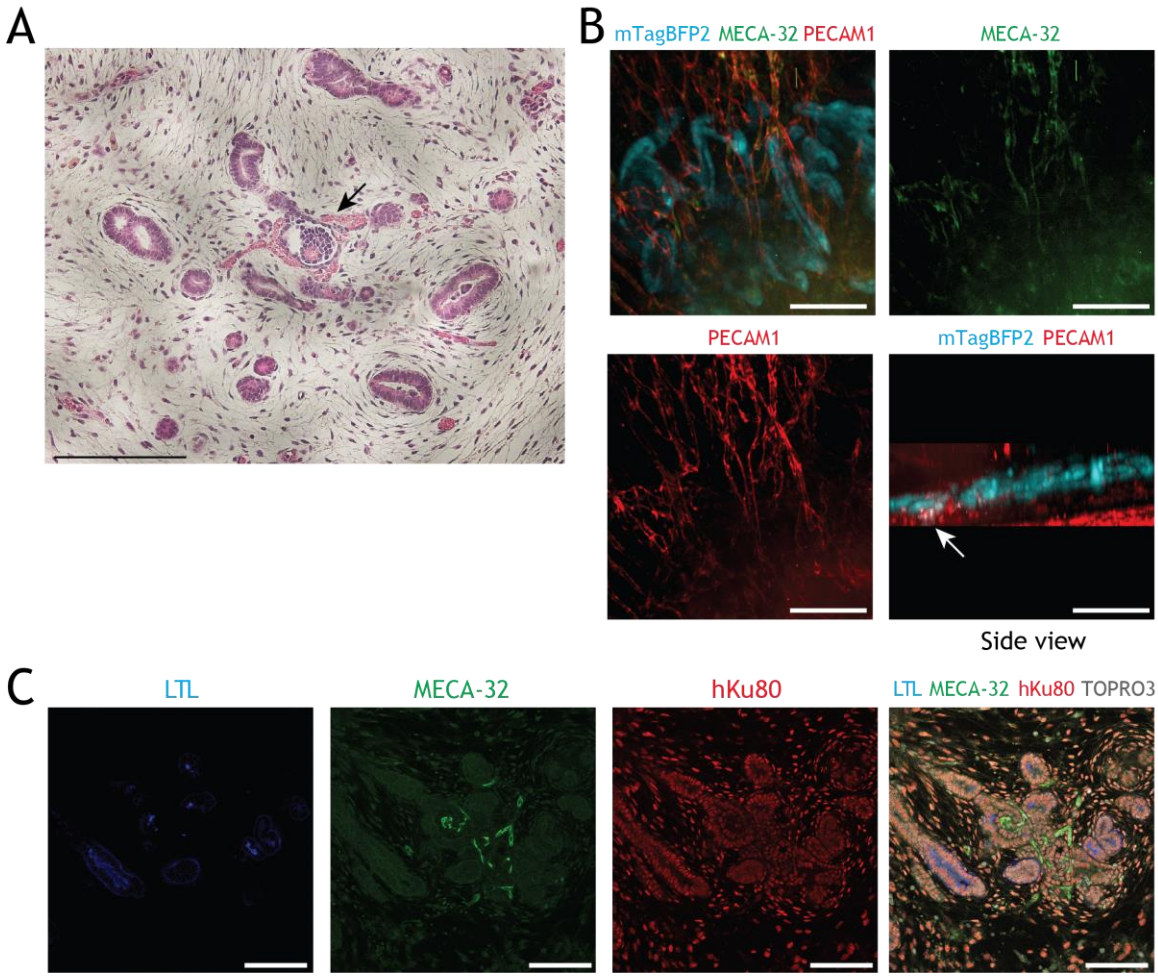

Figure 5.2 Paraffin-embedded sections and whole mounts of organoids transplanted onto the omental fat pad. A: H&E stain of an organoid transplanted onto the omental fat pad at D7+9 and retrieved after 21 days *in vivo*. Arrow marks a vascularised glomerulus. B: 3D projection of whole mount immunofluorescence staining of organoids transplanted onto the omental fat pad at D7+9 and retrieved after 21 days *in vivo*. Side view panel shows the separation between mTagBFP2^{+} tubules and the vascular bed. White arrow marks the closest interaction between the tubules and the vasculature. C: Immunofluorescence staining of an organoid transplanted onto the omental fat pad at D7+9, retrieved after 21 days *in vivo*, and sectioned. LTL marks proximal tubules. MECA-32 marks mouse vasculature and hKu80 marks human nuclei. TOPRO3 stains all nuclei. All scale bars 100 µm.

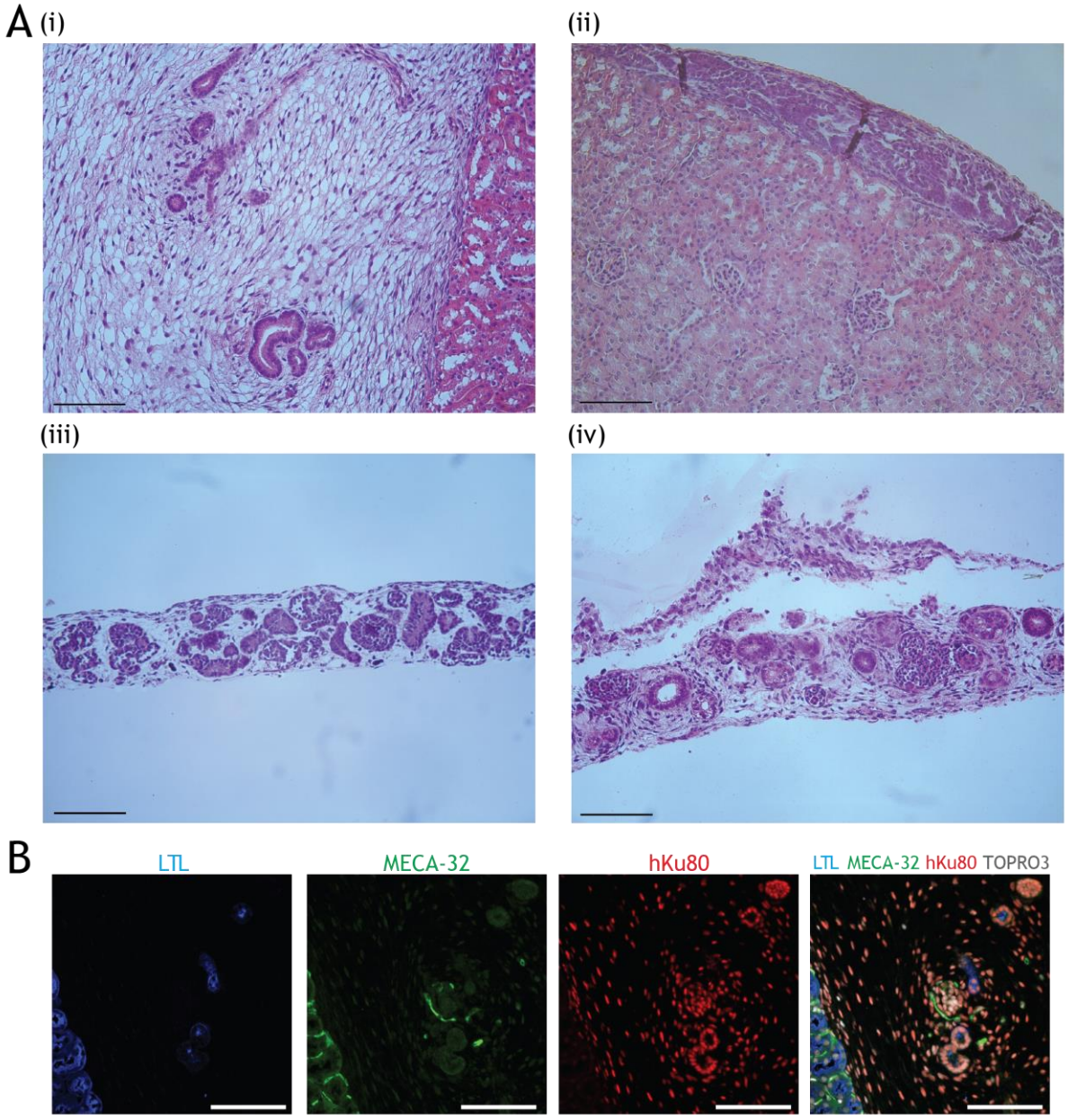

Figure 5.3 Paraffin-embedded sections of organoids transplanted under the renal capsule and organoids maintained *in vitro*. A: Haematoxylin and eosin (H&E) stains of (i) an organoid transplanted at D7+11 and retrieved after 21 days *in vivo*, (ii) an organoid transplanted at D7+11 and retrieved after 2 days *in vivo*, (iii) an organoid fixed at D7+11, (iv) an organoid maintained *in vitro* until D7+33 (i.e. the same span of time as the transplants). B: Immunofluorescence staining of an organoid transplanted subcutaneously at D7+11 and retrieved after 21 days *in vivo*. LTL marks proximal tubules. MECA-32 marks mouse vasculature and hKu80 marks human nuclei. TOPRO3 stains all nuclei. All scale bars 100 µm.

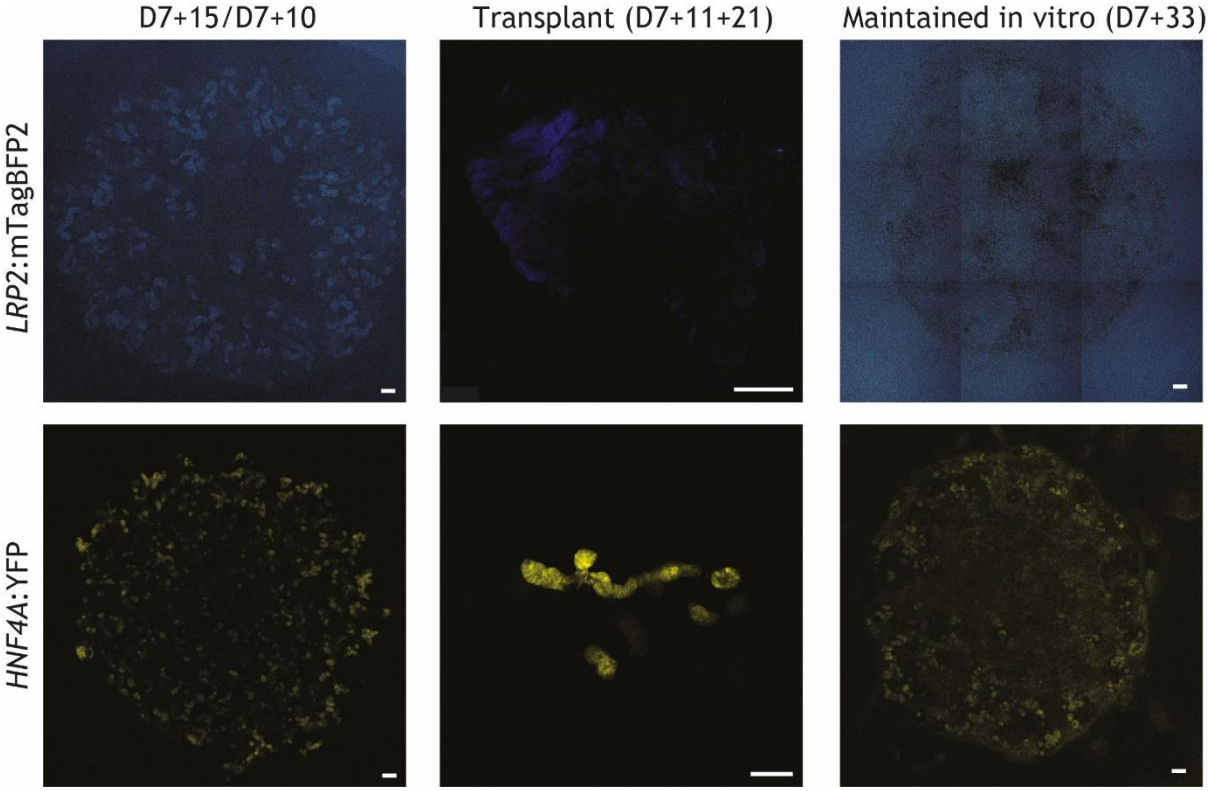

Figure 5.4 Live fluorescent images of organoids transplanted under the renal capsule and organoids maintained *in vitro*. *LRP2*:mTagBFP2 organoids (top) and *HNF4A*:YFP organoids (bottom) at D7+15 and D7+10 respectively (left), transplanted at D7+11 and retrieved after 21 days *in vivo* (middle), or maintained *in vitro* until D7+33 (right). Intensities were adjusted for visibility using the "best fit" setting in ZEN image processing software (Zeiss) for all images. For the *LRP2*:mTagBFP2 line, background subtraction was performed using ZEN image processing software based on autofluorescence in 493-574 nm. All scale bars 100 µm.

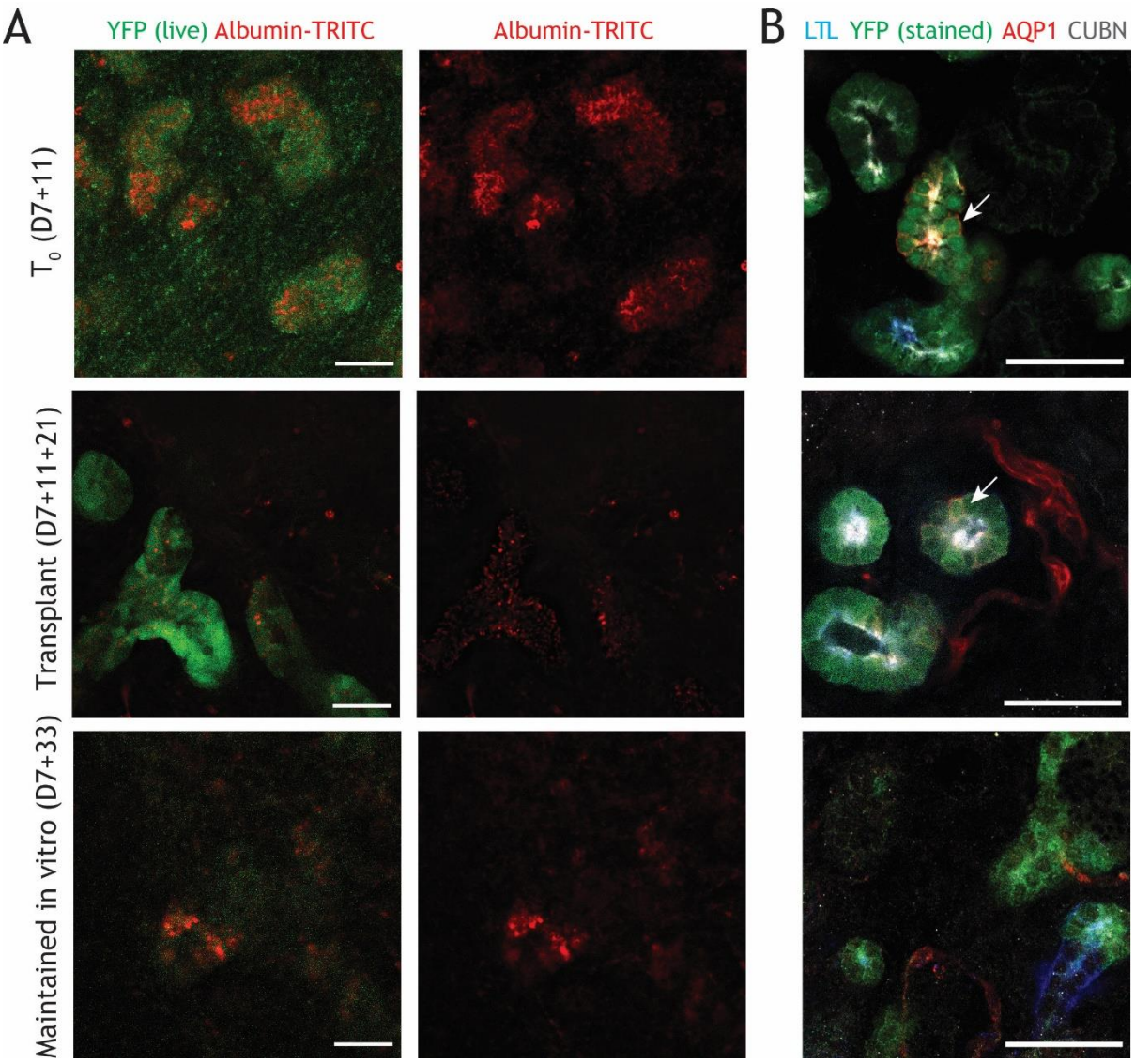

Figure 5.5 Immunofluorescence analysis of organoids transplanted under the renal capsule or maintained *in vitro*. A: Live imaging of YFP and albumin labelled with TRITC in *HNF4A*:YFP organoids at T_0 (D7+11) (top), organoids transplanted under the renal capsule and retrieved after 21 days *in vivo* (D7+11+21) (middle), and organoids maintained *in vitro* to a matched age (D7+33) (bottom). The first panel in the top left has previously been presented in Chapter 3. B: Immunofluorescence staining of *HNF4A*:YFP organoids for YFP, LTL and CUBN in proximal tubules, and AQP1 in proximal tubules and vascular cells. White arrows mark examples of $AQP1^+$ tubular cells. All scale bars 50 µm.

5.4 Discussion

5.4.1 Summary of findings and limitations of the current work

We attempted to vascularise organoids by transplanting them into immunocompromised mice to determine if this would improve proximal tubule maturity. Organoids transplanted subcutaneously, onto the omental fat pad, or under the renal capsule of immunocompromised mice all developed overgrowths of non-renal tissue, such that only a few areas of tubules remained in the grafts which were retrieved. The non-renal tissue in the grafts was derived from the organoids and differed in appearance based on the transplant site, suggesting that it arose from non-renal populations which existed in the organoid prior to transplant and were induced to proliferate and differentiate under cues from the transplant site. Nevertheless, the grafts developed vasculature near the remaining tubules, whether it was host-derived or organoid-derived, which was absent at the time of transplant. In subcapsular transplants, the proximal tubules which remained in the graft, identified by their reporter expression, maintained reporter, LTL, CUBN, and AQP1 expression better than organoids maintained for the same amount of time *in vitro*.

The overgrowth of non-renal tissue in the grafts introduced a number of technical challenges. The first of these was that qRT-PCR or RNA sequencing of the grafts to quantitate proximal tubule marker expression would have been skewed by the low number of tubules in the grafts compared to organoids *in vitro*. Similarly, FACS of proximal tubule cells from the grafts was unlikely to produce sufficient cell yields for profiling. Because of this, without antibodies which could detect markers of the mature proximal tubule such as SLC22A2 by immunofluorescence, we have not yet conclusively demonstrated that transplantation improved proximal tubule maturity in grafts compared to organoids prior to transplant, as opposed to simply maintaining the proximal tubule phenotype better than standard *in vitro* conditions. The latter does not imply the former, since proximal tubules in standard organoid culture conditions lose marker expression over time, as shown here and in further detail in Chapter 4. One method of addressing this is to perform uptake assays for fluorescent substrates of the SLC transporters as previously described [12,170,333]. However, with only a few tubules detectable per graft, multiple grafts would be required to compare uptake with and without transport inhibitors, to demonstrate that uptake was occurring via active transport. Another method of addressing these limitations would be to determine the cause of non-renal

tissue proliferation in the grafts and create conditions which favour tubular growth. Possible approaches are discussed in the next section.

5.4.2 Alternative approaches and future work

The overgrowth of non-renal tissue in transplanted organoids is not a unique issue. Non-renal overgrowth has been observed in transplanted iPSC-derived renal cells in various stages of development prior to transplant, ranging from putative nephron progenitors [209] to kidney organoids cultured up to D7+18 [210]. Transplanted whole or dissociated embryonic kidneys do not demonstrate the same overgrowth [373–376], so the cell types or conditions which give rise to the non-renal tissue are more prevalent in renal cells generated *in vitro*. Off-target stromal progenitors which are produced during induction of renal cells from iPSCs are a likely source [208]. If this is the case, the differentiation protocol should be optimised to minimise off-target cell induction, and the organoid culture protocol could also be optimised to suppress the growth of such populations. Alternatively, it is possible that the non-renal tissue arises from nephron progenitors or renal stromal cells differentiating inappropriately after transplantation, as uncommitted nephron progenitor-like cells are present in organoids at D7+11 and D7+18, even though true nephrogenic niches of progenitors surrounding ureteric tips are not seen in organoids [289]. The uncommitted nephron progenitors could be depleted by forcing another wave of nephrogenesis in organoids *in vitro* a few days prior to transplant. Kidney organoid protocols which recreate the higher-order structure of the kidney by providing a branching ureteric epithelium and nephrogenic niches [196] may also show more appropriate differentiation following transplant.

Increased maturity in the renal tissue in transplanted organoids has been attributed to vascularisation of the grafts, and blood flow between host and graft vasculature into organoid glomeruli has been demonstrated [210], but the process of host vasculature invasion into the grafts and/or the development of graft-derived vasculature during the transplant period has not yet been extensively studied. Organoid podocytes *in vitro* secrete VEGF, which forms a gradient that attract endothelial cells, but under standard conditions organoid-derived endothelial cells typically do not invade the glomeruli as they form and thus the glomeruli remain avascular [207]. In our hands the organoid vascular network developed later than the nephrons, as it was not detectable at the time points chosen for transplant (D7+9 to D7+12), and our collaborators have also found that organoids produce less VEGF at D7+10 compared to D7+17 [210], which suggests that younger organoids will be less capable of attracting host

vasculature compared to older organoids. To determine if this is the case and if this affects the survival or maturation of renal tissue in the grafts, comparisons of organoids transplanted at earlier and later time points are required. It is also worth noting that unilateral nephrectomy in the host accelerates the maturation of transplanted embryonic kidneys, although the underlying mechanism has not been characterised [372,376].

While the organoid vascular network and VEGF production both peak at later time points in standard organoid culture, proximal tubule marker expression peaks earlier, at around D7+11, and progressively declines, as detailed in Chapter 4. Hence, it may be necessary to optimise *in vitro* culture conditions to ensure that all cell populations of interest are healthy prior to transplant so that they can be appropriately vascularised and mature during the transplant period.

If a graft receives sufficient blood flow from the host and has mature proximal tubules, nephrotoxic drugs administered to the host may cause injury to the grafts. While this is too low-throughput and costly to use as a screening method, it may be a useful "humanised" *in vivo* model of nephrotoxicity caused by drug metabolites, vascular dysfunction, or other mechanisms of injury which are difficult to replicate *in vitro*. A proximal tubule injury reporter line could be used to characterise the responses of grafts to known nephrotoxicants as a proof-of-concept of this approach.

In summary, proximal tubule reporter organoids transplanted onto the omental fat pad or under the renal capsule of immunocompromised mice demonstrated an overgrowth of non-renal tissue which was consistent with previous findings. Proximal tubules which survived within the grafts maintained expression of proximal tubule markers such as LTL, CUBN, AQP1, and reporter protein better than organoids maintained to an equivalent age *in vitro*, showing that vascularisation and blood flow was beneficial. Further work will be required to optimise organoid culture and transplant protocols, and to determine how much organoid proximal tubules can mature under these conditions.

6 DISCUSSION AND CONCLUDING REMARKS

Drug-induced nephrotoxicity is an ongoing challenge in healthcare, given the wide range of drugs which are currently in use that can cause acute kidney injury as a side effect [32]. To address this challenge, drugs with improved renal safety profiles need to be developed, which in turn requires *in vitro* models of nephrotoxicity that can accurately predict if a compound will be nephrotoxic *in vivo* and also allow the mechanism of injury to be characterised. Because the proximal tubule cells within the kidney are the primary target of drug-induced injury, primary proximal tubule cells and immortalised cell lines cultured in 2D have been used to model nephrotoxicity *in vitro*. However, these models lose expression of the unique transporters and receptors which underpin the proximal tubule's vulnerability to drug toxicity [12]. Hence, there is a need for new *in vitro* models of nephrotoxicity which express functional proximal tubule markers at appropriate levels, and we have reviewed advances in this field in Soo *et al*.[12]. Among these are techniques for differentiating pluripotent stem cells to kidney tissues which have produced kidney organoids containing multiple renal cell types, including proximal tubules that show the capacity for endocytosis and sensitivity to known nephrotoxicants [112,113,187,188]. Based on this, we investigated proximal tubule marker expression in organoids to determine their suitability for modelling nephrotoxicity *in vitro*.

Our initial characterisation of proximal tubules in organoids showed that while organoids had better expression of some proximal tubule markers, such as the endocytotic receptor *CUBN*, than primary proximal tubule cells cultured in 2D, expression was still low overall compared to expression in human foetal kidney, and expression of some key solute channel transporters was lacking. To determine how organoid proximal tubules might be induced to mature, we performed bioinformatics analysis of single-cell RNA sequencing datasets prepared from foetal and adult mouse and human kidneys which were made available to us from within our group, from publications, or from collaborators, to identify genes and pathways which might drive proximal tubule maturation *in vivo*. Then, to aid the characterisation of organoid proximal tubules, we used CRISPR/Cas9 gene editing of pluripotent stem cell lines to develop two reporter lines for proximal tubule markers, *HNF4A*:YFP and *LRP2*:mTagBFP2, as well as a third reporter line for an injury marker, *HAVCR1*:mCherry. We validated the proximal tubule reporter lines and also published the validation results in Vanslambrouck *et al*. [290] as part of a range of reporter lines developed by our group for characterising renal development *in vitro*. Using these reporter lines, we experimentally validated the pathways

identified in our bioinformatics analysis by culturing organoids in a maturation medium after the initial differentiation, and found that a low glucose maturation medium with TGFβ inhibition significantly increased the expression of proximal tubule markers. We also found that xenotransplantation of reporter organoids caused overgrowth of non-renal tissue in the grafts but also maintained reporter expression in the surviving tubules. In summary, through this PhD project, we have developed a range of tools and approaches for optimising organoid proximal tubules to make better models of nephrotoxicity.

Building on these tools and approaches, there are many other aspects of proximal tubule maturation which need to be studied further. A lineage tracing study by Howden *et al*. [289] showed that under standard culture conditions, organoid nephrons are chimeric, incorporating some cells which are apparently not derived from *SIX2*-expressing metanephric nephron progenitors, in contrast to how the metanephric kidney forms *in vivo*. Hence, it is possible that the nephrons in organoids are more similar to mesonephric nephrons rather than metanephric nephrons. While there is considerable overlap in gene expression between mesonephric and metanephric tubules [377] and mesonephric tubules in mice are capable of transporting anions and cations [378], this suggests that standard organoid nephrons may be limited in their capacity for functional maturation even under modified culture conditions, as the mesonephros degenerates when the metanephros develops *in vivo*. Several protocols have been developed for maintaining and propagating metanephric nephron progenitors *in vitro* [270,379,380]. If these protocols could be used to expand iPSC-derived metanephric nephron progenitors for differentiation to metanephric nephrons, these may show increased proximal tubule maturation when cultured in a maturation medium compared to organoids from standard differentiations.

Another gap in our knowledge of proximal tubule maturation is in the differences in gene expression between the three sub-segments of the proximal tubule and how these differences arise during development. As some of the transporters which are of interest in drug-induced nephrotoxicity, such as *SLC5A2* and *SLC22A2*, are expressed in different sub-segments in adult proximal tubules, a better understanding of proximal tubule sub-segmentation will aid in developing *in vitro* models with appropriate expression of these transporters. The development of the pronephros in lower vertebrates, such as zebrafish and *Xenopus*, has been used to model nephron and proximal tubule segmentation [381–383]. However, while some of the segment-specific transcription factors in the zebrafish pronephros, such as *hnf4a* and *gata3*, are conserved with their mammalian counterparts [384], others such as *etv5* occur in different

segments in mammals [216]. It is worth noting that unlike the metanephric kidney where the metanephric nephron progenitors first differentiate into an epithelial renal vesicle which elongates into tubules, the pronephric tubule segments, including the proximal sub-segments, arise from transcriptionally distinct domains of pronephric mesenchyme, suggesting that commitment to sub-segment fates occurs prior to epithelialisation [382–384]. Based on this, it is possible that cells in the metanephric proximal tubule commit to sub-segments relatively early, around when pan-proximal tubule markers such as *HNF4A* are expressed.

To investigate proximal tubule sub-segmentation further, one could analyse the scRNA-seq and snRNA-seq datasets of foetal and adult mouse and human kidneys which multiple groups have recently produced and characterised [195,216,217,385–387] (Jason Spence, unpublished data). A potential challenge is that proximal tubule cells are generally a much smaller proportion of cells in foetal kidneys compared to adult kidneys, making it more difficult to identify sub-segments in foetal datasets (assuming they are present). To address this, one might enrich for proximal tubule cells prior to scRNA-seq. Alternatively, we note that Ransick *et al*. [385] and Wu *et al*. [195] identified cell clusters representing proximal tubule sub-segments in adult mouse and human kidneys respectively, based on expression of known sub-segment markers. Using this data, one could identify transcription factors and gene regulatory networks which are differentially expressed between adult proximal sub-segments and determine whether these are expressed in foetal proximal tubules or developing nephrons. This assumes that the gene regulatory networks driving sub-segmentation persist in the adult proximal tubule.

The tools we have used in this project could also be developed further to complement these studies. We note that the loci selected for our proximal tubule reporter lines described in Chapter 3, *HNF4A* and *LRP2*, were selected partly because they were expressed in both early and mature proximal tubules, allowing proximal tubule development in organoids to be tracked. However, this also means that reporter fluorescence intensity has to be quantified to screen for improved maturation. In the case of the *HNF4A*:YFP reporter line, we predict that fluorescence quantification will also become limited by the fact that *HNF4A* is not strongly differentially expressed between early and mature proximal tubules. A dual reporter for an early marker such as *HNF4A* or *LRP2* and a late marker such as *SLC22A6* or *SLC22A2* may aid the rapid identification of conditions which improve proximal tubule maturation, and also allow maturation or sub-segmentation to be closely examined by profiling cells which express both markers and comparing them with any single-positive cells. One of the other uses of fluorescent proximal tubule reporter lines which we have noted is to perform assays

of proximal tubule transporter function, using charged fluorescent dyes such as 5(6)-carboxyfluorescein or ASP^+ which are substrates for organic anion and cation transporters [12]. However, many of these dyes intrinsically emit green fluorescence, so if these assays are required, green fluorescent proteins should be avoided when designing reporter lines.

The long-term goal of this project was to develop an *in vitro* model of nephrotoxicity in the proximal tubule. Organoids are composed of multiple cell types, which has been hypothesised to increase the maturation of the various cell types and also provides an opportunity to model nephrotoxicity in cell types other than the proximal tubule, such as the glomerulus, distal tubule, or interstitial cells, which are also clinically relevant [12]. Since organoids are capable of endocytosing labelled dextran [113] or albumin, the presence of other cell types and a lack of fluid flow do not completely prevent substrates of apical proximal tubule transporters from accumulating in proximal tubules. However, while organoids have an endothelial network, it is not physically addressable, which limits the ability to simulate blood flow and filtration in organoids. Directional fluid flow over the surface of organoids has been shown to make their vascular network more extensive and improve polarisation of proximal tubule cells, but does not necessarily produce fluid flow within the vasculature or the tubules [207]. To address this, iPSC-derived proximal tubule cells could be isolated and seeded in three-dimensional kidneys-on-a-chip, using methods similar to those described for primary proximal tubule cells in Chapter 1 [95,154,159]. While this approach would remove the influences of other cell types on the proximal tubules, this may be the best way to model blood and filtrate access to the proximal tubule *in vitro* and would simplify analysis.

One issue with isolating proximal tubule cells from organoids is that they have a relatively small proportion of proximal tubule cells which can vary between differentiations [194]. To produce more proximal tubule cells, one could use the Kumar *et al.* [188] micro-organoid protocol, which aggregates iPSC-derived intermediate mesoderm cells into micro-organoids cultured in suspension, in contrast to the larger aggregates seen in standard organoid protocols. While the proportion of proximal tubule cells produced by the Kumar protocol is similar to standard organoid protocols, the total yield of cells is larger and more cost-effective, as the Kumar protocol produces 8,000-10,000 micro-organoids per differentiation [188]. Another method of addressing this issue is to create differentiation protocols which selectively induce three-dimensional proximal tubules, similar to the protocol developed by Yoshimura *et al.* [200] for selectively inducing podocytes. A low dose of a Wnt agonist like CHIR after renal vesicle formation may ablate podocyte formation in favour of tubules [200,264].

Alternatively, a low dose of Wnt inhibition while tubules are elongating may expand the medial tubule segment which gives rise to the proximal tubule [264]. Tubule-specific or segment-specific pathways which we identified through our bioinformatics analysis in Chapter 2, such as HGF signalling, may also aid proliferation of tubules prior to inducing the metabolic shifts and downregulation of patterning signals which are characteristic of the mature proximal tubule. Yet another method of obtaining isolated proximal tubule cells would be to develop a protocol for expanding them after isolation. As primary proximal tubule cells lose transporter expression when cultured in 2D [4,34,126,154], the isolated cells would have to be cultured and propagated in 3D by embedding them in collagen or Matrigel. This method has been demonstrated for ureteric bud cells isolated from mouse kidney [388]. However, while differentiated proximal tubule cells in juvenile rats are capable of proliferating when given a mitotic stimulus [389,390], it is not clear if isolated proximal tubule cells can be passaged like ureteric bud cells, as unlike ureteric bud cells *in vivo*, proximal tubules do not undergo iterative branching.

Ultimately, modelling drug-induced toxicity to the proximal tubule *in vitro* will require a high-throughput screening platform. This may involve high-content imaging of organoids with fluorescent reporters marking the mature proximal tubule and/or injury to the proximal tubule, or high-content imaging of iPSC-derived mature proximal tubule cells seeded in an array of kidneys-on-a-chip to allow controlled administration of substances to the basolateral and apical surfaces of the cells. In the latter case the effluent could also be assayed for injury markers or transporter substrates. In all platforms, a rapid fluorescent readout of injury will be required. The *HAVCR1*:mCherry reporter line described in Chapter 3 was developed during this project for this purpose, although we were unable to validate reporter expression due to the lack of specific KIM-1 upregulation in organoids following exposure to nephrotoxicants. Recent RNA-seq characterisation of mouse acute kidney injury models has identified a wide range of genes whose expression changes over the course of injury and repair [227]. Some of these markers of injury, such as *HMOX1*, may be more rapidly upregulated in response to injury compared to *HAVCR1* and might be more suitable for an injury reporter [131,227]. A fluorescent injury reporter will be useful for *in situ* imaging in organoids or isolated proximal tubule cells, while a secreted luciferase reporter may be useful if efficient methods are available for measuring luciferase content in the effluent of kidneys-on-a-chip. The readout of injury must be correlated with the nephrotoxicity of a compound. To do this, the model must be tested with known nephrotoxic and non-nephrotoxic

compounds to measure its sensitivity and specificity and define readout thresholds for nephrotoxicity [391], before new compounds can be tested. Then, for proof-of-concept, compounds from case studies [33] which showed different levels of nephrotoxicity in *in vitro* models, animal models, and/or humans could be tested. This will allow the predictivity of the model to be evaluated.

In Chapter 5 we noted that xenotransplantation of organoids was not useful as a high-throughput screening method. However, if the growth of these organoids after transplant could be optimised, they may be useful as an adjunct to screening as a "humanised" *in vivo* model of nephrotoxicity to characterise mechanisms of injury. Drugs administered to the host animal, metabolised, and carried in the blood to the graft would be transported by the human complement of proximal tubule transporters, and the graft's response to a drug might reflect the injury response in humans more closely than the host's response. As with the *in vitro* screens, an injury reporter will be useful for detecting the graft response. More work will be required to characterise and validate such a model compared to the *in vitro* screens.

In conclusion, we have characterised proximal tubules in organoids cultured using standard methods and identified potential methods of increasing their maturity using bioinformatics analysis of mouse and human kidneys. We have also developed reporter lines as tools for characterising proximal tubule maturation and injury, and used these reporter lines to optimise culture conditions for improving proximal tubule maturation based on the bioinformatics analysis. The reporter lines were also used to characterise proximal tubules in organoids transplanted into immunocompromised mice. These tools, analytical approaches, and experimental approaches can be used for further investigation into proximal tubule maturation in organoids and *in vivo*, as well as for optimising the use of iPSC-derived proximal tubule cells as an *in vitro* model of nephrotoxicity.

7 MATERIALS AND METHODS

7.1 Cell culture

7.1.1 Culture on mouse embryonic fibroblast (MEF) feeders

iPSCs cultured throughout this project were maintained according to the methods described in Takasato *et al*. [212] and Howden *et al*. [289]. hESC medium for maintaining feeder-dependent iPSC lines was prepared according to Table 1.2. CRL1502 clone C32 iPSCs were thawed and grown on MEFs with hESC medium supplemented with 10 ng/mL bFGF (Merck) until they reached 80% confluency. Prior to organoid differentiation, cells were adapted to feeder-free culture on Matrigel by dissociation with TrypLE Select (Thermofisher) and plating cells on Matrigel with MEF-conditioned hESC medium supplemented with 10 ng/mL bFGF.

Table 7.1 Components of hESC medium.

Component	Supplier	Catalogue number	Volume (mL)
DMEM/F-12	Thermofisher	11320-082	386.5
Knockout Serum Replacement	Thermofisher	10828-028	100
GlutaMAX	Thermofisher	35050-061	5
Non-essential Amino Acids	Thermofisher	11140-050	5
Penicillin/streptomycin	Thermofisher	15070-063	2.5
2-mercaptoethanol (55 mM)	Thermofisher	21985-023	1

7.1.2 Feeder-free iPSC culture

iPSC cell lines which were generated under feeder-free conditions (Table 7.2) were maintained on tissue culture plates or flasks coated with hESC-qualified Geltrex (Thermofisher) or Matrigel (Corning) with Essential 8™ medium (Thermofisher) and passaged every 3-4 days with 0.5 mM EDTA in PBS, according to previously described methods [343].

Table 7.2 Cell lines used for experiments in this project.

Name	Parental line	Sex	Culture conditions	Reporter (if any)	Reporter expression (if any)
CRL-1502 clone C32	CRL-1502 (ATCC)	F	Feeders	-	-
1502.3	CRL-1502 (ATCC)	F	Feeder-free	-	-
MAFB:mTagBFP2	CRL-2429 (ATCC)	M	Feeder-free	mTagBFP2	Glomerulus
MAFB:mTagBFP2/ *GATA3*:mCherry	*MAFB*:mTagBFP2 iPSC (clone m33e)	M	Feeder-free	mTagBFP2, mCherry	Glomerulus, connecting segment/collecting duct, $GATA3^{+}$ interstitium
LRP2:mTagBFP2	CRL-2429 (ATCC)	M	Feeder-free	mTagBFP2	Proximal tubule
HNF4A:YFP	PCS-201-010 (ATCC)	M	Feeder-free	YFP	Proximal tubule
HAVCR1:mCherry	CRL-2429 (ATCC)	M	Feeder-free	mCherry	Proximal tubule post-injury

7.2 Differentiation of iPSC to form kidney organoids

7.2.1 Standard organoids

iPSCs were differentiated to create kidney organoids according to the protocol of Takasato *et al*. [212] with minor modifications. The basal media used for individual experiments is indicated, where relevant, as APEL (Stemcell Technologies), APEL2 (Stemcell Technologies), or E6 (TeSR™-E6, Stemcell Technologies). These changes were made partly because the manufacture of APEL, the basal media in which the Takasato protocol was originally developed, was discontinued in 2017.

On D -1 of the protocol timeline, pluripotent stem cells were dissociated to single cells using TrypLE Select (Thermofisher) and harvested by gentle pipetting. Cell yield was then

determined by counting cells with a haemocytometer. Cells were plated at a density of 1.0 × 10^4 cells/cm^2. To plate cell lines indicated as "feeder-free" in Table 7.2 on Matrigel, single cell suspensions were centrifuged at 300 ×g for 3 minutes and resuspended in E8 media (Thermofisher) supplemented with either 5 μM Y-27632 (Tocris) or RevitaCell™ Supplement (Thermofisher) at the recommended dilution. Single cell suspensions from "feeder-free" lines can also be plated on recombinant laminin-521 (Biolamina) coated on standard 6-well tissue culture plates (Thermofisher) according to manufacturer's instructions.

The Takasato organoid differentiation protocol uses CHIR99021 (CHIR) to induce differentiation of pluripotent stem cells to posterior primitive streak and intermediate mesoderm [113]. The dosage and duration of CHIR affects the balance of putative anterior and posterior intermediate mesoderm, with higher doses or longer durations producing more posterior intermediate mesoderm as a general rule, though this can be optimised for different culture conditions or cell lines [212]. On D0 of the differentiation timeline, 8 μM CHIR99021 (CHIR) or 6 μM CHIR was added to APEL or E6 respectively to induce posterior primitive streak and intermediate mesoderm. Media was refreshed every two days. On D4 or D5, cells were treated with 200 ng/mL FGF9 and 1 μg/mL heparin in the same basal media until D7. On D7, cells were dissociated to single cells using TrypLE Select and counted using a haemocytometer.

Organoids were either hand-plated as described in Takasato *et al.* [212] or bioprinted according to the method of Higgins *et al.* [202]. For hand-plating, the cell suspension was distributed in microcentrifuge tubes and centrifuged three times at 300 ×g for 3 minutes to create aggregates of 2 × 10^5 cells per organoid. The aggregates were gently aspirated into a wide-bore pipette tip and placed on 0.4 μm polyester Transwell® filters (Corning). For bioprinting, the cell suspension was centrifuged at 300 ×g for 3 minutes in a 15 mL conical tube and the supernatant was discarded. The cell pellet was then resuspended in residual medium and gently aspirated into a NovoGen MMX bioprinter syringe. The bioprinter was used to deposit cell paste in aggregates of 1 × 10^5 cells per organoid on Transwell® filters. To induce nephrogenesis, organoids were incubated at 37° C for 1 hour with 5 μM CHIR in basal medium added to the base of each Transwell®. After this CHIR pulse, the medium was removed and replaced with basal media with 200 ng/mL FGF9 and 1 μg/mL heparin. Media was changed every two days according to the protocol timeline.

7.2.2 Swirler micro-organoids

Differentiation of iPSCs to swirler micro-organoids was performed according to the protocol of Kumar *et al.* [188]. Briefly, iPSCs were differentiated to intermediate mesoderm as a monolayer, similar to the protocol described in section 7.2.1, but with 1 μM CHIR added along with FGF9 and heparin from D4 to D7. On D7, cells were gently dissociated with 0.5 mM EDTA in PBS and cultured in basal media (APEL2 or E6) with 0.1% polyvinyl alcohol (PVA), 0.1% methylcellulose (MC), 5 μM Y-27632, 200 ng/mL FGF9, 1 μg/mL heparin, and 1 μM CHIR in low-adhesion culture dishes on an orbital shaker set to rotate at 60 rpm. On D7+1, Y-27632 was withdrawn, and on D7+5, FGF9, heparin, and CHIR were withdrawn. Media was changed every two days otherwise.

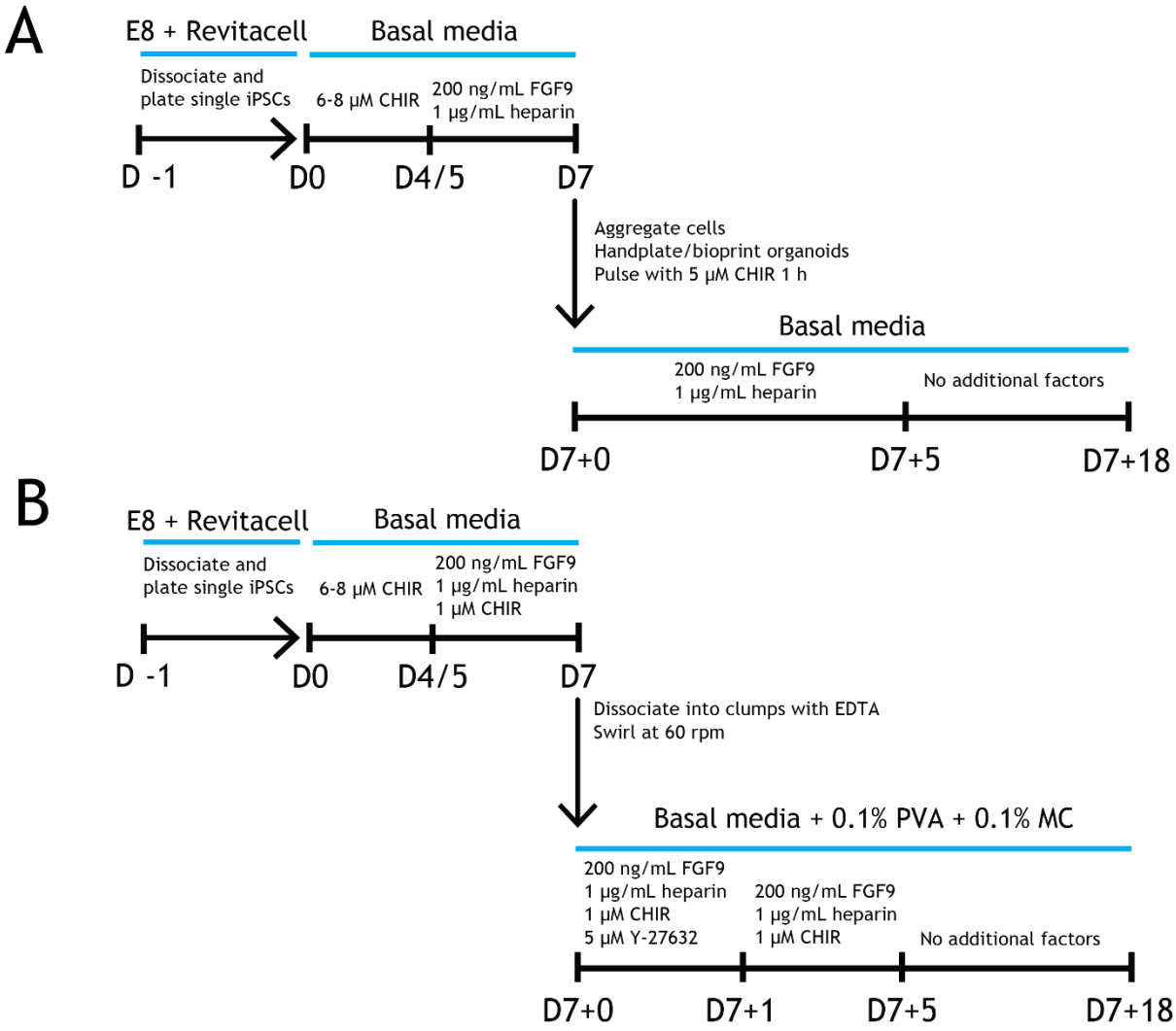

Figure 7.1 Diagrams of protocols used in this project for differentiating iPSCs to kidney organoids. A: Diagram of the Takasato organoid protocol [212] showing stepwise addition of growth factors to induce differentiation from pluripotent stem cells to posterior primitive streak, intermediate mesoderm, and aggregation of intermediate mesoderm cells to form organoids which are cultured for up to 18 additional days. The basal media used was APEL, APEL2, or E6 and is indicated where relevant. Any variations to this protocol made in specific experiments are indicated in their respective chapters. B: Diagram of the Kumar micro-organoid protocol [188] showing similar stepwise differentiation to the Takasato protocol, with some differences in the timing of growth factor addition and the growth factors used. Basal media was APEL, APEL2, or E6 and is indicated where relevant.

7.3 qRT-PCR analysis

7.3.1 RNA extraction and cDNA synthesis

RNA was extracted from samples using a PureLink RNA mini kit (Life Technologies) according to manufacturer's instructions. The concentration of the eluted RNA was

determined using a NanoDrop 1000 spectrophotometer (Thermofisher) so that the amount of RNA used for cDNA synthesis could be standardised for each experiment. RNA was stored at -80° C until use.

cDNA was synthesised with a GoScript™ Reverse Transcriptase Kit (Promega) or a SensiFAST™ cDNA Synthesis Kit (Bioline) according to manufacturer's instructions. cDNA was stored at -30° C until use.

7.3.2 qRT-PCR

Reactions were prepared with GoTaq® qPCR Master Mix (Promega) or SensiFast™ Probe Lo-ROX Kit (Bioline). Amplification was performed in 96-well plates using an Applied Biosystems™ 7500 Real-Time PCR System (Thermofisher) or a QuantStudio™ 5 Real-Time PCR System (Thermofisher). Measured C_T values were used to calculate gene expression normalised to the housekeeping gene *GAPDH* per sample ($-\Delta C_T$) and fold changes in normalised gene expression relative to a control sample ($-\Delta\Delta C_T$) [392]. Primers used for qRT-PCR in this project are listed in Table 7.3.

Table 7.3 qRT-PCR primer sequences.

Gene	Forward primer (5'→3')	Reverse primer (5'→3')
GAPDH	AGCCACATCGCTCAGACAC	GCCCAATACGACCAAATCC
SLC22A6	GCTGGCATCTCCCTCAACTG	TGAATGGGCATCCACTCCAC
SLC22A2	AAGGACTGGTCAGCAAAGCA	CCGATATCTCCGCCCAACAA
CUBN	AACTTCCTAATCCCCAGCGG	GTCCACCTCCTCAGTTCCTG
EPCAM	GCTGGCCGTAAACTGCTTTG	ACATTTGGCAGCCAGCTTTG
LRP2	GGTGGGGCCTTCTATGAACC	AGAGCTGTCCCATCATTGGC
SLC5A2	ATCTATGCCTCCGTCATCGC	GAAGGTCTGTACCGTGTCCG
HNF4A	ACCCTCGTCGACATGGACA	GCCTTCTGATGGGGACGTG
SLC47A1	GGAGTGATGGGTCTGTGGTC	ACTCCGAGGCACGTTGTTTA
GATA3	GCCCCTCATTAAGCCCAA	TTGTGGTGGTCTGACAGTTCG

7.4 Imaging

7.4.1 Live fluorescence imaging

Live fluorescence images in organoids were captured using a Zeiss LSM 780 or an Andor Dragonfly Spinning Disk confocal microscope while the organoids were still in their culture vessel. Images were analysed using ZEN 2 (Zeiss) or Imaris 9.3.0 (Bitplane).

7.4.2 Immunofluorescence staining

Antibodies and stains used are listed in Table 7.4 and Table 7.5. Fixation and staining methods for various types of samples are detailed in the following sections.

Table 7.4 Primary antibodies/lectins and dilutions used in this project.

Target/lectin (known cross-reactivity)	Host/conjugate	Supplier	Catalogue number	Dilution
Lotus tetragonolobus lectin – LTL	Biotin	Vector Laboratories	B-1325	1:300
ECAD	Mouse	BD Biosciences	610182	1:300
ECAD	Rabbit	Cell Signaling Technology	3195S	1:300
GATA3	Rabbit	Cell Signaling Technology	5852S	1:300
NPHS1	Sheep	Bioscientific	AF4269	1:300
GFP (YFP)	Chicken	Abcam	ab13970	1:300
TagRFP (mTagBFP2)	Rabbit	Evrogen	AB233	1:500
LRP2	Mouse	Novus Biological	NB110-96417	1:300
CUBN	Goat	Santa Cruz	sc-20607	1:150
HNF4α	Mouse	Life Technologies	MA1-199	1:500
HNF4α	Rabbit	Cell Signaling Technologies	3113	1:300
SLC22A6	Rabbit	Abcam	ab135924	1:200
SLC22A2	Mouse	R&D	MAB6547	1:100
Peanut agglutinin – PNA	Biotin	Vector Laboratories	B-1075	1:300
PECAM1	Goat	Santa Cruz	sc-1506	1:300
MECA-32	Rat	Novus Biological	NB100-77668	1:300
CD13	Mouse	Biolegend	301713	1:300

Target/lectin (known cross-reactivity)	Host/conjugate	Supplier	Catalogue number	Dilution
AQP1	Rabbit	Chemicon	AB3065	1:300
Human-specific Ku80	Rabbit	Cell Signaling Technologies	2180S	1:300

Table 7.5 Secondary antibodies and stains used in this project.

Antibody/stain	Host	Supplier	Catalogue number	Dilution
DAPI (nuclear stain)	-	Thermofisher	62248	1:2000
TOPRO3 (nuclear stain)	-	Thermofisher	T3605	1:3000
Alexa Fluor 405 Streptavidin	-	Thermofisher	S32351	1:400
Alexa Fluor 647 Streptavidin	-	Thermofisher	S21374	1:400
Alexa Fluor 488 anti-goat	Donkey	Thermofisher	A11055	1:400
Alexa Fluor 488 anti-mouse	Donkey	Thermofisher	A21202	1:400
Alexa Fluor 488 anti-rat	Donkey	Thermofisher	A21208	1:400
Alexa Fluor 488 anti-chicken	Goat	Thermofisher	A11039	1:400
Alexa Fluor 488 anti-rabbit	Donkey	Thermofisher	A21206	1:400
Alexa Fluor 568 anti-rabbit	Donkey	Thermofisher	A10042	1:400
Alexa Fluor 568 anti-mouse	Donkey	Thermofisher	A10037	1:400
Alexa Fluor 647 anti-goat	Donkey	Thermofisher	A21447	1:400
Alexa Fluor 647 anti-mouse	Donkey	Thermofisher	A31571	1:400
Alexa Fluor 647 anti-sheep	Donkey	Thermofisher	A21448	1:400
Alexa Fluor 568 anti-goat	Donkey	Abcam	ab175704	1:400

Antibody/stain	Host	Supplier	Catalogue number	Dilution
Alexa Fluor 647 anti-rabbit	Donkey	Abcam	ab150075	1:400
Alexa Fluor 488 anti-chicken	Donkey	Jackson ImmunoResearch	703-545-155	1:400
Alexa Fluor 647 anti-rabbit	Donkey (monovalent Fab fragment)	Jackson ImmunoResearch	711-607-003	1:400
Brilliant Violent 421 anti-rabbit	Donkey	Jackson ImmunoResearch	711-675-152	1:200

7.4.2.1 Whole mount samples

Samples were fixed in 2% paraformaldehyde (PFA) at 4° C for 20 minutes, then washed three times with PBS and stored at 4° C submerged in PBS until use.

For blocking, samples were submerged in blocking buffer (PBS + 10% donkey serum + 0.2% TritonX) in 24-well plates on a rocker at room temperature for at least 2 hours. After blocking, samples were incubated with primary antibodies in 150 µL blocking buffer on a rocker at 4° C overnight. Samples were then washed with PBS + 0.2% TritonX six times on a rocker at room temperature for 10 minutes each.

After primary incubation, samples were incubated with 150 µL of secondary antibodies in PBS + 0.2% TritonX (Sigma) on a rocker at 4° C overnight. Samples were then washed with PBS six times on a rocker at room temperature for 10 minutes each, then mounted on glass coverslips in 50% glycerol in PBS (v/v). Images were captured using a Zeiss LSM 780 or an Andor Dragonfly Spinning Disk confocal microscope and analysed using ZEN 2 or Imaris 9.3.0.

For thicker samples such as grafts from xenotransplantation of organoids, or to acquire complete 3D images of swirler micro-organoids, BABB (1:2 benzyl alcohol:benzyl benzoate [Sigma]) clearing was performed. Samples were dehydrated in a methanol series (25%, 50%, 75%, 100% and 100% in PBS v/v) for 5 minutes at each step, then mounted in a few drops of BABB in a glass-bottomed tissue culture dish and immediately imaged.

7.4.2.2 Cryosections

Fresh-frozen adult kidney sections (Zyagen) were warmed to room temperature and fixed with 2% PFA at room temperature for 6 minutes. Slides were washed with PBS five times and blocked with 200 µL blocking buffer (PBS + 10% donkey serum) at room temperature for 30 minutes. After blocking, slides were incubated with primary antibodies in 100 µL blocking buffer for 30 minutes at 37° C and then washed three times with PBS. Samples were then incubated with secondary antibodies in PBS for 60 minutes at room temperature and washed three times with PBS. Slides were dried by tapping the slide on a clean laboratory wipe, then coverslipped with ProLong® Diamond (Thermofisher) and imaged.

7.4.2.3 Paraffin-embedded sections

Samples were fixed in 4% PFA at room temperature for 6 hours, then placed in a petri dish and pre-embedded in agar by placing a drop of molten 2% agar over the sample and setting at room temperature. The sample in agar was then placed in a tissue cassette and processed using an Excelsior AS system (Thermofisher) programmed with the cycle shown in Table 7.6 prior to paraffin embedding. Blocks were stored at room temperature until 4 µm sections were cut for slides.

For immunofluorescence staining, sections on slides were dewaxed and rehydrated as in Table 7.7, then incubated with Tris-EDTA buffer (pH 9.0) at 100° C for 30 minutes for antigen retrieval. Slides were left to cool for 30 minutes before washing with PBS three times. After washing, slides were incubated in permeabilisation buffer (PBS + 0.5% TritonX) at room temperature for 30 minutes, then blocked with blocking buffer (PBS + 10% donkey serum) and incubated with primary antibodies at 4° C overnight. After primary antibody incubation, slides were washed with PBS three times and incubated with secondary antibodies at room temperature for 60 minutes, then washed with PBS three times. Slides were coverslipped with ProLong® Diamond before imaging.

Table 7.6: Processing cycle to prepare samples for embedding.

Treatment	Time (min)
70% ethanol	20
80% ethanol	20
90% ethanol	20
100% ethanol	20
100% ethanol	40
100% ethanol	60
Xylene	30
Xylene	30
Xylene	60
Wax	20
Wax	30
Wax	60

Table 7.7: Dewaxing and rehydration of paraffin-embedded sections on slides.

Treatment	Time (min)
Xylene	2
Xylene	2
Xylene	2
100% ethanol	3
100% ethanol	3
70% ethanol	3
dH_2O	5

7.4.3 Haematoxylin and eosin staining

Sections were dewaxed and rehydrated, stained in Harris' haematoxylin (Merck) for 3 minutes, then washed with gentle running water until the water ran clear. Sections were then placed in Scott's Blueing Solution (Trajan Scientific) for 1 minute, washed in dH_2O for 5 minutes, and stained in 1% eosin (Sigma) for 1 minute. To wash, sections were dipped in

dH_2O once, in 100% ethanol three times, and then washed in histolene three times for 3 minutes each. Slides were then coverslipped and imaged.

7.5 Flow cytometry and fluorescence-activated cell sorting (FACS)

Organoids were prepared for flow cytometry using the method described in Howden *et al.* [289]. Kidney organoids were dissociated in 200 µL of 1:1 TrypLE Select/Accutase (Stemcell Technologies) in microcentrifuge tubes for 15-25 minutes at 37° C with occasional flicking until large clumps were no longer visible. PBS + 1% foetal calf serum was added to the cell suspensions before passing suspensions through a 40 µm cell strainer (Falcon) into FACS round-bottom tubes. Samples were then centrifuged at 300 ×g for 3 minutes and resuspended in PBS + 1% foetal calf serum, then kept on ice until analysis. Where required, staining for cell surface markers prior to FACS was performed by diluting antibodies in PBS + 1% foetal calf serum and incubating samples in antibody on ice for 1 hour. Cells were then centrifuged at 300 ×g for 3 minutes and resuspended in PBS + 1% foetal calf serum three times to remove excess antibody and kept on ice until analysis. Flow cytometry was performed using a BD Fortessa X-20 analyser. FACS was performed by the MCRI Flow Cytometry and Imaging core facility using a BD InFlux cell sorter. Data was analysed with FACSDiva (BD) and FCS Express (De Novo Software).

Table 7.8 Antibodies for FACS and dilutions used in this project.

Target	Fluorophore	Supplier	Catalogue number	Dilution
CD13	PerCP/Cyanine5.5	Biolegend	301713	1:100
EPCAM	Alexa Fluor 488	Biolegend	324210	1:100

8 REFERENCES

1. Khan, K. N. M. & Alden, C. L. Kidney. in *Handbook of Toxicologic Pathology* vol. 2 255–336 (Academic Press, 2002).
2. Jang, K.-J. *et al.* Human kidney proximal tubule-on-a-chip for drug transport and nephrotoxicity assessment. *Integr. Biol.* **5**, 1119 (2013).
3. Denker, B. M. & Sabath, E. The biology of epithelial cell tight junctions in the kidney. *J. Am. Soc. Nephrol.* **22**, 622–625 (2011).
4. Qi, W., Johnson, D. W., Vesey, D. A., Pollock, C. A. & Chen, X. Isolation, propagation and characterization of primary tubule cell culture from human kidney (Methods in Renal Research). *Nephrology* **12**, 155–159 (2007).
5. Raghavan, V. & Weisz, O. A. Discerning the role of mechanosensors in regulating proximal tubule function. *Am. J. Physiol. - Ren. Physiol.* (2015) doi:10.1152/ajprenal.00373.2015.
6. Martinez-Guerrero, L. J., Evans, K. K., Dantzler, W. H. & Wright, S. H. The multidrug transporter, MATE1, sequesters OCs within an intracellular compartment that has no influence on OC secretion in renal proximal tubules. *Am. J. Physiol. - Ren. Physiol.* (2015) doi:10.1152/ajprenal.00318.2015.
7. Pfaller, W. & Rittinger, M. Quantitative morphology of the rat kidney. *Int. J. Biochem.* **12**, 17–22 (1980).
8. Hall, A. M., Rhodes, G. J., Sandoval, R. M., Corridon, P. R. & Molitoris, B. A. *In vivo* multiphoton imaging of mitochondrial structure and function during acute kidney injury. *Kidney Int.* **83**, 72–83 (2013).
9. Sands, J. M. & Layton, H. E. Advances in understanding the urine-concentrating mechanism. *Annu. Rev. Physiol.* **76**, 387–409 (2014).

10. Subramanya, A. R. & Ellison, D. H. Distal convoluted tubule. *Clin. J. Am. Soc. Nephrol.* **9**, 2147–2163 (2014).
11. Hall, A. M., Unwin, R. J., Parker, N. & Duchen, M. R. Multiphoton imaging reveals differences in mitochondrial function between nephron segments. *J. Am. Soc. Nephrol.* **20**, 1293–1302 (2009).
12. Soo, J. Y.-C., Jansen, J., Masereeuw, R. & Little, M. H. Advances in predictive *in vitro* models of drug-induced nephrotoxicity. *Nat. Rev. Nephrol.* **14**, 378–393 (2018).
13. Rabelink, T. J. & Little, M. H. Stromal cells in tissue homeostasis: balancing regeneration and fibrosis. *Nat. Rev. Nephrol.* **9**, 747–753 (2013).
14. Davidson, A. J. Mouse kidney development. in *StemBook* (Harvard Stem Cell Institute, 2008).
15. Takasato, M. & Little, M. H. The origin of the mammalian kidney: implications for recreating the kidney *in vitro*. *Dev. Camb. Engl.* **142**, 1937–1947 (2015).
16. Mugford, J. W., Sipilä, P., Kobayashi, A., Behringer, R. R. & McMahon, A. P. *Hoxd11* specifies a program of metanephric kidney development within the intermediate mesoderm of the mouse embryo. *Dev. Biol.* **319**, 396–405 (2008).
17. Nishinakamura, R. Kidney development conserved over species: essential roles of *Sall1*. *Semin. Cell Dev. Biol.* **14**, 241–247 (2003).
18. Little, M., Takasato, M., Soo, J. Y.-C. & Forbes, T. A. Recapitulating development to generate kidney organoid cultures. in *Organ Regeneration - 3D Stem Cell Culture & Manipulation* (ed. Tsuji, T.) 195–206 (2017).
19. Lawlor, K. T. *et al.* Nephron progenitor commitment is a stochastic process influenced by cell migration. *eLife* **8**, e41156 (2019).
20. Lindström, N. O. *et al.* Conserved and divergent molecular and anatomic features of human and mouse nephron patterning. *J. Am. Soc. Nephrol.* **29**, 825–840 (2018).

21. Rumballe, B. A. *et al.* Nephron formation adopts a novel spatial topology at cessation of nephrogenesis. *Dev. Biol.* **360**, 110–122 (2011).
22. Hartman, H. A., Lai, H. L. & Patterson, L. T. Cessation of renal morphogenesis in mice. *Dev. Biol.* **310**, 379–387 (2007).
23. Little, M. H., Combes, A. N. & Takasato, M. Understanding kidney morphogenesis to guide renal tissue regeneration. *Nat. Rev. Nephrol.* **12**, 624–635 (2016).
24. Little, M. & Combes, A. N. Kidney organoids: accurate models or fortunate accidents. *Genes Dev.* **in press**, (2019).
25. Georgas, K. *et al.* Analysis of early nephron patterning reveals a role for distal RV proliferation in fusion to the ureteric tip via a cap mesenchyme-derived connecting segment. *Dev. Biol.* **332**, 273–286 (2009).
26. Little, M. H. & Kairath, P. Does renal repair recapitulate kidney development? *J. Am. Soc. Nephrol.* **28**, 34–46 (2017).
27. Silver, S. A. & Chertow, G. M. The economic consequences of acute kidney injury. *Nephron* **137**, 297–301 (2017).
28. Yamout, H., Levin, M. L., Rosa, R. M., Myrie, K. & Westergaard, S. Physician prevention of acute kidney injury. *Am. J. Med.* **128**, 1001–1006 (2015).
29. Naughton, C. A. Drug-induced nephrotoxicity. *Am. Fam. Physician* **78**, 743–750 (2008).
30. Nolin, T. D. & Himmelfarb, J. Mechanisms of drug-induced nephrotoxicity. in *Adverse Drug Reactions* (ed. Uetrecht, J.) vol. 196 111–130 (Springer Berlin Heidelberg, 2010).
31. Grünfeld, J.-P. & Rossier, B. C. Lithium nephrotoxicity revisited. *Nat. Rev. Nephrol.* **5**, 270–276 (2009).
32. Rewa, O. & Bagshaw, S. M. Acute kidney injury—epidemiology, outcomes and economics. *Nat. Rev. Nephrol.* **10**, 193–207 (2014).

33. Magee, T. V. *et al.* Discovery of Dap-3 polymyxin analogues for the treatment of multidrug-resistant Gram-negative nosocomial infections. *J. Med. Chem.* **56**, 5079–5093 (2013).
34. Tiong, H. Y. *et al.* Drug-induced nephrotoxicity: clinical impact and preclinical *in vitro* models. *Mol. Pharm.* **11**, 1933–1948 (2014).
35. Huang, J. X. *et al.* Evaluation of biomarkers for *in vitro* prediction of drug-induced nephrotoxicity: comparison of HK-2, immortalized human proximal tubule epithelial, and primary cultures of human proximal tubular cells. *Pharmacol. Res. Perspect.* **3**, (2015).
36. Dekant, W. & Vamvakas, S. Biotransformation and membrane transport in nephrotoxicity. *Crit. Rev. Toxicol.* **26**, 309–334 (1996).
37. Hawksworth, G. M. *et al.* Site specific drug and xenobiotic induced renal toxicity. in *Toxicology - From Cells to Man* 184–192 (Springer, Berlin, Heidelberg, 1996). doi:10.1007/978-3-642-61105-6_19.
38. Lock, E. A. & Reed, C. J. Xenobiotic metabolizing enzymes of the kidney. *Toxicol. Pathol.* **26**, 18–25 (1998).
39. Knops, N. *et al.* The functional implications of common genetic variation in *CYP3A5* and *ABCB1* in human proximal tubule cells. *Mol. Pharm.* **12**, 758–768 (2015).
40. Bhargava, P. & Schnellmann, R. G. Mitochondrial energetics in the kidney. *Nat. Rev. Nephrol.* **13**, 629–646 (2017).
41. Fisel, P., Renner, O., Nies, A. T., Schwab, M. & Schaeffeler, E. Solute carrier transporter and drug-related nephrotoxicity: the impact of proximal tubule cell models for preclinical research. *Expert Opin. Drug Metab. Toxicol.* **10**, 395–408 (2014).
42. Lemke, A., Kiderlen, A. F. & Kayser, O. Amphotericin B. *Appl. Microbiol. Biotechnol.* **68**, 151–162 (2005).

43. Mamoulakis, C. *et al.* Contrast-induced nephropathy: basic concepts, pathophysiological implications and prevention strategies. *Pharmacol. Ther.* **180**, 99–112 (2017).
44. Paueksakon, P. & Fogo, A. B. Drug-induced nephropathies. *Histopathology* **70**, 94–108 (2017).
45. Perazella, M. A. & Markowitz, G. S. Bisphosphonate nephrotoxicity. *Kidney Int.* **74**, 1385–1393 (2008).
46. Xia, L., Zhou, M., Kalhorn, T. F., Ho, H. T. B. & Wang, J. Podocyte-specific expression of organic cation transporter PMAT: implication in puromycin aminonucleoside nephrotoxicity. *Am. J. Physiol.-Ren. Physiol.* **296**, F1307–F1313 (2009).
47. Yilmaz, M., Taninmis, H., Kara, E., Ozagari, A. & Unsal, A. Nephrotic syndrome after oral bisphosphonate (alendronate) administration in a patient with osteoporosis. *Osteoporos. Int.* **23**, 2059–2062 (2012).
48. Liebeskind, D. S. Chapter 26 - Nephrotic syndrome. in *Handbook of Clinical Neurology* (eds. Biller, J. & Ferro, J. M.) vol. 119 405–415 (Elsevier, 2014).
49. Cheng, H. F. & Harris, R. C. Renal effects of non-steroidal anti-inflammatory drugs and selective cyclooxygenase-2 inhibitors. *Curr. Pharm. Des.* **11**, 1795–1804 (2005).
50. Perazella, M. A. Drug-induced renal failure: update on new medications and unique mechanisms of nephrotoxicity. *Am. J. Med. Sci.* **325**, 349–362 (2003).
51. Kramann, R., Tanaka, M. & Humphreys, B. D. Fluorescence microangiography for quantitative assessment of peritubular capillary changes after AKI in mice. *J. Am. Soc. Nephrol.* **25**, 1924–1931 (2014).
52. Basile, D. P., Donohoe, D., Roethe, K. & Osborn, J. L. Renal ischemic injury results in permanent damage to peritubular capillaries and influences long-term function. *Am. J. Physiol.-Ren. Physiol.* **281**, F887–F899 (2001).

53. Verma, S. K. & Molitoris, B. A. Renal endothelial injury and microvascular dysfunction in acute kidney injury. *Semin. Nephrol.* **35**, 96–107 (2015).
54. Dimke, H. *et al.* Tubulovascular cross-talk by vascular endothelial growth factor A maintains peritubular microvasculature in kidney. *J. Am. Soc. Nephrol.* **26**, 1027–1038 (2015).
55. Lameire, N. Nephrotoxicity of recent anti-cancer agents. *Clin. Kidney J.* **7**, 11–22 (2014).
56. Breljak, D. *et al.* Distribution of organic anion transporters NaDC3 and OAT1-3 along the human nephron. *Am. J. Physiol. - Ren. Physiol.* **311**, F227–F238 (2016).
57. Motohashi, H. *et al.* Gene expression levels and immunolocalization of organic ion transporters in the human kidney. *J. Am. Soc. Nephrol.* **13**, 866–874 (2002).
58. Ingraham, L. *et al.* A plasma concentration of α-ketoglutarate influences the kinetic interaction of ligands with organic anion transporter 1. *Mol. Pharmacol.* **86**, 86–95 (2014).
59. Budiman, T., Bamberg, E., Koepsell, H. & Nagel, G. Mechanism of electrogenic cation transport by the cloned organic cation transporter 2 from rat. *J. Biol. Chem.* **275**, 29413–29420 (2000).
60. Cihlar, T. *et al.* The antiviral nucleotide analogs cidofovir and adefovir are novel substrates for human and rat renal organic anion transporter 1. *Mol. Pharmacol.* **56**, 570–580 (1999).
61. Ho, E. S., Lin, D. C., Mendel, D. B. & Cihlar, T. Cytotoxicity of antiviral nucleotides adefovir and cidofovir is induced by the expression of human renal organic anion transporter 1. *J. Am. Soc. Nephrol.* **11**, 383–393 (2000).
62. Nieskens, T. T. G. *et al.* A human renal proximal tubule cell line with stable organic anion transporter 1 and 3 expression predictive for antiviral-induced toxicity. *AAPS J.* **18**, 465–475 (2016).

63. Hagos, Y. & Wolff, N. A. Assessment of the role of renal organic anion transporters in drug-induced nephrotoxicity. *Toxins* **2**, 2055–2082 (2010).

64. Ciarimboli, G. Role of organic cation transporters in drug-induced toxicity. *Expert Opin. Drug Metab. Toxicol.* **7**, 159–174 (2011).

65. Pabla, N., Murphy, R. F., Liu, K. & Dong, Z. The copper transporter Ctr1 contributes to cisplatin uptake by renal tubular cells during cisplatin nephrotoxicity. *Am. J. Physiol. - Ren. Physiol.* **296**, F505–F511 (2009).

66. Hori, Y. *et al.* Megalin blockade with cilastatin suppresses drug-induced nephrotoxicity. *J. Am. Soc. Nephrol.* (2017) doi:10.1681/ASN.2016060606.

67. Nagai, J. & Takano, M. Entry of aminoglycosides into renal tubular epithelial cells via endocytosis-dependent and endocytosis-independent pathways. *Biochem. Pharmacol.* **90**, 331–337 (2014).

68. GUDMAP Genitourinary Development Molecular Anatomy Project. http://www.gudmap.org/.

69. Harding, S. D. *et al.* The GUDMAP database – an online resource for genitourinary research. *Development* **138**, 2845–2853 (2011).

70. Jenkinson, S. E. *et al.* The limitations of renal epithelial cell line HK-2 as a model of drug transporter expression and function in the proximal tubule. *Pflüg. Arch. - Eur. J. Physiol.* **464**, 601–611 (2012).

71. van Aubel, R. A., Smeets, P. H., Peters, J. G., Bindels, R. J. & Russel, F. G. The MRP4/*ABCC4* gene encodes a novel apical organic anion transporter in human kidney proximal tubules: putative efflux pump for urinary cAMP and cGMP. *J. Am. Soc. Nephrol.* **13**, 595–603 (2002).

72. Huls, M. *et al.* The breast cancer resistance protein transporter *ABCG2* is expressed in the human kidney proximal tubule apical membrane. *Kidney Int.* **73**, 220–225 (2008).

73. Motohashi, H. & Inui, K. Multidrug and toxin extrusion family SLC47: physiological, pharmacokinetic and toxicokinetic importance of MATE1 and MATE2-K. *Mol. Aspects Med.* **34**, 661–668 (2013).
74. Wen, X. *et al.* MDR1 transporter protects against paraquat-induced toxicity in human and mouse proximal tubule cells. *Toxicol. Sci.* **141**, 475–483 (2014).
75. Yokoo, S. *et al.* Differential contribution of organic cation transporters, OCT2 and MATE1, in platinum agent-induced nephrotoxicity. *Biochem. Pharmacol.* **74**, 477–487 (2007).
76. Hahn, K., Ejaz, A. A., Kanbay, M., Lanaspa, M. A. & Johnson, R. J. Acute kidney injury from SGLT2 inhibitors: potential mechanisms. *Nat. Rev. Nephrol.* **12**, 711–712 (2016).
77. Nadkarni, G. N. *et al.* Acute kidney injury in patients on SGLT2 inhibitors: a propensity-matched analysis. *Diabetes Care* **40**, 1479–1485 (2017).
78. Saly, D. & Perazella, M. A. Harnessing basic and clinic tools to evaluate SGLT2 inhibitor nephrotoxicity. *Am. J. Physiol. - Ren. Physiol.* **313**, F951–F954 (2017).
79. Yu, A. S. L. Claudins and the kidney. *J. Am. Soc. Nephrol.* **26**, 11–19 (2015).
80. Markadieu, N. *et al.* A primary culture of distal convoluted tubules expressing functional thiazide-sensitive NaCl transport. *Am. J. Physiol. - Ren. Physiol.* **303**, F886–F892 (2012).
81. Fromm, M., Piontek, J., Rosenthal, R., Günzel, D. & Krug, S. M. Tight junctions of the proximal tubule and their channel proteins. *Pflüg. Arch. - Eur. J. Physiol.* **469**, 877–887 (2017).
82. Günzel, D. & Yu, A. S. L. Claudins and the modulation of tight junction permeability. *Physiol. Rev.* **93**, 525–569 (2013).
83. Trujillo, J. *et al.* Renal tight junction proteins are decreased in cisplatin-induced nephrotoxicity in rats. *Toxicol. Mech. Methods* **24**, 520–528 (2014).

84. Balkovetz, D. F. Tight junction claudins and the kidney in sickness and in health. *Biochim. Biophys. Acta BBA - Biomembr.* **1788**, 858–863 (2009).
85. Lash, L. H., Putt, D. A. & Cai, H. Drug metabolism enzyme expression and activity in primary cultures of human proximal tubular cells. *Toxicology* **244**, 56–65 (2008).
86. Miners, J., Yang, X., Knights, K. & Zhang, L. The role of the kidney in drug elimination: transport, metabolism, and the impact of kidney disease on drug clearance. *Clin. Pharmacol. Ther.* **102**, 436–449 (2017).
87. Bolbrinker, J. *et al. CYP3A5* genotype-phenotype analysis in the human kidney reveals a strong site-specific expression of *CYP3A5* in the proximal tubule in carriers of the *CYP3A5*1* Allele. *Drug Metab. Dispos.* **40**, 639–641 (2012).
88. Yu, J., Zhou, Z., Owens, K. H., Ritchie, T. K. & Ragueneau-Majlessi, I. What can be learned from recent new drug applications? A systematic review of drug interaction data for drugs approved by the US FDA in 2015. *Drug Metab. Dispos.* **45**, 86–108 (2017).
89. Dekant, W. The role of biotransformation and bioactivation in toxicity. *EXS* **99**, 57–86 (2009).
90. Liu, S. *et al.* The role of renal proximal tubule P450 enzymes in chloroform-induced nephrotoxicity: utility of renal specific P450 reductase knockout mouse models. *Toxicol. Appl. Pharmacol.* **272**, 230–237 (2013).
91. Fliedl, L. Controversial role of gamma-glutamyl transferase activity in cisplatin nephrotoxicity. *ALTEX* **31**, 269–278 (2014).
92. Meister, A., Tate, S. S. & Griffith, O. W. γ-glutamyl transpeptidase. in *Methods in Enzymology* vol. 77 237–253 (Academic Press, 1981).
93. King, S. M. *et al.* 3D proximal tubule tissues recapitulate key aspects of renal physiology to enable nephrotoxicity testing. *Front. Physiol.* **8**, (2017).

94. Wieser, M. *et al.* hTERT alone immortalizes epithelial cells of renal proximal tubules without changing their functional characteristics. *Am. J. Physiol. - Ren. Physiol.* **295**, F1365–F1375 (2008).

95. Weber, E. J. *et al.* Development of a microphysiological model of human kidney proximal tubule function. *Kidney Int.* **90**, 627–637 (2016).

96. Kortenoeven, M. L. A. *et al.* Amiloride blocks lithium entry through the sodium channel thereby attenuating the resultant nephrogenic diabetes insipidus. *Kidney Int.* **76**, 44–53 (2009).

97. Thomsen, K. & Shirley, D. G. A hypothesis linking sodium and lithium reabsorption in the distal nephron. *Nephrol. Dial. Transplant.* **21**, 869–880 (2006).

98. Christensen, B. M., Kim, Y.-H., Kwon, T.-H. & Nielsen, S. Lithium treatment induces a marked proliferation of primarily principal cells in rat kidney inner medullary collecting duct. *Am. J. Physiol. - Ren. Physiol.* **291**, F39–F48 (2006).

99. Ledeganck, K. J. *et al.* Expression of renal distal tubule transporters *TRPM6* and NCC in a rat model of cyclosporine nephrotoxicity and effect of EGF treatment. *Am. J. Physiol. - Ren. Physiol.* **301**, F486–F493 (2011).

100. Sonneveld, R. *et al.* Glucose specifically regulates *TRPC6* expression in the podocyte in an AngII-dependent manner. *Am. J. Pathol.* **184**, 1715–1726 (2014).

101. Ambrus, L. *et al.* Inhibition of *TRPC6* by protein kinase C isoforms in cultured human podocytes. *J. Cell. Mol. Med.* **19**, 2771–2779 (2015).

102. Eyre, J. *et al.* Statin-sensitive endocytosis of albumin by glomerular podocytes. *Am. J. Physiol. - Ren. Physiol.* **292**, F674–F681 (2007).

103. Jansen, J. *et al.* Bioengineered kidney tubules efficiently excrete uremic toxins. *Sci. Rep.* **6**, 26715 (2016).

104. Kido, Y., Matsson, P. & Giacomini, K. M. Profiling of a prescription drug library for potential renal drug–drug interactions mediated by the organic cation transporter 2. *J. Med. Chem.* **54**, 4548–4558 (2011).

105. Schophuizen, C. M. S. *et al.* Cationic uremic toxins affect human renal proximal tubule cell functioning through interaction with the organic cation transporter. *Pflüg. Arch. - Eur. J. Physiol.* **465**, 1701–1714 (2013).

106. Caetano-Pinto, P. *et al.* Fluorescence-based transport assays revisited in a human renal proximal tubule cell line. *Mol. Pharm.* **13**, 933–944 (2016).

107. Shaik, N., Giri, N., Pan, G. & Elmquist, W. F. P-glycoprotein-mediated active efflux of the anti-HIV1 nucleoside abacavir limits cellular accumulation and brain distribution. *Drug Metab. Dispos.* **35**, 2076–2085 (2007).

108. Kusuhara, H. *et al.* Effects of a MATE protein inhibitor, pyrimethamine, on the renal elimination of metformin at oral microdose and at therapeutic dose in healthy subjects. *Clin. Pharmacol. Ther.* **89**, 837–844 (2011).

109. Ito, S. *et al.* Potent and specific inhibition of mMate1-mediated efflux of type I organic cations in the liver and kidney by pyrimethamine. *J. Pharmacol. Exp. Ther.* **333**, 341–350 (2010).

110. Wilmer, M. J. *et al.* Novel conditionally immortalized human proximal tubule cell line expressing functional influx and efflux transporters. *Cell Tissue Res.* **339**, 449–457 (2010).

111. Zhai, X. Y. *et al.* Cubilin- and megalin-mediated uptake of albumin in cultured proximal tubule cells of opossum kidney. *Kidney Int.* **58**, 1523–1533 (2000).

112. Freedman, B. S. *et al.* Modelling kidney disease with CRISPR-mutant kidney organoids derived from human pluripotent epiblast spheroids. *Nat Commun* **6**, (2015).

113. Takasato, M. *et al.* Kidney organoids from human iPS cells contain multiple lineages and model human nephrogenesis. *Nature* **526**, 564–568 (2015).

114. Moreno, E. *et al.* Affinity-defining domains in the Na-Cl cotransporter: a different location for Cl- and thiazide binding. *J. Biol. Chem.* **281**, 17266–17275 (2006).

115. Andrukhova, O. *et al.* FGF23 promotes renal calcium reabsorption through the TRPV5 channel. *EMBO J.* **33**, 229–246 (2014).

116. Bonventre, J. V., Vaidya, V. S., Schmouder, R., Feig, P. & Dieterle, F. Next-generation biomarkers for detecting kidney toxicity. *Nat. Biotechnol.* **28**, 436–440 (2010).

117. Bailly, V. *et al.* Shedding of kidney injury molecule-1, a putative adhesion protein involved in renal regeneration. *J. Biol. Chem.* **277**, 39739–39748 (2002).

118. Ichimura, T. Kidney injury molecule-1: a tissue and urinary biomarker for nephrotoxicant-induced renal injury. *Am. J. Physiol. - Ren. Physiol.* **286**, 552F – 563 (2004).

119. Ichimura, T. *et al.* Kidney injury molecule–1 is a phosphatidylserine receptor that confers a phagocytic phenotype on epithelial cells. *J. Clin. Invest.* **118**, 1657–1668 (2008).

120. Vaidya, V. S. Urinary kidney injury molecule-1: a sensitive quantitative biomarker for early detection of kidney tubular injury. *Am. J. Physiol. - Ren. Physiol.* **290**, F517–F529 (2006).

121. Vaidya, V. S. *et al.* Kidney injury molecule-1 outperforms traditional biomarkers of kidney injury in preclinical biomarker qualification studies. *Nat. Biotechnol.* **28**, 478–485 (2010).

122. Vaidya, V. S. *et al.* Urinary biomarkers for sensitive and specific detection of acute kidney injury in humans. *Clin. Transl. Sci.* **1**, 200–208 (2008).

123. Dieterle, F. *et al.* Renal biomarker qualification submission: a dialog between the FDA-EMEA and Predictive Safety Testing Consortium. *Nat. Biotechnol.* **28**, 455–462 (2010).

124. Rached, E. *et al.* Evaluation of putative biomarkers of nephrotoxicity after exposure to ochratoxin A *in vivo* and *in vitro*. *Toxicol. Sci.* **103**, 371–381 (2008).

125. Sohn, S.-J. *et al. In vitro* evaluation of biomarkers for cisplatin-induced nephrotoxicity using HK-2 human kidney epithelial cells. *Toxicol. Lett.* **217**, 235–242 (2013).

126. Li, Y. *et al.* An *in vitro* method for the prediction of renal proximal tubular toxicity in humans. *Toxicol. Res.* **2**, 352 (2013).

127. Luo, Q.-H. *et al.* Evaluation of KIM-1 and NGAL as early indicators for assessment of gentamycin-induced nephrotoxicity *in vivo* and *in vitro*. *Kidney Blood Press. Res.* **41**, 911–918 (2016).

128. Gozzelino, R., Jeney, V. & Soares, M. P. Mechanisms of cell protection by heme oxygenase-1. *Annu. Rev. Pharmacol. Toxicol.* **50**, 323–354 (2010).

129. Lever, J. M., Boddu, R., George, J. F. & Agarwal, A. Heme oxygenase-1 in kidney health and disease. *Antioxid. Redox Signal.* (2016) doi:10.1089/ars.2016.6659.

130. Zager, R. A., Johnson, A. C. M. & Becker, K. Plasma and urinary heme oxygenase-1 in AKI. *J. Am. Soc. Nephrol.* **23**, 1048–1057 (2012).

131. Adler, M. *et al.* A quantitative approach to screen for nephrotoxic compounds in vitro. *J. Am. Soc. Nephrol.* **27**, 1015–1028 (2016).

132. Akdis, M. *et al.* Interleukins, from 1 to 37, and interferon-γ: Receptors, functions, and roles in diseases. *J. Allergy Clin. Immunol.* **127**, 701-721.e70 (2011).

133. Tramma, D., Hatzistylianou, M., Gerasimou, G. & Lafazanis, V. Interleukin-6 and interleukin-8 levels in the urine of children with renal scarring. *Pediatr. Nephrol.* **27**, 1525–1530 (2012).

134. Grigoryev, D. N. *et al.* The local and systemic inflammatory transcriptome after acute kidney injury. *J. Am. Soc. Nephrol.* **19**, 547–558 (2008).

135. Araki, M. *et al.* Expression of IL-8 during reperfusion of renal allografts is dependent on ischemic time. *Transplantation* **81**, 783–788 (2006).

136. Su, H., Lei, C.-T. & Zhang, C. Interleukin-6 signaling pathway and its role in kidney disease: an update. *Front. Immunol.* **8**, (2017).

137. Mihajlovic, M. *et al.* Allostimulatory capacity of conditionally immortalized proximal tubule cell lines for bioartificial kidney application. *Sci. Rep.* **7**, 7103 (2017).

138. Cowland, J. B. & Borregaard, N. Molecular characterization and pattern of tissue expression of the gene for neutrophil gelatinase-associated lipocalin from humans. *Genomics* **45**, 17–23 (1997).

139. Charlton, J. R., Portilla, D. & Okusa, M. D. A basic science view of acute kidney injury biomarkers. *Nephrol. Dial. Transplant.* **29**, 1301–1311 (2014).

140. Paragas, N. *et al.* The Ngal reporter mouse detects the response of the kidney to injury in real time. *Nat. Med.* **17**, 216–222 (2011).

141. McIlroy, D. R., Wagener, G. & Lee, H. T. Neutrophil gelatinase-associated lipocalin and acute kidney injury after cardiac surgery: the effect of baseline renal function on diagnostic performance. *Clin. J. Am. Soc. Nephrol.* **5**, 211–219 (2010).

142. Mårtensson, J. & Bellomo, R. The rise and fall of NGAL in acute kidney injury. *Blood Purif.* **37**, 304–310 (2014).

143. Haase, M. *et al.* Accuracy of neutrophil gelatinase-associated lipocalin (NGAL) in diagnosis and prognosis in acute kidney injury: a systematic review and meta-analysis. *Am. J. Kidney Dis.* **54**, 1012–1024 (2009).

144. Scotcher, D., Jones, C., Posada, M., Galetin, A. & Rostami-Hodjegan, A. Key to opening kidney for *in vitro-in vivo* extrapolation entrance in health and disease: Part II: mechanistic models and in vitro-in vivo extrapolation. *AAPS J.* **18**, 1082–1094 (2016).

145. Hilgendorf, C. *et al.* Expression of thirty-six drug transporter genes in human intestine, liver, kidney, and organotypic cell lines. *Drug Metab. Dispos.* **35**, 1333–1340 (2007).

146. Chu, X., Bleasby, K. & Evers, R. Species differences in drug transporters and implications for translating preclinical findings to humans. *Expert Opin. Drug Metab. Toxicol.* **9**, 237–252 (2013).

147. Yonezawa, A. & Inui, K. Importance of the multidrug and toxin extrusion MATE/SLC47A family to pharmacokinetics, pharmacodynamics/toxicodynamics and pharmacogenomics. *Br. J. Pharmacol.* **164**, 1817–1825 (2011).

148. Aoki, M. *et al.* Kidney-specific expression of human organic cation transporter 2 (OCT2/SLC22A2) is regulated by DNA methylation. *Am. J. Physiol. - Ren. Physiol.* **295**, F165–F170 (2008).

149. Tanaka, Y., Slitt, A. L., Leazer, T. M., Maher, J. M. & Klaassen, C. D. Tissue distribution and hormonal regulation of the breast cancer resistance protein (Bcrp/*Abcg2*) in rats and mice. *Biochem. Biophys. Res. Commun.* **326**, 181–187 (2004).

150. Soldin, O. P. & Mattison, D. R. Sex differences in pharmacokinetics and pharmacodynamics. *Clin. Pharmacokinet.* **48**, 143–157 (2009).

151. Joseph, S. *et al.* Expression of drug transporters in human kidney: impact of sex, age, and ethnicity. *Biol. Sex Differ.* **6**, (2015).

152. Veiras, L. C. *et al.* Sexual dimorphic pattern of renal transporters and electrolyte homeostasis. *J. Am. Soc. Nephrol.* (2017) doi:10.1681/ASN.2017030295.

153. Food and Drug Administration. Advancing regulatory science - validating human stem cell cardiomyocyte technology for better predictive assessment of drug-induced cardiac toxicity. https://www.fda.gov/ScienceResearch/SpecialTopics/RegulatoryScience/ucm507998.htm (2016).

154. Wilmer, M. J. *et al.* Kidney-on-a-chip technology for drug-induced nephrotoxicity screening. *Trends Biotechnol.* **34**, 156–170 (2016).

155. Ryan, M. J. *et al.* HK-2: An immortalized proximal tubule epithelial cell line from normal adult human kidney. *Kidney Int.* **45**, 48–57 (1994).

156. Aschauer, L., Carta, G., Vogelsang, N., Schlatter, E. & Jennings, P. Expression of xenobiotic transporters in the human renal proximal tubule cell line RPTEC/TERT1. *Toxicol. In Vitro* **30**, 95–105 (2015).

157. Mutsaers, H. A. M. *et al.* Uremic toxins inhibit renal metabolic capacity through interference with glucuronidation and mitochondrial respiration. *Biochim. Biophys. Acta BBA - Mol. Basis Dis.* **1832**, 142–150 (2013).

158. Ivliev, A. E., 't Hoen, P. A. C., van Roon-Mom, W. M. C. van, Peters, D. J. M. & Sergeeva, M. G. Exploring the transcriptome of ciliated cells using in silico dissection of human tissues. *PLOS ONE* **7**, e35618 (2012).

159. Homan, K. A. *et al.* Bioprinting of 3D convoluted renal proximal tubules on perfusable chips. *Sci. Rep.* **6**, 34845 (2016).

160. Tourovskaia, A., Fauver, M., Kramer, G., Simonson, S. & Neumann, T. Tissue-engineered microenvironment systems for modeling human vasculature. *Exp. Biol. Med.* **239**, 1264–1271 (2014).

161. Masereeuw, R. *et al.* Probenecid interferes with renal oxidative metabolism: a potential pitfall in its use as an inhibitor of drug transport. *Br. J. Pharmacol.* **131**, 57–62 (2000).

162. Tsai, M. *et al. In vitro* modeling of the microvascular occlusion and thrombosis that occur in hematologic diseases using microfluidic technology. *J. Clin. Invest.* **122**, 408–418 (2012).

163. Ligresti, G. *et al.* A novel three–dimensional human peritubular microvascular system. *J. Am. Soc. Nephrol.* **27**, 2370–2381 (2016).

164. Kelly, E. J. *et al.* Innovations in preclinical biology: *ex vivo* engineering of a human kidney tissue microperfusion system. *Stem Cell Res. Ther.* **4**, S17 (2013).

165. Phan, D. T. T. *et al.* A vascularized and perfused organ-on-a-chip platform for large-scale drug screening applications. *Lab. Chip* **17**, 511–520 (2017).

166. van Duinen, V. *et al.* 96 perfusable blood vessels to study vascular permeability in vitro. *Sci. Rep.* **7**, (2017).

167. Musah, S. *et al.* Mature induced-pluripotent-stem-cell-derived human podocytes reconstitute kidney glomerular-capillary-wall function on a chip. *Nat. Biomed. Eng.* **1**, (2017).

168. Vernetti, L. *et al.* Functional coupling of human microphysiology systems: intestine, liver, kidney proximal tubule, blood-brain barrier and skeletal muscle. *Sci. Rep.* **7**, 42296 (2017).

169. Chang, S.-Y. *et al.* Human liver-kidney model elucidates the mechanisms of aristolochic acid nephrotoxicity. *JCI Insight* **2**, (2017).

170. Jansen, J. *et al.* Human proximal tubule epithelial cells cultured on hollow fibers: living membranes that actively transport organic cations. *Sci. Rep.* **5**, (2015).

171. Mihajlovic, M. *et al.* Role of vitamin D in maintaining renal epithelial barrier function in uremic conditions. *Int. J. Mol. Sci.* **18**, (2017).

172. Nguyen, D. G. *et al.* Bioprinted 3D primary liver tissues allow assessment of organ-level response to clinical drug induced toxicity *in vitro*. *PLOS ONE* **11**, e0158674 (2016).

173. Miya, M. *et al.* Enhancement of *in vitro* human tubulogenesis by endothelial cell-derived factors: implications for *in vivo* tubular regeneration after injury. *Am. J. Physiol. - Ren. Physiol.* **301**, F387–F395 (2011).

174. Tasnim, F. & Zink, D. Cross talk between primary human renal tubular cells and endothelial cells in cocultures. *Am. J. Physiol. - Ren. Physiol.* **302**, F1055–F1062 (2012).

175. Takahashi, K. *et al.* Induction of pluripotent stem cells from adult human fibroblasts by defined factors. *Cell* **131**, 861–872 (2007).

176. Yu, J. *et al.* Human induced pluripotent stem cells free of vector and transgene sequences. *Science* **324**, 797–801 (2009).

177. Kaji, K. *et al.* Virus-free induction of pluripotency and subsequent excision of reprogramming factors. *Nature* **458**, 771–775 (2009).

178. Woltjen, K. *et al. piggyBac* transposition reprograms fibroblasts to induced pluripotent stem cells. *Nature* **458**, 766–770 (2009).

179. Soldner, F. *et al.* Parkinson's disease patient-derived induced pluripotent stem cells free of viral reprogramming factors. *Cell* **136**, 964–977 (2009).

180. Kandasamy, K. *et al.* Prediction of drug-induced nephrotoxicity and injury mechanisms with human induced pluripotent stem cell-derived cells and machine learning methods. *Sci. Rep.* **5**, 12337 (2015).

181. Imberti, B. *et al.* Renal progenitors derived from human iPSCs engraft and restore function in a mouse model of acute kidney injury. *Sci. Rep.* **5**, 8826 (2015).

182. Chuah, J. K. C. & Zink, D. Stem cell-derived kidney cells and organoids: recent breakthroughs and emerging applications. *Biotechnol. Adv.* **35**, 150–167.

183. Kang, M. & Han, Y.-M. Differentiation of human pluripotent stem cells into nephron progenitor cells in a serum and feeder free system. *PLOS ONE* **9**, e94888 (2014).

184. Narayanan, K. *et al.* Human embryonic stem cells differentiate into functional renal proximal tubular–like cells. *Kidney Int.* **83**, 593–603 (2013).

185. Taguchi, A. *et al.* Redefining the *in vivo* origin of metanephric nephron progenitors enables generation of complex kidney structures from pluripotent stem cells. *Cell Stem Cell* **14**, 53–67 (2014).

186. Takasato, M. *et al.* Directing human embryonic stem cell differentiation towards a renal lineage generates a self-organizing kidney. *Nat. Cell Biol.* **16**, 118–126 (2014).

187. Morizane, R. *et al.* Nephron organoids derived from human pluripotent stem cells model kidney development and injury. *Nat. Biotechnol.* **33**, 1193–1200 (2015).

188. Kumar, S. V. *et al.* Kidney micro-organoids in suspension culture as a scalable source of human pluripotent stem cell-derived kidney cells. *Development* **146**, dev172361 (2019).

189. Przepiorski, A. *et al.* A simple bioreactor-based method to generate kidney organoids from pluripotent stem cells. *Stem Cell Rep.* **11**, 470–484 (2018).

190. Islam, M. & Nishinakamura, R. How to rebuild the kidney: recent advances in kidney organoids. *J. Biochem. (Tokyo)* **166**, 7–12 (2019).

191. Nishinakamura, R. Human kidney organoids: progress and remaining challenges. *Nat. Rev. Nephrol.* 1–12 (2019) doi:10.1038/s41581-019-0176-x.

192. Morizane, R. & Bonventre, J. V. Generation of nephron progenitor cells and kidney organoids from human pluripotent stem cells. *Nat. Protoc.* **12**, 195–207 (2017).

193. Subramanian, A. *et al.* Kidney organoid reproducibility across multiple human iPSC lines and diminished off target cells after transplantation revealed by single cell transcriptomics. *bioRxiv* 516807 (2019) doi:10.1101/516807.

194. Phipson, B. *et al.* Evaluation of variability in human kidney organoids. *Nat. Methods* **16**, 79–87 (2019).

195. Wu, H. *et al.* Comparative analysis and refinement of human PSC-derived kidney organoid differentiation with single-cell transcriptomics. *Cell Stem Cell* **23**, 869-881.e8 (2018).

196. Taguchi, A. & Nishinakamura, R. Higher-order kidney organogenesis from pluripotent stem cells. *Cell Stem Cell* **21**, 730-746.e6 (2017).

197. Forbes, T. A. *et al.* Patient-iPSC-derived kidney organoids show functional validation of a ciliopathic renal phenotype and reveal underlying pathogenetic mechanisms. *Am. J. Hum. Genet.* **102**, 816–831 (2018).

198. Cruz, N. M. *et al.* Organoid cystogenesis reveals a critical role of microenvironment in human polycystic kidney disease. *Nat. Mater.* **16**, 1112–1119 (2017).

199. Hale, L. J. *et al.* 3D organoid-derived human glomeruli for personalised podocyte disease modelling and drug screening. *Nat. Commun.* **9**, 5167 (2018).

200. Yoshimura, Y. *et al.* Manipulation of nephron-patterning signals enables selective induction of podocytes from human pluripotent stem cells. *J. Am. Soc. Nephrol.* **30**, 304–321 (2019).

201. Czerniecki, S. M. *et al.* High-throughput screening enhances kidney organoid differentiation from human pluripotent stem cells and enables automated multidimensional phenotyping. *Cell Stem Cell* **22**, 929–940 (2018).

202. Higgins, J. W. *et al.* Bioprinted pluripotent stem cell-derived kidney organoids provide opportunities for high content screening. *bioRxiv* 505396 (2018) doi:10.1101/505396.

203. Leuning, D. G. *et al.* Vascular bioengineering of scaffolds derived from human discarded transplant kidneys using human pluripotent stem cell–derived endothelium. *Am. J. Transplant.* **19**, 1328–1343 (2019).

204. Orlova, V. V. *et al.* Generation, expansion and functional analysis of endothelial cells and pericytes derived from human pluripotent stem cells. *Nat. Protoc.* **9**, 1514–1531 (2014).

205. Gupta, A. K. *et al.* Scaffolding kidney organoids on silk. *J. Tissue Eng. Regen. Med.* **13**, 812–822 (2019).

206. Garreta, E. *et al.* Fine tuning the extracellular environment accelerates the derivation of kidney organoids from human pluripotent stem cells. *Nat. Mater.* **18**, 397–405 (2019).

207. Homan, K. A. *et al.* Flow-enhanced vascularization and maturation of kidney organoids *in vitro*. *Nat. Methods* **16**, 255–262 (2019).

208. Sharmin, S. *et al.* Human induced pluripotent stem cell–derived podocytes mature into vascularized glomeruli upon experimental transplantation. *J. Am. Soc. Nephrol.* **27**, 1778–1791 (2016).

209. Bantounas, I. *et al.* Generation of functioning nephrons by implanting human pluripotent stem cell-derived kidney progenitors. *Stem Cell Rep.* **10**, 766–779 (2018).

210. van den Berg, C. W. *et al.* Renal subcapsular transplantation of PSC-derived kidney organoids induces neo-vasculogenesis and significant glomerular and tubular maturation *in vivo*. *Stem Cell Rep.* **10**, 751–765 (2018).

211. Tanigawa, S. *et al.* Organoids from nephrotic disease-derived iPSCs identify impaired NEPHRIN localization and slit diaphragm formation in kidney podocytes. *Stem Cell Rep.* **11**, 727–740 (2018).

212. Takasato, M., Er, P. X., Chiu, H. S. & Little, M. H. Generation of kidney organoids from human pluripotent stem cells. *Nat. Protoc.* **11**, 1681–1692 (2016).

213. Martovetsky, G., Tee, J. B. & Nigam, S. K. Hepatocyte nuclear factors 4α and 1α regulate kidney developmental expression of drug-metabolizing enzymes and drug transporters. *Mol. Pharmacol.* **84**, 808–823 (2013).

214. Wilson, P. C. & Humphreys, B. D. Kidney and organoid single-cell transcriptomics: the end of the beginning. *Pediatr. Nephrol.* (2019) doi:10.1007/s00467-018-4177-y.

215. Haque, A., Engel, J., Teichmann, S. A. & Lönnberg, T. A practical guide to single-cell RNA-sequencing for biomedical research and clinical applications. *Genome Med.* **9**, 75 (2017).

216. Combes, A. N. *et al.* Single cell analysis of the developing mouse kidney provides deeper insight into marker gene expression and ligand-receptor crosstalk. *Development* (2019) doi:10.1242/dev.178673.

217. Park, J. *et al.* Single-cell transcriptomics of the mouse kidney reveals potential cellular targets of kidney disease. *Science* **360**, 758–763 (2018).

218. Butler, A., Hoffman, P., Smibert, P., Papalexi, E. & Satija, R. Integrating single-cell transcriptomic data across different conditions, technologies, and species. *Nat. Biotechnol.* **36**, 411–420 (2018).

219. Ilicic, T. *et al.* Classification of low quality cells from single-cell RNA-seq data. *Genome Biol.* **17**, (2016).

220. Van der Hauwaert, C. *et al.* Isolation and characterization of a primary proximal tubular epithelial cell model from human kidney by CD10/CD13 double labeling. *PLoS ONE* **8**, e66750 (2013).

221. Ohtsuki, S. *et al.* Simultaneous absolute protein quantification of transporters, cytochromes P450, and UDP-glucuronosyltransferases as a novel approach for the characterization of individual human liver: comparison with mRNA levels and activities. *Drug Metab. Dispos.* **40**, 83–92 (2012).

222. Engel, U., Breborowicz, D., Bøg-Hansen, T. & Francis, D. Lectin staining of renal tubules in normal kidney. *APMIS* **105**, 31–34 (1997).

223. Özcelik, D. *et al.* Zinc supplementation attenuates metallothionein and oxidative stress changes in kidney of streptozotocin-induced diabetic rats. *Biol. Trace Elem. Res.* **150**, 342–349 (2012).

224. Ogawa, D. *et al.* High glucose increases metallothionein expression in renal proximal tubular epithelial cells. *Exp. Diabetes Res.* **2011**, 1–8 (2011).

225. Heliot, C. *et al. HNF1B* controls proximal-intermediate nephron segment identity in vertebrates by regulating Notch signalling components and *Irx1/2*. *Development* **140**, 873–885 (2013).

226. Georgas, K. *et al.* Use of dual section mRNA *in situ* hybridisation/immunohistochemistry to clarify gene expression patterns during the early stages of nephron development in the embryo and in the mature nephron of the adult mouse kidney. *Histochem. Cell Biol.* **130**, 927 (2008).

227. Liu, J. *et al.* Molecular characterization of the transition from acute to chronic kidney injury following ischemia/reperfusion. *JCI Insight* **2**, (2017).

228. Vilar, J., Gilbert, T., Moreau, E. & Merlet-Bénichou, C. Metanephros organogenesis is highly stimulated by vitamin A derivatives in organ culture. *Kidney Int.* **49**, 1478–1487 (1996).

229. Lazzeri, E., Peired, A. J., Lasagni, L. & Romagnani, P. Retinoids and glomerular regeneration. *Semin. Nephrol.* **34**, 429–436 (2014).

230. Rosselot, C. *et al.* Non-cell-autonomous retinoid signaling is crucial for renal development. *Dev. Camb. Engl.* **137**, 283–292 (2010).

231. Wingert, R. A. *et al.* The *cdx* genes and retinoic acid control the positioning and segmentation of the zebrafish pronephros. *PLOS Genet.* **3**, e189 (2007).

232. Li, Y., Cheng, C. N., Verdun, V. A. & Wingert, R. A. Zebrafish nephrogenesis is regulated by interactions between retinoic acid, *mecom*, and Notch signaling. *Dev. Biol.* **386**, 111–122 (2014).

233. Trapnell, C. *et al.* The dynamics and regulators of cell fate decisions are revealed by pseudotemporal ordering of single cells. *Nat. Biotechnol.* **32**, 381–386 (2014).

234. Qiu, X. *et al.* Single-cell mRNA quantification and differential analysis with Census. *Nat. Methods* **14**, 309–315 (2017).

235. Qiu, X. *et al.* Reversed graph embedding resolves complex single-cell trajectories. *Nat. Methods* **14**, 979–982 (2017).

236. Gerich, J. E., Meyer, C., Woerle, H. J. & Stumvoll, M. Renal gluconeogenesis: its importance in human glucose homeostasis. *Diabetes Care* **24**, 382–391 (2001).

237. Jacquillet, G. & Unwin, R. J. Physiological regulation of phosphate by vitamin D, parathyroid hormone (PTH) and phosphate (Pi). *Pflugers Arch.* **471**, 83–98 (2019).

238. Edwards, A. & Bonny, O. A model of calcium transport and regulation in the proximal tubule. *Am. J. Physiol. - Ren. Physiol.* **315**, F942–F953 (2018).

239. Ibarra, F. *et al.* Prolactin, a natriuretic hormone, interacting with the renal dopamine system. *Kidney Int.* **68**, 1700–1707 (2005).

240. Duda, K., Chi, Y.-I. & Shoelson, S. E. Structural basis for HNF-4α activation by ligand and coactivator binding. *J. Biol. Chem.* **279**, 23311–23316 (2004).

241. Glosse, P. & Föller, M. AMP-activated protein kinase (AMPK)-dependent regulation of renal transport. *Int. J. Mol. Sci.* **19**, 3481 (2018).

242. Sato, Y. *et al.* Hypoxia reduces HNF4α/MODY1 protein expression in pancreatic β-cells by activating AMP-activated protein kinase. *J. Biol. Chem.* **292**, 8716–8728 (2017).

243. Adelsberg, J. van *et al.* Activation of hepatocyte growth factor (HGF) by endogenous HGF activator is required for metanephric kidney morphogenesis *in vitro*. *J. Biol. Chem.* **276**, 15099–15106 (2001).

244. Stracke, S. Differentiating and proliferative effects of HGF in renal proximal tubular cells are mediated via different signalling pathways. *Nephrol. Dial. Transplant.* **13**, 1398–1405 (1998).

245. Nakasatomi, M. *et al.* Enhancement of HGF-induced tubulogenesis by endothelial cell-derived GDNF. *PLoS ONE* **14**, (2019).

246. Blutke, A., Schneider, M. R., Wolf, E. & Wanke, R. Growth hormone (GH)-transgenic insulin-like growth factor 1 (IGF1)-deficient mice allow dissociation of excess GH and IGF1 effects on glomerular and tubular growth. *Physiol. Rep.* **4**, e12709.

247. Woda, C. B. *et al.* Regulation of renal NaPi-2 expression and tubular phosphate reabsorption by growth hormone in the juvenile rat. *Am. J. Physiol.-Ren. Physiol.* **287**, F117–F123 (2004).

248. Ornitz, D. M. & Itoh, N. The fibroblast growth factor signaling pathway. *Wiley Interdiscip. Rev. Dev. Biol.* **4**, 215–266 (2015).

249. Colvin, J. S., Feldman, B., Nadeau, J. H., Goldfarb, M. & Ornitz, D. M. Genomic organization and embryonic expression of the mouse fibroblast growth factor 9 gene. *Dev. Dyn. Off. Publ. Am. Assoc. Anat.* **216**, 72–88 (1999).

250. Combes, A. N., Davies, J. A. & Little, M. H. Cell-cell interactions driving kidney morphogenesis. *Curr. Top. Dev. Biol.* **112**, 467–508 (2015).

251. Weinstein, M., Xu, X., Ohyama, K. & Deng, C. X. FGFR-3 and FGFR-4 function cooperatively to direct alveogenesis in the murine lung. *Development* **125**, 3615–3623 (1998).

252. Bates, C. M. Role of fibroblast growth factor receptor signaling in kidney development. *Pediatr. Nephrol.* **22**, 343–349 (2007).

253. Gattineni, J., Twombley, K., Goetz, R., Mohammadi, M. & Baum, M. Regulation of serum 1,25$(OH)_2$Vitamin D_3 levels by fibroblast growth factor 23 is mediated by FGF receptors 3 and 4. *Am. J. Physiol.-Ren. Physiol.* **301**, F371–F377 (2011).

254. Evans, R. M., Barish, G. D. & Wang, Y.-X. PPARs and the complex journey to obesity. *Nat. Med.* **10**, 355–361 (2004).

255. Yang, T. *et al.* Expression of peroxisomal proliferator-activated receptors and retinoid X receptors in the kidney. *Am. J. Physiol.-Ren. Physiol.* **277**, F966–F973 (1999).

256. Braissant, O., Foufelle, F., Scotto, C., Dauça, M. & Wahli, W. Differential expression of peroxisome proliferator-activated receptors (PPARs): tissue distribution of PPAR-alpha, -beta, and -gamma in the adult rat. *Endocrinology* **137**, 354–366 (1996).

257. Lyu, Z. *et al.* PPARγ maintains the metabolic heterogeneity and homeostasis of renal tubules. *EBioMedicine* **38**, 178–190 (2018).

258. Aseem, O., Barth, J. L., Klatt, S. C., Smith, B. T. & Argraves, W. S. Cubilin expression is monoallelic and epigenetically augmented via PPARs. *BMC Genomics* **14**, 405 (2013).

259. Cabezas, F. *et al.* Megalin/LRP2 expression is induced by peroxisome proliferator-activated receptor -alpha and -gamma: implications for PPARs' roles in renal function. *PLOS ONE* **6**, e16794 (2011).

260. Thiagarajan, R. D. *et al.* Identification of anchor genes during kidney development defines ontological relationships, molecular subcompartments and regulatory pathways. *PLOS ONE* **6**, e17286 (2011).

261. Kispert, A., Vainio, S. & McMahon, A. P. Wnt-4 is a mesenchymal signal for epithelial transformation of metanephric mesenchyme in the developing kidney. *Development* **125**, 4225–4234 (1998).

262. Stark, K., Vainio, S., Vassileva, G. & McMahon, A. P. Epithelial transformation of metanephric mesenchyme in the developing kidney regulated by Wnt-4. *Nature* **372**, 679–683 (1994).

263. Schneider, J., Arraf, A. A., Grinstein, M., Yelin, R. & Schultheiss, T. M. Wnt signaling orients the proximal-distal axis of chick kidney nephrons. *Dev. Camb. Engl.* **142**, 2686–2695 (2015).

264. Lindström, N. O. *et al.* Integrated β-catenin, BMP, PTEN, and Notch signalling patterns the nephron. *eLife* **4**, e04000 (2015).

265. Lau, W. de, Peng, W. C., Gros, P. & Clevers, H. The R-spondin/Lgr5/Rnf43 module: regulator of Wnt signal strength. *Genes Dev.* **28**, 305–316 (2014).

266. Chung, E., Deacon, P. & Park, J.-S. Notch is required for the formation of all nephron segments and primes nephron progenitors for differentiation. *Development* **144**, 4530–4539 (2017).

267. Guo, X. & Wang, X.-F. Signaling cross-talk between TGF-β/BMP and other pathways. *Cell Res.* **19**, 71–88 (2009).

268. Kitisin, K. *et al.* TGF-β signaling in development. *Sci. Signal.* (2007) doi:10.1126/stke.3992007cm1.

269. Plisov, S. Y. *et al.* TGF beta 2, LIF and FGF2 cooperate to induce nephrogenesis. *Development* **128**, 1045–1057 (2001).

270. Tanigawa, S., Taguchi, A., Sharma, N., Perantoni, A. O. & Nishinakamura, R. Selective *in vitro* propagation of nephron progenitors derived from embryos and pluripotent stem cells. *Cell Rep.* **15**, 801–813 (2016).

271. Li, Z., Araoka, T. & Belmonte, J. C. I. Gene editing in 3D cultured nephron progenitor cell lines. in *Kidney Organogenesis: Methods and Protocols* (ed. Vainio, S.) 151–159 (Springer New York, 2019). doi:10.1007/978-1-4939-9021-4_13.

272. Gewin, L. *et al.* Deleting the TGF-β receptor attenuates acute proximal tubule injury. *J. Am. Soc. Nephrol.* **23**, 2001–2011 (2012).

273. Lan, R. *et al.* Mitochondrial pathology and glycolytic shift during proximal tubule atrophy after ischemic AKI. *J. Am. Soc. Nephrol.* **27**, 3356–3367 (2016).

274. Nakao, A. *et al.* Identification of Smad7, a TGFβ-inducible antagonist of TGF-β signalling. *Nature* **389**, 631–635 (1997).

275. Miyazaki, Y., Oshima, K., Fogo, A., Hogan, B. L. M. & Ichikawa, I. Bone morphogenetic protein 4 regulates the budding site and elongation of the mouse ureter. *J. Clin. Invest.* **105**, 863–873 (2000).

276. Cain, J. E. & Bertram, J. F. Ureteric branching morphogenesis in BMP4 heterozygous mutant mice. *J. Anat.* **209**, 745–755 (2006).

277. Lindström, N. O. *et al.* Conserved and divergent features of mesenchymal progenitor cell types within the cortical nephrogenic niche of the human and mouse kidney. *J. Am. Soc. Nephrol.* (2018) doi:10.1681/ASN.2017080890.

278. Habib, N. *et al.* Massively parallel single-nucleus RNA-seq with DroNc-seq. *Nat. Methods* **14**, 955–958 (2017).

279. Lake, B. B. *et al.* A comparative strategy for single-nucleus and single-cell transcriptomes confirms accuracy in predicted cell-type expression from nuclear RNA. *Sci. Rep.* **7**, 1–8 (2017).

280. Mutsaers, H. A. M. *et al.* Switch in FGFR3 and -4 expression profile during human renal development may account for transient hypercalcemia in patients with sotos syndrome due to 5q35 microdeletions. *J. Clin. Endocrinol. Metab.* **99**, E1361–E1367 (2014).

281. Matsuzaki, T. *et al.* The distribution and function of aquaporins in the kidney: resolved and unresolved questions. *Anat. Sci. Int.* **92**, 187–199 (2017).

282. Dutta, D., Heo, I. & Clevers, H. Disease modeling in stem cell-derived 3D organoid systems. *Trends Mol. Med.* **23**, 393–410 (2017).

283. Schutgens, F. *et al.* Tubuloids derived from human adult kidney and urine for personalized disease modeling. *Nat. Biotechnol.* **37**, 303–313 (2019).

284. Mills, R. J. *et al.* Functional screening in human cardiac organoids reveals a metabolic mechanism for cardiomyocyte cell cycle arrest. *Proc. Natl. Acad. Sci.* 201707316 (2017) doi:10.1073/pnas.1707316114.

285. Rech, M. *et al.* Assessing fatty acid oxidation flux in rodent cardiomyocyte models. *Sci. Rep.* **8**, 1–6 (2018).

286. Guo, M., Wang, H., Potter, S. S., Whitsett, J. A. & Xu, Y. SINCERA: a pipeline for single-cell RNA-Seq profiling analysis. *PLOS Comput. Biol.* **11**, e1004575 (2015).

287. Aibar, S. *et al.* SCENIC: single-cell regulatory network inference and clustering. *Nat. Methods* **14**, 1083–1086 (2017).

288. Boreström, C. *et al.* A CRISP(e)R view on kidney organoids allows generation of an induced pluripotent stem cell–derived kidney model for drug discovery. *Kidney Int.* **94**, 1099–1110 (2018).

289. Howden, S. E., Vanslambrouck, J. M., Wilson, S. B., Tan, K. S. & Little, M. H. Reporter-based fate mapping in human kidney organoids confirms nephron lineage relationships and reveals synchronous nephron formation. *EMBO Rep.* **20**, e47483 (2019).

290. Vanslambrouck, J. M. *et al.* A toolbox to characterize human induced pluripotent stem cell–derived kidney cell types and organoids. *J. Am. Soc. Nephrol.* (2019) doi:10.1681/ASN.2019030303.

291. Cong, L. *et al.* Multiplex genome engineering using CRISPR/Cas systems. *Science* **339**, 819–823 (2013).

292. Mali, P. *et al.* RNA-guided human genome engineering via Cas9. *Science* **339**, 823–826 (2013).

293. Smith, J. *et al.* A combinatorial approach to create artificial homing endonucleases cleaving chosen sequences. *Nucleic Acids Res.* **34**, e149 (2006).

294. Miller, J. C. *et al.* An improved zinc-finger nuclease architecture for highly specific genome editing. *Nat. Biotechnol.* **25**, 778–785 (2007).

295. Joung, J. K. & Sander, J. D. TALENs: a widely applicable technology for targeted genome editing. *Nat. Rev. Mol. Cell Biol.* **14**, 49–55 (2013).

296. Horvath, P. & Barrangou, R. CRISPR/Cas, the immune system of bacteria and archaea. *Science* **327**, 167–170 (2010).

297. Hsu, P. D., Lander, E. S. & Zhang, F. Development and applications of CRISPR-Cas9 for genome engineering. *Cell* **157**, 1262–1278 (2014).

298. Howden, S. E. *et al.* Simultaneous reprogramming and gene correction of patient fibroblasts. *Stem Cell Rep.* **5**, 1109–1118 (2015).

299. Hsu, P. D. *et al.* DNA targeting specificity of RNA-guided Cas9 nucleases. *Nat. Biotechnol.* **31**, 827–832 (2013).

300. Cho, S. W. *et al.* Analysis of off-target effects of CRISPR/Cas-derived RNA-guided endonucleases and nickases. *Genome Res.* **24**, 132–141 (2014).

301. Fu, Y. *et al.* High-frequency off-target mutagenesis induced by CRISPR-Cas nucleases in human cells. *Nat. Biotechnol.* **31**, 822–826 (2013).

302. Bae, S., Park, J. & Kim, J.-S. Cas-OFFinder: a fast and versatile algorithm that searches for potential off-target sites of Cas9 RNA-guided endonucleases. *Bioinformatics* **30**, 1473–1475 (2014).

303. Doench, J. G. *et al.* Rational design of highly active sgRNAs for CRISPR-Cas9-mediated gene inactivation. *Nat. Biotechnol.* **32**, 1262–1267 (2014).

304. Kleinstiver, B. P. *et al.* High-fidelity CRISPR–Cas9 nucleases with no detectable genome-wide off-target effects. *Nature* **529**, 490–495 (2016).

305. Slaymaker, I. M. *et al.* Rationally engineered Cas9 nucleases with improved specificity. *Science* **351**, 84–88 (2016).

306. Smith, C. *et al.* Whole-genome sequencing analysis reveals high specificity of CRISPR/Cas9 and TALEN-based genome editing in human iPSCs. *Cell Stem Cell* **15**, 12–13 (2014).

307. Crosetto, N. *et al.* Nucleotide-resolution DNA double-strand breaks mapping by next-generation sequencing. *Nat. Methods* **10**, 361–365 (2013).

308. Tsai, S. Q. *et al.* GUIDE-Seq enables genome-wide profiling of off-target cleavage by CRISPR-Cas nucleases. *Nat. Biotechnol.* **33**, 187–197 (2015).

309. Kim, D. *et al.* Digenome-seq: genome-wide profiling of CRISPR-Cas9 off-target effects in human cells. *Nat. Methods* **12**, 237–243 (2015).

310. Howden, S. E. *et al.* A Cas9 variant for efficient generation of indel-free knockin or gene-corrected human pluripotent stem cells. *Stem Cell Rep.* **7**, 508–517 (2016).

311. Howden, S. E., Thomson, J. A. & Little, M. H. Simultaneous reprogramming and gene editing of human fibroblasts. *Nat. Protoc.* **13**, 875–898 (2018).

312. Ran, F. A. *et al.* Genome engineering using the CRISPR-Cas9 system. *Nat. Protoc.* **8**, 2281–2308 (2013).

313. Paquet, D. *et al.* Efficient introduction of specific homozygous and heterozygous mutations using CRISPR/Cas9. *Nature* **533**, 125–129 (2016).

314. Nielsen, R., Christensen, E. I. & Birn, H. Megalin and cubilin in proximal tubule protein reabsorption: from experimental models to human disease. *Kidney Int.* **89**, 58–67 (2016).

315. Prabakaran, T. *et al.* Receptor-mediated endocytosis of α-galactosidase A in human podocytes in Fabry disease. *PLoS ONE* **6**, e25065 (2011).

316. Subach, O. M., Cranfill, P. J., Davidson, M. W. & Verkhusha, V. V. An enhanced monomeric blue fluorescent protein with the high chemical stability of the chromophore. *PLOS ONE* **6**, e28674 (2011).

317. Cranfill, P. J. *et al.* Quantitative assessment of fluorescent proteins. *Nat. Methods* **13**, 557–562 (2016).

318. Vuong, L. M. *et al.* Differential effects of hepatocyte nuclear factor 4α isoforms on tumor growth and T-Cell factor 4/AP-1 interactions in human colorectal cancer cells. *Mol. Cell. Biol.* **35**, 3471–3490 (2015).

319. Marable, S. S., Chung, E., Adam, M., Potter, S. S. & Park, J.-S. *Hnf4a* deletion in the mouse kidney phenocopies Fanconi renotubular syndrome. *JCI Insight* **3**, (2018).

320. Brogna, S. & Wen, J. Nonsense-mediated mRNA decay (NMD) mechanisms. *Nat. Struct. Mol. Biol.* **16**, 107–113 (2009).

321. May, P., Bock, H. H. & Herz, J. Integration of endocytosis and signal transduction by lipoprotein receptors. *Sci. Signal.* (2003) doi:10.1126/stke.2003.176.pe12.

322. Naccache, S. N., Hasson, T. & Horowitz, A. Binding of internalized receptors to the PDZ domain of GIPC/synectin recruits myosin VI to endocytic vesicles. *Proc. Natl. Acad. Sci.* **103**, 12735–12740 (2006).

323. Chittenden, T. W. *et al.* Selective regulation of arterial branching morphogenesis by synectin. *Dev. Cell* **10**, 783–795 (2006).

324. Fisher, C. E. & Howie, S. E. M. The role of megalin (LRP-2/Gp330) during development. *Dev. Biol.* **296**, 279–297 (2006).

325. Shih, D. Q. *et al.* Genotype/phenotype relationships in HNF-4alpha/MODY1: haploinsufficiency is associated with reduced apolipoprotein (AII), apolipoprotein (CIII), lipoprotein(a), and triglyceride levels. *Diabetes* **49**, 832–837 (2000).

326. Kim, J. H. *et al.* High cleavage efficiency of a 2A peptide derived from porcine teschovirus-1 in human cell Lines, zebrafish and mice. *PLoS ONE* **6**, (2011).

327. Sylvain, E., Rajaraman, S., Megyesi, J. & Bello-Reuss, E. N. Expression of MDR1 (multidrug resistance) gene and its protein in normal human kidney. *Nephron* **77**, 284–9 (1997).

328. Konieczna, A. *et al.* Differential expression of ABC transporters (MDR1, MRP1, BCRP) in developing human embryos. *J. Mol. Histol.* **42**, 567–574 (2011).

329. Costantini, L. M., Subach, O. M., Jaureguiberry-bravo, M., Verkhusha, V. V. & Snapp, E. L. Cysteineless non-glycosylated monomeric blue fluorescent protein, secBFP2, for studies in the eukaryotic secretory pathway. *Biochem. Biophys. Res. Commun.* **430**, 1114–1119 (2013).

330. Burckhardt, G. Drug transport by organic anion transporters (OATs). *Pharmacol. Ther.* **136**, 106–130 (2012).

331. Kumar, S. *et al.* Sox9 activation highlights a cellular pathway of renal repair in the acutely injured mammalian kidney. *Cell Rep.* **12**, 1325–1338 (2015).

332. Magyar, A. *et al.* HO-1 concentrations 24 hours after cardiac surgery are associated with the incidence of acute kidney injury: a prospective cohort study. *Int. J. Nephrol. Renov. Dis.* **12**, 9–18 (2019).

333. Nagle, M. A. *et al.* Analysis of three-dimensional systems for developing and mature kidneys clarifies the role of OAT1 and OAT3 in antiviral handling. *J. Biol. Chem.* **286**, 243–251 (2011).

334. Yang, X., Pabon, L. & Murry, C. E. Engineering adolescence: maturation of human pluripotent stem cell-derived cardiomyocytes. *Circ. Res.* **114**, 511–523 (2014).

335. Parr, C. J. C., Yamanaka, S. & Saito, H. An update on stem cell biology and engineering for brain development. *Mol. Psychiatry* **22**, 808–819 (2017).

336. Gstraunthaler, G., Seppi, T. & Pfaller, W. Impact of culture conditions, culture media volumes, and glucose content on metabolic properties of renal epithelial cell cultures. *Cell. Physiol. Biochem. Int. J. Exp. Cell. Physiol. Biochem. Pharmacol.* **9**, 150–172 (1999).

337. Hale, L. J. & Coward, R. J. M. Insulin signalling to the kidney in health and disease. *Clin. Sci.* **124**, 351–370 (2013).

338. Duong Van Huyen, J.-P. *et al.* Spatiotemporal distribution of insulin-like growth factor receptors during nephrogenesis in fetuses from normal and diabetic rats. *Cell Tissue Res.* **314**, 367–379 (2003).

339. Artunc, F. *et al.* The impact of insulin resistance on the kidney and vasculature. *Nat. Rev. Nephrol.* **12**, 721–737 (2016).

340. Courjault-Gautier, F., Chevalier, J., Abbou, C. C., Chopin, D. K. & Toutain, H. J. Consecutive use of hormonally defined serum-free media to establish highly differentiated human renal proximal tubule cells in primary culture. *J. Am. Soc. Nephrol.* **5**, 1949–1963 (1995).

341. Mather, A. & Pollock, C. Glucose handling by the kidney. *Kidney Int.* **79**, S1–S6 (2011).

342. Francis, G. L. Albumin and mammalian cell culture: implications for biotechnology applications. *Cytotechnology* **62**, 1–16 (2010).

343. Chen, G. *et al.* Chemically defined conditions for human iPSC derivation and culture. *Nat. Methods* **8**, 424–429 (2011).

344. Ng, E. S., Davis, R., Stanley, E. G. & Elefanty, A. G. A protocol describing the use of a recombinant protein-based, animal product-free medium (APEL) for human embryonic stem cell differentiation as spin embryoid bodies. *Nat. Protoc.* **3**, 768–776 (2008).

345. Ghezzi, C. & Wright, E. M. Regulation of the human Na^+-dependent glucose cotransporter hSGLT2. *Am. J. Physiol. - Cell Physiol.* **303**, C348–C354 (2012).

346. Nakamura, N., Matsui, T., Ishibashi, Y. & Yamagishi, S. Insulin stimulates SGLT2-mediated tubular glucose absorption via oxidative stress generation. *Diabetol. Metab. Syndr.* **7**, (2015).

347. Brewer, G. J., Torricelli, J. R., Evege, E. K. & Price, P. J. Optimized survival of hippocampal neurons in B27-supplemented neurobasal™, a new serum-free medium combination. *J. Neurosci. Res.* **35**, 567–576 (1993).

348. Harper, M.-E. & Seifert, E. L. Thyroid hormone effects on mitochondrial energetics. *Thyroid* **18**, 145–156 (2008).

349. Sayre, N. L. & Lechleiter, J. D. Fatty acid metabolism and thyroid hormones. *Curr. Trends Endocrinol.* **6**, 65–76 (2012).

350. Shah, M., Quigley, R. & Baum, M. Maturation of proximal straight tubule NaCl transport: role of thyroid hormone. *Am. J. Physiol.-Ren. Physiol.* **278**, F596–F602 (2000).

351. Gupta, N. Maturation of the Na^+/H^+ antiporter (NHE3) in the proximal tubule of the hypothyroid adrenalectomized rat. *Am. J. Physiol. - Ren. Physiol.* **287**, F521–F527 (2004).

352. Ali, R., Amlal, H., Burnham, C. E. & Soleimani, M. Glucocorticoids enhance the expression of the basolateral Na^+:$HCO3^-$ cotransporter in renal proximal tubules. *Kidney Int.* **57**, 1063–1071 (2000).

353. Sabolić, I. *et al.* Gender differences in kidney function. *Pflüg. Arch. - Eur. J. Physiol.* **455**, 397 (2007).

354. Ljubojević, M. *et al.* Rat renal cortical OAT1 and OAT3 exhibit gender differences determined by both androgen stimulation and estrogen inhibition. *Am. J. Physiol.-Ren. Physiol.* **287**, F124–F138 (2004).

355. Morris, M. E., Lee, H.-J. & Predko, L. M. Gender differences in the membrane transport of endogenous and exogenous compounds. *Pharmacol. Rev.* **55**, 229–240 (2003).

356. Herak-Kramberger, C. M. *et al.* Sex-dependent expression of water channel AQP1 along the rat nephron. *Am. J. Physiol. - Ren. Physiol.* **308**, F809–F821 (2015).

357. Yuan, Y., Zhang, A., Huang, S., Ding, G. & Chen, R. A PPARγ agonist inhibits aldosterone-induced mesangial cell proliferation by blocking ROS-dependent EGFR intracellular signaling. *Am. J. Physiol.-Ren. Physiol.* **300**, F393–F402 (2010).

358. Slusser, A. *et al.* Cadherin expression, vectorial active transport, and metallothionein isoform 3 mediated EMT/MET responses in cultured primary and immortalized human proximal tubule cells. *PLOS ONE* **10**, e0120132 (2015).

359. Paul, R. *et al.* Cadherin-6, a cell adhesion molecule specifically expressed in the proximal renal tubule and renal cell carcinoma. *Cancer Res.* **57**, 2741–2748 (1997).

360. Hu, D. *et al.* Metabolic maturation of human pluripotent stem cell-derived cardiomyocytes by inhibition of HIF1α and LDHA. *Circ. Res.* **123**, 1066–1079 (2018).

361. Li, S. *et al.* PPARα ligand protects during cisplatin-induced acute renal failure by preventing inhibition of renal FAO and PDC activity. *Am. J. Physiol.-Ren. Physiol.* **286**, F572–F580 (2004).

362. Schwartzentruber, J. *et al.* Molecular and functional variation in iPSC-derived sensory neurons. *Nat. Genet.* **50**, 54–61 (2018).

363. Nicholas, C. R. *et al.* Functional maturation of hPSC-derived forebrain interneurons requires an extended timeline and mimics human neural development. *Cell Stem Cell* **12**, 573–586 (2013).

364. Khanna, A. K., Plummer, M. S., Hilton, G., Pieper, G. M. & Ledbetter, S. Anti–transforming growth factor antibody at low but not high doses limits cyclosporine-mediated nephrotoxicity without altering rat cardiac allograft survival. *Circulation* **110**, 3822–3829 (2004).

365. Forbes, J. M. & Thorburn, D. R. Mitochondrial dysfunction in diabetic kidney disease. *Nat. Rev. Nephrol.* **14**, 291–312 (2018).

366. Takebe, T. *et al.* Vascularized and functional human liver from an iPSC-derived organ bud transplant. *Nature* **499**, 481–484 (2013).

367. Watson, C. L. *et al.* An *in vivo* model of human small intestine using pluripotent stem cells. *Nat. Med.* **20**, 1310–1314 (2014).

368. Francipane, M. G. *et al.* Kidney-in-a-lymph node: a novel organogenesis assay to model human renal development and test nephron progenitor cell fates. *J. Tissue Eng. Regen. Med.* **13**, 1724–1731 (2019).

369. Finkbeiner, S. R. *et al.* Transcriptome-wide analysis reveals hallmarks of human intestine development and maturation *in vitro* and *in vivo*. *Stem Cell Rep.* **4**, 1140–1155 (2015).

370. Cho, G.-S. *et al.* Neonatal transplantation confers maturation of PSC-derived cardiomyocytes conducive to modeling cardiomyopathy. *Cell Rep.* **18**, 571–582 (2017).

371. Long, K. R. *et al.* Proximal tubule apical endocytosis is modulated by fluid shear stress via an mTOR-dependent pathway. *Mol. Biol. Cell* (2017) doi:10.1091/mbc.E17-04-0211.

372. Rogers, S. A., Lowell, J. A., Hammerman, N. A. & Hammerman, M. R. Transplantation of developing metanephroi into adult rats. *Kidney Int.* **54**, 27–37 (1998).

373. Dekel, B. *et al.* Engraftment and differentiation of human metanephroi into functional mature nephrons after transplantation into mice is accompanied by a profile of gene expression similar to normal human kidney development. *J. Am. Soc. Nephrol.* **13**, 977–990 (2002).

374. Dekel, B. *et al.* Human and porcine early kidney precursors as a new source for transplantation. *Nat. Med.* **9**, 53–60 (2003).

375. Hammerman, M. R. Organogenesis of kidneys following transplantation of renal progenitor cells. *Transpl. Immunol.* **12**, 229–239 (2004).

376. Francipane, M. G. & Lagasse, E. The lymph node as a new site for kidney organogenesis. *STEM CELLS Transl. Med.* **4**, 295–307 (2015).

377. Georgas, K. M., Chiu, H. S., Lesieur, E., Rumballe, B. A. & Little, M. H. Expression of metanephric nephron-patterning genes in differentiating mesonephric tubules. *Dev. Dyn.* **240**, 1600–1612 (2011).

378. Lawrence, M. L., Chang, C.-H. & Davies, J. A. Transport of organic anions and cations in murine embryonic kidney development and in serially-reaggregated engineered kidneys. *Sci. Rep.* **5**, 9092 (2015).

379. Brown, A. C., Muthukrishnan, S. D. & Oxburgh, L. A synthetic niche for nephron progenitor cells. *Dev. Cell* **34**, 229–241 (2015).

380. Li, Z. *et al.* 3D culture supports long-term expansion of mouse and human nephrogenic progenitors. *Cell Stem Cell* **19**, 1–14 (2016).

381. Chambers, J. M., Poureetezadi, S. J., Addiego, A., Lahne, M. & Wingert, R. A. *ppargc1a* controls nephron segmentation during zebrafish embryonic kidney ontogeny. *eLife* **7**, e40266 (2018).

382. Cheng, C. N. & Wingert, R. A. Nephron proximal tubule patterning and corpuscles of Stannius formation are regulated by the *sim1a* transcription factor and retinoic acid in zebrafish. *Dev. Biol.* **399**, 100–116 (2015).

383. Wessely, O. & Tran, U. Xenopus pronephros development—past, present, and future. *Pediatr. Nephrol.* **26**, 1545–1551 (2011).

384. Wingert, R. A. & Davidson, A. J. Zebrafish nephrogenesis involves dynamic spatiotemporal expression changes in renal progenitors and essential signals from retinoic acid and *irx3b*. *Dev. Dyn.* **240**, 2011–2027 (2011).

385. Ransick, A. *et al.* Single cell profiling reveals sex, lineage and regional diversity in the mouse kidney. *bioRxiv* 673335 (2019) doi:10.1101/673335.

386. Lindström, N. O. *et al.* Progressive recruitment of mesenchymal progenitors reveals a time-dependent process of cell fate acquisition in mouse and human nephrogenesis. *Dev. Cell* **45**, 651-660.e4 (2018).

387. Sivakamasundari, V. *et al.* Comprehensive cell type specific transcriptomics of the human kidney. *bioRxiv* 238063 (2017) doi:10.1101/238063.

388. Yuri, S., Nishikawa, M., Yanagawa, N., Jo, O. D. & Yanagawa, N. *In vitro* propagation and branching morphogenesis from single ureteric bud cells. *Stem Cell Rep.* **8**, 401 (2017).

389. Vogetseder, A., Palan, T., Bacic, D., Kaissling, B. & Le Hir, M. Proximal tubular epithelial cells are generated by division of differentiated cells in the healthy kidney. *Am. J. Physiol.-Cell Physiol.* **292**, C807–C813 (2007).

390. Vogetseder, A. *et al.* Proliferation capacity of the renal proximal tubule involves the bulk of differentiated epithelial cells. *Am. J. Physiol.-Cell Physiol.* **294**, C22–C28 (2008).

391. Su, R., Xiong, S., Zink, D. & Loo, L.-H. High-throughput imaging-based nephrotoxicity prediction for xenobiotics with diverse chemical structures. *Arch. Toxicol.* **90**, 2793–2808 (2016).

392. Schmittgen, T. D. & Livak, K. J. Analyzing real-time PCR data by the comparative C_T method. *Nat. Protoc.* **3**, 1101–1108 (2008).

APPENDIX

Please see the next page for appendix content.

Advances in predictive in vitro models of drug-induced nephrotoxicity

*Joanne Y.-C. Soo[1,2], Jitske Jansen[3], Rosalinde Masereeuw[3] and Melissa H. Little[1,2,4]**

Abstract | In vitro screens for nephrotoxicity are currently poorly predictive of toxicity in humans. Although the functional proteins that are expressed by nephron tubules and mediate drug susceptibility are well known, current in vitro cellular models poorly replicate both the morphology and the function of kidney tubules and therefore fail to demonstrate injury responses to drugs that would be nephrotoxic in vivo. Advances in protocols to enable the directed differentiation of pluripotent stem cells into multiple renal cell types and the development of microfluidic and 3D culture systems have opened a range of potential new platforms for evaluating drug nephrotoxicity. Many of the new in vitro culture systems have been characterized by the expression and function of transporters, enzymes, and other functional proteins that are expressed by the kidney and have been implicated in drug-induced renal injury. In vitro platforms that express these proteins and exhibit molecular biomarkers that have been used as readouts of injury demonstrate improved functional maturity compared with static 2D cultures and represent an opportunity to model injury to renal cell types that have hitherto received little attention. As nephrotoxicity screening platforms become more physiologically relevant, they will facilitate the development of safer drugs and improved clinical management of nephrotoxicants.

The specialized role of the kidney in filtering substances from the blood to maintain volume and electrolyte homeostasis, coupled with the high metabolic activity of the renal tubule epithelium, makes the kidney particularly vulnerable to drug-induced injury. A wide variety of commonly used pharmaceutical compounds are nephrotoxic; therefore, the degree of nephrotoxicity of each compound has to be balanced against its utility and is often dose limiting. For example, antibiotics (such as gentamicin and vancomycin) and immunosuppressive agents (including ciclosporin) can induce tubular injury[1], whereas lithium, which is frequently prescribed for bipolar disorder, can cause damage to the collecting duct[2]. Several epidemiological studies have shown a strong association between the use of common drugs, such as antiretroviral agents and aminoglycoside antibiotics, and the risk of acute kidney injury (AKI)[3]. However, the development of drug derivatives with improved renal safety profiles has proved challenging as currently available in vitro screening methods are poorly predictive of nephrotoxicity in animal models or humans[4]. Of note, preclinical studies can also fail to identify nephrotoxicity owing to species-specific variations in the metabolic response to various pharmaceutical agents and in the expression of certain genes[4].

The failure of in vitro drug screening methods to identify nephrotoxic activity results from a combination of factors. A major contributing factor is the lack of valid in vitro cell models of the kidney[5]. A second is the lack of robust markers of kidney injury in both in vitro and in vivo studies[5,6]. The fact that drugs can interact with each other and/or compete for detoxification enzyme complexes further complicates screening and presents difficulties in terms of predicting which drug combinations can be safely used by a patient[7–9]. Finally, the market has failed to develop models with which to predict drug responses of individual patients, for example, owing to genetic variations in cytochrome P450 (CYP) enzymes[10].

Current in vitro screens for nephrotoxic compounds have focused mostly on proximal tubule cells because this segment of the nephron is an important target of nephrotoxic injury in vivo. The proximal tubules secrete xenobiotics into the filtrate and reabsorb glucose, albumin, and various electrolytes via an array of transporters and receptors that can also transport drugs. To generate energy for these processes, proximal tubule cells are rich in mitochondria; thus, proximal tubule cells are also sensitive to disruptions in oxidative phosphorylation[11]. Moreover, metabolic enzymes such as β-lyase, expressed in renal proximal tubule cells, can bioactivate xenobiotics, potentiating the toxicity of these agents. However, nephrotoxic injury is not restricted to the proximal tubules, with all segments of the nephron,

[1]*Department of Paediatrics, The University of Melbourne, Parkville, Victoria, Australia.*

[2]*Murdoch Children's Research Institute, Parkville, Victoria, Australia.*

[3]*Division of Pharmacology, Utrecht Institute for Pharmaceutical Sciences, Utrecht University, Utrecht, Netherlands.*

[4]*Department of Anatomy and Neuroscience, The University of Melbourne, Parkville, Victoria, Australia.*

[5]*These authors contributed equally: Joanne Y-C Soo, Jitske Jansen*

**e-mail: melissa.little@mcri.edu.au*

https://doi.org/10.1038/s41581-018-0003-9

Key points

- Currently available in vitro and animal models of drug-induced nephrotoxicity are poorly predictive of toxicity in humans.
- Functional proteins that underlie the susceptibility of various renal cell types to specific drugs, and molecular biomarkers of injury, can be used to characterize the functional maturity of in vitro models and their capacity to respond to nephrotoxicants.
- In vitro models derived using new protocols for the directed differentiation of pluripotent stem cells to renal cells and new 3D in vitro culture systems demonstrate improved functional maturity over static 2D systems.
- Improved functional maturity of cultured renal cells in systems that more closely replicate the physiology of the renal tubule and its supporting cells will improve the predictive ability of in vitro models of nephrotoxicity.

including the podocytes, distal nephrons, and collecting ducts, displaying specific drug sensitivities (FIG. 1). In addition, the kidney microvasculature is also susceptible to drug-induced injury, which can cause diminished blood flow, hypoxic injury, and inflammation with consequences on tubule function[12].

The development of in vitro models to reliably predict the nephrotoxicity of potential pharmacologic agents requires a solid understanding of the specific cellular targets and consequences of nephrotoxicants as well as robust and reliable mechanistic biomarkers of nephrotoxicity. Two-dimensional cultures of primary or conditionally immortalized renal epithelial cells have traditionally represented the gold standard in vitro model for nephrotoxicant assessment. However, proximal tubular epithelial cells cultured using this approach exhibit poor apical–basal polarization and low levels of key protein transporters such as organic anion transporters (OATs) and organic cation transporter 2 (OCT2), hindering their utility as tools for predicting the effects of nephrotoxic agents in vivo[13,14]. Advances in the directed differentiation of human pluripotent stem cells (hPSCs) to multiple renal cell types, as well as in microfluidic culture systems, have opened up a range of potential novel platforms for in vitro nephrotoxicity screening. Here, we discuss the transporters, enzymes, and proteins expressed by the many different cell types in the kidney that have been implicated in drug-induced injury as well as molecular biomarkers that have been used as readouts of injury in in vitro models. We describe mechanisms of nephrotoxic injury, the functional features of tubular cell models that are essential for predicting the toxicity of pharmaceutical compounds, and novel in vitro cell models that are currently under development.

Mechanisms of nephrotoxic injury

Nephrotoxicants cause injury by selectively injuring specific cell types or by nonselectively injuring multiple cell types within the kidney, depending on their mechanism of action[1] (FIG. 1). The direct effects of nephrotoxicants have been most extensively studied for epithelial cells in the proximal tubule. However, tubular epithelial cells express a wide range of transporters, many of which are unique to specific segments of the tubule; hence, drugs with an affinity for those transporters can cause cell death in specific nephron segments. By contrast, some drugs, such as amphotericin B, cause tubular toxicity by nonspecifically damaging the membranes of epithelial cells throughout the tubule[15]. In addition, tubular epithelial cells can suffer injury as a result of the osmotic effects of pharmaceutical compounds, drug-induced nephrolithiasis, or from drug-induced ischaemic events. For example, contrast media used for procedures such as angiography can induce nephropathy through the induction of oxidative stress and osmotic effects as well as haemodynamic changes[16].

The interstitial cells that surround the tubules are also targets of drug toxicity. Acute interstitial nephritis is most often the result of an inflammatory, non-dose-dependent response to a drug that causes immunoglobulin deposition in tubule basement membranes. By contrast, chronic interstitial nephritis is often associated with the long-term use of drugs such as ciclosporin, which can also cause acute tubular injury through the induction of inflammatory changes and interstitial fibrosis[1].

Podocytes, which maintain the filtration barrier in glomeruli, are also targets of drug-induced nephrotoxicity[17]. Similar to acute interstitial nephritis, drug-induced podocyte injury is often mediated by immune mechanisms. However, certain drugs have direct toxic effects on podocytes. For example, puromycin, which is taken up by podocytes via the plasma membrane monoamine transporter (PMAT; also known as ENT4 and encoded by *SLC29A4*), and bisphosphonates[18–20] are thought to cause podocyte injury by disrupting their cytoskeleton[18]. Once injured, podocytes undergo a dedifferentiation programme, which disrupts the glomerular filtration barrier, leading to nephrotic syndrome. The resulting proteinuria can cause secondary tubular injury (FIG. 1).

Beyond their nephrotoxic effects on specific renal cell types, drugs can exert injurious effects on the haemodynamic regulatory mechanisms of the kidney. Renal blood flow and glomerular filtration rate (GFR) are regulated by complex mechanisms, including prostaglandin and renin–angiotensin system signalling pathways[1]. Several drug classes, such as nonsteroidal anti-inflammatory drugs (NSAIDs) and angiotensin-converting enzyme (ACE) inhibitors, can disrupt these pathways[21,22], reducing GFR and potentially causing renal ischaemia and cell death through excessive vasoconstriction.

The kidney also contains a highly diverse population of endothelial cells that form its microvasculature. These cells are also sensitive to drug-induced injury. Unlike the renal tubules, these endothelial cells lack regenerative capacity[12]; hence, acute injury of the renal vasculature can predispose patients to the development of chronic kidney disease[23]. Nephrotoxicants can directly affect vascular responsiveness by modulating endothelial barrier function, coagulation cascades, and/or inflammatory processes[24]. Tubulovascular crosstalk takes place through vascular endothelial growth factor A (VEGFA), which is expressed in renal tubular epithelial cells, and its receptor, VEGF receptor 2 (VEGFR2), located almost exclusively on peritubular capillary endothelial cells[25]. This interaction is essential for the maintenance of the peritubular microvasculature. Anticancer drugs that target the VEGF pathway can induce thrombotic microangiopathy, proteinuria, and hypertension[26]. Thrombotic microangiopathy — involving thrombocytopenia, microangiopathic haemolytic anaemia, and

Nephrotoxicants
Any compounds, natural and synthetic, that exert an adverse effect on a specific kidney cell type or mediate an unwanted event affecting kidney functioning. By contrast, a toxin is a poisonous substance produced within living cells or organisms.

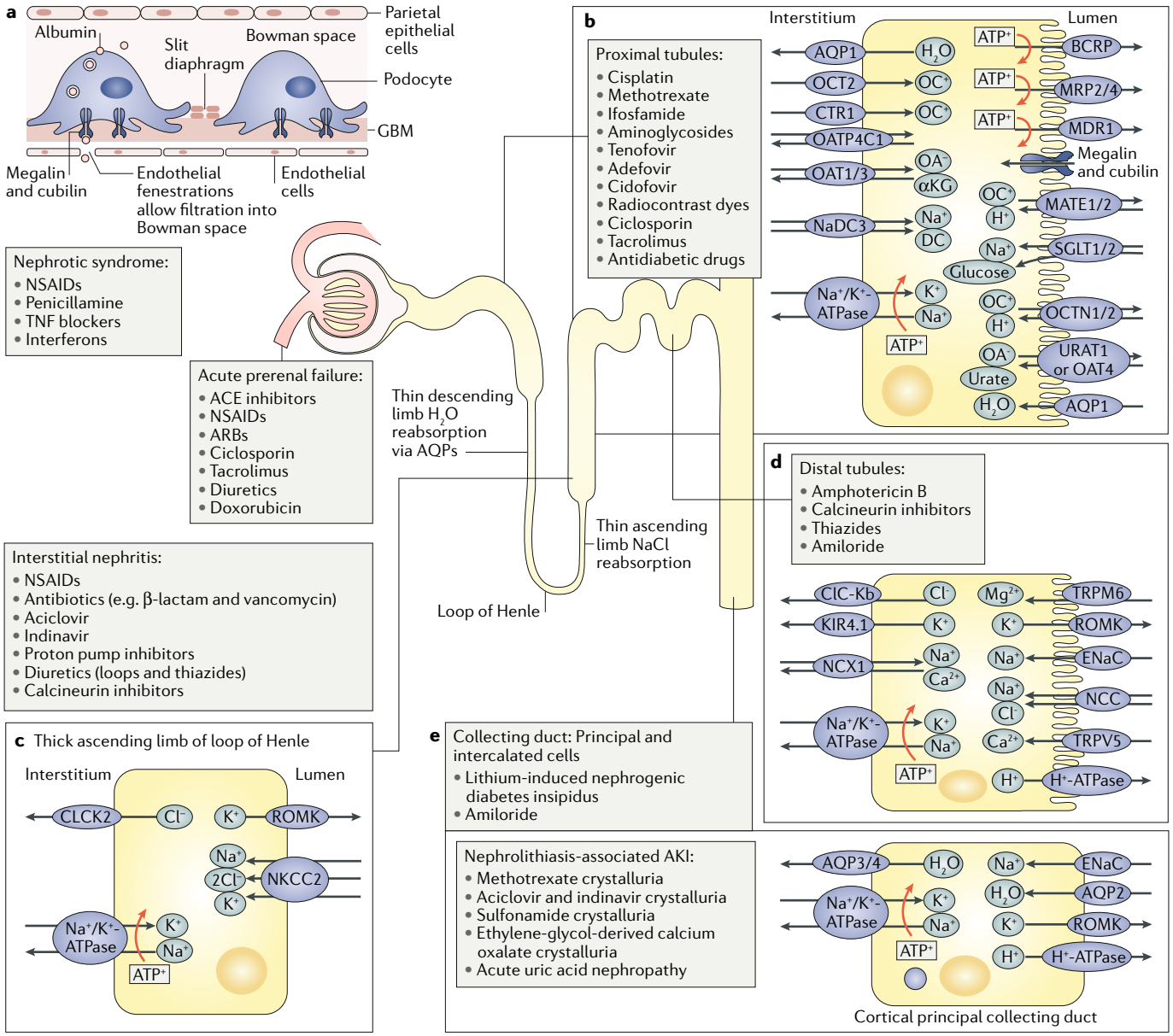

Fig. 1 | **Renal transporters and targets of nephrotoxicants.** Different segments of the nephron express various transporters and receptors that affect the susceptibility of the segments to the nephrotoxic effects of different drugs. **a** | In addition to the specific nephrotoxic effects of agents on different transporters in the tubule (discussed below), drugs such as nonsteroidal anti-inflammatory drugs (NSAIDs) can cause nephrotic syndrome by inducing immunoglobulin deposition on the glomerular basement membrane (GBM), damaging the membrane and podocytes. **b** | The proximal tubule expresses many transporters and receptors that are affected by pharmaceutical agents. For example, tenofovir, cisplatin, and gentamicin have affinity for organic anion transporters (OATs), organic cation transporters (OCTs), and endocytic receptors, respectively, allowing them to accumulate within the cell and cause toxic injury. **c** | The loop of Henle expresses aquaporins (AQPs) and ion transporters in different segments. **d** | The distal tubule expresses unique ion transporters. Drugs such as ciclosporin can affect the expression of these transporters and cause adverse effects such as Mg^{2+} and Na^+ loss. **e** | The collecting duct is composed of principal and intercalated cells. The principal cells express epithelial sodium channel (ENaC), which can transport lithium, contributing to lithium-induced diabetes insipidus. In addition, pharmaceutical agents can cause nonspecific nephrotoxic injury by inducing ischaemia, interstitial nephritis, or microangiopathy (not shown). αKG, α-ketoglutarate; ACE, angiotensin-converting enzyme; AKI, acute kidney injury; ARB, angiotensin receptor blocker; BCRP, breast cancer resistance protein; CLCK2, H^+/Cl^- exchange transporter 5 (also known as CLCN5); ClC-Kb, chloride channel protein ClC-Kb (also known as CLCNKB); CTR1, copper transporter 1; DC, dicarboxylate cotransporter; KIR4.1, ATP-dependent inwardly rectifying potassium channel KIR4.1 (also known as KCNJ10); MATE, multidrug and toxin extrusion protein; MDR1, multidrug resistance protein 1; MRP, multidrug resistance-associated protein; NaDC3, Na^+/dicarboxylate cotransporter 3; NCC, Na^+/Cl^- cotransporter; NCX1, Na^+/Ca^{2+}-exchange protein 1 (also known as SLC8A1); NKCC2, solute carrier family 12 member 1 (also known as SLC12A1); OA, organic anion; OATP4C1, solute carrier organic anion transporter family member 4C1 (also known as SLCO4C1); OC, organic cation; OCTN1, organic cation/carnitine transporter 1 (also known as SLC22A4); ROMK, ATP-sensitive inward rectifier potassium channel 1 (also known as KCNJ1); SGLT, sodium/glucose cotransporter; TNF, tumour necrosis factor; TRPM6, transient receptor potential cation channel subfamily M member 6; TRPV5, transient receptor potential cation channel subfamily V member 5; URAT1, urate anion exchanger 1 (also known as SLC22A12).

microvascular occlusion — can be immune-mediated and often leads to acute tubular necrosis. Drugs associated with thrombotic microangiopathy include quinine, ciclosporin, and tacrolimus[27].

Assessment of the potential nephrotoxic effects of pharmaceutical compounds on different components of the kidney therefore requires the use of different model systems. Direct injurious effects of a compound on tubular cells are the easiest mechanisms to model in vitro, whereas injury mechanisms that require blood flow, urine or filtrate production, or immune-mediated injury — or those that involve secondary injury — are more challenging as they require a model system in which complex cellular architecture is combined with functional components. Below, we discuss current in vitro models that are used to assess the nephrotoxicity of pharmaceutical agents and the development of novel systems that more closely recapitulate the complexity of the kidney.

Characterization of cellular models

Markers of functional maturity

An in vitro model that recapitulates the in vivo response of renal cells to nephrotoxicants requires appropriate expression of the transporters and receptors that interact with the drug of interest. Much work has been done to identify the transporters and enzymes that are associated with drug-induced nephrotoxicity; the degree to which in vitro models express physiological levels of these proteins will affect the ability of the models to accurately predict drug nephrotoxicity in clinical studies. In addition to detecting expression of transporters at the transcript and protein level by quantitative PCR and immunohistochemistry, the function of transporters and endocytic receptors can be investigated by assessing the effect of fluorescent substrates and transport inhibitors (TABLE 1). Inhibition of substrate uptake routes will decrease intracellular fluorescence, whereas inhibition of efflux transporters will increase intracellular fluorescence. Of importance, these transporters, receptors, and enzymes do not act in isolation. For example, drug transporters might rely on Na^+/K^+-ATPase activity to generate an electrochemical gradient that is then used to transport the substrate. A drug can also act as a substrate for multiple transporters and receptors or can become a substrate after bioactivation by an enzyme. Thus, for a model to accurately predict drug nephrotoxicity, it must express appropriate levels of all key transporters and enzymes and carry out the metabolic activities required for these transporters and enzymes to function.

The polarized, mature proximal tubule expresses a range of transporters that have overlapping substrate affinities and allow the transcellular secretion of drugs and endogenous compounds from the interstitial compartment into the pro-urine. Major influx transporters include the family of OATs and OCT2, which are expressed on the basolateral surface of the proximal tubule. OAT1–OAT3 and OCT2 are not expressed in other nephron segments in adult humans[28,29]. OAT-mediated transport is driven by an α-ketoglutarate gradient generated by the Na^+/K^+-ATPase and Na^+/dicarboxylate cotransporter 3 (NaDC3; encoded by *SLC13A3*), whereas OCT2 operates by electrogenic transport[30,31]. Multiple studies, including mouse knockout models and in vitro transfection models, have demonstrated that OAT1–OAT3 and OCT2 transporters increase sensitivity to known nephrotoxic drugs such as nucleoside analogue antivirals and cisplatin[32–36]. In addition to OCT2, copper transporter 1 (CTR1; encoded by *SLC31A1*), which is also expressed on the basolateral surface of the proximal tubule in mice, is also involved in cisplatin uptake and contributes to its toxicity[37] (BOX 1). Similarly, the megalin–cubilin endocytic receptor complex expressed on the apical surface of proximal tubule cells and in podocytes increases sensitivity of these cells to aminoglycoside, polymyxin, and glycopeptide antibiotics as these drugs bind to the receptor and are endocytosed[38,39].

Efflux transporters residing in the proximal tubule include the ATP-binding cassette transporters breast cancer resistance protein (BCRP; also known as ABCG2), multidrug resistance-associated proteins (MRPs), and multidrug resistance protein 1 (MDR1; also known as P-gp and ABCB1) as well as the multidrug and toxin and extrusion proteins (MATEs). According to the GUDMAP database, most of these transporters are expressed at the mRNA level before nephron formation in the developing mouse kidney[40,41]. If these transporters are also present in the developing human kidney, their expression in an in vitro model would not necessarily provide evidence of functional maturity and should be interpreted with caution. Indeed, HK-2 immortalized proximal tubule epithelial cells express MDR1 and demonstrate efflux function even when their influx transporter expression and function are close to zero[42]. Within the adult human nephron, these markers (that is, BCRP, MRPs, MDR1, and MATEs) are expressed only on the apical surface of the proximal tubule[43–45]. As these transporters export substances from the cell, their overexpression or upregulation attenuates renal toxicity of their substrates. Different affinities for these transporters could distinguish nephrotoxic drugs from less nephrotoxic derivatives[10,46,47].

Other transporters expressed in the renal proximal tubule include the sodium/glucose cotransporter 2 (SGLT2; encoded by *SLC5A2*) and aquaporin 1 (encoded by *AQP1*). SGLT2 is a target for a new class of drug for type 2 diabetes mellitus (SGLT2 inhibitors), but concerns exist that these agents might cause AKI in some patients[48,49], possibly owing to increased intratubular oxidative stress, uricosuria (with or without crystal formation), or an as-yet unidentified indirect mechanism[48,49]. Further insights into the underlying mechanism of SGLT2 inhibitor nephrotoxicity could potentially be provided by using an in vitro model of the renal proximal tubule that expresses SGLT2 (REF.[50]).

In addition to active transcellular transport via transporter proteins, ATP-independent paracellular transport also occurs in the proximal tubule. The proximal tubule epithelium has a leaky barrier, characterized by a transepithelial electrical resistance (TEER) of merely 5–7 Ω^*cm^2 compared with isolated renal distal tubular cells, which form a less leaky monolayer and have a TEER of 630 Ω^*cm^2 (REFS[51,52]). Ions, such as

Electrogenic transport
Transport that leads to a change in net charge across a cell membrane.

Transepithelial electrical resistance
(TEER). The electrical resistance across a cell monolayer. The higher the value, the less permeable the monolayer.

Table 1 | **Approaches to functionally characterize renal transporters, receptors, and ion channels in vitro**

Protein (gene)	Labelled substrate	Inhibitors	Refs
Glomerulus			
TRPC6 (*TRPC6*)	Fura-2-AM (10 μM)	2-Aminoethoxydiphenyl borate (100 μM)	156,157
Megalin (*LRP2*)	FITC–human serum albumin (K_m 4.5 mg/ml)	Equimolar transferrin or IgG	158
PMAT (*SLC29A4*)	PAN (100–250 μM, unlabelled)	Decynium-22 (2 μM)	19
Proximal tubule			
OAT1 (*SLC22A6*)	Fluorescein (K_m 0.8 ± 0.1 μM)	• Para-aminohippuric acid (IC_{50} 18 ± 4 μM) • Probenecid (IC_{50} 12.7 ± 5 μM) • Kynurenic acid (IC_{50} 6 ± 1 μM)	34,116
OAT3 (*SLC22A8*)	Fluorescein (K_m 3.7 ± 0.5 μM)	• Estrone sulfate (IC_{50} 2.1 ± 0.3 μM) • Probenecid (IC_{50} 1.9 ± 0.6 μM) • Kynurenic acid (IC_{50} 6 ± 1 μM)	34,116
OCT2 (*SLC22A2*)	ASP^+ (K_m 36.4 ± 6.8 μM)	• TPA (IC_{50} 16 ± 2 μM) • Metformin (IC_{50} 3.9 ± 1.2 μM) • Cimetidine (IC_{50} 8 ± 2 μM) • Verapamil (IC_{50} 10 ± 2 μM)	114,159
BCRP (*ABCG2*)	• Hoechst 33342 (1.25 μM) • Fluorescein (1 μM)	• KO143 (IC_{50} 4.4 ± 0.9 μM) • MK571 (IC_{50} 5.1 ± 0.9 μM) • PSC833 (IC_{50} 1.3 ± 0.3 μM)	116,160
MRPs (*ABCC2* and *ABCC4*)	• CMFDA (1.25 μM) • Fluorescein (1 μM)	• KO143 (IC_{50} 2.7 ± 0.2 μM) • MK571 (IC_{50} 6.4 ± 1.3 μM) • PSC833 (IC_{50} 1.0 ± 0.2 μM)	116,160
MDR1 (*ABCB1*)	Calcein-AM (1 μM)	• KO143 (IC_{50} 2.5 ± 0.5 μM) • MK571 (IC_{50} 10.2 ± 3.1 μM) • PSC833 (IC_{50} 0.7 ± 0.5 μM) • Zosuquidar (0.07 μM)[a]	160,161
MATE2K (*SLC47A2*)	ND	Pyrimethamine[b]	162,163
Megalin (*LRP2*)	FITC-bovine serum albumin (K_m 126 μg/ml)	RAP (IC_{50} 0.02 μM)[c]	112,164
	RAP–GST (2.5 μg/ml)	–	160
	Rhodamine–dextran (5 μM)	–	123
	Alexa 488–dextran (10 μg/ml)	–	124
SGLT2 (*SLC5A2*)	2-NBDG (200 μg/ml)	• Apigenin (50 μM) • Dapagliflozin (0.5 μM)	67
Distal tubule			
NCC (*SLC12A3*)	$^{22}Na^+$ (2 μCi/ml)	• Hydrochlorothiazide (100 μM) • Spironolactone (100 μM) • Metolazone (0.3 ± 0.001 μM)	52,165
TRPV5 (*TRPV5*)	Fluo-4 (2 μM)	Ruthenium red (10 μM)	166
Collecting duct			
ENaC (*SCNN1A*)	Lithium (10 mM, unlabelled)	Amiloride (10 μM)	68

2-NBDG, 2-(*N*-(7-nitrobenz-2-oxa-1,3-diazol-4-yl)amino)2-deoxyglucose; ASP^+, 4-(4-(dimethylamino)styryl)-*N*-methylpyridinium; BCRP, breast cancer resistance protein; CMFDA, 5-chloromethylfluorescein diacetate; ENaC, epithelial Na^+ channel; FITC, fluorescein isothiocyanate; IgG, immunoglobulin G; MATE2K, multidrug and toxin extrusion protein 2; MDR1, multidrug resistance protein 1; MRP, multidrug resistance-associated protein; NCC, Na^+/Cl^- cotransporter; ND, not done; OAT, organic anion transporter; OCT, organic cation transporter; PAN, puromycin aminonucleoside; PMAT, plasma membrane monoamine transporter; RAP–GST, receptor-associated protein–glutathione *S*-transferase fusion protein; SGLT2, sodium/glucose cotransporter 2; TPA, tetrapentylammonium; TRPC6, short transient receptor potential channel; TRPV5, transient receptor potential cation channel subfamily V member 5. [a]IC_{50} abacavir inhibition. Zosuquidar 1 μM is a potent inhibitor of MDR1-mediated calcein efflux (R.M., unpublished observation). [b]Inhibits efflux of *N*-methylnicotinamide and metformin in low micromolar range. [c]Concentration used in assay 1 μM[112].

Na^+, Cl^-, and K^+, and, to a lesser extent, compounds such as water are reabsorbed via passive diffusion and osmosis through paracellular tight junctions to the interstitial space. The tight junctions consist of a variety of proteins — including claudin 2, claudin 10a, claudin 11, and claudin 17 as well as occludin and tricellulin — that form ion-selective channels with a pore size of ~4 Å in radius[51,53]. Functional analyses have shown that claudin 2 channels facilitate the diffusion of cations (for example, Na^+, K^+, Ca^{2+} and H_2O), whereas claudin

Box 1 | **The many faces of cisplatin**

Cisplatin is a well-known nephrotoxic drug and is often used to study nephrotoxic injury responses in both animal and in vitro models. As it is a cationic drug, the prevailing paradigm is that cisplatin in the plasma enters proximal tubule cells via cation transporters and causes injury by inducing mitochondrial DNA damage and oxidative stress, with some efflux occurring via multidrug and toxin extrusion (MATE) transporters[103,153,154]. However, deletion of organic anion transporters or the endocytic receptor megalin also attenuates cisplatin toxicity in mouse models[38,155], suggesting that alternative modes of cisplatin uptake exist. Cisplatin is also a substrate for γ-glutamyltransferase (GGT), which is expressed by proximal tubules, but conflicting reports exist as to whether GGT processing attenuates or exacerbates cisplatin toxicity[63]. Cisplatin also shows general cytotoxicity at high doses, suggesting that nonspecific toxicity responses are possible. Hence, the induction of a nephrotoxic effect in response to cisplatin cannot necessarily be used to determine which transporters and metabolic functions are present in the model.

10a and possibly claudin 17 are involved in anion diffusion. Claudin 2 expression is regulated by components of the immune system (including IL-2, tumour necrosis factor (TNF), IL-13, IL-15, and IL-17) and growth factor signalling (including pro-epidermal growth factor (EGF), hepatocyte growth factor (HGF), extracellular signal-regulated kinase 1 (ERK1; also known as MAPK3), ERK2, and the RACα serine/threonine-protein kinase (AKT) pathways)[54]. Under pathophysiological conditions such as cisplatin-induced nephrotoxicity, ischaemic injury, or metabolic acidosis, claudin 2 expression is reduced, resulting in impaired paracellular transport of cations, which may contribute to disruption of the proximal tubule epithelium[55,56]. Tight junction injury can be visualized in vitro by tracking immunofluorescence or leakage of labelled inulin.

Proximal tubule cells also express a range of biotransformation enzymes on their brush border and cytoplasm, including γ-glutamyltransferase (GGT) as well as CYPs, glutathione *S*-transferases (GSTs), flavin-containing monooxygenase (FMO), and UDP-glucuronosyltransferases (UGTs)[7,57,58]. These renal enzymes, especially CYP3A4 and CYP3A5 and UGT1A9 and UGT2B7, might facilitate drug detoxification and efflux[10,58,59], which could lead to drug–drug interactions because substrates that inhibit these enzymes could cause other drugs to accumulate in the proximal tubule, thereby exacerbating their nephrotoxic effects[60]. In addition to their detoxifying effects, various studies have demonstrated that these enzymes can also bioactivate xenobiotics, potentially exacerbating their nephrotoxic effects[61–63]. However, the degree to which renal biotransformation contributes to the nephrotoxic effects of pharmaceutical compounds in vivo is not yet clear. GGT activity in proximal tubule models has been measured using a colorimetric assay reported in 1981 or with commercially available kits, although a difficulty in normalizing the assay readout to total protein content has been reported[64–66]. Acivicin, a GGT inhibitor, can be used to demonstrate the specificity of a chosen GGT assay[67]. Fluorometric assays for CYP enzymes, GSTs, and UGTs are also available from various suppliers.

The glomerulus, loop of Henle, distal tubule, and collecting duct also express transporters and receptors unique to those segments. Although some of these transporters have been linked to drug nephrotoxicity, less is known about the contributions of these transporters to nephrotoxicity than those of the proximal tubule. In principal cells of the collecting duct, lithium is absorbed via the epithelial sodium channel (ENaC), inducing downregulation of AQP2 expression, which leads to diabetes insipidus and with chronic exposure can lead to remodelling of the collecting duct, characterized by loss of principal cells and an increase in the number of intercalated cells[68–70]. Distinct transporters are also responsible for some of the adverse effects of drugs in the absence of overt renal cell injury; for example, Mg^{2+} and Na^+ loss following ciclosporin treatment is caused by downregulation of transient receptor potential cation channel subfamily M member 6 (TRPM6) and Na^+/Cl^- cotransporter (NCC) in the distal tubule[71].

Thus, the sensitivity of the kidney to nephrotoxicants is mediated by a multitude of unique functional proteins that are present in distinct epithelial components of the tubule. Therefore, modelling nephrotoxicity in vitro requires characterization of the functional identity of the cells under study, regardless of the cell source used. Such characterization requires substantially more than evaluation of gene expression and should also include characterization of protein localization and function.

Readouts of injury

Studies that use in vitro models to assess the nephrotoxicity of pharmaceutical agents usually rely on general cytotoxicity measures — such as cell death, the degree of cytoskeletal defects or mitochondrial function as determined by lactate production, or ATP content — as a measure of injury. The assumption is that in a relatively homogeneous population of renal cells, any compound that is cytotoxic to these cells is nephrotoxic. This assumption fails, however, when using a model that has more than one cell type by design. In addition, these cytotoxicity responses might reflect only advanced stages of injury elicited by high doses of the drug and therefore might fail to detect subtle injury that could still lead to acute or chronic kidney injury in vivo.

The past decade has witnessed a push to identify biomarkers of renal injury with improved specificity and sensitivity over the current standards of serum creatinine (SCr) and blood urea nitrogen (BUN)[72]. The fact that many of these biomarkers are proteins that are upregulated in response to injury led to the assumption that their in vitro expression could be used as a readout of the nephrotoxic potential of a given drug. However, not all biomarkers with potential utility in vivo are reliable indicators of nephrotoxicity in vitro.

Kidney injury molecule 1 (KIM1), also known as hepatitis A virus cellular receptor 1 (encoded by *HAVCR1*), is a type I membrane glycoprotein that is expressed in the liver, in activated immune cells, and in proximal tubules following injury[73,74]. Following AKI, KIM1 is expressed

on the apical surface of proximal tubule cells where it acts as a phagocytic receptor, enabling the removal of apoptotic cell debris by surviving cells[75]. The KIM1 ectodomain is shed into the urine following metalloproteinase cleavage, enabling it to be used as a biomarker of kidney injury[73]. The demonstration that urinary KIM1 concentration is a more sensitive and specific readout of in vivo kidney injury in rats and humans than SCr and BUN led to US Food and Drug Administration (FDA) and European Medicines Agency (EMA) approval of KIM1 as one of seven biomarkers to be used in addition to SCr and BUN for monitoring drug-induced nephrotoxicity in preclinical trials[76–79]. However, KIM1 has not performed as well in in vitro models, with a number of studies of primary proximal tubule cells or cell lines being unable to consistently detect significant differences in KIM1 expression between controls and cultures exposed to nephrotoxicants[80–83]. These inconsistent findings might suggest that additional cell types are required within the organ for KIM1 expression to be induced or that deficits exist in the in vitro cell models with respect to their cellular identity and/or response to injury.

Haem oxygenase 1 (HO1; encoded by *HMOX1*) is a 32 kDa enzyme that is induced in response to oxidative stress[84]. Within the kidney, HO1 is expressed following injury to the proximal tubules, glomeruli, or interstitial cells and is upregulated in renal mononuclear phagocytes in response to injury[85]. One study showed that levels of plasma and urinary HO1 are significantly higher in rats and humans with AKI than in healthy controls, although sample sizes used in that study were smaller than those of studies that have validated the specificity of other novel biomarkers, such as the 2008 and 2010 studies validating the performance of KIM1[77,78,86]. A study that performed transcriptional profiling of an in vitro primary proximal tubule cell model exposed to nephrotoxicants showed that *HMOX1* was the marker that correlated positively with dose for the largest number of nephrotoxic compounds tested[87]. HO1 expression also showed greater specificity and sensitivity for distinguishing between nephrotoxic and non-nephrotoxic compounds than the cell viability measures of cell death and ATP levels. Moreover, upregulation of HO1 expression was detectable by immunofluorescence in a kidney-on-a-chip model following exposure to cadmium chloride, whereas KIM1 expression was not detectable before exposure and only marginally increased after exposure, suggesting that the HO1 response to this nephrotoxic metal is more robust than that of KIM1 in vitro[87].

IL-6 is a multifunctional cytokine that is expressed by macrophages, endothelial cells, and fibroblasts, whereas IL-8 attracts neutrophils and is expressed by a number of immune cells as well as by endothelial and epithelial cells[88]. In the kidney, tubular epithelial cells and podocytes produce these interleukins as part of an inflammatory response following most types of injury, including ischaemia–reperfusion injury and pyelonephritis[89–92]. The potential utility of IL-6 and IL-8 as in vivo biomarkers of AKI is unclear, but a pilot study that assessed the effects of gentamicin and cadmium chloride on primary proximal tubule cells from two different donors showed greater upregulation of IL-6 and IL-8 than KIM1 levels in response to the compounds[82]. Upregulation of IL-6 and IL-8 expression also occurs in conditionally immortalized proximal tubule cell lines in response to uraemic toxins[93]. Together, these findings suggest that IL-6 and IL-8 are used as readouts of injury in vitro.

Neutrophil gelatinase-associated lipocalin (NGAL), also known as lipocalin 2 (encoded by *LCN2*), is expressed in maturing granulocytes and in various epithelial tissues including the stomach, lung, and kidney[94]. The healthy kidney filters serum NGAL through the glomerulus, whereupon it is endocytosed by the proximal tubule[95]. Kidney injury leads to upregulation of NGAL levels in the distal tubules and collecting ducts and shedding of NGAL into the urine[96]. The utility of urinary NGAL as a clinical biomarker of AKI is, however, limited by the finding that inflammation affects NGAL levels[78,97–99]. NGAL is expressed at relatively high levels in proximal tubule cells in vitro, which may indicate the poor phenotype retention of proximal tubule cells when cultured using standard techniques as NGAL is not upregulated in mouse or rat proximal tubules following injury in vivo[6,82,83]. NGAL might be useful as a marker of distal tubule and collecting duct injury in vitro, although this possibility has not been extensively investigated.

Preclinical screens of nephrotoxicity

Animal models

Preclinical testing of drug candidates using animal models is required to study safety and efficacy on a systems biology level before moving to clinical studies. However, animal pharmacokinetic profiles often differ considerably from those of humans; hence, animal models are often poor predictors of adverse drug effects of drug disposition in humans[100,101]. This mismatch between animal and human outcomes is largely due to the many differences in drug transporter and metabolizing enzyme expression between species[102]. For example, expression levels of OCT1 and OCT2 are comparable in the rodent kidney, whereas OCT2 predominates in the human kidney[103,104]. Similarly, renal expression of BCRP is much higher in male FVB mice and Wistar Hanover rats than in humans[44]. Other transporters, such as MATE2K, have been detected only in humans[103]. Transporter expression and function can also differ between different non-human animal species. For example, renal expression of BCRP is lower in female Sprague-Dawley rats than in female C57BL/6J mice[105]. In the process of developing polymyxin analogues, a compound that was selected for further investigation on the basis of promising safety results in rats was subsequently found to be nephrotoxic in dogs[4]. Sex can also influence transporter expression and, hence, drug kinetics, which creates the potential for toxicity screen results to differ between sexes[106,107]. In rats, for example, sex differences have been observed in the expression of tubule transporters and tight junction proteins, including claudin 2, AQP1, NCC, and ENaC[108].

The differences in transporter expression between animals and humans, and between different non-human species, limit the utility of animal models to study adverse drug effects. Therefore, the development of more suitable and predictive in vitro models is key to

Kidney-on-a-chip
Renal cells seeded in a 2D or 3D configuration in a microfluidic device. For proximal tubule chips, these devices typically allow flow of media across the cells' apical surface, basolateral surface, or both. Other cell types such as endothelial cells might be included; in these cases, the organization of the different cell types is defined by the design of the chip.

providing more reliable measures of the efficacy and safety of novel drug candidates in early stages of their development. In addition, the development of such in vitro models will greatly reduce preclinical toxicity testing in animals. Of note, in the area of cardiotoxicity, the FDA is in the process of validating induced pluripotent stem cell (iPSC)-derived human cardiomyocytes as a model in which to screen compounds for cardiac toxicity[109].

In vitro models of nephrotoxicity

Primary and immortalized cell lines. In vitro models for nephrotoxicity screening commonly use primary human renal proximal tubule cells, usually acquired from cadaveric specimens and cultured in 2D. However, primary cells display large interdonor variability, have limited expansion capacity, and are prone to dedifferentiation and loss of transporter expression[5,13,82,110]. To overcome difficulties in expanding primary proximal tubule cells, lines of immortalized or conditionally immortalized proximal tubule cells have been developed, for example, using oncogenes (such as E6/E7 or SV40 large T antigen) or telomerase (for example TERT1)[66,111,112]. Although TERT1-immortalized renal proximal tubule cells can undergo at least 90 population doublings and possess several characteristics of proximal tubule cells, including microvilli, tight junctions, GGT activity, endocytic activity, and functional drug transporters, the functional characteristics of early and late passage cells have not been compared[66,113]. Conditionally immortalized proximal tubule cells exhibit tight junctions, endocytic activity, OCT2 and MDR1 function, and UGT activity, but like all renal proximal tubule cells in 2D culture, these conditionally immortalized proximal tubule cells lose OAT1 and OAT3 expression unless the proteins are transduced[34,112,114,115].

The difficulty in maintaining transporter and metabolic function in primary cells and cell lines, and in reaching levels of transporter function comparable to those observed in vivo, are likely to result from the use of static 2D culture formats. In vitro renal transport or toxicity assays often use primary proximal tubule cells or cell lines cultured in a monolayer on a permeable support system, such as a Transwell insert, that is coated with an extracellular matrix[67,87,112,116]. The insert is placed in a well with media on top and underneath, enabling cells with appropriate transporters to transport substances from one side of the insert to the other. The major advantages of this system are that it is simple and that transporter and barrier function can be assayed by analysing substrate content on the top and bottom of the Transwell insert. However, the simplicity of this model also results in the loss of the environmental cues to which kidney tubules are normally exposed in vivo, such as fluid flow across the apical surface or signals from other adjacent cell types[14,110,117]. This deficiency has led to the development of more complex 3D culture systems and systems in which more than one renal cell type can be investigated; although, of note, Transwell inserts are still commonly used as a base for kidney organoids and renal tissue arrays, which are discussed later.

Pluripotent stem-cell-derived renal cells and reprogrammed cells. hPSCs have sparked considerable interest in terms of their potential to develop into fully functional renal cells. These cells can give rise to any cell type within the human body and can be easily expanded[118]. Including both embryonic stem cells and human iPSCs (hiPSCs), hPSCs have now been used to generate renal cells in vitro using combinations of growth factors and small molecules to mimic progression through normal embryonic kidney development[119–127]. Although the differentiation protocols developed so far vary in their duration, culture configuration, and timing of growth factor administration, most protocols involve an initial stimulation of WNT signalling followed by the use of fibroblast growth factor 9 (FGF9) with or without accompanying bone morphogenetic protein (BMP), retinoic acid, or activin A signalling (TABLE 2).

In one study of hiPSCs, use of a short differentiation protocol gave rise to proximal tubule-like cells, which when cultured in 2D showed expression of the tight junction protein ZO1 and the transporters OAT3, SGLT1, glucose transporter type 1 GLUT1, AQP1, and peptide transporter 1 (PEPT1) (REF.[126]). However, similar to 2D cultures of renal proximal tubule cells, these hiPSC-derived cells exhibited high baseline expression of the injury marker KIM1 and the dedifferentiation marker vimentin. In addition, immunofluorescence staining for transporters did not show correct polarization of transporter expression. Transcript expression analysis also demonstrated expression of markers of nephron segments other than the proximal tubule, which could indicate the presence of a mixed population of renal tubular cells, transdifferentiation of individual cells within the cultures, or the presence of nonspecific gene expression due to a lack of clear lineage commitment. Nonetheless, the study describes the use of these cells and IL-6 and IL-8 expression levels to classify compounds as nephrotoxic or nontoxic.

Two studies have described protocols for the generation of hiPSC-derived podocytes[128,129]. Although one of these protocols described the production of a cell population containing >90% podocytes[128], a direct comparison of the transcriptional signature of the cells with that of freshly isolated podocytes has not been presented[129]. In addition, in one of the studies[128], immunofluorescence staining for the podocyte marker Wilms tumour protein (WT1) was not nuclear, as would be anticipated for this protein.

A 2016 paper described a protocol to enable the direct reprogramming of fibroblasts to renal epithelial cells without first reprogramming the cells to a pluripotent state[130]. This approach has been described for other cell types and typically involves the overexpression of transcription factors associated with the target cell type[131]. Kaminski et al. determined that overexpression of homeobox protein EMX2, paired box protein PAX8, and hepatocyte nuclear factors 1β and 4α could induce mouse or human fibroblasts to differentiate directly into induced renal epithelial cells (iRECs), which expressed GGT and megalin and had a transcriptional profile more similar to that of whole human kidney lysate than that of human fibroblasts. Mouse iRECs could transport albumin and demonstrated greater cytotoxic responses

Kidney organoids
Three-dimensional aggregates of interstitial cells and nephron structures with characteristic segments, typically formed by directing pluripotent stem cells to a renal fate and aggregating these cells to enable self-organization, with or without additional extracellular matrix.

Renal tissue arrays
Three-dimensional co-cultures of renal epithelial cells, renal fibroblasts, and endothelial cells. Cell suspensions are prepared in biocompatible gels and bioprinted. The composition of the suspensions and the spatial arrangement of the different suspensions used define the organization of the different cell types. Scaffolds composed of extracellular matrix may or may not be used.

Table 2 | **Protocols and characterization of iPSC-derived kidney lineages**

iPSC origin	Differentiation protocol			PTEC markers			Nephrotoxicity response	Refs
	Inducing factors	Configuration	Total time (days)	Genes	Proteins	Function		
Human foreskin (ATCC); human dermal fibroblast-α (Invitrogen)	• IM[a]: CHIR, FGF2, and RA • MM and nephrogenesis: activin A, CHIR, and FGF9	2D	11	• *AQP1* • *MGLL*	• LTL • N-cadherin	ND	ND	119
Human pluripotent stem cells; exact source unknown	IM[a]: activin A, BMP7 and CHIR	2D; 3D embryonic bodies	• 2D: 20 • 3D: 3 + 17[b]	*AQP1*	• AQP1[c] • LTL[c]	ND	ND	120
Human pluripotent stem cells; exact source unknown	• IM: BMP4 and bFGF • UB: RA, activin A, and BMP2	3D chimeric aggregates (E12.5 mouse MM and human)	4 + 6	ND	ND	ND	ND	121
Human dermal fibroblasts (RIKEN BioResource Center)	IM: activin A, BMP4, CHIR, RA and bFGF	MM: 3D embryonic bodies	11 + 3	ND	• SALL1 • Cadherin 6	ND	ND	122
	MM and nephrogenesis: activin A, BMP4, CHIR, RA and FGF9	Nephrogenesis: 3D co-culture spheroids	14 + 8–12					
Human BJ foreskin fibroblasts (ATCC CRL-2522), human HDFα dermal fibroblasts (Invitrogen C-013-5C), human LR5-iPSCs (Hubrecht Institute, Netherlands), and human fibroblast hfib2-iPS4 and hfib2-iPS5 iPSCs (Boston Children's Hospital)	• IM[a]: CHIR • MM and nephrogenesis: B27 supplement (Thermo Fisher)	3D spheroid cultures towards organoids	23	ND	• LTL[d] • Megalin • Cubilin	• Endocytosis using rhodamine–dextran • Organic anion transport activity detected by fluorescein methotrexate • Barrier integrity measured by Lucifer yellow[e]	Organoids: KIM1 expression in response to cisplatin (50 μM) and gentamycin treatment (5 mM)	123
Human female fibroblasts (ATCC line CRL1502)	• IM: CHIR, FGF9 and heparin • MM and nephrogenesis: CHIR pulse, FGF9; after 5 days FGF9, no GF days 12–25	3D organoids	7 + 18	ND	• LTL • Cubilin	Endocytosis using dextran–Alexa 488	Organoids: caspase 3 expression in LTL^+ECAD^+ PTECs in response to cisplatin (5 and 20 μM) treatment	124
Human foreskin fibroblasts (WiCell Research Institute)	IM[a] + MM towards HPTC-like cells: BMP2 and BMP7	2D	8	• *SLC34A1* • *SLC4A4* • SLC5A2 • *SLC2A5* • *SLC22A6* • *SLC22A8* • *SLC22A2* • *SLC22A5* • *ABCB1* • *LRP2* • *SLC15A1* • *AQP1* • *ANPEP* • *GGT* • ATPase	• GLUT1[c] • SGLT[c] • AQP1[c] • OAT3[c] • PEPT1[c] • ATPase[c]	OAT activity determined by citrinin and OCT2 activity by cimetidine (indirect approaches: IL-6 and IL-8 induction)	2D cells: NF-κB, γH2AX, and 4-HNE expression in response to cisplatin (100 μg/ml = 333 μM) and aristolochic acid (1,000 μg/ml = 2,932 μM)	126
Human dermal fibroblasts (Invitrogen C-013-5C)	• IM: CHIR, Noggin and activin A • MM and nephrogenesis: FGF9, CHIR; no GFs days 14–28	2D; 3D organoids	• 2D: 21 • 3D: 9 + 12	ND	• LTL and AQP1 • N-cadherin	ND	Organoids: KIM1 expression in response to cisplatin (5 μM) and gentamycin treatment (5 mg/ml = 10 mM); γH2AX expression in response to cisplatin (5 μM and 50 μM)	125

Table 2 (cont.) | **Protocols and characterization of iPSC-derived kidney lineages**

iPSC origin	Differentiation protocol			PTEC markers			Nephrotoxicity response	Refs
	Inducing factors	Configuration	Total time (days)	Genes	Proteins	Function		
Human foreskin fibroblasts (System Biosciences International, SC101A-1)	• IM: activin A, CCG-1423, LY294002, and RA • MM towards renal progenitors: BMP7, FGF2, and GDNF	2D	19	ND	AQP1	ND	Regenerative effect in cisplatin AKI mice model	[127]

4-HNE, 4-hydroxynonenal; γH2AX, phosphorylated histone H2AX; AKI, acute kidney injury; AQP1, aquaporin 1; bFGF, basic fibroblast growth factor; BMP, bone morphogenetic protein; CCG-1423, RHOA inhibitor; CHIR, CHIR99201; E12.5, embryonic day 12.5; ECAD, epithelial cadherin; FGF, fibroblast growth factor; GDNF, glial cell line-derived neurotrophic factor; GF, growth factor; GLUT1, glucose transporter type 1; HDFα, human dermal fibroblast-α; HPTC, human proximal tubule cell; IM, intermediate mesoderm; iPSC, induced pluripotent stem cell; KIM1, kidney injury molecule 1; LTL, *Lotus tetragonolobus* lectin; LY294002, phosphoinositide 3-kinase–RACα serine/threonine-protein kinase inhibitor; MM, metanephric mesenchyme; MRP, multidrug resistance-associated protein; N-cadherin, neural cadherin; ND, not done; NF-κB, nuclear factor-κB; OAT, organic anion transporter; OCT2, organic cation transporter 2; PEPT1, peptide transporter 1; PTEC, proximal tubular epithelial cell; RA, retinoic acid; RKi, RHO-kinase inhibitor; SALL1, Sal-like protein 1; SGLT, sodium/glucose cotransporter; UB, ureteric bud. [a]RKi was added to support single-cell passaging before differentiation start. [b]Indicates 3D aggregate formation after 3 days of 2D differentiation and additional culture in 3D for 17 days. [c]Specificity not shown by cellular localization or double staining with proximal tubule marker. [d]LTL-positive tubules remained stable upon long-term culturing up to 120 days. [e]Lucifer yellow is also an OAT and MRP substrate[167].

to cisplatin, gentamicin, and tacrolimus than mouse fibroblasts, suggesting that the cells contained functional renal transporters. The cisplatin response was ameliorated by administration of the OCT antagonist cimetidine, suggesting functional OCT2 involvement in cisplatin tubulotoxicity, although expression of OCT2 or of other proximal tubule cell transporters was not confirmed. KIM1 expression was also significantly increased in response to gentamicin; however, KIM1 was also expressed at low levels in untreated iRECs, consistent with earlier observations that KIM1 is expressed by untreated, hiPSC-derived proximal tubule-like cells cultured in 2D[126] and suggesting that KIM1 is a nonspecific marker of tubule cell injury in in vitro models. In addition to the above caveats, the protocol for direct reprogramming produced a mixed population of iRECs that expressed markers of different nephron segments, with some individual cells expressing markers of multiple segments, suggesting that this approach generates pan-epithelial cells, which might represent an endogenous progenitor or tubular intermediate but might also represent nonspecific epithelial cell types that are not analogous to any cell type found in vivo. Further refinement of the protocol to control the types of cells produced and increase their functional maturity might enable the use of direct reprogramming to generate proximal tubule cells for in vitro nephrotoxicity screening.

Organoids. Several protocols now exist to enable the directed differentiation of hPSCs (human embryonic stem cells and hiPSCs) into complex multicellular kidney organoids (TABLE 2). These protocols exploit the ability of cells grown in 3D cultures to self-organize, which is reminiscent of the processes that occur during embryonic development, and can produce nephrons with evidence of glomeruli as well as segmentation of proximal and distal tubules, with some models showing additional evidence of surrounding stroma, vasculature, and collecting duct epithelium[122–125,132] (FIG. 2a). As with all protocols for the directed differentiation of hPSCs into complex structures, the kidney organoids produced to date are representative of the early developing nephron and do not necessarily represent a mature functional epithelium[124]. Nevertheless, proximal tubules within kidney organoids developed by different groups demonstrate some characteristic functions of mature tubules. Organoids produced by Takasato et al. had proximal tubules that were capable of dextran uptake and had greater sensitivity to cisplatin (as determined by the induction of apoptosis) than other cell types within the organoid, although injury marker expression was not determined[124]. Using a different protocol, Morizane et al. developed organoids in which proximal tubules expressed KIM1 in response to cisplatin and gentamicin and demonstrated that cisplatin induced proximal tubule-specific DNA damage as determined by phosphorylated histone H2AX (γH2AX) staining[125]. These findings show that organoids could potentially be used as a nephrotoxicity screening platform, although further characterization of the functional maturity and their injury response to known nephrotoxicants is needed.

Three-dimensional multicellular models are particularly valuable because they overcome the cellular simplicity of 2D cultures, wherein a single renal cell type is typically cultured in a monolayer, and instead provide a system with which to model the complex intercellular relationships involved in the response to a toxic insult. These intercellular relationships include interactions between adjacent epithelial cells and surrounding stromal cells but also include the microvasculature surrounding the tubules. Some protocols for the generation of organoids can induce the formation of vascular progenitors along with evidence of endothelial cells, perivascular cells, and pericytes[124]. Ideally, these would allow both for the modelling of vascular toxicity, such as that induced by VEGF inhibitors, and for studying the role of the endothelial network in tubular injury. However, the endothelial vessels in organoids arise between the forming nephrons with no convenient access point for perfusion. Thus, current kidney organoids do not yet recapitulate microvascular function to the extent required to study peritubular vasculature injury and/or downstream tubular effects in vitro.

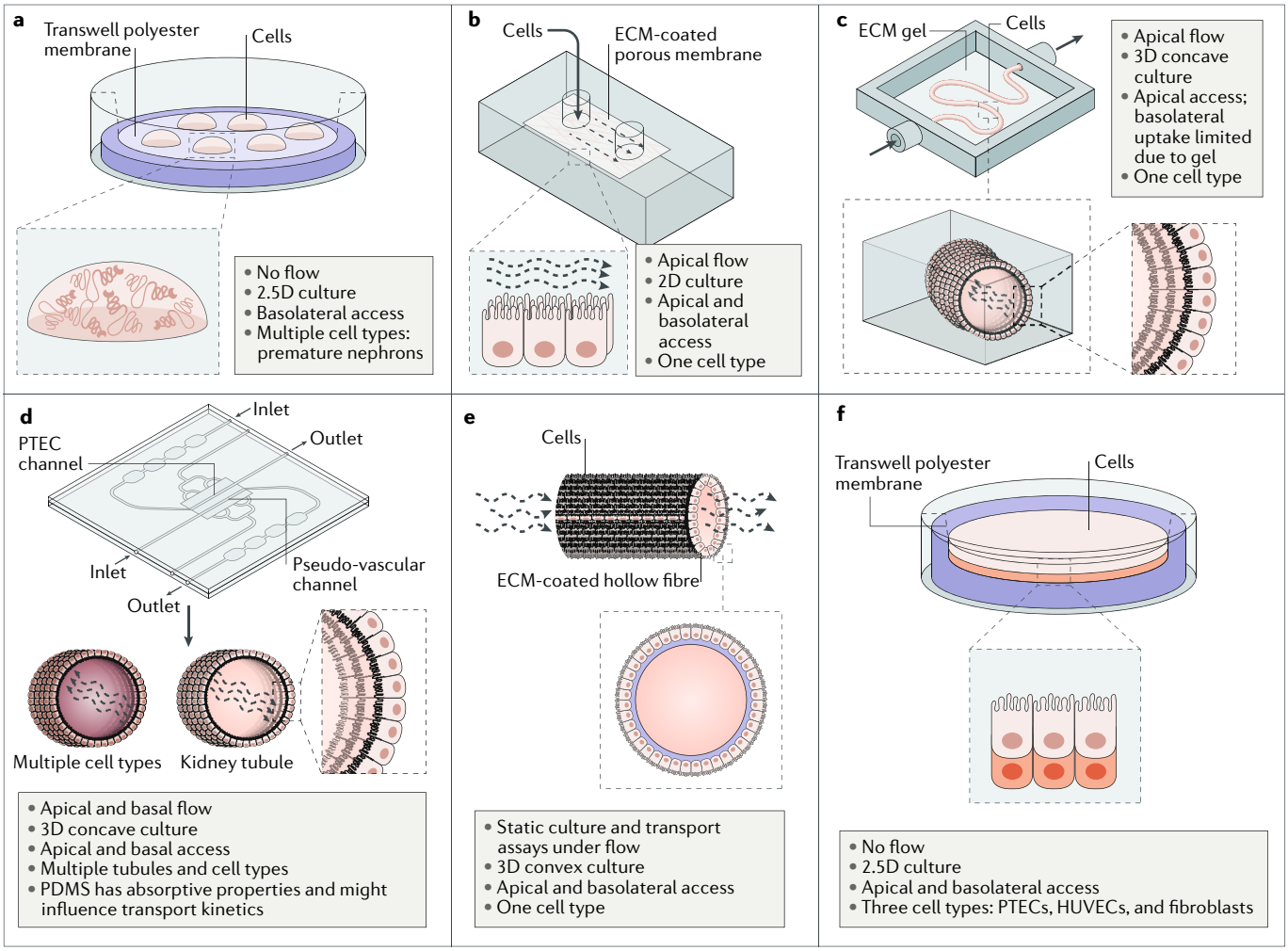

Fig. 2 | **Novel culture platforms for modelling nephrotoxicity in vitro.** **a** | Organoids consist of multiple immature nephrons and interstitial cells that self-organize in response to developmental cues and overcome the cellular simplicity of 2D cultures. **b** | A simple kidney-on-a-chip model allows media containing the compound of interest to flow across a cell monolayer. **c** | A kidney-on-a-chip that comprises a perfusable, convoluted 3D tubule within an extracellular matrix (ECM) enables fluid flow and the administration of test compounds to the apical surface of the cells. **d** | A kidney-on-a-chip with parallel 3D channels enables multiple cell types (for example, vasculature) to be modelled on a single chip with tubules. **e** | A biofunctionalized hollow fibre is coated with ECM and seeded with proximal tubule cells on its external surface, rendering both the basolateral and apical surfaces of the cells accessible for testing compounds. **f** | A 3D engineered renal tissue array consists of a monolayer of proximal tubule cells with an interstitial layer (comprising human umbilical vein endothelial cells (HUVECs) and fibroblasts) on their basolateral side, arranged on a Transwell. This model enables control over the spatial arrangement of cell types and media access to the basolateral and apical surfaces of the cells. PDMS, poly(dimethylsiloxane); PTEC, proximal tubule epithelial cell. Part **b** is reproduced with permission from REF.[133], Royal Society of Chemistry. Part **c** is reproduced from REF.[134], Macmillan Publishers Limited. Part **d** is reproduced with permission from REF.[67], Elsevier.

Although organoids are a relatively straightforward way to derive and co-culture a variety of renal cell types, and the presence of distinct nephron segments should enable detection of segment-specific toxicity during screens, their use is also associated with unique challenges. For instance, the presence of multiple cell types within a single structure also means that a solid understanding of the markers of functional maturity of each cell type is required to properly characterize an organoid model. Cell-type-specific readouts of injury also become more important for identifying the mechanism of injury of a test compound. To date, none of the available organoid protocols produce an anatomically functional organoid with collecting ducts that merge into a single ureter. Moreover, tubules within the organoids cannot be directionally perfused, which makes the administration of test compounds more challenging. In addition, the lack of direct access to either the apical or basolateral surface of the tubular epithelium, as is possible with 2D cultures, could hinder the delivery of toxic compounds to the cells of interest following their addition to the medium.

Kidney-on-a-chip. We define kidneys-on-a-chip as renal cells that are seeded in a microfluidic device that allows flow of media across the cell surface and/or cell surfaces[110] (FIG. 2b). One of the first studies of this technology seeded primary human proximal tubule cells on 2D chips with apical and basolateral media compartments and demonstrated that fluid flow across the apical surface stimulated MDR1 expression and function and induced the formation of tight junctions and columnar

Fugitive ink
Biocompatible material that can be printed and later evacuated to leave a hollow space within a mould.

morphology[133]. Cells in fluidic culture were also better protected by cimetidine from cisplatin-induced apoptosis than were cells in static culture, although OCT2 function and expression were not directly assessed and injury marker expression was not determined by the researchers.

Although cells grown on 2D microfluidic chips demonstrate better proximal tubule cell function than cells grown in static cultures, 3D chip designs might more closely replicate the architecture of the proximal tubule and may offer further improvements (FIG. 2c). Indeed, a bioprinting approach has been used to fabricate a 3D chip containing a convoluted tubule filled with a fugitive ink within a gelatin–fibrinogen matrix. After flushing, the tubules were seeded with immortalized proximal tubule cells[134], which, similar to the 2D chips, could then be perfused with media to provide fluid flow and administer test compounds to the apical surface of the cells. Epithelial cells cultured within these 3D models had higher expression of megalin and greater albumin uptake than cells cultured under static conditions and on 2D microfluidic chips, indicative of greater functional maturity. These bioprinted cells also showed evidence of tight junction damage following exposure to ciclosporin; however, the expression of injury markers was not assessed.

Although these 3D bioprinted chips are an improvement on static and 2D designs, further improvements are needed to develop 'vascular' networks that surround the tubule in order to gain access to the basolateral surface of the printed proximal tubule[134]. A 2014 study described the development of chips for modelling human vasculature, which contained a collagen matrix and two parallel 3D channels that could be perfused independently[135]. This system has since been used to culture primary human proximal tubule cells, seeding one channel with the cells and using the second channel as a cell-free, pseudo-vascular channel[67] (FIG. 2d). Proximal tubule cells cultured in this 3D flow-directed microphysiological system demonstrated GGT activity and SGLT2-mediated transport of a fluorescent glucose analogue, indicating the presence of mature, functional proximal tubule cells. Perfusion of the OAT substrates para-aminohippurate or indoxyl sulfate through the pseudo-vascular channel was followed by their detection in the 'proximal tubule' effluent, suggesting transepithelial transport. Moreover, the amount of each substrate in the effluent relative to the inflow was decreased in the presence of probenecid (an OAT and MRP inhibitor), suggesting active transport of each substrate via OATs and/or MRPs, although the use of high concentrations of probenecid might have compromised cell metabolism[136]. Nevertheless, this study demonstrates that primary proximal tubule cells cultured in this chip design show characteristic functions of this cell type and that the pseudo-vascular channel can be used to administer compounds to the basolateral surface of these cells, although nephrotoxic injury responses were not determined in this study.

Several chips with vascular channels have been designed and can theoretically also be used to model injury to the renal and extrarenal microvasculature. For example, one microfluidic device seeded with human microvascular endothelial cells has been used for modelling haematologic diseases[137]. Activation of these endothelial cells with TNF resulted in decreased flow and microchannel occlusion, whereas exposure of the cells to Shiga-like toxin 2 resulted in the formation of thrombi that occluded the microchannels, indicating that this design would be suitable for studying drug-induced thrombotic microangiopathy. More recently, a protocol has been developed for isolating human kidney peritubular microvascular endothelial cells (HKMECs) and culturing them in a microfluidic device[138]. These HKMECs have a markedly different transcriptional profile from that of human umbilical vein endothelial cells (HUVECs) cultured under the same conditions and showed lower angiogenic potential and increased responsiveness to flow, demonstrating that the kidney microvasculature has specific properties that might not be replicated in models that use other endothelial cell types or lack physiological features such as flow.

Modelling the interactions between renal tubular cells and the microvasculature during injury requires the use of chips with dedicated renal epithelial tubules, vasculature seeded with appropriate endothelial cells, and, possibly, pericytes incorporated into the extracellular matrix of the chip[139]. Advances in the past couple of years have led to the development of high-throughput platforms with vascularized microorgans in a 96-well format, with the intent of recreating tissues with multiple cell types for rapid screening of large drug libraries. So far, however, the microorgans studied with these platforms have been restricted to simple architectures, such as tumour models, and renal models have not yet been produced with this design[140,141].

Most kidney-on-a-chip systems to date have used primary proximal tubule cells; however, it should also be possible to seed chips with hPSC-derived proximal tubule cells or other tubular cells. Although no system has yet assessed multiple nephron cell types on a single chip, a 2017 study reported the development of a 'glomerulus-on-a-chip', in which hPSC-derived podocytes were seeded on one side of a porous membrane and primary endothelial cells were seeded on the other[128]. The chip design also permitted cyclic stretching of the membrane to model the mechanical strain of blood pulsation in glomeruli in vivo. As no specific molecular biomarker of podocyte injury has been identified, the researchers used albumin leakage across the membrane as a readout of injury following adriamycin exposure. Although extensive characterization of the hPSC-derived podocytes was not carried out, evidence for the differential retention of albumin and inulin across the chip membrane suggests the existence of barrier function.

Kidneys-on-a-chip have also been used in in vitro systems to model multiorgan toxicity and pharmacodynamics, whereby the kidney chip is functionally coupled (via the manual transfer of media) or physically coupled to in vitro models of other organ systems[142,143]. One 2017 study demonstrated that human proximal tubules on a chip showed increased KIM1 production and cell death in response to aristolochic acid I when a hepatocyte-containing chip was coupled upstream

compared with when the proximal tubule chip was isolated, consistent with bioactivation of aristolochic acid I by hepatocytes[143]. This study provides proof of concept that a multiorgan in vitro model can assess the nephrotoxicity of a test compound and its metabolites. The benefits of multiorgan models and the challenges of designing them have been discussed elsewhere[142].

Kidneys-on-a-chip are advantageous as they afford precise control over the spatial arrangement of different cell types and the perfusion of test compounds, making them a potentially valuable tool for nephrotoxicity screening. Further improvements in the engineering and design of these chips to enable the study of multiple 'tubules' in parallel will facilitate high-throughput screening[110]. However, additional characterization of injury marker expression of renal cells cultured on chips is required to enable rapid assessment of injury.

Biofunctionalized hollow fibres. A 2015 study showed that conditionally immortalized proximal tubule epithelial cells could be seeded onto the exterior surface of hollow fibres coated with an extracellular matrix, creating biofunctionalized hollow fibres with a monolayer of cells[144] (FIG. 2e). The proximal tubule cells grown on these fibres demonstrated improved tight junction formation and OAT1 expression compared with that of the same cells cultured in 2D even in the absence of flow through the fibres, suggesting that the 3D culture itself improved the expression of these markers. The integrity of the tight junction and OAT1 function were confirmed using fluorescein isothiocyanate (FITC)-labelled inulin leakage and fluorescein uptake assays, respectively, demonstrating that both the basolateral and apical surfaces of the cells are accessible for testing compounds. Flow through the basolateral compartment is also possible. Exposure of these hollow fibres to uraemic toxins increased IL-6 expression and induced leakage of FITC-labelled inulin, indicating disruption of the epithelial tight junctions[145]. Notably, the convex arrangement of tubular epithelial cells on the exterior of the hollow fibre is not reflective of their arrangement in vivo — a caveat that should be addressed in future designs.

Engineered renal tissue arrays. Tissue arrays are a form of multicellular 3D culture that has been used for in vitro hepatotoxicity screening, and they have now been adapted for the assessment of nephrotoxicity in renal tissue[65,146] (FIG. 2f). To generate these renal tissue arrays, a suspension of renal fibroblasts and HUVECs in a proprietary gel were bioprinted into Transwells to create a 3D interstitial layer[65], after which a second suspension of primary human proximal tubule cells was bioprinted over the interstitial layer. This method produced a 3D tissue array consisting of a monolayer of proximal tubule cells with a thicker interstitial layer on their basolateral side. The proximal tubule cells in these arrays expressed polarized, functional MDR1, OAT1, OAT3, OCT2, and SGLT2 transporters and showed ACE and GGT activity. The arrays also had TEER values of 18.1 $\Omega^{*}cm^{2}$, higher than those seen in proximal tubule cells in vivo but better than values typical of cells cultured in static 2D systems. The proximal tubule cells desquamated and proliferated in response to cisplatin, whereas cimetidine exhibited protective effects. Furthermore, the interstitial layer showed a fibrotic response to transforming growth factor-β (TGFβ). To our knowledge, this is one of the first proof-of-concept models of renal fibrosis in vitro.

Renal tissue arrays enable the co-culture of multiple renal cell types and enable investigation of injury to different cell types, with control over the spatial arrangement of cell types and media access to the basolateral and apical surfaces of proximal tubule cells. Current designs involve bioprinting of cells into 24-well Transwell plates, which enable moderate-throughput toxicity screens. However, rapid readouts of proximal tubule injury will be required to increase throughput; therefore, further characterization of injury markers is needed. Improved tissue array designs that permit laminar flow (possibly requiring microfabrication similar to that used for kidneys-on-a-chip) might further improve the functional maturity of the proximal tubule cells cultured in these tissue arrays[65].

Future directions

The development of in vitro nephrotoxicity screens that more accurately predict the in vivo response than currently available approaches is likely to occur with improvement of the approaches described above. The development of approaches to obtain functionally mature 3D models of individual nephron segments or even entire nephrons will improve the predictive ability of screens of novel compounds. However, these models will eventually require higher-throughput screening approaches with rapid readouts of injury that can be measured by an automated system in order for these models to be adopted by industry.

Advances in automated imaging and image analysis have given rise to high-content screening, in which fluorescent probes or reporter lines are used to visualize specific cellular features (for example, specific injury markers, general apoptotic markers, or the actin cytoskeleton), followed by automated imaging and quantification of changes in those features across the test conditions[147]. Machine-learning algorithms, trained on a set of reference compounds, can then be used to classify test compounds as either toxic or nontoxic on the basis of the imaging readouts[148]. The feasibility of this approach was demonstrated in a 2016 study, in which a high-content screen and classification algorithm in primary human proximal tubule cells were used to correctly identify 15 of 24 compounds known to be nephrotoxic to proximal tubule cells and 17 of 20 compounds that are not toxic to proximal tubule cells[148]. Such high-content screening enables large amounts of data to be collected and interpreted, which will be useful for analysing compound responses in the above-described complex nephrotoxicity models under development.

As nephrotoxicity models become more physiologically relevant, their clinical predictive value will lie in screening not only for single drug effects but also for drug–drug interactions and the effects of individual variations such as the effects of underlying kidney disease or CYP enzyme polymorphisms on drug metabolism and toxicity[100,149,150]. Such analyses will require in vitro-to-in

Biofunctionalized hollow fibres
Hollow, porous polymer fibres coated with extracellular matrix on which renal cells can be cultured.

Desquamated
Peeling and shedding of the top layer of an epithelium.

vivo extrapolations, involving mathematical models that can numerically simulate the behaviour of a drug in a complex system using results obtained experimentally in an in vitro system as the input parameter. The success of these mechanistic models is highly dependent on in-depth quantitative knowledge of renal physiology, such as relevant flow rates, the total number of nephrons and cells in a kidney, and absolute protein expression levels of transporters and enzymes[100,151]. In physiologically based pharmacokinetic modelling, drug pharmacokinetics or toxicokinetics can be predicted in silico by incorporating relevant drug disposition data such as renal drug metabolism and renal accumulation during excretion[152]. Such computational models not only might be useful for early-phase predictions of drug nephrotoxicity but also might guide the design of clinical studies and reduce reliance on animal testing. A final challenge in this area is to predict the individual response of a patient to any compound. As many drugs in clinical use have dose-limiting nephrotoxicity, understanding the capacity of an individual patient to detoxify a given drug will aid dose management. Such a precision approach will require integration of pharmacogenomics data into the computational models and might also require the development of multiorgan in vitro models to obtain relevant data from nonrenal systems[152]. At present, this goal is some time off.

Conclusions

The failure of existing in vitro cell and preclinical models to accurately predict nephrotoxicity highlights the need for more accurate models. Advances in our understanding of kidney development, regeneration of human kidney cell types from pluripotent stem cells, and increasingly complex 3D platforms for tissue culture have sparked the development of new approaches to address this challenge. The main goal will be to generate cellular models that demonstrate improved functional maturity and consequently improved injury responses and predictivity for known and new nephrotoxicants. Further technological advances will lead to the development of models that contain multiple renal cell types and nephron segments and enable access to both basolateral and apical sides of the model nephron, improving the physiological relevance of the models. Improved throughput in compound testing and data collection is also needed. Ultimately, the integration of information gained from these in vitro models into computational algorithms that incorporate patient-specific physiological parameters will not only reduce the late loss of drugs from the development pipeline but also facilitate the development of safer drugs and improve management of clinically important compounds with nephrotoxic adverse effects.

Published online 06 Apr 2018

1. Nolin, T. D. & Himmelfarb, J. in *Adverse Drug Reactions* (ed. Uetrecht, J.) 111–130 (Springer, Berlin, Heidelberg, 2010).
2. Grünfeld, J.-P. & Rossier, B. C. Lithium nephrotoxicity revisited. *Nat. Rev. Nephrol.* **5**, 270–276 (2009).
3. Rewa, O. & Bagshaw, S. M. Acute kidney injury — epidemiology, outcomes and economics. *Nat. Rev. Nephrol.* **10**, 193–207 (2014).
4. Magee, T. V. et al. Discovery of Dap-3 polymyxin analogues for the treatment of multidrug-resistant Gram-negative nosocomial infections. *J. Med. Chem.* **56**, 5079–5093 (2013).
5. Tiong, H. Y. et al. Drug-induced nephrotoxicity: clinical impact and preclinical in vitro models. *Mol. Pharm* **11**, 1933–1948 (2014).
6. Huang, J. X. et al. Evaluation of biomarkers for in vitro prediction of drug-induced nephrotoxicity: comparison of HK-2, immortalized human proximal tubule epithelial, and primary cultures of human proximal tubular cells. *Pharmacol. Res. Perspect.* **3**, e00148 (2015).
7. Dekant, W. & Vamvakas, S. Biotransformation and membrane transport in nephrotoxicity. *Crit. Rev. Toxicol.* **26**, 309–334 (1996).
8. Hawksworth, G. M. et al. in Toxicology — From Cells to Man (eds Seiler, S. P., Kroftová, O. & Eybl, V.) 184–192 (Springer, Berlin, Heidelberg, 1996).
9. Lock, E. A. & Reed, C. J. Xenobiotic metabolizing enzymes of the kidney. *Toxicol. Pathol.* **26**, 18–25 (1998).
10. Knops, N. et al. The functional implications of common genetic variation in CYP3A5 and ABCB1 in human proximal tubule cells. *Mol. Pharm.* **12**, 758–768 (2015).
11. Bhargava, P. & Schnellmann, R. G. Mitochondrial energetics in the kidney. *Nat. Rev. Nephrol.* **13**, 629–646 (2017).
12. Kramann, R., Tanaka, M. & Humphreys, B. D. Fluorescence microangiography for quantitative assessment of peritubular capillary changes after AKI in mice. *J. Am. Soc. Nephrol.* **25**, 1924–1931 (2014).
13. Qi, W., Johnson, D. W., Vesey, D. A., Pollock, C. A. & Chen, X. Isolation, propagation and characterization of primary tubule cell culture from human kidney (Methods in Renal Research). *Nephrology* **12**, 155–159 (2007).
14. Fisel, P., Renner, O., Nies, A. T., Schwab, M. & Schaeffeler, E. Solute carrier transporter and drug-related nephrotoxicity: the impact of proximal tubule cell models for preclinical research. *Expert Opin. Drug Metab. Toxicol.* **10**, 395–408 (2014).
15. Lemke, A., Kiderlen, A. F. & Kayser, O. Amphotericin, B. *Appl. Microbiol. Biotechnol.* **68**, 151–162 (2005).
16. Mamoulakis, C. et al. Contrast-induced nephropathy: Basic concepts, pathophysiological implications and prevention strategies. *Pharmacol. Ther.* **180**, 99–112 (2017).
17. Pauksakon, P. & Fogo, A. B. Drug-induced nephropathies. *Histopathology* **70**, 94–108 (2017).
18. Perazella, M. A. & Markowitz, G. S. Bisphosphonate nephrotoxicity. *Kidney Int.* **74**, 1385–1393 (2008).
19. Xia, L., Zhou, M., Kalhorn, T. F., Ho, H. T. B. & Wang, J. Podocyte-specific expression of organic cation transporter PMAT: implication in puromycin aminonucleoside nephrotoxicity. *Am. J. Physiol.-Ren. Physiol.* **296**, F1307–F1313 (2009).
20. Yilmaz, M., Taninmis, H., Kara, E., Ozagari, A. & Unsal, A. Nephrotic syndrome after oral bisphosphonate (alendronate) administration in a patient with osteoporosis. *Osteoporos. Int.* **23**, 2059–2062 (2012).
21. Cheng, H. F. & Harris, R. C. Renal effects of non-steroidal anti-inflammatory drugs and selective cyclooxygenase-2 inhibitors. *Curr. Pharm. Des.* **11**, 1795–1804 (2005).
22. Perazella, M. A. Drug-induced renal failure: update on new medications and unique mechanisms of nephrotoxicity. *Am. J. Med. Sci.* **325**, 349–362 (2003).
23. Basile, D. P., Donohoe, D., Roethe, K. & Osborn, J. L. Renal ischemic injury results in permanent damage to peritubular capillaries and influences long-term function. *Am. J. Physiol. Renal Physiol.* **281**, F887–F899 (2001).
24. Verma, S. K. & Molitoris, B. A. Renal endothelial injury and microvascular dysfunction in acute kidney injury. *Semin. Nephrol.* **35**, 96–107 (2015).
25. Dimke, H. et al. Tubulovascular cross-talk by vascular endothelial growth factor a maintains peritubular microvasculature in kidney. *J. Am. Soc. Nephrol.* **26**, 1027–1038 (2015).
26. Lameire, N. Nephrotoxicity of recent anti-cancer agents. *Clin. Kidney J.* **7**, 11–22 (2014).
27. Al-Nouri, Z. L., Reese, J. A., Terrell, D. R., Vesely, S. K. & George, J. N. Drug-induced thrombotic microangiopathy: a systematic review of published reports. *Blood* **125**, 616–618 (2015).
28. Breljak, D. et al. Distribution of organic anion transporters NaDC3 and OAT1-3 along the human nephron. *Am. J. Physiol. Renal Physiol.* **311**, F227–F238 (2016).
29. Motohashi, H. et al. Gene expression levels and immunolocalization of organic ion transporters in the human kidney. *J. Am. Soc. Nephrol.* **13**, 866–874 (2002).
30. Ingraham, L. et al. A plasma concentration of α-ketoglutarate influences the kinetic interaction of ligands with organic anion transporter 1. *Mol. Pharmacol.* **86**, 86–95 (2014).
31. Budiman, T., Bamberg, E., Koepsell, H. & Nagel, G. Mechanism of electrogenic cation transport by the cloned organic cation transporter 2 from rat. *J. Biol. Chem.* **275**, 29413–29420 (2000).
32. Cihlar, T. et al. The antiviral nucleotide analogs cidofovir and adefovir are novel substrates for human and rat renal organic anion transporter 1. *Mol. Pharmacol.* **56**, 570–580 (1999).
33. Ho, E. S., Lin, D. C., Mendel, D. B. & Cihlar, T. Cytotoxicity of antiviral nucleotides adefovir and cidofovir is induced by the expression of human renal organic anion transporter 1. *J. Am. Soc. Nephrol.* **11**, 383–393 (2000).
34. Nieskens, T. T. G. et al. A human renal proximal tubule cell line with stable organic anion transporter 1 and 3 expression predictive for antiviral-induced toxicity. *AAPS J.* **18**, 465–475 (2016).
35. Hagos, Y. & Wolff, N. A. Assessment of the role of renal organic anion transporters in drug-induced nephrotoxicity. *Toxins* **2**, 2055–2082 (2010).
36. Ciarimboli, G. Role of organic cation transporters in drug-induced toxicity. *Expert Opin. Drug Metab. Toxicol.* **7**, 159–174 (2011).
37. Pabla, N., Murphy, R. F., Liu, K. & Dong, Z. The copper transporter Ctr1 contributes to cisplatin uptake by renal tubular cells during cisplatin nephrotoxicity. *Am. J. Physiol. Renal Physiol.* **296**, F505–F511 (2009).
38. Hori, Y. et al. Megalin blockade with cilastatin suppresses drug-induced nephrotoxicity. *J. Am. Soc. Nephrol.* **28**, 1783–1791 (2017).
39. Nagai, J. & Takano, M. Entry of aminoglycosides into renal tubular epithelial cells via endocytosis-dependent and endocytosis-independent pathways. *Biochem. Pharmacol.* **90**, 331–337 (2014).
40. [No authors listed.] Genitourinary Development Molecular Anatomy Project. GUDMAP http://www.gudmap.org/ (2017).

41. Harding, S. D. et al. The GUDMAP database — an online resource for genitourinary research. *Development* **138**, 2845–2853 (2011).
42. Jenkinson, S. E. et al. The limitations of renal epithelial cell line HK-2 as a model of drug transporter expression and function in the proximal tubule. *Pflüg. Arch.* **464**, 601–611 (2012).
43. van Aubel, R. A., Smeets, P. H., Peters, J. G., Bindels, R. J. & Russel, F. G. The MRP4/ABCC4 gene encodes a novel apical organic anion transporter in human kidney proximal tubules: putative efflux pump for urinary cAMP and cGMP. *J. Am. Soc. Nephrol.* **13**, 595–603 (2002).
44. Huls, M. et al. The breast cancer resistance protein transporter ABCG2 is expressed in the human kidney proximal tubule apical membrane. *Kidney Int.* **73**, 220–225 (2008).
45. Motohashi, H. & Inui, K. Multidrug and toxin extrusion family SLC47: Physiological, pharmacokinetic and toxicokinetic importance of MATE1 and MATE2-K. *Mol. Aspects Med.* **34**, 661–668 (2013).
46. Wen, X. et al. MDR1 transporter protects against paraquat-induced toxicity in human and mouse proximal tubule cells. *Toxicol. Sci.* **141**, 475–483 (2014).
47. Yokoo, S. et al. Differential contribution of organic cation transporters, OCT2 and MATE1, in platinum agent-induced nephrotoxicity. *Biochem. Pharmacol.* **74**, 477–487 (2007).
48. Hahn, K., Ejaz, A. A., Kanbay, M., Lanaspa, M. A. & Johnson, R. J. Acute kidney injury from SGLT2 inhibitors: potential mechanisms. *Nat. Rev. Nephrol.* **12**, 711–712 (2016).
49. Nadkarni, G. N. et al. Acute kidney injury in patients on SGLT2 inhibitors: a propensity-matched analysis. *Diabetes Care* **40**, 1479–1485 (2017).
50. Saly, D. & Perazella, M. A. Harnessing basic and clinic tools to evaluate SGLT2 inhibitor nephrotoxicity. *Am. J. Physiol. Renal Physiol.* **313**, F951–F954 (2017).
51. Yu, A. S. L. Claudins and the kidney. *J. Am. Soc. Nephrol.* **26**, 11–19 (2015).
52. Markadieu, N. et al. A primary culture of distal convoluted tubules expressing functional thiazide-sensitive NaCl transport. *Am. J. Physiol. Renal Physiol.* **303**, F886–F892 (2012).
53. Fromm, M., Piontek, J., Rosenthal, R., Günzel, D. & Krug, S. M. Tight junctions of the proximal tubule and their channel proteins. *Pflüg. Arch.* **469**, 877–887 (2017).
54. Günzel, D. & Yu, A. S. L. Claudins and the modulation of tight junction permeability. *Physiol. Rev.* **93**, 525–569 (2013).
55. Trujillo, J. et al. Renal tight junction proteins are decreased in cisplatin-induced nephrotoxicity in rats. *Toxicol. Mech. Methods* **24**, 520–528 (2014).
56. Balkovetz, D. F. Tight junction claudins and the kidney in sickness and in health. *Biochim. Biophys. Acta* **1788**, 858–863 (2009).
57. Lash, L. H., Putt, D. A. & Cai, H. Drug metabolism enzyme expression and activity in primary cultures of human proximal tubular cells. *Toxicology* **244**, 56–65 (2008).
58. Miners, J., Yang, X., Knights, K. & Zhang, L. The role of the kidney in drug elimination: transport, metabolism, and the impact of kidney disease on drug clearance. *Clin. Pharmacol. Ther.* **102**, 436–449 (2017).
59. Bolbrinker, J. et al. CYP3A5 genotype-phenotype analysis in the human kidney reveals a strong site-specific expression of CYP3A5 in the proximal tubule in carriers of the CYP3A5*1 allele. *Drug Metab. Dispos.* **40**, 639–641 (2012).
60. Yu, J., Zhou, Z., Owens, K. H., Ritchie, T. K. & Ragueneau-Majlessi, I. What can be learned from recent new drug applications? A systematic review of drug interaction data for drugs approved by the US FDA in 2015. *Drug Metab. Dispos.* **45**, 86–108 (2017).
61. Dekant, W. The role of biotransformation and bioactivation in toxicity. *EXS* **99**, 57–86 (2009).
62. Liu, S. et al. The role of renal proximal tubule P450 enzymes in chloroform-induced nephrotoxicity: Utility of renal specific P450 reductase knockout mouse models. *Toxicol. Appl. Pharmacol.* **272**, 230–237 (2013).
63. Fliedl, L. Controversial role of gamma-glutamyl transferase activity in cisplatin nephrotoxicity. *ALTEX* **31**, 269–278 (2014).
64. Meister, A., Tate, S. S. & Griffith, O. W. Gamma-glutamyl transpeptidase. *Methods Enzymol.* **77**, 237–253 (1981).
65. King, S. M. et al. 3D proximal tubule tissues recapitulate key aspects of renal physiology to enable nephrotoxicity testing. *Front. Physiol.* **8**, 123 (2017).
66. Wieser, M. et al. hTERT alone immortalizes epithelial cells of renal proximal tubules without changing their functional characteristics. *Am. J. Physiol. Renal Physiol.* **295**, F1365–F1375 (2008).
67. Weber, E. J. et al. Development of a microphysiological model of human kidney proximal tubule function. *Kidney Int.* **90**, 627–637 (2016).
68. Kortenoeven, M. L. A. et al. Amiloride blocks lithium entry through the sodium channel thereby attenuating the resultant nephrogenic diabetes insipidus. *Kidney Int.* **76**, 44–53 (2009).
69. Thomsen, K. & Shirley, D. G. A hypothesis linking sodium and lithium reabsorption in the distal nephron. *Nephrol. Dial. Transplant.* **21**, 869–880 (2006).
70. Christensen, B. M., Kim, Y.-H., Kwon, T.-H. & Nielsen, S. Lithium treatment induces a marked proliferation of primarily principal cells in rat kidney inner medullary collecting duct. *Am. J. Physiol. Renal Physiol.* **291**, F39–F48 (2006).
71. Ledeganck, K. J. et al. Expression of renal distal tubule transporters TRPM6 and NCC in a rat model of cyclosporine nephrotoxicity and effect of EGF treatment. *Am. J. Physiol. Renal Physiol.* **301**, F486–F493 (2011).
72. Bonventre, J. V., Vaidya, V. S., Schmouder, R., Feig, P. & Dieterle, F. Next-generation biomarkers for detecting kidney toxicity. *Nat. Biotechnol.* **28**, 436–440 (2010).
73. Bailly, V. et al. Shedding of kidney injury molecule-1, a putative adhesion protein involved in renal regeneration. *J. Biol. Chem.* **277**, 39739–39748 (2002).
74. Ichimura, T. Kidney injury molecule-1: a tissue and urinary biomarker for nephrotoxicant-induced renal injury. *Am. J. Physiol. Renal Physiol.* **286**, 552F–563 (2004).
75. Ichimura, T. et al. Kidney injury molecule-1 is a phosphatidylserine receptor that confers a phagocytic phenotype on epithelial cells. *J. Clin. Invest.* **118**, 1657–1668 (2008).
76. Vaidya, V. S. Urinary kidney injury molecule-1: a sensitive quantitative biomarker for early detection of kidney tubular injury. *Am. J. Physiol. Renal Physiol.* **290**, F517–F529 (2006).
77. Vaidya, V. S. et al. Kidney injury molecule-1 outperforms traditional biomarkers of kidney injury in preclinical biomarker qualification studies. *Nat. Biotechnol.* **28**, 478–485 (2010).
78. Vaidya, V. S. et al. Urinary biomarkers for sensitive and specific detection of acute kidney injury in humans. *Clin. Transl Sci.* **1**, 200–208 (2008).
79. Dieterle, F. et al. Renal biomarker qualification submission: a dialog between the FDA-EMEA and Predictive Safety Testing Consortium. *Nat. Biotechnol.* **28**, 455–462 (2010).
80. Rached, E. et al. Evaluation of putative biomarkers of nephrotoxicity after exposure to ochratoxin A in vivo and in vitro. *Toxicol. Sci* **103**, 371–381 (2008).
81. Sohn, S.-J. et al. In vitro evaluation of biomarkers for cisplatin-induced nephrotoxicity using HK-2 human kidney epithelial cells. *Toxicol. Lett.* **217**, 235–242 (2013).
82. Li, Y. et al. An in vitro method for the prediction of renal proximal tubular toxicity in humans. *Toxicol. Res* **2**, 352 (2013).
83. Luo, Q.-H. et al. Evaluation of KIM-1 and NGAL as early indicators for assessment of gentamycin-induced nephrotoxicity in vivo and in vitro. *Kidney Blood Press. Res* **41**, 911–918 (2016).
84. Gozzelino, R., Jeney, V. & Soares, M. P. Mechanisms of cell protection by heme oxygenase-1. *Annu. Rev. Pharmacol. Toxicol.* **50**, 323–354 (2010).
85. Lever, J. M., Boddu, R., George, J. F. & Agarwal, A. Heme oxygenase-1 in kidney health and disease. Antioxid. Redox Signal. https://doi.org/10.1089/ars.2016.6659 (2016).
86. Zager, R. A., Johnson, A. C. M. & Becker, K. Plasma and urinary heme oxygenase-1 in AKI. *J. Am. Soc. Nephrol.* **23**, 1048–1057 (2012).
87. Adler, M. et al. A quantitative approach to screen for nephrotoxic compounds in vitro. *J. Am. Soc. Nephrol.* **27**, 1015–1028 (2016).
88. Akdis, M. et al. Interleukins, from 1 to 37, and interferon-γ: receptors, functions, and roles in diseases. *J. Allergy Clin. Immunol.* **127**, 701–721.e70 (2011).
89. Tramma, D., Hatzistylianou, M., Gerasimou, G. & Lafazanis, V. Interleukin-6 and interleukin-8 levels in the urine of children with renal scarring. *Pediatr. Nephrol.* **27**, 1525–1530 (2012).
90. Grigoryev, D. N. et al. The local and systemic inflammatory transcriptome after acute kidney injury. *J. Am. Soc. Nephrol.* **19**, 547–558 (2008).
91. Araki, M. et al. Expression of IL-8 during reperfusion of renal allografts is dependent on ischemic time. *Transplantation* **81**, 783–788 (2006).
92. Su, H., Lei, C.-T. & Zhang, C. Interleukin-6 signaling pathway and its role in kidney disease: an update. *Front. Immunol.* **8**, 405 (2017).
93. Mihajlovic, M. et al. Allostimulatory capacity of conditionally immortalized proximal tubule cell lines for bioartificial kidney application. *Sci. Rep.* **7**, 7103 (2017).
94. Cowland, J. B. & Borregaard, N. Molecular characterization and pattern of tissue expression of the gene for neutrophil gelatinase-associated lipocalin from humans. *Genomics* **45**, 17–23 (1997).
95. Charlton, J. R., Portilla, D. & Okusa, M. D. A basic science view of acute kidney injury biomarkers. *Nephrol. Dial. Transplant.* **29**, 1301–1311 (2014).
96. Paragas, N. et al. The Ngal reporter mouse detects the response of the kidney to injury in real time. *Nat. Med.* **17**, 216–222 (2011).
97. McIlroy, D. R., Wagener, G. & Lee, H. T. Neutrophil gelatinase-associated lipocalin and acute kidney injury after cardiac surgery: the effect of baseline renal function on diagnostic performance. *Clin. J. Am. Soc. Nephrol.* **5**, 211–219 (2010).
98. Mårtensson, J. & Bellomo, R. The rise and fall of NGAL in acute kidney injury. *Blood Purif.* **37**, 304–310 (2014).
99. Haase, M. et al. Accuracy of neutrophil gelatinase-associated lipocalin (NGAL) in diagnosis and prognosis in acute kidney injury: a systematic review and meta-analysis. *Am. J. Kidney Dis.* **54**, 1012–1024 (2009).
100. Scotcher, D., Jones, C., Posada, M., Galetin, A. & Rostami-Hodjegan, A. Key to opening kidney for in vitro-in vivo extrapolation entrance in health and disease: Part II: mechanistic models and in vitro-in vivo extrapolation. *AAPS J.* **18**, 1082–1094 (2016).
101. Hilgendorf, C. et al. Expression of thirty-six drug transporter genes in human intestine, liver, kidney, and organotypic cell lines. *Drug Metab. Dispos.* **35**, 1333–1340 (2007).
102. Chu, X., Bleasby, K. & Evers, R. Species differences in drug transporters and implications for translating preclinical findings to humans. *Expert Opin. Drug Metab. Toxicol.* **9**, 237–252 (2013).
103. Yonezawa, A. & Inui, K. Importance of the multidrug and toxin extrusion MATE/SLC47A family to pharmacokinetics, pharmacodynamics/toxicodynamics and pharmacogenomics. *Br. J. Pharmacol.* **164**, 1817–1825 (2011).
104. Aoki, M. et al. Kidney-specific expression of human organic cation transporter 2 (OCT2/SLC22A2) is regulated by DNA methylation. *Am. J. Physiol. Renal Physiol.* **295**, F165–F170 (2008).
105. Tanaka, Y., Slitt, A. L., Leazer, T. M., Maher, J. M. & Klaassen, C. D. Tissue distribution and hormonal regulation of the breast cancer resistance protein (Bcrp/Abcg2) in rats and mice. *Biochem. Biophys. Res. Commun.* **326**, 181–187 (2004).
106. Soldin, O. P. & Mattison, D. R. Sex differences in pharmacokinetics and pharmacodynamics. *Clin. Pharmacokinet.* **48**, 143–157 (2009).
107. Joseph, S. et al. Expression of drug transporters in human kidney: impact of sex, age, and ethnicity. *Biol. Sex Differ.* **6**, 4 (2015).
108. Veiras, L. C. et al. Sexual dimorphic pattern of renal transporters and electrolyte homeostasis. *J. Am. Soc. Nephrol.* **28**, 3504–3517 (2017).
109. [No authors listed.] Validating human stem cell cardiomyocyte technology for better predictive assessment of drug-induced cardiac toxicity. U.S. Food & Drug Administration https://www.fda.gov/ScienceResearch/SpecialTopics/RegulatoryScience/ucm507998.htm (2016).
110. Wilmer, M. J. et al. Kidney-on-a-chip technology for drug-induced nephrotoxicity screening. *Trends Biotechnol.* **34**, 156–170 (2016).
111. Ryan, M. J. et al. HK-2: An immortalized proximal tubule epithelial cell line from normal adult human kidney. *Kidney Int.* **45**, 48–57 (1994).
112. Wilmer, M. J. et al. Novel conditionally immortalized human proximal tubule cell line expressing functional influx and efflux transporters. *Cell Tissue Res.* **339**, 449–457 (2010).
113. Aschauer, L., Carta, G., Vogelsang, N., Schlatter, E. & Jennings, P. Expression of xenobiotic transporters in the human renal proximal tubule cell line RPTEC/TERT1. *Toxicol. In Vitro* **30**, 95–105 (2015).

114. Schophuizen, C. M. S. et al. Cationic uremic toxins affect human renal proximal tubule cell functioning through interaction with the organic cation transporter. *Pflüg. Arch.* **465**, 1701–1714 (2013).
115. Mutsaers, H. A. M. et al. Uremic toxins inhibit renal metabolic capacity through interference with glucuronidation and mitochondrial respiration. *Biochim. Biophys. Acta* **1832**, 142–150 (2013).
116. Jansen, J. et al. Bioengineered kidney tubules efficiently excrete uremic toxins. *Sci. Rep.* **6**, 26715 (2016).
117. Ivliev, A. E., 't Hoen, P. A. C., Roon-Mom, W. M. C., van, Peters, D. J. M. & Sergeeva, M. G. Exploring the transcriptome of ciliated cells using in silico dissection of human tissues. *PLoS ONE* **7**, e35618 (2012).
118. Ohnuki, M. & Takahashi, K. Present and future challenges of induced pluripotent stem cells. *Phil. Trans. R. Soc. B Biol Sci.* **370**, 20140367 (2015).
119. Lam, A. Q. et al. Rapid and efficient differentiation of human pluripotent stem cells into intermediate mesoderm that forms tubules expressing kidney proximal tubular markers. *J. Am. Soc. Nephrol.* **25**, 1211–1225 (2014).
120. Mae, S.-I. et al. Monitoring and robust induction of nephrogenic intermediate mesoderm from human pluripotent stem cells. *Nat. Commun.* **4**, 1367 (2013).
121. Xia, Y. et al. The generation of kidney organoids by differentiation of human pluripotent cells to ureteric bud progenitor-like cells. *Nat. Protoc.* **9**, 2693–2704 (2014).
122. Taguchi, A. et al. Redefining the in vivo origin of metanephric nephron progenitors enables generation of complex kidney structures from pluripotent stem cells. *Cell Stem Cell* **14**, 53–67 (2014).
123. Freedman, B. S. et al. Modelling kidney disease with CRISPR-mutant kidney organoids derived from human pluripotent epiblast spheroids. *Nat. Commun.* **6**, 8715 (2015).
124. Takasato, M. et al. Kidney organoids from human iPS cells contain multiple lineages and model human nephrogenesis. *Nature* **526**, 564–568 (2015).
125. Morizane, R. et al. Nephron organoids derived from human pluripotent stem cells model kidney development and injury. *Nat. Biotechnol.* **33**, 1193–1200 (2015).
126. Kandasamy, K. et al. Prediction of drug-induced nephrotoxicity and injury mechanisms with human induced pluripotent stem cell-derived cells and machine learning methods. *Sci. Rep.* **5**, 12337 (2015).
127. Imberti, B. et al. Renal progenitors derived from human iPSCs engraft and restore function in a mouse model of acute kidney injury. *Sci. Rep.* **5**, 8826 (2015).
128. Musah, S. et al. Mature induced-pluripotent-stem-cell-derived human podocytes reconstitute kidney glomerular-capillary-wall function on a chip. *Nat. Biomed. Eng.* **1**, 0069 (2017).
129. Song, B. et al. The directed differentiation of human iPS cells into kidney podocytes. *PLoS ONE* **7**, e46453 (2012).
130. Kaminski, M. M. et al. Direct reprogramming of fibroblasts into renal tubular epithelial cells by defined transcription factors. *Nat. Cell Biol.* **18**, 1269–1280 (2016).
131. Xu, J., Du, Y. & Deng, H. Direct lineage reprogramming: strategies, mechanisms, and applications. *Cell Stem Cell* **16**, 119–134 (2015).
132. Takasato, M. et al. Directing human embryonic stem cell differentiation towards a renal lineage generates a self-organizing kidney. *Nat. Cell Biol.* **16**, 118–126 (2014).
133. Jang, K.-J. et al. Human kidney proximal tubule-on-a-chip for drug transport and nephrotoxicity assessment. *Integr. Biol.* **5**, 1119 (2013).
134. Homan, K. A. et al. Bioprinting of 3D convoluted renal proximal tubules on perfusable chips. *Sci. Rep.* **6**, 34845 (2016).
135. Tourovskaia, A., Fauver, M., Kramer, G., Simonson, S. & Neumann, T. Tissue-engineered microenvironment systems for modeling human vasculature. *Exp. Biol. Med.* **239**, 1264–1271 (2014).
136. Masereeuw, R. et al. Probenecid interferes with renal oxidative metabolism: a potential pitfall in its use as an inhibitor of drug transport. *Br. J. Pharmacol.* **131**, 57–62 (2000).
137. Tsai, M. et al. In vitro modeling of the microvascular occlusion and thrombosis that occur in hematologic diseases using microfluidic technology. *J. Clin. Invest.* **122**, 408–418 (2012).
138. Ligresti, G. et al. A novel three-dimensional human peritubular microvascular system. *J. Am. Soc. Nephrol.* **27**, 2370–2381 (2016).
139. Kelly, E. J. et al. Innovations in preclinical biology: ex vivo engineering of a human kidney tissue microperfusion system. *Stem Cell Res. Ther.* **4**, S17 (2013).
140. Phan, D. T. T. et al. A vascularized and perfused organ-on-a-chip platform for large-scale drug screening applications. *Lab Chip* **17**, 511–520 (2017).
141. van Duinen, V. et al. 96 perfusable blood vessels to study vascular permeability in vitro. *Sci. Rep.* **7**, 18071 (2017).
142. Vernetti, L. et al. Functional coupling of human microphysiology systems: intestine, liver, kidney proximal tubule, blood-brain barrier and skeletal muscle. *Sci. Rep.* **7**, 42296 (2017).
143. Chang, S.-Y. et al. Human liver-kidney model elucidates the mechanisms of aristolochic acid nephrotoxicity. *JCI Insight* **2**, 95978 (2017).
144. Jansen, J. et al. Human proximal tubule epithelial cells cultured on hollow fibers: living membranes that actively transport organic cations. *Sci. Rep.* **5**, 16702 (2015).
145. Mihajlovic, M. et al. Role of vitamin D in maintaining renal epithelial barrier function in uremic conditions. *Int. J. Mol. Sci.* **18**, 2531 (2017).
146. Nguyen, D. G. et al. Bioprinted 3D primary liver tissues allow assessment of organ-level response to clinical drug induced toxicity in vitro. *PLoS ONE* **11**, e0158674 (2016).
147. Persson, M. & Hornberg, J. J. Advances in predictive toxicology for discovery safety through high content screening. *Chem. Res. Toxicol.* **29**, 1998–2007 (2016).
148. Su, R., Xiong, S., Zink, D. & Loo, L.-H. High-throughput imaging-based nephrotoxicity prediction for xenobiotics with diverse chemical structures. *Arch. Toxicol.* **90**, 2793–2808 (2016).
149. Abdullah, R., Alhusainy, W., Woutersen, J., Rietjens, I. M. C. M. & Punt, A. Predicting points of departure for risk assessment based on in vitro cytotoxicity data and physiologically based kinetic (PBK) modeling: The case of kidney toxicity induced by aristolochic acid I. *Food Chem. Toxicol.* **92**, 104–116 (2016).
150. Zhou, S.-F., Liu, J.-P. & Chowbay, B. Polymorphism of human cytochrome P450 enzymes and its clinical impact. *Drug Metab. Rev.* **41**, 89–295 (2009).
151. Scotcher, D. et al. Microsomal and cytosolic scaling factors in dog and human kidney cortex and application for in vitro-in vivo extrapolation of renal metabolic clearance. *Drug Metab. Dispos.* **45**, 556–568 (2017).
152. Leclerc, E., Hamon, J. & Bois, F. Y. Investigation of ifosfamide and chloroacetaldehyde renal toxicity through integration of in vitro liver–kidney microfluidic data and pharmacokinetic-system biology models. *J. Appl. Toxicol.* **36**, 330–339 (2016).
153. Miller, R. P., Tadagavadi, R. K., Ramesh, G. & Reeves, W. B. Mechanisms of cisplatin nephrotoxicity. *Toxins* **2**, 2490–2518 (2010).
154. Nakamura, T., Yonezawa, A., Hashimoto, S., Katsura, T. & Inui, K. Disruption of multidrug and toxin extrusion MATE1 potentiates cisplatin-induced nephrotoxicity. *Biochem. Pharmacol.* **80**, 1762–1767 (2010).
155. Hu, S. et al. Identification of OAT1/OAT3 as contributors to cisplatin toxicity. *Clin. Transl Sci.* **10**, 412–420 (2017).
156. Sonneveld, R. et al. Glucose specifically regulates TRPC6 expression in the podocyte in an AngII-dependent manner. *Am. J. Pathol.* **184**, 1715–1726 (2014).
157. Ambrus, L. et al. Inhibition of TRPC6 by protein kinase C isoforms in cultured human podocytes. *J. Cell. Mol. Med.* **19**, 2771–2779 (2015).
158. Eyre, J. et al. Statin-sensitive endocytosis of albumin by glomerular podocytes. *Am. J. Physiol. Renal Physiol.* **292**, F674–F681 (2007).
159. Kido, Y., Matsson, P. & Giacomini, K. M. Profiling of a prescription drug library for potential renal drug–drug interactions mediated by the organic cation transporter 2. *J. Med. Chem.* **54**, 4548–4558 (2011).
160. Caetano-Pinto, P. et al. Fluorescence-based transport assays revisited in a human renal proximal tubule cell line. *Mol. Pharm.* **13**, 933–944 (2016).
161. Shaik, N., Giri, N., Pan, G. & Elmquist, W. F. P-Glycoprotein-mediated active efflux of the anti-HIV1 nucleoside abacavir limits cellular accumulation and brain distribution. *Drug Metab. Dispos.* **35**, 2076–2085 (2007).
162. Kusuhara, H. et al. Effects of a MATE protein inhibitor, pyrimethamine, on the renal elimination of metformin at oral microdose and at therapeutic dose in healthy subjects. *Clin. Pharmacol. Ther.* **89**, 837–844 (2011).
163. Ito, S. et al. Potent and specific inhibition of mMate1-mediated efflux of type I organic cations in the liver and kidney by pyrimethamine. *J. Pharmacol. Exp. Ther.* **333**, 341–350 (2010).
164. Zhai, X. Y. et al. Cubilin- and megalin-mediated uptake of albumin in cultured proximal tubule cells of opossum kidney. *Kidney Int.* **58**, 1523–1533 (2000).
165. Moreno, E. et al. Affinity-defining domains in the Na-Cl cotransporter: a different location for Cl^- and thiazide binding. *J. Biol. Chem.* **281**, 17266–17275 (2006).
166. Andrukhova, O. et al. FGF23 promotes renal calcium reabsorption through the TRPV5 channel. *EMBO J.* **33**, 229–246 (2014).
167. Masereeuw, R., Moons, M. M., Toomey, B. H., Russel, F. G. M. & Miller, D. S. Active lucifer yellow secretion in renal proximal tubule: evidence for organic anion transport system crossover. *J. Pharmacol. Exp. Ther.* **289**, 1104–1111 (1999).

Acknowledgements
J.Y.-C.S. is supported by a University of Melbourne Research Scholarship and a Murdoch Children's Research Institute Top up scholarship. J.J. is supported by the Dutch Kidney Foundation (Kolff postdoctoral fellowship abroad grant 170KK05), EMBO (short-term fellowship 6893), and by the partners of Regenerative Medicine Crossing Borders powered by Health ~ Holland, Top Sector Life Sciences & Health. R.M. is supported by a grant from the UK National Centre for the Replacement, Refinement and Reduction of Animals in Research (NC3Rs), the NephroTube CRACK IT Challenge, and the RegMed XB consortium. M.H.L. is an Australian National Health and Medical Research Council (NHMRC) Senior Principal Research Fellow (GNT1042093) and is supported by funding from the NHMRC (GNT1100970) and the US National Institutes of Health (DK107344).

Author contributions
J.J. researched data for the article. J.Y.-C.S., J.J., and R.M. wrote the article. All authors contributed substantially to discussion of the article's content and reviewed and edited the manuscript before submission.

Competing interests
M.H.L. holds a research contract with Organovo, Inc. The other authors declare no competing interests.

Publisher's note
Springer Nature remains neutral with regard to jurisdictional claims in published maps and institutional affiliations.

Reviewer information
Nature Reviews Nephrology thanks J. Lewis, R. Morizane and the other, anonymous reviewer(s) for their contribution to the peer review of this work.

RELATED LINKS
GUDMAP: www.gudmap.org
Regenerative Medicine Crossing Borders: www.regmedxb.com